

**PARTIAL DISCHARGE BEHAVIOURS AND BREAKDOWN
MECHANISMS OF ESTER TRANSFORMER LIQUIDS
UNDER AC STRESS**

A thesis submitted to The University of Manchester for the degree of

PhD

in the Faculty of Engineering and Physical Sciences

2011

XIN WANG

School of Electrical and Electronic Engineering

Content

Content	3
List of Figures	7
List of Tables	12
Abstract	14
Declaration	15
Copyright Statement	16
Acknowledgement	17
Terminologies	18
Chapter 1. Introduction	21
1.1 Background.....	21
1.2 Insulating Liquids Used in Thesis.....	23
1.2.1 Mineral Oil - Nytro Gemini X	23
1.2.2 Synthetic Ester - Midel 7131	25
1.2.3 Natural Ester - Envirotemp FR3.....	26
1.3 Research Objectives	27
1.4 Outline of Thesis.....	28
Chapter 2. Literature Review of Breakdown Mechanism of Mineral Oil	33
2.1 Introduction.....	33
2.2 Breakdown Theories	33
2.2.1 Ionization Theory	34
2.2.2 Weakest-link Theory	34
2.2.3 Streamer Theory.....	35
2.2.4 Summary.....	36
2.3 Breakdown of Mineral Oil in Uniform Fields	37
2.3.1 Conditioning Effect	37
2.3.2 Influence of Water.....	38
2.3.3 Influence of Particles.....	44
2.3.4 Influence of Gas	50
2.3.5 Influence of Electrodes.....	55
2.3.6 Streamer Study in Uniform Fields.....	57
2.4 Breakdown of Mineral Oil in Divergent Fields	59
2.4.1 Introduction.....	59
2.4.2 Definitions of Pre-breakdown Phenomena	61
2.4.3 Streamer Initiation.....	62
2.4.4 Streamer Propagation	64
2.4.5 Streamer-led Breakdown	68
2.4.6 Influence of Some Factors	71
2.5 Comparison between Breakdown in Uniform and Divergent Fields.....	75
2.6 Summary.....	76
Chapter 3. Experimental Study on Breakdown in AC Uniform Fields	79
3.1 Introduction.....	79
3.2 Breakdown Strengths of Transformer Liquids	80

3.2.1	Introduction.....	80
3.2.2	Sample Preparation	80
3.2.3	AC breakdown Voltages.....	81
3.2.4	Breakdown Voltage Distributions.....	84
3.3	Withstand Strengths of Transformer liquids	89
3.3.1	Introduction.....	89
3.3.2	Prediction of Withstand Voltages	89
3.3.3	Examination of Withstand Voltages	92
3.3.4	Comparison of Prediction Results and Measurement Results.....	97
3.4	Particle Effect on Breakdown Voltages	99
3.4.1	Contaminations in Power Transformers.....	99
3.4.2	Experimental Description	100
3.4.3	Experimental Results.....	101
3.4.4	Influence of Viscosity on Breakdown Voltages	105
3.4.5	Particle Movement in Transformer Liquids	107
3.5	Water Effect on Breakdown Voltages.....	112
3.5.1	Introduction.....	112
3.5.2	Sample Preparation	113
3.5.3	Tests and Results.....	113
3.5.4	Discussion and Further Work	115
3.6	Area Effect on Breakdown Voltages	116
3.6.1	Introduction.....	116
3.6.2	Theoretical Analysis of Area Effect using Weibull Distribution.....	117
3.6.3	Experimental Description	120
3.6.4	Results and Discussions.....	121
3.7	Withstand Voltages of In-service Transformer Liquids.....	125
3.8	Summary	127
Chapter 4.	PD Measurement and PD Performances of Transformer Liquids.....	129
4.1	Introduction	129
4.2	Knowledge Related to PDIV Measurements.....	130
4.2.1	IEC 61294 Test Procedure.....	130
4.2.2	Definitions of PD Inception Voltage.....	131
4.3	Experimental Description.....	134
4.4	Suggestions relating to IEC 61294	135
4.4.1	Ramping Speed	136
4.4.2	Voltage Duration.....	137
4.4.3	PD Detector.....	138
4.4.4	Outline of Suggested Revisions	139
4.5	PDIV Measurements	140
4.5.1	Industrial PDIV Definition	140
4.5.2	Academic PDIV Definition	141
4.6	PD Performances at Overstressed Voltages	143
4.6.1	Experimental Description	143
4.6.2	Experimental Results.....	144
4.7	Summary	149
Chapter 5.	Experimental Study on Breakdown in AC Divergent Fields.....	151

5.1	Introduction.....	151
5.2	Experimental Description.....	152
5.2.1	Experimental Setup	152
5.2.2	Measurement Methods	153
5.3	Streamer Initiation.....	156
5.3.1	General Features.....	156
5.3.2	Inception Voltages.....	159
5.3.3	Φ -Q-N Patterns.....	160
5.4	Streamer Propagation	161
5.4.1	Streamer Structures and Associated Currents.....	161
5.4.2	Maximum Stopping Lengths.....	164
5.4.3	Average Propagation Velocities.....	170
5.4.4	Φ -Q-N Patterns.....	172
5.4.5	Space Charge Effect	173
5.5	Streamer Lead to Breakdown	178
5.5.1	Breakdown Modes.....	179
5.5.2	Influence of Gap Distance	182
5.5.3	Influence of Needle Electrode.....	184
5.5.4	Influence of Ground Electrode.....	187
5.6	Summary.....	188
Chapter 6. Dissolved Gas Analysis under PD Faults.....		191
6.1	Introduction.....	191
6.2	DGA Techniques.....	192
6.2.1	PD Faults in Oil.....	192
6.2.2	Gas Formation under PD Faults	193
6.2.3	PD Fault Diagnosis.....	194
6.3	Experimental Setup and Considerations.....	196
6.4	DGA under PD Faults of Controlled Amplitude	198
6.4.1	Experimental Description	198
6.4.2	Results and Discussions.....	199
6.5	DGA under PD Fault of Controlled Energy	204
6.5.1	Experimental Description	204
6.5.2	Results and Discussions.....	204
6.6	Production of C_2H_6 in Natural Esters.....	209
6.7	DGA Diagnosis Methods	211
6.7.1	Criteria for DGA Diagnosis	211
6.7.2	Key Gas Method.....	212
6.7.3	Duval Triangle Method.....	215
6.8	Summary.....	216
Chapter 7. Conclusions and Future Work.....		219
7.1	Research Areas.....	219
7.2	Summary of Main Findings and Results	220
7.3	Future Work.....	222
Appendix I. Additional Information and Further Tests		225
I.1	Particle Effect on AC Breakdown Strengths of Transformer Liquids	225
I.2	Equipment and Methods used in Breakdown Voltage Tests.....	226

I.3	Sample Preparation of Breakdown Voltage Tests	234
I.4	Experimental Description of Breakdown Voltage Tests.....	235
I.5	Sample Preparation of Water Effect Tests	238
I.6	Influence of Needle Electrode on PDIV	240
I.7	Influence of Electrode Arrangement on Streamer Propagation.....	241
Appendix II. Test Results Used in Thesis		249
Appendix III. List of Publications		269
References		271

Words count: 56645

List of Figures

Figure 1.1 Basic hydrocarbon structures of mineral oil [12].....	24
Figure 1.2 Molecular structure of Midel 7131 [14]	25
Figure 1.3 Molecular structure of Envirotemp FR3 [14].....	26
Figure 2.1 Conditioning effect of successive breakdowns in mineral oil [29]	37
Figure 2.2 Water absorptions from air for 10 types of mineral oil at 20°C [33].....	39
Figure 2.3 Water bonding positions and the length of alkyl chain [37]	40
Figure 2.4 Water saturation levels for transformer liquids at different temperatures [14]40	
Figure 2.5 Water effect on dielectric strength of mineral oil.....	41
Figure 2.6 Water effect on dielectric strength of mineral oil at different gap distances [44]	43
Figure 2.7 Breakdown of a insulating liquid due to instability of a water globule [50] ..	44
Figure 2.8 Influence of water on dielectric strengths of mineral oil and FR3 [16].....	44
Figure 2.9 Motion of a conductive particle in insulating liquids	46
Figure 2.10 Schematic graph of metallic particle motion in mineral oil [54]	47
Figure 2.11 Cellulose particles bridging a gap under DC voltage [77].....	49
Figure 2.12 Schematic of small cellulose particles aggregating into larger particles [78]49	
Figure 2.13 Relation between breakdown strength and particle content factor [80]	50
Figure 2.14 Dissolved gas influence on breakdown strength of mineral oil [82].....	51
Figure 2.15 Deformation of an air bubble in the direction of applied AC field [90].....	53
Figure 2.16 Theoretical and observation decay rate of a zero pressure bubble [20].....	53
Figure 2.17 Breakdown strengths of mineral oil at various gauge pressures [94].....	54
Figure 2.18 Lichtenberg photos obtained in mineral oil at different pressures [95].....	55
Figure 2.19 Electrode area effect on breakdown voltage of mineral oil [103]	56
Figure 2.20 Breakdowns induced by positive and negative streamers under AC voltage in semi-uniform field [109].....	58
Figure 2.21 Streamer structure of mineral oil in semi-uniform and divergent field [25].	58
Figure 2.22 Average propagation velocity of positive streamer in mineral oil [118].....	60
Figure 2.23 Inception voltage of positive streamer versus tip radius [119].	63
Figure 2.24 Bubble growth, detachment, and disappear of a negative streamer [111]....	64
Figure 2.25 Ionization zone of negative and positive streamers [126]	66
Figure 2.26 Re-illumination of a positive streamer with current and light recordings [120]	68
Figure 2.27 Streamer stopping length of positive streamers with applied voltage [124].	69
Figure 2.28 Positive streamer propagating to the plane without causing breakdown [114]	70
Figure 2.29 Return streamer channel developed from sphere electrode[130].....	70
Figure 2.30 Current and voltage signal for streamer burst breakdown [120].....	70
Figure 2.31 Influence of electrode configuration on positive streamer properties [135].	72
Figure 2.32 Positive streamer propagations of clean and cellulose contaminated oils [114]	73
Figure 2.33 Breakdown voltage with oil gaps for new and carbonized mineral oil [74].	74
Figure 2.34 PD inception voltage of carbonized samples with controlled energy [73] ...	74

Figure 2.35 Impulse streamer inception field of mineral oil versus stressed liquid scale	75
Figure 2.36 AC streamer inception field of mineral oil versus electrode area [142].	76
Figure 3.1 AC breakdown voltages of processed Gemini X	82
Figure 3.2 AC breakdown voltages of processed Midel 7131	82
Figure 3.3 AC breakdown voltages of processed FR3	82
Figure 3.4 Comparison of AC breakdown voltages of processed transformer liquids	83
Figure 3.5 Normal distributions of breakdown voltages of transformer liquids	85
Figure 3.6 Gumbel distributions of breakdown voltages of transformer liquids	85
Figure 3.7 Weibull distributions of breakdown voltages of transformer liquids	86
Figure 3.8 Prediction of withstand voltage from breakdown voltage distribution of Gemini X using Weibull fitting	90
Figure 3.9 Results of 500 withstand tests for Gemini X	93
Figure 3.10 Results of 500 withstand tests for Midel 7131	94
Figure 3.11 Results of 500 withstand tests for FR3	94
Figure 3.12 Probability distributions of breakdown numbers in 500 withstand tests	95
Figure 3.13 Probability density and cumulative probability of failure rate for Gemini X	96
Figure 3.14 Probability density and cumulative probability of failure rate for Midel 7131	96
Figure 3.15 Probability density and cumulative probability of failure rate for FR3	97
Figure 3.16 Examinations of prediction results for Gemini X using various distributions	98
Figure 3.17 Examinations of prediction results for Midel 7131 using various distributions	98
Figure 3.18 Examinations of prediction results for FR3 using various distributions	98
Figure 3.19 Breakdown voltages and standard deviations of transformer liquids contaminated by cellulose particles	102
Figure 3.20 Breakdown voltages and standard deviations of transformer liquids contaminated by copper particles	104
Figure 3.21 Dielectric strengths of transformer liquids with temperature [83]	105
Figure 3.22 Schematic diagram of experimental setup for particle movement test	108
Figure 3.23 Threshold voltages of particle motions in transformer liquids	109
Figure 3.24 Phenomena of spark and breakdown during particle motion	109
Figure 3.25 Particle motions in transformer liquids at 20 kV	110
Figure 3.26 Swing voltages of particle motion in transformer liquids	110
Figure 3.27 AC breakdown voltages of transformer liquids with a steel particle	111
Figure 3.28 Breakdown voltages and standard deviations with absolute water content for transformer liquids	114
Figure 3.29 Breakdown voltages and standard deviations with relative water content for transformer liquids	114
Figure 3.30 Water effect on breakdown voltages of clean and relatively dirty Gemini X	116
Figure 3.31 The parallel breakdown probability model for electrode area effect	118
Figure 3.32 Electrodes used in scale effect test	120
Figure 3.33 Weibull plots of breakdown voltage distributions using various electrodes	122
Figure 3.34 Scale parameters of transformer liquids as a function of electrode area	124

Figure 4.1 Traditional test circuit for PD detection	134
Figure 4.2 Structure of partial discharge test cell	135
Figure 4.3 PD signals in Gemini X recorded at various voltage ramping rates.....	136
Figure 4.4 PD pulses in Gemini X recorded at 26 kV for two minutes	138
Figure 4.5 Maximum PD amplitudes with applied voltage in transformer liquids.....	140
Figure 4.6 PD repetition rates with applied voltage in transformer liquids	142
Figure 4.7 Maximum PD amplitudes with applied voltage in transformer liquids.....	145
Figure 4.8 PD repetition rates with applied voltage for transformer liquids	146
Figure 4.9 Φ -Q-N patterns at applied voltage of 55 kV in transformer liquids.....	146
Figure 4.10 PD equivalent currents with applied voltage in transformer liquids	148
Figure 4.11 PD equivalent powers with applied voltage in transformer liquids	149
Figure 5.1 Schematic view of experimental Setup.....	152
Figure 5.2 Synchronization of measurement methods	155
Figure 5.3 The structure, current and charge recordings of a positive streamer in FR3	156
Figure 5.4 Initiation of a negative streamer in FR3 at 20 kV	157
Figure 5.5 Detachment of a negative streamer from electrode tip in FR3 at 20 kV	157
Figure 5.6 Generation of a positive streamer in Midel 7131 at 24 kV.....	158
Figure 5.7 Detachment of a positive streamer from electrode tip in FR3 at 22 kV	159
Figure 5.8 Streamer repetition rates versus applied voltage in Midel 7131 using two needle electrodes	160
Figure 5.9 Φ -Q-N patterns during 1 minute period recorded by a digital PD detector..	160
Figure 5.10 Structures and associated currents of positive streamers propagation.....	162
Figure 5.11 Structures and associated currents of negative streamers propagation.....	163
Figure 5.12 Structures of negative streamers at breakdown voltage levels.....	164
Figure 5.13 Propagation of a negative streamer in Midel 7131 at 90 kV	165
Figure 5.14 Interpretation of V_{peak} , V_{rms} and $V_{instantaneous}$ for streamers under AC voltage	166
Figure 5.15 Streamer stopping length versus instantaneous voltage in Gemini X at 80 kV	167
Figure 5.16 Maximum stopping lengths for positive streamers in transformer liquids .	168
Figure 5.17 Maximum stopping lengths for negative streamers in transformer liquids	169
Figure 5.18 Propagation velocities of positive streamers in transformer liquids.....	170
Figure 5.19 Propagation velocities of negative streamers in transformer liquids.....	171
Figure 5.20 Φ -Q-N patterns of transformer liquids at 40 kV	172
Figure 5.21 Φ -Q-N patterns of transformer liquids at 70 kV	173
Figure 5.22 Streamer lengths versus instantaneous voltages in FR3	174
Figure 5.23 Streamer inception voltages versus applied voltage in FR3	174
Figure 5.24 Streamer inception voltages versus applied voltage in Gemini X.....	175
Figure 5.25 Space charge disturbance on field distribution near HV point electrode ...	175
Figure 5.26 Streamer sequence versus instantaneous voltage in Midel 7131 at 65 kV .	177
Figure 5.27 Shadowgraph recordings of streamer structures in time sequence.....	178
Figure 5.28 A breakdown induced by a positive streamer in FR3 at 135 kV.....	179
Figure 5.29 A breakdown induced by negative streamer in Midel 7131 at 68 kV	180
Figure 5.30 A re-stroke pre-breakdown in Midel 7131 at 125 kV.....	181
Figure 5.31 A re-stroke breakdown in Midel 7131 at 125 kV.....	182
Figure 5.32 50 % breakdown voltages of transformer liquids versus gap distance.....	183
Figure 5.33 50 % breakdown voltage logarithms versus gap distance logarithms	184

Figure 5.34 50 % breakdown voltages of Midel 7131 versus gap distance	185
Figure 5.35 Probabilities of breakdowns induced by negative streamers in Midel 7131	186
Figure 5.36 50% breakdown voltages versus electrode area in Midel 7131 at various gaps	187
Figure 6.1 Duval triangle graph to diagnosis transformer faults [196]	195
Figure 6.2 Test circuit to generate partial discharge faults	196
Figure 6.3 Structure of partial discharge test container	197
Figure 6.4 PD patterns in Midel 7131 at 24.5 kV	199
Figure 6.5 Total combustible gases concentrations under PD faults of various amplitudes	201
Figure 6.6 H ₂ concentrations under PD faults of various amplitudes.....	202
Figure 6.7 Hydrocarbon gases concentrations under PD faults of various amplitudes ..	202
Figure 6.8 Combustible gases concentrations under PD fault of various durations.....	207
Figure 6.9 Φ -Q-N patterns of transformer liquids under 500 pC PD faults for 15 minutes	208
Figure 6.10 Total combustible gases concentrations with discharge energy	208
Figure 6.11 Percentages of combustible gases produced under PD faults	213
Figure 6.12 Percentages of combustible gases without CO produced under PD faults .	214
Figure 6.13 Percentages of combustible gases without CO in FR3	215
Figure 6.14 Diagnosis of PD faults using Duval triangle method for transformer liquids	216
Figure I.1 Baur DPA75 automatic transformer liquids tester	227
Figure I.2 Breakdown strengths of Gemini X using IEC 60156 and ASTM D1816	229
Figure I.3 Schematic configuration of test container used in AC dielectric strength test	230
Figure I.4 The XB120 scale, 684 Coulometer and 832 Thermoprep of Karl Fischer titration equipment used for water content measurement	230
Figure I.5 HIAC ABS2 bottle sampler and HIAC 8000A liquid particle counter of particle size analyzer.....	232
Figure I.6 Microscopic photo of trapped impurities on filter paper from contaminated transformer oil [224].....	233
Figure I.7 Particle contents of FR3 up to five filtration cycles	235
Figure I.8 The 95% confidence levels of the percentage errors between the measurement value and the actual value of the breakdown voltage	237
Figure I.9 Conditioning and re-conditioning effect of Midel7131 oil.....	238
Figure I.10 Relative humidity of air in a closed container using water-glycerine mixture	239
Figure I.11 Moisture uptake of mineral oil exposed to moisture air at room temperature	239
Figure I.12 PD inception voltages using different needle electrodes	241
Figure I.13 Stopping length of positive streamers in Midel 7131 for two needle electrodes	242
Figure I.14 Stopping length of negative streamers in Midel 7131 for two needle electrode	242
Figure I.15 Stopping length of positive streamers in Midel 7131 for different ground electrodes.....	244

Figure I.16 Stopping length of negative streamers in Midel 7131 for different ground electrodes	244
Figure I.17 Stopping length for positive streamers in Gemini X at different gaps.....	245
Figure I.18 Stopping length for negative streamers in Gemini X at different gaps	245

List of Tables

Table 1.1 Key properties of Nytro Gemini X [13]	24
Table 1.2 Key properties of Midel 7131 [15].....	25
Table 1.3 Key properties of Envirotemp FR3 [16].....	26
Table 1.4 Outline of thesis	31
Table 3.1 AC breakdown voltages of transformer liquids reported by manufacturers	79
Table 3.2 Comparisons of liquid qualities of mineral oil and esters	81
Table 3.3 Summary of S-W test results of normal distributions for transformer liquids .	87
Table 3.4 Summary of K-S test results of various distributions for transformer liquids..	88
Table 3.5 Prediction of withstand voltages using Weibull distribution.....	91
Table 3.6 Prediction results of failure rates and 95% confidence intervals at specified voltages using three distributions	91
Table 3.7 Water and particle contents of transformer liquids before and after tests.....	93
Table 3.8 95% confidence intervals of failure rate for transformer liquids	97
Table 3.9 Contamination levels recommended by CIGRE working group 12.17 [53] ..	100
Table 3.10 Size distributions of cellulose and copper particles in artificially contaminated liquid samples of 100 ml	101
Table 3.11 Curve fitting parameters for particle effect on liquid breakdown voltages ..	106
Table 3.12 Threshold voltages, swing voltages and breakdown voltages of transformer liquids with a steel particle.....	112
Table 3.13 Effective stressed areas of electrodes used in scale effect test	121
Table 3.14 Weibull parameters of transformer liquids using various electrodes.....	123
Table 3.15 Average shape parameters, standard deviations and 90% confidence intervals of transformer liquids.....	123
Table 3.16 Parameters used in area effect equations for transformer liquids	124
Table 4.1 PDIVs of transformer liquids using various discharge detection systems	139
Table 4.2 PDIVs of transformer liquids using IEC 61294 and proposed method.....	141
Table 4.3 PDIVs of transformer liquids using industrial and academic definitions.....	142
Table 6.1 Main fault gases produced by decomposition of mineral oils [129].....	193
Table 6.2 Accuracies of DGA diagnosis methods [204].....	195
Table 6.3 Examples of faults detectable by Duval triangle method [198].....	196
Table 6.4 Dissolved gas contents of controlled samples in ppm unit.....	198
Table 6.5 Applied voltages at controlled discharge amplitude for transformer liquids..	198
Table 6.6 DGA results in ppm under PD faults of various amplitudes	200
Table 6.7 DGA results in ppm under PD faults of 500 pC and various durations	205
Table 6.8 TCG amounts produced by unit energy per Joule.....	209
Table 6.9 Fatty acid compositions in new and in-service FR3.....	209
Table 6.10 90% typical values for mineral oil-filled power transformers [218].....	211
Table I.1 Influence of particles on AC breakdown strengths of transformer liquids	225
Table I.2 Differences between IEC 60156 and ASTM D1816	228
Table I.3 Breakdown strengths of Voltesso using IEC 60156 and ASTM D1816 [220]	229
Table I.4 Saturation levels of water content in mineral oil and esters at ambient temperature of 25° C.....	231
Table I.5 Settings of lower and upper diameter limits for HIAC 8000A particle counter	

.....	233
Table II.1 AC breakdown voltages of transformer liquids in long-term stored conditions	249
.....	249
Table II.2 AC breakdown voltages of transformer liquids in well-processed conditions	249
.....	249
Table II.3 Parameters of AC breakdown strengths of mineral oil and esters	250
Table II.4 500 breakdown voltage tests of transformer liquids to verify withstand voltage	250
.....	250
Table II.5 Parameters of cellulose particle effect on liquid breakdown voltages	251
Table II.6 Parameters of copper particle effect on liquid breakdown voltages	251
Table II.7 Threshold voltages of particle motion in transformer liquids	252
Table II.8 Particle motion (distance from electrode (mm)) in transformer liquids at 20 kV	252
.....	252
Table II.9 Swing voltages of particle motion in transformer liquids	253
Table II.10 Breakdown voltages of particle motion in transformer liquids	253
Table II.11 Parameters of water effect on breakdown voltages of transformer liquids	253
Table II.12 Parameters of water effect for clean and relatively dirty Gemini X	253
Table II.13 Breakdown voltages of transformer liquids for various electrodes	253
Table II.14 PD signals recorded in Gemini X at various ramping rates	257
Table II.15 Maximum PD amplitudes with applied voltage in transformer liquids	258
Table II.16 PDIV test results using IEC 61294 test procedure	258
Table II.17 PD repetition rates with applied voltage in transformer liquids around PDIV	258
.....	258
Table II.18 Maximum PD of transformer liquids at overstressed voltages	258
Table II.19 PD repetition rates of transformer liquids at overstressed voltages	259
Table II.20 PD equivalent currents of transformer liquids at overstressed voltage	259
Table II.21 PD equivalent powers of transformer liquids at overstressed voltage	260
Table II.22 Streamer repetition rates of streamers in Midel 7131 under various needle electrodes	260
Table II.23 Streamer stopping lengths in Gemini X with instantaneous voltage at 80 kV	260
.....	260
Table II.24 Propagation of positive streamers in transformer liquids	261
Table II.25 Propagation of negative streamers in transformer liquids	262
Table II.26 Breakdown voltages of transformer liquids with gap distance	262
Table II.27 Breakdown voltages with various needle electrodes in Midel 7131	263
Table II.28 Probabilities of breakdowns induced by negative streamers in Midel 7131	264
Table II.29 Breakdown voltages of Midel 7131 with ground electrodes	265
Table II.30 Comparison of breakdown strengths of Gemini X using IEC 60156 and ASTM D1816	266
Table II.31 Particle contents of stored FR3 oil after each filtration cycle	266
Table II.32 Preparation of electrodes and conditioning effect for Midel 7131 oil	266

Abstract

Mineral oil has been widely used in liquid insulation of power transformers. However, it is poorly biodegradable and could cause serious contamination to the environment if a spill occurs. With increasingly strict environmental rules and regulations, there is considerable interest from the Utilities to apply esters in power transformers as substitutions to mineral oil. In order to use esters in large power transformers, their dielectric properties should be thoroughly investigated. This PhD thesis covers the experimental studies on the dielectric properties of a type of synthetic ester (Midel 7131) and a type of natural ester (FR3) in both uniform and divergent electric fields, using a mineral oil (Gemini X) as the benchmark.

The dielectric properties of transformer liquids in uniform fields were investigated using breakdown voltage tests. The breakdown voltages of esters should be at least similar to that of mineral oil to allow a replacement in transformers. To obtain a fair comparison, the AC breakdown voltages of well-processed transformer liquids were tested, and their distributions were statistically analyzed. Since the breakdowns of transformer liquids in uniform fields are caused by the weakest-links, conditions representative of in-service transformer liquids were also considered by testing the effects of extraneous factors, such as particles, water and electrode area.

The divergent fields were produced by sharp needle electrodes with tip curvatures of a few micrometers. The dielectric properties of transformer liquids in such fields were studied using several methods. A traditional PD detector was used to study the partial discharge characteristics of insulating liquids, such as the inception voltages and the repetition rates. A high speed camera was utilized to identify the streamer generation, propagation and breakdown phenomena. An oscilloscope was used to investigate the current signals associated with these phenomena. The breakdown voltages of transformer liquids were also determined in the divergent field at various gaps. Furthermore, the fault gases in transformer liquids under partial discharge faults were determined and analyzed.

The following findings and conclusions can be made from the research in this thesis:

- | The AC dielectric strengths of esters in uniform fields are similar to that of mineral oil when they are in a well-processed condition. When practical liquid conditions are considered, the AC dielectric strengths of esters are higher than that of mineral oil.
- | The partial discharge behaviours at overstressed voltages can be used to differentiate various transformer liquids. Esters are relatively inferior to mineral oil in terms of higher discharge amplitude, higher discharge repetition rate and more negative partial discharges.
- | Mineral oil possesses a higher ability to suppress the propagation of negative streamers. Thus, the AC dielectric strength of mineral oil in the divergent field is relatively higher than those of esters.
- | Esters generate the same types of fault gases due to electrical discharge as mineral oil, but in relatively larger amounts.

Declaration

I declare that no part of the work referred to in the thesis has been submitted in support of an application for another degree or qualification of this or any other university or other institutes of learning.

Copyright Statement

- I. The author of this thesis (including any appendices and/or schedules to this thesis) owns certain copyright or related rights in it (the “Copyright”) and he has given The University of Manchester certain rights to use such Copyright, including for administrative purposes.
- II. Copies of this thesis, either in full or in extracts and whether in hard or electronic copy, may be made only in accordance with the Copyright, Designs and Patents Act 1988 (as amended) and regulations issued under it or, where appropriate, in accordance with licensing agreements which the University has from time to time. This page must form part of any such copies made.
- III. The ownership of certain Copyright, patents, designs, trade marks and other intellectual property (the “Intellectual Property”) and any reproductions of copyright works in the thesis, for example graphs and tables (“Reproductions”), which may be described in this thesis, may not be owned by the author and may be owned by third parties. Such Intellectual Property and Reproductions cannot and must not be made available for use without the prior written permission of the owner(s) of the relevant Intellectual Property and/or Reproductions.
- IV. Further information on the conditions under which disclosure, publication and commercialisation of this thesis, the Copyright and any Intellectual Property and/or Reproductions described in it may take place is available in the University IP Policy (see <http://documents.manchester.ac.uk/DocuInfo.aspx?DocID=487>), in any relevant Thesis restriction declarations deposited in the University Library, The University Library’s regulations (see <http://www.manchester.ac.uk/library/aboutus/regulations>) and in The University’s policy on Presentation of Theses

Acknowledgement

Firstly I would like to express my gratitude to my supervisor Professor Zhondong Wang for her support and guidance during my PhD research study at the University of Manchester. Her hard work has ensured my PhD research project's success.

I am also truly grateful to the financial sponsorship from the Engineering and Physical Sciences Research Council (EPSRC) - Dorothy Hodgkin Postgraduate Award (DHPA), Alstom Grid, M&I Materials, National Grid, Scottish Power, and UK Power Networks, which covers my tuition fees and living maintenance.

I would like to thank the technical support from industrial partners of the research project on 'Application of Alternative Oils in Large Transformer Research – Phase 2'. In particular, Fabrice Perrot, Alan Darwin, and Christophe Perrier of Alstomn Grid, Russell Martin and Mark Lashbrook of M&I Materials, Paul Jarman and Gordon Wilson of National Grid, Dave Walker of Scottish Power, Sue Northcote and John Noakhes of TJH2b, and Paul Dyer of UK Power Networks. I would also like to thank Cooper Power System for providing natural ester over the years, and EPSRC Instrument Pool for providing some of the measurement instruments used in this research.

Thanks also to everyone in the research team of our transformer group, including Dr. Hongzhi Ding who helped me a lot at the start of my PhD study, and Mr. Keith Cornick who gave me some wise suggestions about some of my experimental designs.

Last but not least, I would like to take this opportunity to thank my parents and my wife for their selfless love and support. Their support has encouraged me to go through all the hard work all the time.

Terminologies

The following definitions are provided to assist the reader to understand the referred terminologies which appear in this PhD thesis. They are listed in sequence according to their first appearance in this thesis. Their first appearance in the thesis is shown in bold, and the corresponding page numbers are provided in the list.

Ester (page 22)	Esters are chemical compounds derived from an inorganic acid or organic acid in which at least one -OH (hydroxyl) group is replaced by an -O-alkyl (alkoxy) group, and most commonly from carboxylic acids and alcohols
Paraffin (page 23)	Paraffin is a class of saturated hydrocarbons with the general formula of C_nH_{2n+2} . It can be used synonymously with the term "alkane".
Naphthene (page 23)	Naphthene is a class of saturated hydrocarbons which have one or more rings of carbon atoms in their chemical structures.
Partial discharge (page 23)	Partial discharge (PD) is a localised dielectric breakdown of a small portion of a solid or fluid electrical insulation system under high voltage stress, which does not bridge the space between two conductors
Aromatic (page 23)	Aromatic is a class of organic hydrocarbon compounds which have one or more unsaturated rings of carbon atoms characterized by alternating double and single bonds between carbon atoms.
Pentaerythritol (page 25)	Pentaerythritol is a type of white, crystalline polyol with the formula of $C_5H_{12}O_4$. It is often used to manufacture synthetic esters.
Triglyceride (page 26)	Triglyceride is an ester derived from glycerol and three fatty acids. It is the main constituent of vegetable oil and animal fats.
Electron affinity (page 28)	Electron affinity of a molecule or atom is the energy change when an electron is added to the neutral molecule or atom to form a negative ion.
Streamer (page 28)	A streamer is a hot, highly conductive channel of plasma that plays a critical part during dielectric breakdown in liquid dielectrics.
Area effect (page 56)	The 'area effect' is similar to 'volume effect', referring to the decrease of the breakdown strength of a dielectric medium with the increase of

	the stressed electrode area.
Streamer channel (page 55)	The gaseous channel inside which the streamer exists. (The detailed description of 'streamer' and 'streamer channel' are given in page 61)
Volume effect (page 57)	The 'volume effect' refers to a well-known phenomenon that for a dielectric medium, the breakdown strength decreases statistically with the increase of stressed liquid volume.
Shadowgraph (page 153)	Shadowgraph is an optical method that reveals non-uniformities in transparent media by casting a shadow on a screen.
Linoleic (page 209)	Linoleic acid is an unsaturated carboxylic acid with an 18-carbon chain and two cis-double bonds.
Linolenic (page 209)	Linolenic acid is an unsaturated carboxylic acid with an 18-carbon chain and three cis-double bonds.
Radical (page 210)	Radicals are atoms, molecules, or ions with unpaired electrons on an open shell configuration. Free radicals may have positive, negative, or zero charge.
Triplet oxygen (page 210)	Triplet oxygen is the ground state of the oxygen molecule. The electron configuration of the molecule has two unpaired electrons occupying two degenerate molecular orbitals.
Singlet oxygen (page 210)	Singlet oxygen is the common name used for the diamagnetic form of molecular oxygen, which is less stable than the normal triplet oxygen.
Hydroperoxides (page 210)	Hydroperoxides are organic compounds containing the hydroperoxide functional group (R-OOH), where R is a hydrocarbon chain.
Alkoxy (page 210)	Alkoxy group is an alkyl (hydrocarbon chain) group singularly bonded to oxygen, in the form of R-O-R', where R and R' are hydrocarbon chains.
β -scission (page 210)	Beta scission is an important reaction in the chemistry of thermal cracking of hydrocarbons and the formation of free radicals. Free radicals are formed by splitting the carbon-carbon bond. Free radicals are extremely reactive and short-lived.



Chapter 1. Introduction

1.1 Background

Transformers are one of the most expensive and critical components in electrical power systems. A transformer failure would cause a number of losses to the electrical industry, including the economic losses during the interruption of power supply, the capital cost to purchase and install new transformers, the penalty payment to government regulators due to environmental contaminations, or even compensation for fatalities and injuries [1]. Thus, it is essential to ensure the safe operation of power transformers during their working lives.

Transformer post-failure analysis shows that insulation failures are the leading cause of transformer failures [1]. Oil and paper has been the choice of insulation for power transformers over the past century. Transformer oil impregnates the voids in paper insulation and fills the gaps between components in the transformer tank to increase the dielectric strength of the insulation. It not only functions as insulating liquid, but also transfers heat which is generated from losses of transformer windings and cores. Furthermore, oil also acts as the information carrier for monitoring the condition of a power transformer.

Mineral oil has a number of the desirable electrical and thermal-physical properties for transformers. With low cost and wide availability, it has been used in oil-filled transformers of all voltage ratings from the beginning of the transformer industry. However, it is poorly biodegradable and can cause serious contamination to the environment if a spill occurs. With increasingly strict environmental rules and regulations, the transformer industry is paying more attention to the environmental aspect of a transformer along with sufficient technical performances. Increasingly depleted resources, which could lead to a serious shortage of mineral oil in the forthcoming decades, also raise the desire of the power industry to look for alternatives to mineral oil. As a result, the use of new insulating fluids with high biodegradability is becoming extremely attractive [2].

Among all the environmentally friendly substitutions to mineral oil, **esters** are probably the most widely used insulating fluids up to now. Generally speaking, two types of esters are available on the market, one being natural ester based on ‘renewably sourced’ vegetable oils, and the other being synthetic ester which is manufactured from petroleum products. Although some poor features of esters limit their usage, e.g. low oxidation stability for natural esters, they have been used worldwide for many years in from small to medium distribution transformers up to 66 kV [3]. The most attractive feature of esters is that they are highly biodegradable and non-toxic, which put no risk to the surrounding environment of ester-filled transformers in case of a spill. Two other fundamental advantages which also motivate the growing interest in esters are their high fire safety and high moisture absorption ability. Indeed, the flash and fire points of esters are usually above 300 °C [4], ensuring more operation safety for in-service transformers than mineral oil. The high moisture saturation levels of esters result in the absorption of water from the cellulose materials, thus protecting the insulation paper from ageing and deterioration.

The technical challenge we are facing in recent years is to extend the usage of esters from distribution transformers to high voltage power transformers. The power industry has already tried to apply esters in large power transformers, e.g. a 132 kV/90 MVA transformer filled with FR3 was manufactured by ALSTOM Grid (previously AREVA T&D) and put into service by UK Power Networks (previously EDF Energy) in 2009 [5], a 238 kV/ 135MVA transformer filled with Midel 7131 is being operated in Sweden [6]. In the USA, some transformers up to 230 kV and 200 MVA have been retro-filled with esters in order to extend their working lives [7]. Since the physical and chemical properties of esters are different from those of mineral oil, both the design and manufacturing process of power transformers might be affected, supposing there is a substitution of mineral oil by esters. Thus, a complete understanding of the dielectric properties of esters and their impact on transformer design and operation is required.

Previous studies provided an extensive knowledge of the differences between the properties of esters and mineral oil [3, 8-10]. However, limited data is available on the properties of the pre-breakdown and breakdown phenomena in esters, and the breakdown mechanism of

esters is still open to question. When we consider the structural arrangement inside a transformer, the conductors and earthed components creates a very complex situation in terms of electric field distribution. It is therefore essential to study the breakdown mechanisms of esters in various electric fields. A good understanding of the dielectric properties of esters is of critical importance in the application of esters in large power transformers.

Since the chemical compositions and molecular structures of esters are different from those of mineral oil, there are also uncertainties associated with the application of standard diagnostic techniques to monitor the condition of a transformer. **Partial discharge** detection and dissolved gas analysis are two of the most important and currently available diagnostic techniques. With the conventional liquid, mineral oil, replaced by esters, it is essential to investigate the differences between the partial discharge behaviours of esters and mineral oil, and to determine whether the DGA technique used for mineral oil is still applicable to esters.

1.2 Insulating Liquids Used in Thesis

This PhD thesis reports an investigation into the suitability of esters to replace conventional mineral oil in large power transformers. Three types of insulating liquids investigated in this work are:

- | Nytro Gemini X as mineral oil
- | Midel 7131 as synthetic ester
- | Envirotemp FR3 as natural ester

1.2.1 Mineral Oil - Nytro Gemini X

Nytro Gemini X is a type of inhibited insulating oil (with anti-oxidation additives), produced by the Nynas Oil Company, to replace previously used uninhibited Nytro 10GBN. It mainly consists of saturated hydrocarbon molecules, such as **paraffins**, **naphthenes** and **aromatics**, as shown in Figure 1.1. Due to the saturated molecular structures, Gemini X is chemically stable and has a high anti-oxidation ability. Its dielectric strength is high, above 70 kV/ 2.5 mm (measured by IEC60156 using a 2.5 mm gap distance) when the liquid is treated, but

reduced significantly when the liquid is contaminated by water and particles [11]. The Gemini X has shortcomings mainly with fire hazards and environmental unfriendliness. The low flash point and the slow biodegradability of Gemini X have become a major issue for their application in power transformers due to increasingly strict environmental legislations. The water saturation level of Gemini X is 55 **Parts per Million** (ppm) at ambient temperature. Table 1.1 lists the key properties of Nytro Gemini X.

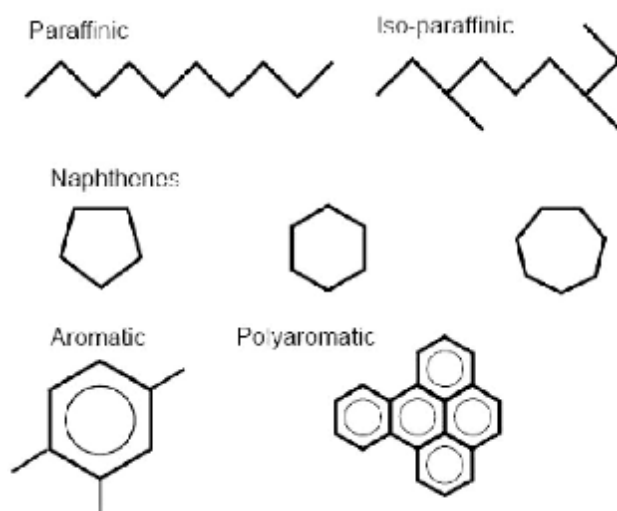


Figure 1.1 Basic hydrocarbon structures of mineral oil [12]

Table 1.1 Key properties of Nytro Gemini X [13]

	Unit	Test method	Typical data
1. Physical			
Density, 20°C	kg/dm ³	ISO 12185	0.882
Viscosity, 40°C	mm ² /s	ISO 3104	8.7
Flash point	°C	ISO 2719	144
Pour point	°C	ISO 3016	-60
Interfacial tension	mN/m	ISO 6295	50
2. Chemical			
Acidity	mg KOH/g	IEC 61125	0.08
Aromatic content (only applicable for mineral oil)	%	IEC 60590	10
Water content	mg/kg (ppm)	IEC 60814	<20
3. Electrical			
Dissipation Factor, 90°C	-	IEC 60247	<0.001
Breakdown Voltage	kV	IEC 60156	
-before treatment			40-60
-after treatment			>70

1.2.2 Synthetic Ester - Midel 7131

Midel 7131 is a type of synthetic ester manufactured by M&I Materials in Manchester, UK. It is derived from **pentaerythritol**, with four fatty acid chains as shown in Figure 1.2. Due to the ester components in the molecular structure, Midel 7131 is highly biodegradable and environmentally friendly. The dielectric strength of Midel 7131 is comparable to that of Gemini X, above 75 kV/ 2.5 mm. Due to its excellent electrical and environmental properties, Midel 7131 is widely used in distribution transformers around Europe [6]. Furthermore, the water saturation level of Midel 7131 is much higher than that of Gemini X, around 2600 ppm at ambient temperature. This feature favours the absorption of water from cellulose materials, and thus protects the insulation paper or the pressboard from deterioration. Table 1.2 lists the key properties of Midel 7131.

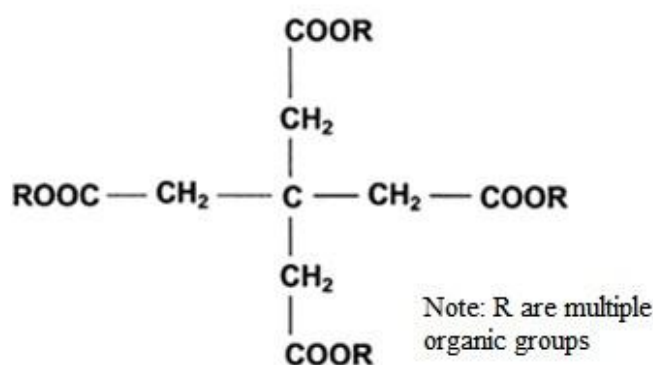


Figure 1.2 Molecular structure of Midel 7131 [14]

Table 1.2 Key properties of Midel 7131 [15]

	Unit	Test method	Typical data
1. Physical			
Density, 20°C	kg/dm ³	ISO 3675	0.97
Viscosity, 40°C	mm ² /s	ASTM D445	28
Flash point	°C	ISO 2719	260
Pour point	°C	ISO 3016	-60
Interfacial tension	mN/m	ASTM D971	26
2. Chemical			
Acidity	mg KOH/g	IEC 62021	<0.03
Water content	mg/kg	IEC 60814	50
3. Electrical			
Dissipation Factor, 90°C	-	IEC 60247	<0.03
Breakdown Voltage	kV	IEC 60156	>75

1.2.3 Natural Ester - Envirotemp FR3

Envirotemp FR3 is a type of natural ester manufactured by Cooper Power Systems in the USA from edible vegetable oils. As shown in Figure 1.3, the molecular structure of this liquid is based on **triglycerides**, containing carbon double bonds or even carbon triple bonds. Therefore, FR3 is highly biodegradable and unstable to oxidation. This liquid possesses a high dielectric strength, above 56 kV/ 2mm (measured by ASTM D1816 using a 2 mm gap distance). Currently, this liquid is mainly used in power equipments in North and South America, up to 242 kV and 200 MVA [7]. The water saturation level of FR3 is higher than that of Gemini X, around 1100 ppm at ambient temperature. Table 1.3 lists the key properties of FR3.

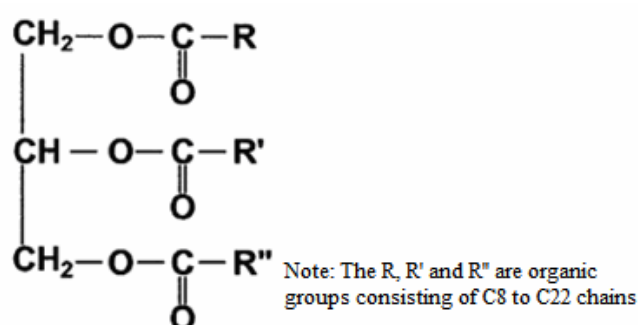


Figure 1.3 Molecular structure of Envirotemp FR3 [14]

Table 1.3 Key properties of Envirotemp FR3 [16]

	Unit	Test method	Typical data
1. Physical			
Density, 20 °C	kg/dm ³	ASTM D1298	0.92
Viscosity, 40 °C	mm ² /s	ASTM D445	32
Flash point	°C	ASTM D92	330
Pour point	°C	ASTM D97	-20
Interfacial tension, 25 °C	mN/m	ASTM D971	24
2. Chemical			
Acidity	mg KOH/g	ASTM D974	0.02
Water content	mg/kg	ASTM D1533	30
3. Electrical			
Dissipation Factor, 100°C	-	ASTM D924	0.03
Breakdown Voltage	kV	ASTM D1816	56 (2mm)

1.3 Research Objectives

The investigations reported in this PhD thesis is aimed at answering a number of questions related to the breakdown mechanisms of various insulating liquids used in power transformers under both uniform and divergent AC fields, and investigating the differences between the partial discharge behaviours of esters and mineral oil. From these investigations, it is hoped to contribute to the research on the suitability of esters to replace mineral oil in power transformers, and to assist the transformer manufacturers to choose between mineral oil and esters. The objectives of this PhD thesis are summarized below for PD characteristics and breakdown mechanism of ester transformer liquids in both uniform and divergent field.

1 Breakdown Mechanisms of Transformer Liquids in AC Uniform Fields

The usage of conventional mineral oil in power transformers has been well-established by transformer manufacturers based on years of experience. The main conclusion reached so far is that the impurities (particle, moisture and gas) are the key parameters initiating an electrical breakdown rather than the liquid itself. On the other hand, esters have different intrinsic properties (i.e. more polar molecular structures) and physical properties (i.e. higher viscosities) from mineral oil, which might affect the moisture affinity, and particle movement in esters. These influences should be taken into consideration when studying the breakdown mechanisms of esters. Experiments are carried out in this part to obtain an understanding of the breakdown mechanisms of esters in AC uniform fields.

1 Partial Discharge (PD) Measurement and PD Performance of Transformer Liquids

Partial discharge is one of the main contributor to the insulation failure in power transformers. To evaluate the partial discharge properties of insulating liquids, the **Partial Discharge Inception Voltage** (PDIV) is commonly used, and it is usually measured following IEC 61294 test procedure. With the replacement of mineral oil by esters, this procedure might not be applicable to esters due to their different chemical compositions from those of mineral oil. It is also of concern that the PDIV might not be a good parameter to differentiate various transformer liquids. Therefore, new parameters, such as the PD performances at

over-stressed voltage, are proposed to differentiate various transformer liquids. The over-stressed voltage refers to the applied voltage higher than the PDIV. In this part, the experiments on the PD performances of esters at both the inception voltage and the over-stressed voltage were carried out in laboratory, using mineral oil as a bench mark.

1 Breakdown Mechanisms of Transformer Liquids in AC Divergent Fields

The breakdown mechanism of mineral oil has been well studied in divergent AC fields by other researchers. With the help of a high speed camera, identifying the pre-breakdown phenomena has become one of the most important methods in evaluating the dielectric performances of transformer liquids. The pre-breakdown phenomena are characterized by the **streamers**, which can develop themselves into full-path propagations and lead to breakdowns. However, the streamers will not necessarily lead to breakdowns, and they might extinguish during the propagation process. Due to the differences between their intrinsic properties (e.g. **electron affinities**), changing the insulating liquids in power transformers from mineral oil to esters might affect the threshold voltage for the streamers to propagate, thus affecting their breakdown strengths. In this part, experiments on the streamer properties of mineral oil and esters were carried out in divergent AC fields to evaluate the differences between their breakdown mechanisms.

1 DGA Diagnosis Technique for PD Phenomena

Dissolved Gas Analyses (DGA) techniques have been well-accepted as a diagnosis tool to detect the incipient faults of a power transformer. Various methods were developed to interpret the DGA results, in which the key gas method and the Duval Triangle method were proved to be among the most reliable ones. However, limited data is available now for the application of the DGA technique to esters. In this part, PD activity is generated in laboratory condition and associated fault gases are analysed in esters, using mineral oil as a benchmark. Furthermore, the interpretation methods are examined for esters.

1.4 Outline of Thesis

The outline of this thesis is summarized and listed in Table 1.4. The breakdown study of the

transformer liquids is carried out in uniform fields or in divergent fields separately, due to the fact that the breakdown process in uniform fields is dominated by extraneous factors, while the breakdown process in divergent fields is determined by the intrinsic properties of the liquid. A detailed introduction of the contents for each chapter is presented as follows.

Chapter 1 Introduction

This chapter briefly introduces the research background of this thesis, the research objectives and the thesis outline.

Chapter 2 Literature Review of Breakdown Mechanism of Mineral Oil

This chapter provides a general literature review of the breakdown mechanism of mineral oil used in power transformers under AC voltage, in both uniform fields and divergent field. This review will assist the study of the breakdown processes in esters.

Chapter 3 Electrical Breakdown in AC Uniform Fields

The influence of several extraneous factors on the breakdown strengths of esters are studied and compared to mineral oil in this chapter.

With mineral oil as a benchmark, the breakdown voltages of esters are firstly measured. Since the breakdown voltage of a transformer liquid is a statistically distributed parameter, the breakdown voltage distributions of investigated transformer liquids are modelled. Then, Weibull function is used to extrapolate the withstand voltages of transformer liquids.

Information about the breakdown process suggests that extraneous factors play important roles in the liquid breakdowns in uniform fields. Thus, the experiments in this chapter study the influence of some extraneous factors, i.e. moisture, particles, and electrode area, on the breakdown strengths of mineral oil and esters.

Chapter 4 PD Measurement and PD Performances of Transformer Liquids

After the evaluation of the traditional PDIV measurement method, the PD performances of esters are determined in divergent AC fields at both the inception and over-stressed voltages.

Firstly, the effectiveness of IEC 61294 for the measurement of PDIVs of transformer liquids

is discussed. Improved procedures are proposed for a reasonable measurement of PDIVs in both mineral oil and esters. Then, the PDIVs of investigated transformer liquids are measured following the proposed method. Their PD performances at over-stressed voltage are also determined. As a preliminary study to the research reported in Chapter 5, this chapter studies the PD phenomena in transformer liquids using the electrical measurement method, and proposes a suitable test procedure for esters.

Chapter 5 Electrical Breakdown in AC Divergent Fields

Using a similar arrangement to that in the previous chapter, this chapter investigates the differences between the pre-breakdown and breakdown phenomena in mineral oil and esters using optical measurement, current measurement and charge measurement methods.

The ‘partial discharges’ are also referred to as ‘streamers’ in laboratory research. The pre-breakdown and breakdown phenomena of transformer liquids are characterized by streamers in divergent fields. With the help of a high speed camera, the streamer properties in both mineral oil and esters are investigated, of which the development is classified into generation stage, propagation stage, and final breakdown stage. It is found that the local electric field determines the streamer initiation, while the overall electric field determines the streamer propagation and breakdown. Furthermore, the space charge is also an important factor which affects the streamer properties, especially in esters under AC voltage.

Chapter 6 DGA Diagnosis Technique under PD Faults

This chapter correlates the amount of fault gases with PD faults in both mineral oil and esters. Based on the literature from the food industry, the generation of large amount of ethane in natural esters is explained. The key gas method and the Duval triangle method are also examined in terms of their application to the test results. Suggestions are made for a better recognition of the PD faults in esters.

Chapter 7 Conclusions and Future Work

This chapter summarizes the main conclusions in this PhD thesis and suggests further work to continue the study on breakdown mechanisms of esters under AC voltage.

Table 1.4 Outline of thesis

Chapter 1: Introduction												
Chapter 2: literature review	Breakdown theories		Ionization theory	Weakest-link theory	Streamer theory							
	Breakdown in uniform field		Moisture	Particle	Gas	Electrode						
	Breakdown in divergent field		Under impulse voltage		Under AC voltage							
	Connection		Volume effect		Area effect							
Study in uniform field	Chapter 3: Breakdown mechanism	AC dielectric strength		Breakdown voltage								
				Breakdown voltage distribution								
				Extrapolation to withstand voltage								
		Particle effect										
		Water effect										
		Scale effect (electrode area effect)										
		Case study										
Study in divergent field	Chapter 4: PD performances	Introduction to IEC61294		Chapter 5: Breakdown mechanism								
		Improvements to IEC61294										
		Measurement of PDIV										
		PD performances at overstressed voltages										
	Chapter 6: DGA technique	PD fault of controlled amplitude					Streamer observation methods		General features			
		PD fault of controlled energy							Inception voltages			
		Production of Ethane in natural ester							Streamer propagation		General features	
											Stopping length	
	Interpretation methods		Streamer lead to breakdown				Average velocity					
							Space charge effect					
		General features										
				Breakdown strength								
				Influence of electrodes								
Chapter 7: Summary and future work												

Chapter 2. Literature Review of Breakdown Mechanism of Mineral Oil

2.1 Introduction

In this chapter, the breakdown theories in insulating liquids will be reviewed first, followed by a discussion of breakdown processes in both uniform fields and divergent fields. By choosing the most significant experimental results from extensive literature, it is hoped to present an overall background and research achievement of breakdown mechanisms in transformer liquids over the past 100 years.

It should be kept in mind that most of the previous investigations made use of mineral oil or saturated hydrocarbon liquids. With the successful usage of esters in distribution transformers in recent years, much research effort was devoted to preparing for the application of esters in power apparatus at higher voltage ratings. It is therefore of great importance to understand the dielectric characteristics of esters, especially at large oil gaps and high voltage ratings. Nevertheless, a thorough review of breakdown mechanisms in mineral oil is still of great necessity, to provide both the experimental methods and the inspiring thoughts to the study of breakdown mechanisms in esters.

2.2 Breakdown Theories

The breakdown of insulating liquids is not simple to explain and the mechanism responsible for the initiation of breakdown is still open to controversy. Many breakdown theories have been put forward since the start of research on this subject, which can be generally divided into three categories.

- Ionization theory believes that electrons can be accelerated to ionization energy at high voltage, and the accumulative ionization-collision process will lead to the final

breakdown.

- | Weakest-link theory, which postulates that the breakdown in liquid dielectrics starts with a local instability caused by the presence of either the inhomogeneities in the bulk liquid or irregularities on the electrode surface.
- | Streamer theory, which regards that the breakdown in insulating liquids is composed of the initiation and propagation of a gaseous channel, called streamer. Breakdown occurs when this channel bridges both electrodes.

2.2.1 Ionization Theory

The ionization theory used to be a popular theory to explain the breakdowns in insulating liquids before 1940s. However, Felici pointed out that the collision ionization can not exist in insulating liquids at an electric field of several MV/cm [17]. One reason is that the collisions of electrons in insulating liquids are mainly inelastic and the electrons can not gather enough momentum for collision-ionization. The other reason is that free electrons are conspicuously rare in insulating liquids since most electrons are attached to liquid molecules in the form of negative ions. Thus, the number of free electrons is far less than that to trigger a breakdown.

2.2.2 Weakest-link Theory

Between 1940 and 1980, researchers gradually realized that it was impossible to attribute all the observed breakdown phenomena to a single hypothesis or factor. The weakest-link theory was then put forward to interpret the dependence of liquid dielectric strength on a large number of factors, most of which are extraneous to the natural properties of liquid. According to this theory, the liquid breakdown was initiated by the weakest-links either exists in the bulk liquid or on the surface of the electrode. Due to the uncertainty of these weakest-links, the breakdowns of insulating liquids might be influenced by the impurities, the chemical additives, the dissolved water, the nature and amount of dissolved gases, the geometry/ material/ surface condition/ gap distance of the electrodes, the temperature and hydrostatic pressure, the waveshape of applied voltage and so on [18]. These factors

interact with each other and the overall effect can be expressed by the breakdown voltage. Therefore, a breakdown theory, applicable for one set of experimental conditions, might not necessarily be applicable if the test condition changes.

Once this had been realized, researchers were able to assess the extent to which each of these factors affects the breakdown process, by carefully controlling the test condition with the change of only one variable. At this stage, the investigations were usually carried out in uniform electric fields, since the breakdown voltage of an insulating liquid in uniform fields is more sensitive to the extraneous factors than to the intrinsic properties of the insulating liquid [19].

2.2.3 Streamer Theory

With the development of high speed imaging techniques, the streamer theory was put forward to explain the breakdown processes in insulating liquids. This theory was first developed in the early 1970s to explain the dependence of the breakdown strengths of insulating liquids on the applied pressure and the generation of gas bubbles from highly stressed liquids [20]. The early form of this theory was also called ‘bubble theory’, which came from the gas bubble observation before a breakdown occurs. A detailed study of the influence of thermal bubbles was summarized by Hayakawa [21].

After the 1980s, the microscopic technique was used together with the high speed imaging technique in the investigations. This enabled researchers to investigate detailed breakdown processes in insulating liquids. In divergent field produced by needle-plane electrode configuration, a small gas or vapour bubble with radius of about 50 μm was observed near the tip of the needle electrode several μs before a breakdown occurs [22, 23]. The streamer theory considers the gas or vapour bubble as a general environment, inside which the breakdown mechanism is similar to that in air. Through cumulative collision-ionization processes, the gas bubble is elongated and the breakdown of insulating liquids is actually the breakdown of this elongated gas channel [19].

The streamer theory has become more dominant in recent years. It is widely accepted that

the breakdown processes in insulating liquids are composed of streamer initiation, streamer propagation and final breakdown. Many researches have demonstrated the differences between the breakdown mechanisms in uniform and divergent electric fields [24, 25]. In uniform or quasi-uniform fields, the dielectric strengths of transformer liquids measured in laboratory conditions and encountered in industrial applications are in the range of 0.1 MV/cm to 1 MV/cm [19]. Electric field in this range is high enough to allow the propagation of a streamer until the final breakdown. Therefore, the breakdown process in uniform fields is dominated by the streamer initiation, where the ‘weakest-link theory’ can be applied. On the other hand, in divergent fields, the streamers are produced easily by enhanced local fields. However, their propagation is limited by the low average field. When the applied voltage is high enough, the streamers can propagate until reaching the opposite electrode and leading to the final breakdown. Therefore, the breakdown process in divergent fields is dominated by the streamer propagation [26].

Due to high resolution of the microscopic recording, only limited areas can be observed during the experiment. Therefore, most of the research uses a strongly divergent field and it proved that the oil conditions have limited influence on the overall breakdown strength under divergent field.

2.2.4 Summary

In recent publications, the weakest-link theory and the streamer theory are both commonly used to interpret the breakdown process of transformer liquids. Either in uniform or in divergent field, there are two pre-requisite conditions to trigger the breakdowns.

- ı A necessary instability (intrinsic or extrinsic) to produce an initial streamer.
- ı A sufficient field to enable the streamer propagating through the liquid.

2.3 Breakdown of Mineral Oil in Uniform Fields

2.3.1 Conditioning Effect

The conditioning effect was observed both under AC and impulse voltage in uniform field. Hancox found that the first few breakdowns in mineral oil using new electrodes usually yielded low breakdown strengths [27]. It was increased noticeably during the next few breakdowns and gradually stabilized after the first few breakdowns acting as conditioning, as shown in Figure 2.1 [28].

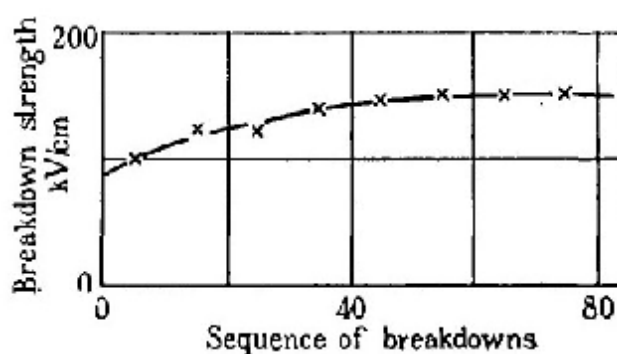


Figure 2.1 Conditioning effect of successive breakdowns in mineral oil [28]

Watson attributed the conditioning effect to the removal of small fibres by successive breakdowns, which might reduce the possibility of breakdown initiation and thus increase the breakdown voltage [28]. In [29], the breakdown test using circulated oil also showed the conditioning effect. This indicated the conditioning effect should be related to the electrodes rather than the insulating liquid. [28, 30] found that the conditioning effect was significantly reduced when the mineral oil was degassed under vacuum conditions or when the electrode surface was carefully polished before the breakdown tests. Therefore, the conditioning effect might be attributed to the micro-gas bubbles or irregularities on the electrode surface.

If there was a long interval before carrying out another breakdown test, the breakdown strength of the oil would drop to approximately the same value as for the first few breakdown [27]. This indicates that the conditioning effect can be reversed, probably due to the reattachment of gases bubbles on the electrode surface.

2.3.2 Influence of Water

2.3.2.1 Introduction

The water in transformers mainly originates from three sources: residual water, ingressing from the atmosphere and aging products [31]. During the transformer manufacturing, the paper insulated windings are subjected to extensive drying process and a well-dried transformer should have a moisture content of less than 0.5 % by weight in paper [32]. Less dried paper insulation might have a high residual water content, which will gradually migrate into the transformer oil during service. Moisture might also ingress into transformers from the atmosphere by poor working practices or through poorly maintained seals. Furthermore, a large amount of water is produced by thermal aging of cellulose materials. The water will further accelerate the cellulose aging and produce more water.

The solubilities of water in transformer liquids depend on their molecular structures and ambient temperature. For new liquids, the water saturation level W (in ppm) can be expressed by Equation 2.1, where T is the temperature in °C, A and K are coefficients dependent on the liquids [33]. However, the saturation level for aged oil might be increased due to the aging by-products with polar structures, such as the carboxyl hydrocarbons. When a liquid is exposed to the atmosphere, the amount of water absorbed from the ambience is directly proportional to the relative humidity in air, as shown in Figure 2.2 [33]. The relative humidity in air is equal to the final **relative water content** in liquid. The relative water content is defined as the ratio of water absorbed by oil to the maximum water that the oil can contain at that temperature [34].

$$\log W = A + \frac{K}{T} \qquad \text{Equation 2.1}$$

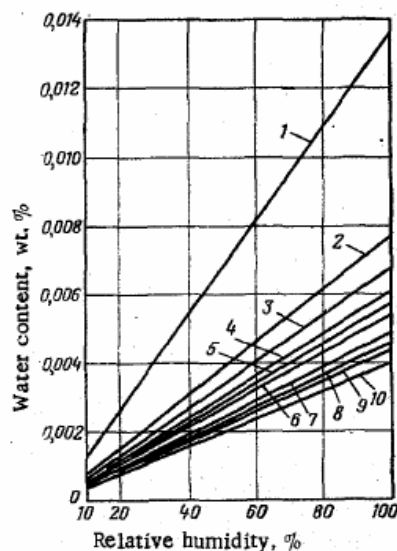


Figure 2.2 Water absorptions from air for 10 types of mineral oil at 20°C [33]
 (1) ABT, (2) Gorai00-Iraq, (3) TKp, (4) T-750, (5) TSp, (6) Detroit Edison-USA, (7) TSp-hydrotreated, (8) Esso Univolt 84-France, (9) T-1500 and (10) ShellDiala Dx-England

2.3.2.2 States of Water in Oil

Water may exist in transformer liquids in three states: **associated water**, **dissociated water** and water drops. The associated water refers to a small number of dissolved water molecules tightly linked to the polar/charged groups of the liquid molecules by hydrogen bonds [35]. The dissociated water refers to most of the dissolved water molecules either as ‘monomer’ or ‘clusters’. The ‘monomer’ is a free water molecule suspended in liquid, and ‘cluster’ is several free water molecules accumulated together [36]. The water drops appear when water in liquids exceeds the saturation levels. They might either suspend in the liquid or deposit at the tank bottom depending on the drop size. Recent techniques have enabled researchers to recognize the states of water in transformer liquids using the OH vibration method and Fourier infrared spectroscopy [36].

The states of water in mineral oil are dependent on the polarity of the liquid molecules. Since water molecules are easier to bond with polar molecules, liquids with polar structures can retain more associated water. This is confirmed in [37] where the states of water in saturated hydrocarbon liquid with carboxyl groups are studied. The water molecules were classified into four groups according to their bonding positions: *A.* attached to the carboxyl groups, *B.* attached to alkyl chains, *C.* attached to other water

molecules, and *D*. free water. Since the molecular polarity increases with the increase of the alkyl chain, more water is attached to the carboxyl groups (type a) and more associated water is attained, as shown in Figure 2.3.

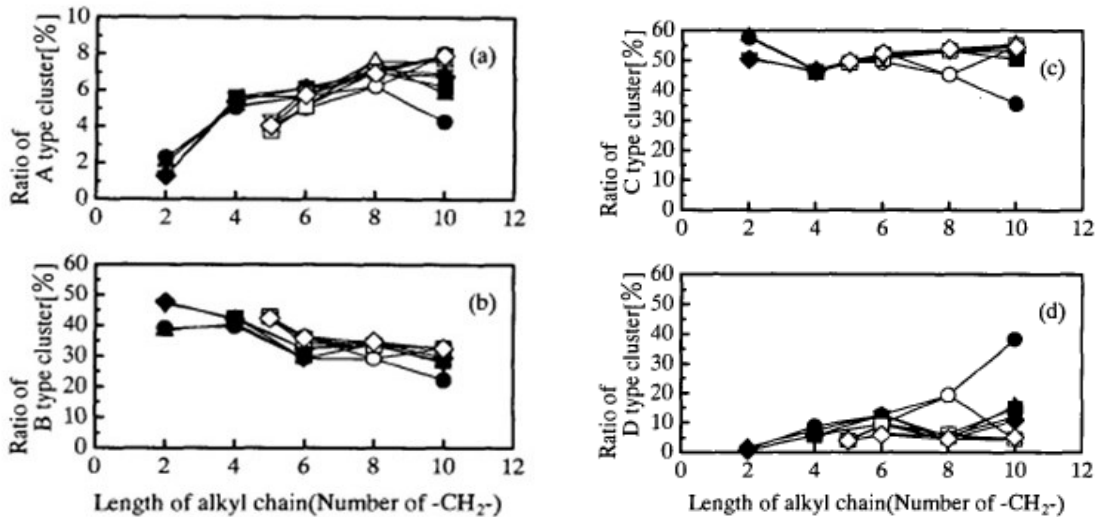


Figure 2.3 Water bonding positions and the length of alkyl chain [37]

For the same reason, esters could retain more water than mineral oil due to their polar structures, such as carboxyl group and unsaturated carbon bonds [33, 36-38]. Their water saturation levels are more than 20 times of mineral oil at 20° C, as shown in Figure 2.4.

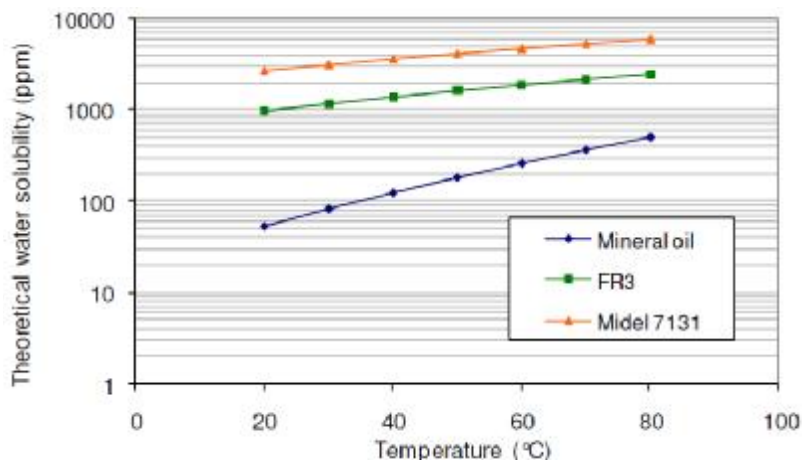


Figure 2.4 Water saturation levels for transformer liquids at different temperatures [14]

2.3.2.3 Influence of Dissolved Water

Dielectric strengths of mineral oil are heavily dependent on the water content, and the most widely accepted relationship in uniform field is shown in Figure 2.5 (a) [39]. The liquid breakdown strength reduces sharply with the increase of the water content from 5

ppm to 20 ppm. The reduction gradually levels off when the water content approaches saturation level. Although similar trends were reported in different publications [39-45], no quantitative agreement was found in them. This might be attributed to different test conditions, such as different liquids, electrode shapes, conditioning effect, and gap distances.

Somewhat different results were also reported. As shown in Figure 2.5 (b), Clark found an almost linear relationship between the dielectric strength and water content using ramping voltage and well- purified mineral oil [31]. Brinkman and Beyer divided the relationship curve into four parts as shown in Figure 2.5 (c) [46]. Compared with Figure 2.5 (a), there is a plateau between 20 ppm and 40 ppm in Figure 2.5 (c). This plateau is correlated with the steady state when almost all the water is molecularly dispersed and dissolved in the liquid. A similar trend was found by Miner in Figure 2.5 (d) between 10 ppm and 20 ppm, and there another plateau was also found where the water content is lower than 5 ppm [47].

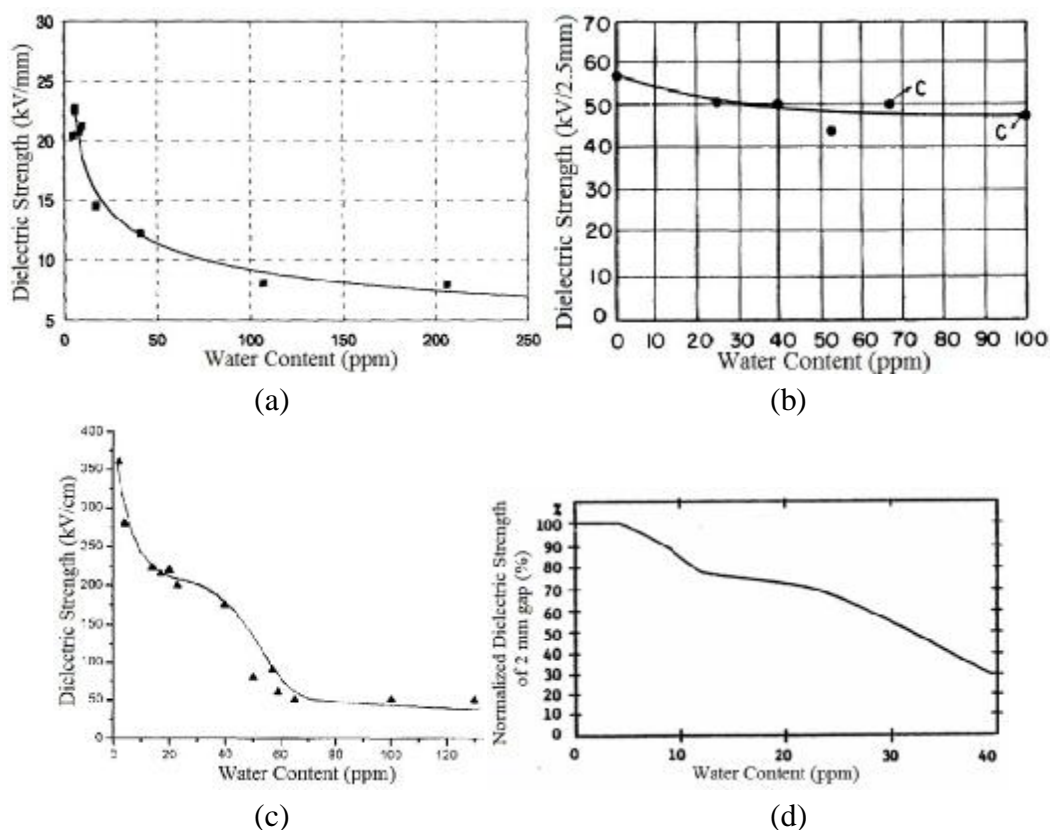


Figure 2.5 Water effect on dielectric strength of mineral oil in different papers (a) Farooq [39], (b) Clark [31], (c) Brinkman [46], (d) Miner [47]

The deleterious effect of water on liquid breakdown strengths is mainly attributed to the absorption of moisture by solid impurities. The moisturized impurities function as the weakest-links in mineral oil and significantly reduce their dielectric strengths [48]. This is evidenced by the fact that a well-purified mineral oil can retain a good dielectric strength even at high water content [31]. Some other reasons were also used to interpret the water effect, such as the low boiling point of water compared to mineral oil [44]. Due to the low boiling point, water vapour bubbles are more easily formed than liquid vapour bubbles when the discharge current heats the local region surrounding the electrode. Since pre-breakdown phenomena in uniform fields are featured by bubble occurrence, the liquid breakdown occurs at lower voltages in the presence of water.

When water content approaches the saturation level, free water clusters or water drops appear and a two-phase emulsion might be formed. A further elevation of water content does not yield a pronounced reduction of the breakdown strength. This is because the liquid breakdown is governed by free water drops, and the dielectric strength is already low.

The water effect on liquid dielectric strength also depends on other factors, such as gap distance and applied voltage [44]. Figure 2.6 shows that the water effect is more significant at small gaps than large gaps. This is attributed to higher field enhancement at small gaps when moisturized particles approach the electrodes. When the duration of applied voltage is shorter, the water effect is found to be less significant due to less time for the particles to move [49]. This further confirms that the water effect is attributed to the movement of moisturized impurities within the liquid gap.

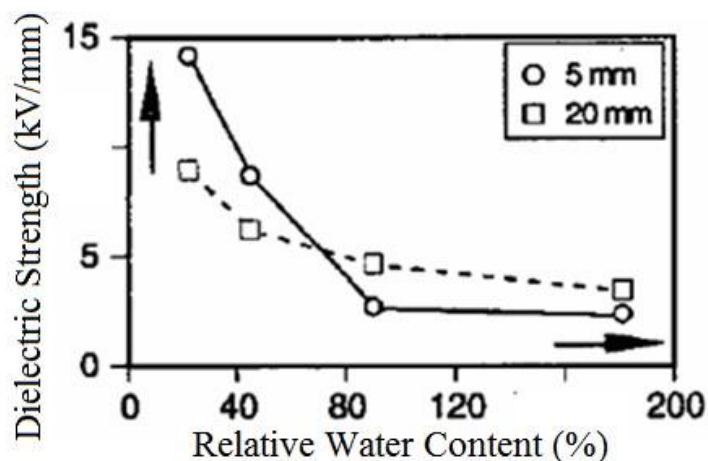


Figure 2.6 Water effect on dielectric strength of mineral oil at different gap distances [44]

2.3.2.4 Influence of Water drops

When the water content exceeds the saturation levels (i.e. a transformer is suddenly cooled down from high temperature), free water drops will appear in transformer liquids. These water drops could function as the weakest-links and significantly reduce the dielectric strengths of transformer liquids.

The effect of water drops has been widely studied using a high speed camera, and the deformation of water droplets was observed [50]. In general, the water droplets are periodically compressed and elongated under the electrical force of AC voltage [51, 52]. The field distortion for a compressed water droplet is the smallest during the deformation. However, the elongated water droplet could form a complete water channel (contact both electrodes) or a partial water channel (contact one electrode). The water channel would act as an extension of the electrode and greatly enhance the electric field at the channel tip [50]. Since most of the voltage is applied on the oil gap due to a higher relative permittivity of water ($\epsilon=80$) than oil ($\epsilon=2.2$), local breakdown might occur between the deformed water and electrode. The local breakdown would easily develop into a full liquid breakdown as shown in Figure 2.7 in a 16 mm liquid gap.

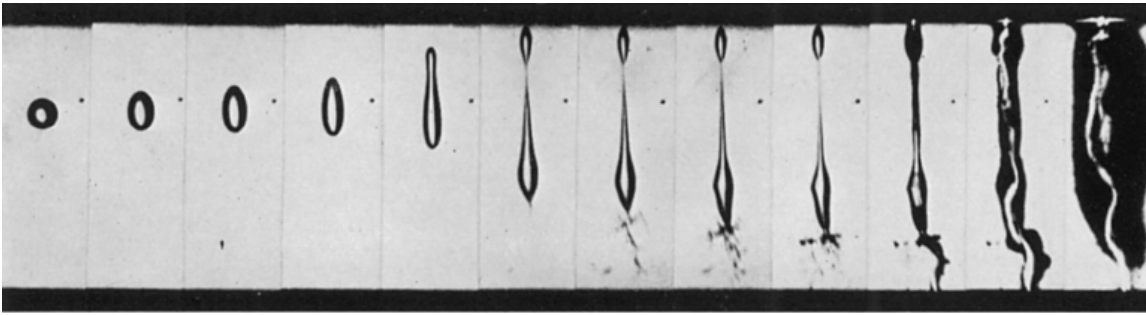


Figure 2.7 Breakdown of a insulating liquid due to instability of a water globule [50]

2.3.2.5 Water Effect of Esters

With the application of esters in power transformers, researches have been carried out to study the water effect on the dielectric strengths of esters [14, 16, 43, 45]. Since the saturation levels in esters are much higher than those of mineral oil, ‘relative water content’ should be used to compare the water effects in various transformer liquids. As shown in Figure 2.8, [16] compared the water effect of esters and mineral oil in terms of relative water content. It is generally accepted that the hygroscopic nature of esters is the main reason for their high water saturation levels and different water effects from that of mineral oil [14].

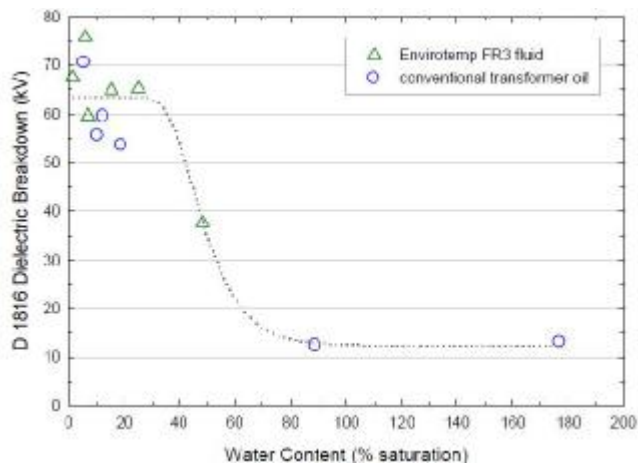


Figure 2.8 Influence of water on dielectric strengths of mineral oil and FR3 [16]

2.3.3 Influence of Particles

The particles in transformers come from various sources. During the manufacturing process, particles are left in the transformer tank either attached to the walls or on the winding surfaces. Although the oil filled into transformers is usually filtered to remove

impurities, the purified oil might be re-contaminated by the residual particles. Therefore, a multiple filtering process is needed before a transformer goes through factory routine tests. During the operations, periodic inspections involving lids and covers removal introduce dust and particles from the surrounding atmosphere to the transformer liquid. For in-service transformers, the cellulose materials continuously release particles into the liquid during the transformer aging.

Using spectroscopy and X-ray diffractions, experts have identified that iron, copper, carbon, and cellulose fibre are the main constituents of particles for in-service transformers. The metallic particles are generally regarded as more dangerous than cellulose particles in dry oil. However, the detrimental effect of cellulose particles is more pronounced in the presence of water. According to the CIGRE survey, the field transformer failures are usually related with high content of particle contaminations [53]. Laboratory work also confirmed the vital function of particles in the process of electrical breakdowns in insulating liquids [54-56].

2.3.3.1 Influence of Metallic Particles

The breakdown process of mineral oil in uniform fields has been associated closely to particle movement. Partial discharges can be produced when charged particles, especially metallic particles, approach high voltage electrodes due to local field enhancement. Thus, particle contaminations play an important role in the initiation of a liquid breakdown [57]. Generally speaking, two methods are applied to study the effect of metallic particles on the dielectric strength of mineral oil. One is to study the motion and effect of a single metallic particle in mm size, and the other is to study the effects of fine metallic particles, usually in μm size.

The motion of a single metallic particle in mineral oil has been well-studied [54-56]. The particle motion is affected by many factors, such as the particle material, the oil type, the field distribution. When a particle is placed between two horizontal electrodes, it will be charged and lifted up when the voltage is high enough [58]. This voltage can be calculated if the shape and material of the particle is known, as shown in Equation 2.2

and Equation 2.3, where R is particle diameter, ρ_s and ρ_i is particle and oil densities, ϵ is oil permittivity, and g is acceleration of gravity [58].

$$E = 0.494[R(r_s - r_l)g / e]^{1/2} \quad (\text{Spherical particle}) \quad \text{Equation 2.2}$$

$$E = 0.836[R(r_s - r_l)g / e]^{1/2} \quad (\text{Cylinder particle}) \quad \text{Equation 2.3}$$

Once the metallic particle is lifted up, it starts to bounce between electrodes [59-63]. The bouncing motion depends on the applied voltage [59], oil type, and electrode arrangement [60]. Figure 2.9 (a) shows the speed of a metallic particle in two types of mineral oil [60]. The uplift speed is generally lower than the drop speed due to gravity. The particle weight acts as a resistance in the uplift motion and as a driving force in the drop motion. In Figure 2.9 (a), the particle motion is affected by the liquid viscosity. Since the viscous resistance in liquid with larger viscosity is higher, the particle motion is retarded and the speed is reduced, as well as the associated current passing through the liquid [61].

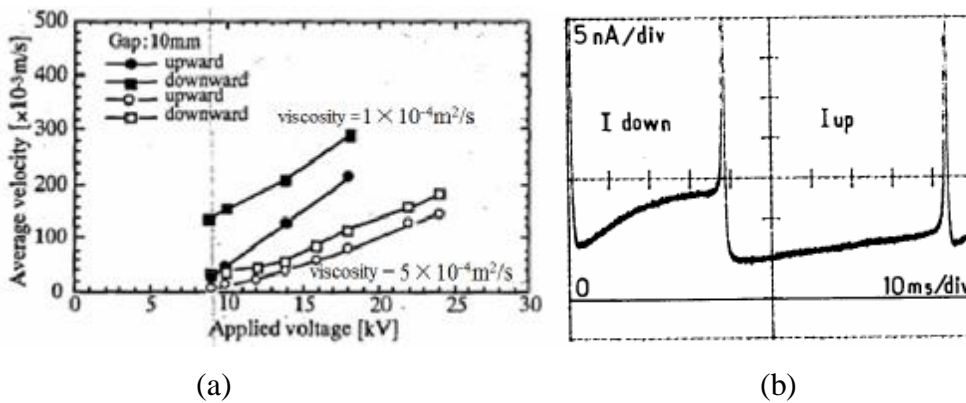


Figure 2.9 Motion of a conductive particle in insulating liquids
(a) motion speed [60], (b) transient current [56]

When charged particles approach the electrode, the local field can be significantly enhanced and current peaks appear as shown in Figure 2.9 (b) [56]. Calculation shows that the enhanced field can be as high as 700 kV/cm for a gap distance of 0.25mm, exceeding the breakdown voltage of the oil gap [62]. This indicates the initiation of micro-discharges due to charge transfer between the metallic particles and electrodes. The current peaks are usually accompanied by visually available small sparks or arcs

[62-64]. Under certain conditions, the micro-discharges may trigger the breakdown of the whole oil gap. Figure 2.10 schematically shows the particle motion and the breakdown process in an insulating liquid [54].

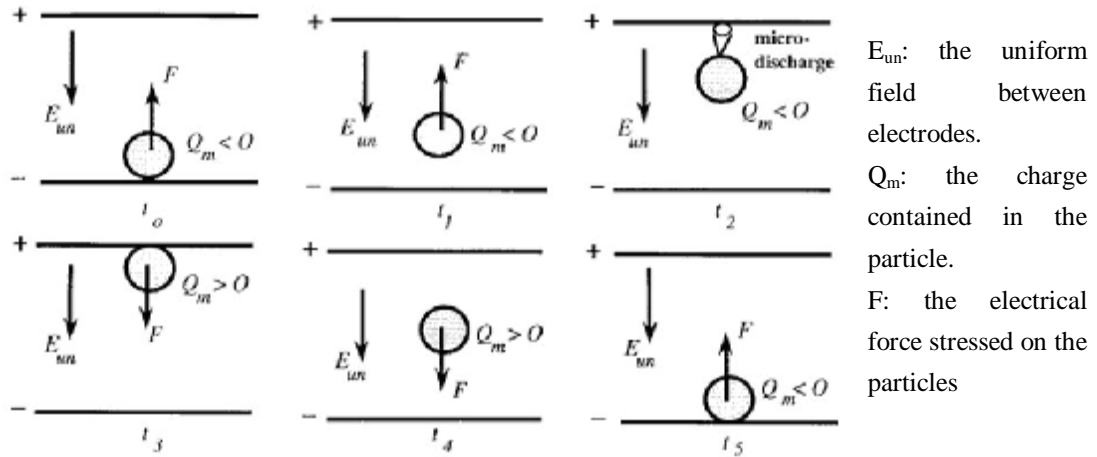


Figure 2.10 Schematic graph of metallic particle motion in mineral oil [54]

The deleterious effect of μm -size metallic particles on the dielectric strength of mineral oil was also well-studied [48, 53, 65-67]. Since the charge transfer between the small particles and the electrode are of such small magnitudes, they can not be observed as small sparks but as continuous discharges in the form of a faint glow [68].

Further studies indicated that the small particles affect both the streamer initiation and the streamer propagation during the liquid breakdown. The metallic particles with diameter ranging from 200\AA ($1\text{\AA} = 1 \times 10^{-9} \text{ m}$) to 500\AA favour the development of zero pressure areas at their surface under certain fields [20]. The zero pressure areas will develop into small cavities, inside which the streamers are initiated. The required field can be calculated by Equation 2.4, where P is the hydrostatic pressure, σ is the oil surface tension, ϵ is oil permittivity and R is the particle radius. After initiation, the streamers propagate much faster in the presence of small metallic particles. Study of the time lag between the application of voltage and breakdown occurrence showed that the streamer velocity is doubled in the presence of copper particles [69]. This is confirmed by the fact that the electron mobility in mineral oil with copper powder is $2 \times 10^{-2} (\text{cm}^2/\text{Vs})$, twice the mobility in clean mineral oil.

$$E = 358 \sqrt{\left\{ \frac{1}{e} \left(P + \frac{2S}{R} \right) \right\}} \quad \text{Equation 2.4}$$

However when there are too many small particles in the liquid, they tend to agglomerate into large particles and fall to the container bottom [70]. The agglomeration and falling process depend on the applied field, the temperature and the liquid viscosity [71].

2.3.3.2 Influence of Carbon Particles

Carbon particles exist in transformers mainly as a by-product of carbonized oil during the operation of on-load tap changers (OLTC). Thermal aging of the oil/paper insulation system can also create a large number of carbon particles. The existence of carbon particles has both beneficial and deleterious effects on the dielectric strengths of mineral oil.

The carbon contaminations have a high affinity to dissolved water in mineral oil [72]. When carbon particles are added into liquid samples, the relative water contents of the samples will be reduced, increasing their breakdown strengths. Therefore in some studies, the dielectric properties of mineral oil are improved when carbon particles are introduced [73]. On the other hand, the conductive carbon particles were found to agglomerate and line up into a carbon chain between electrodes, leading to the reduction of breakdown strengths. Therefore, in other studies, the dielectric strengths of mineral oil were significantly improved after removing the carbon particles from the liquid by filtering [39, 73-75].

2.3.3.3 Influence of Cellulose Particles

Cellulose particles mainly come from the paper insulation materials used in power transformers. When an insulating liquid is stressed under electric field E , the cellulose particles are polarised. The charge contained in the particle and the electrical force can be calculated by Equation 2.5 and Equation 2.6 respectively, where ϵ_1 and ϵ_2 are the permittivities for oil and cellulose particles, r is particle radius and $grad(E^2)$ is the gradient of E^2 in a three dimensional space.

$$\pm q = \pm p r^2 (e_2 - e_1) e_1 \text{grad}(E) \quad \text{Equation 2.5}$$

$$F = \frac{1}{2} r^3 \frac{e_2 - e_1}{2e_1 + e_2} \text{grad}(E^2) \quad \text{Equation 2.6}$$

The polarized particles will eventually migrate to highly stressed regions, such as the protrusion of electrode, and form cellulose chains, either partially or fully bridging the electrodes [76]. Figure 2.11 shows the formation of cellulose chains in a 10 mm oil gap under the DC voltage of 7.5 kV [77]. Under the AC voltage, the migration speed of cellulose particles is much slower, and the oscillatory motion could be observed using the microscopic laser beam technique [68].

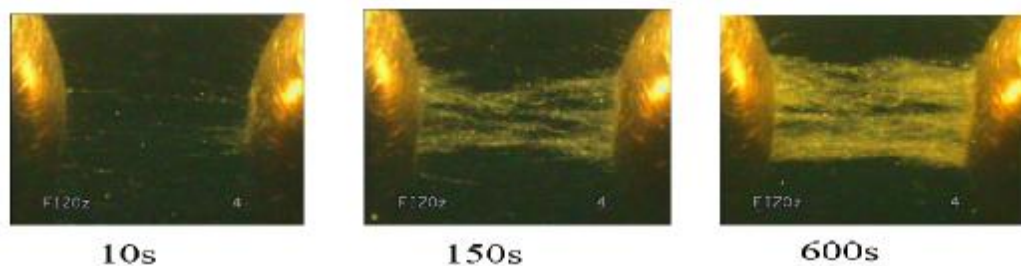


Figure 2.11 Cellulose particles bridging a gap under DC voltage [77]

For in-service transformers, the cellulose particles in liquids are usually in a relatively large concentration and wet condition. Consequently, as shown in Figure 2.12, small cellulose particles might agglomerate into larger particles due to the polar components of the oil and the high surface energy of the particle [78]. For moisturized particles, their dielectric constant will increase from 3.2 up to 70 [79], enhancing their movement in the oil according to Equation 2.5.

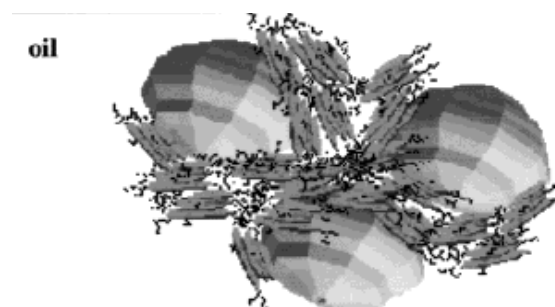


Figure 2.12 Schematic of small cellulose particles aggregating into larger particles [78]

The cellulose chains are generally recognized as partially conducting paths between the electrodes, favouring the liquid breakdowns. Therefore, the dielectric strength of mineral oil is significantly reduced in the presence of cellulose particles. The dependence of liquid breakdown strength on cellulose particle content can be clarified by ‘particle content factor δ ’ expressed in Equation 2.7 [65], where n is the particle number with diameters greater than 1 μm in 10 ml sample, and d is the size of the largest particle. As shown in Equation 2.7, the breakdown strength of mineral oil is enhanced by removing suspended particles [80].

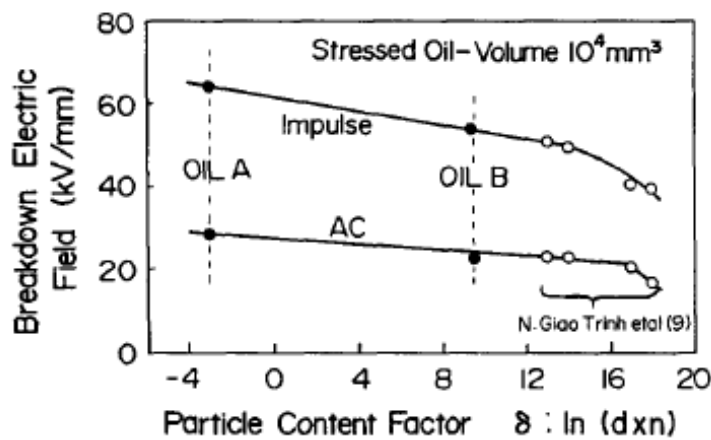


Figure 2.13 Relation between breakdown strength and particle content factor [80]

$$d = \ln(n \cdot d) \quad \text{Equation 2.7}$$

2.3.3.4 Summary

From the above discussion, it can be concluded that particles play a detrimental role in the breakdown process of mineral oil. The breakdown strength of mineral oil is significantly reduced in the presence of particles. A detailed summary of the particle influence on the breakdown strengths of mineral oil under AC voltage is presented in Appendix I.1.

2.3.4 Influence of Gas

The gas in transformer liquids can originate from several sources [81]. The gas can be air absorbed from the atmosphere, hydrocarbon gases due to thermal or electrical stresses, or

even evaporated water and oil molecules due to a sudden change of temperature. When the gas amount is relatively low, the gas exists in the transformer liquid in the form of dissolved gas. When the saturation level is reached, gas bubbles are produced in the transformer liquid.

The existence of gas has a significant detrimental effect on the dielectric strength of mineral oil [25]. This detrimental effect is indirectly evidenced by the dependence of the dielectric strength of mineral oil on the hydraulic pressure [40, 41]. In this section, the influences of dissolved gas, gas bubbles, and hydraulic pressure on the dielectric strength of mineral oil are discussed respectively.

2.3.4.1 Influence of Dissolved Gas

It has been recognized for a long time that the dielectric strength of mineral oil was a function of its dissolved air content [82]. As shown in Figure 2.14, the breakdown strength of well-degassed oil was measured continuously when it was exposed to air. A minimum in the dielectric strength of the oil was obtained for 6 minutes of air exposure, and a recovery was observed in approximately 25 minutes, after which the existence of dissolved gas only slightly reduced the dielectric strength of mineral oil. Further research in [83] and [84] confirmed that the dielectric breakdown strength of mineral oil depended on the relative gas content, rather than the absolute value of the gas content.

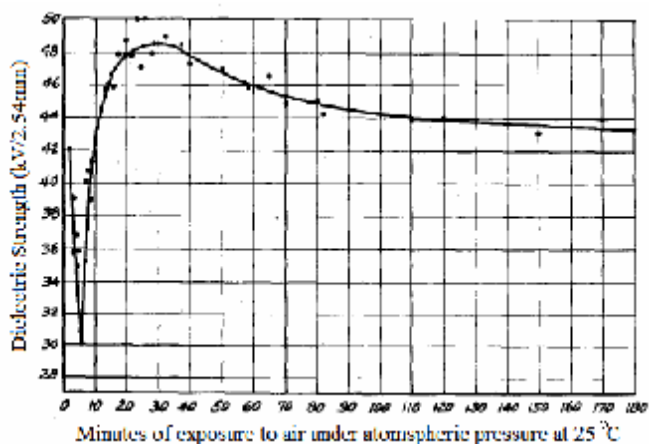


Figure 2.14 Dissolved gas influence on breakdown strength of mineral oil [82]

The breakdown strength of mineral oil was not only dependent on the dissolved gas

amount, but also on the type of dissolved gas. [85, 86] studied the influence of various dissolved gases on the breakdown strength of insulating liquids. In uniform fields, oxygen with a partial pressure of 130 torr increases the dielectric strength of a mineral oil from 0.9MV/cm to 1.3MV/cm. However, hydrogen, nitrogen and carbon dioxide had nearly no influence on the breakdown strength, even with a large gas content [86].

Further study explained the influence of dissolved gases by their electron affinities. A gas with a high electron affinity, such as oxygen, will trap electrons emitted from the cathode, reducing the number of free electrons in the bulk liquid, thus reducing the chance of breakdown [85]. On the other hand, hydrogen, nitrogen and carbon dioxide have small or even no electron affinity. Thus, these gases have limited influence on the breakdown strength of insulating liquids [86]. In order to verify this explanation, sulphur hexafluoride (SF_6) was introduced into a transformer liquid [87]. Since SF_6 has a high electron affinity, a small quantity of SF_6 significantly increases the dielectric strength of the liquid. Analysis using a mass spectrometer confirmed the formation of negative ions such as SF_6^- , SF_5^- , F_2^- and F^- in the liquid [88]. The reduction of free electrons in the bulk liquid was also confirmed by reduced leakage current in [89].

2.3.4.2 Influence of Gas Bubbles

When mineral oil is stressed under uniform fields, its breakdown strengths is significantly reduced if gas bubbles appear due to the temperature or hydrostatic pressure change.

The influence of gas bubbles is usually investigated with the help of a high speed camera [50, 90, 91]. A bubble immersed in a liquid and subjected to an electric field will deform into an elliptic shape along the field direction as shown in Figure 2.15 [90]. Under certain conditions, the bubble is so deformed that partial discharge might appear at the end of the deformed bubble, where the electric field was enhanced to a critical level [92]. The discharge starts progressing toward the electrode and breakdown will occur in several microseconds. For conducting bubbles, the critical shape to induce a particle discharge is ellipse with the ratio of the major to minor semi axis of 1.85 [50].

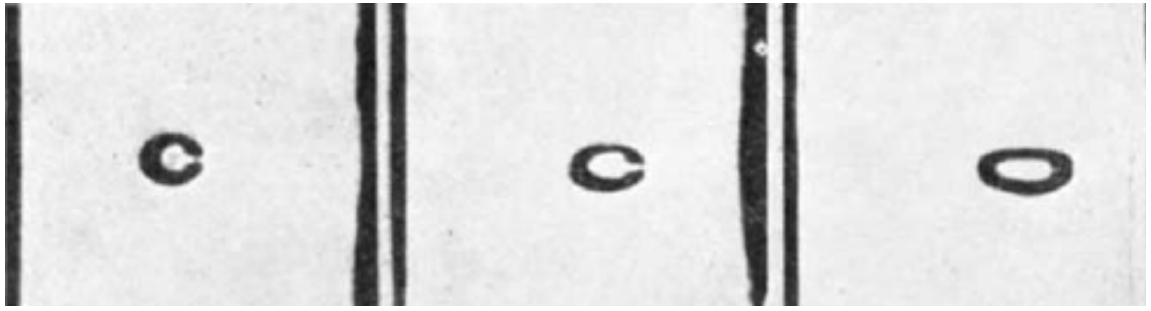


Figure 2.15 Deformation of an air bubble in the direction of applied AC field [90]

Gas bubbles are not only released from gas-saturated transformer liquids. They can also be gaseous water or vaporized oil molecules produced by local heat injection due to electrical or thermal faults [91]. Krasuchi noted that the liquid breakdown was developed through the formation and growth of a gas bubble within the gap [20]. The subsequential decay process of the gas bubble expressed in Equation 2.8 and Figure 2.16 indicated that the internal pressure of the bubble is zero when it decays. The μ , σ and P are the viscosity, surface tension and hydrostatic pressure of the liquid, R_t is the radius at the time t of the bubble with an original radius R_0 .

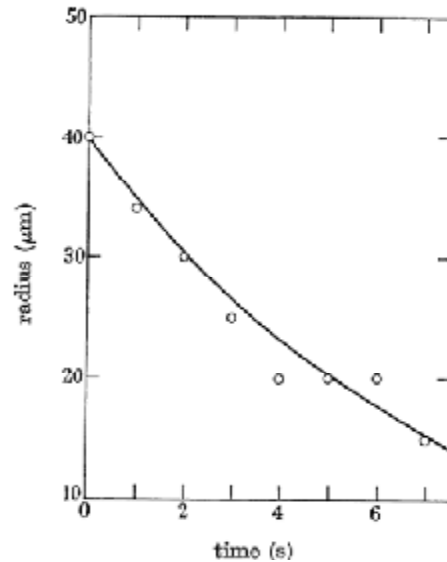


Figure 2.16 Theoretical and observation decay rate of a zero pressure bubble [20]

$$R_t = \left(\frac{2S}{P} + R_0 \right) \exp\left(-\frac{Pt}{4m} \right) - \frac{2S}{P} \quad \text{Equation 2.8}$$

Further calculation showed that if all the energy during a partial discharge is used to vaporize the liquid, the theoretical radius of the vapour bubble is in the same order with

the observed value [20]. Usually, the vapour bubble is produced on the surface of electrodes. But in the presence of particle impurities, the formation of the zero pressure regions preferentially occurs at the site of particles.

2.3.4.3 Influence of Pressure

The dependence of the dielectric strengths of mineral oil on the hydraulic pressure is usually regarded as the indirect evidence of the gas effect. Above atmospheric pressure, the breakdown voltages of mineral oil are generally increased with the increase of pressure [28, 40, 41, 93], with a tendency toward levelling off at higher pressure [94]. However below atmospheric pressure, there is a continuous decrease of breakdown strengths with the decrease of pressure, as shown in Figure 2.17.

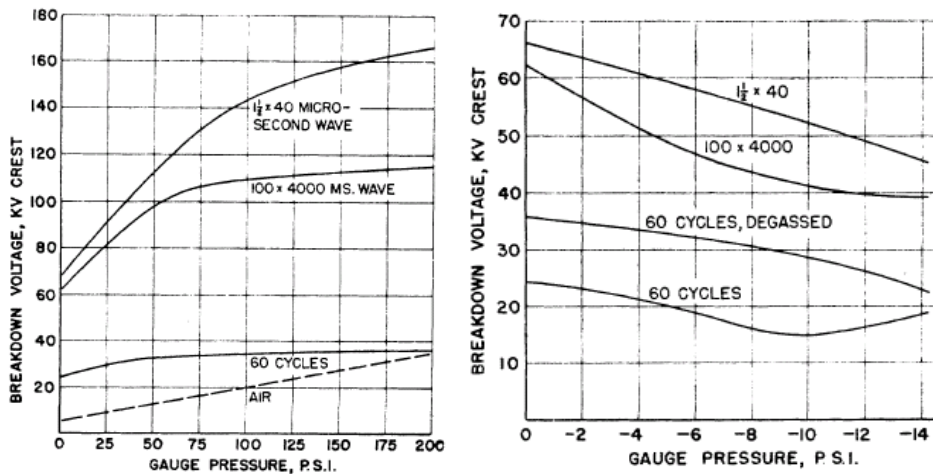
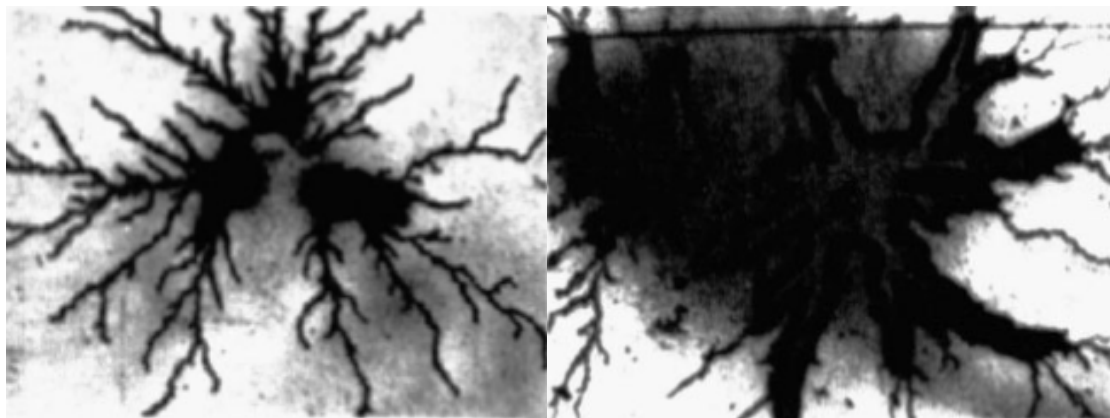


Figure 2.17 Breakdown strengths of mineral oil at various gauge pressures [94]

This behaviour can be attributed to the number and size of gas bubbles [21]. Increased pressure generally decreases the number and size of gas bubbles, leading to reduced ‘weakest-links’ and reduced breakdown voltage. When the number and size of gas bubbles are so small, the solid impurities in liquids become the main ‘weakest links’, which are less affected by pressure. For pressure below atmospheric pressure, the size and number of gas bubbles keep increasing with pressure reduction, reducing the breakdowns strength significantly.

Since gas bubbles can be produced by heat injection during the breakdown process, the dielectric breakdown of a well-degassed liquid is also pressure dependent. Figure 2.18

shows two photos of the breakdown process in mineral oil, recorded using Lichtenberg technique [95]. The thin, filamentary **streamer channels** in the photos represent the traces of the gaseous phase in the breakdown process. After reducing the pressure from 760 mmHg to 100 mmHg, the channel diameter was significantly enlarged. This confirmed that the pressure would affect the breakdown process of well-degassed oil, due to the gaseous nature of the streamer channels [96-98].



(a) Atmospheric pressure, 760 mmHg (b) Reduced pressure, 100mmHg

Figure 2.18 Lichtenberg photos obtained in mineral oil at different pressures [95]

To sum up, the breakdown strength of mineral oil is less dependent on the dissolved gas, but more dependent on the gas bubbles. The hydraulic pressure influences the breakdown strength of mineral oil by affecting the number and size of gas bubbles, as well as by affecting the gas channels during the breakdown process.

2.3.5 Influence of Electrodes

The influence of electrodes on the breakdown strengths of insulating liquids can be discussed in two aspects: electrode material and electrode scale, including electrode area and gap distance [99]. A generally accepted fact is that the breakdown strength is decreased as electrode scale increases [70], due to the increased probability of initiating a breakdown via localized field enhancement. Indeed, the transformer designers routinely subdivide large oil gaps into small gaps of a few millimetres by transformer boards in order to achieve higher breakdown strengths. This indicates a long-held practical belief in the electrode effect.

2.3.5.1 Influence of Electrode Material

It is generally accepted that the breakdown strength of a well-treated oil depends on the electrode material used in the breakdown tests [19, 27]. Further investigation using DC voltage confirmed that the liquid strength depended on the material of the cathode electrode, rather than the anode electrode [100]. A possible explanation is that the breakdown process of clean oil is initiated by the electrons emitted from the electrode. The natural oxide film covered on the cathode surface constitutes an effective layer which may hinder the neutralisation and electron emission, thus affecting the dielectric strength of the liquid [100].

However, for contaminated mineral oil, the influence of electrode material on the breakdown strength is not as significant as in clean oil [101]. Under DC voltage, the breakdowns in contaminated liquids usually occur at much lower voltages due to the contaminations functioning as ‘weakest links’, rather than due to the emitted electrons from the cathode.

2.3.5.2 Influence of Electrode Scale

The influence of electrode scale includes two aspects: the influence of electrode area and the influence of gap distance. Generally speaking, the dielectric strengths of insulating liquids decrease with the increase of electrode area (**electrode area effect**) and gap distance [102-104]. Figure 2.19 shows a typical result of the linear relationship between AC breakdown voltage and the logarithmic of the electrode area [103].

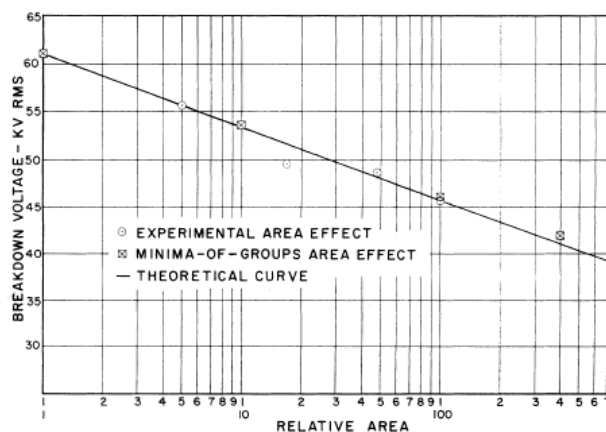


Figure 2.19 Electrode area effect on breakdown voltage of mineral oil [103]

For most investigations, the deleterious effects of electrode area and gap distance were both observed, and they were also referred to as **volume effect** or scale effect [18, 105]. Assuming the statistical distribution of liquid breakdown follows normal distribution, the dielectric strength E_n and the standard deviation σ_n of a liquid can be estimated from Equation 2.9, if the dielectric strength for the unit volume of oil E_1 (kV/cm) and the standard deviation σ_1 (kV/cm) are known [106].

$$\begin{aligned} E_n &= E_1 + AS_1 \\ S_n &= BS_1 \end{aligned} \qquad \text{Equation 2.9}$$

Since the breakdown strength distribution of mineral oil in uniform fields follows the Weibull distribution better than a normal distribution, Equation 2.9 might be further improved to show the scale effect with higher accuracy [14]. The scale effect is usually attributed to the weakest-links in both the bulk liquid and on the electrode surface [99], such as the gas bubbles and micro-protrusions. With the enlargement of the liquid scale stressed under the electric field, more weakest-links were involved in the liquid breakdown, leading to a reduced dielectric strength.

However, somewhat different results were also reported, where the dielectric strengths of testing liquids in uniform fields seem to be independent of the gap distance between the electrodes [27, 41, 107]. It is worth noting that liquids tested in these papers were commonly well degassed and purified. Therefore, it is reasonable to assume that most of weakest-links in bulk oil were removed from these liquids, but the weakest-links on the electrode surface still remained. Consequently, the liquid strengths reduced more significantly with the increase of electrode area than with the increase of the gap distance.

2.3.6 Streamer Study in Uniform Fields

The breakdown of transformer liquids is the consequence of streamer initiation and propagation. Although the dielectric strength in uniform fields is dependent on the liquid quality, the most direct way to investigate the breakdown process in transformer liquids

is to study the streamer behaviours. Only a few papers have reported the streamer behaviours in uniform or semi-uniform fields under AC voltage.

The breakdowns in uniform fields are usually induced by negative streamers originated at the cathode [108]. These streamers propagate towards the anode with velocities of 10 km/s, leading to the ultimate breakdown of the gap. An introduction of ethyl-chloride will promote the propagation velocity of the negative streamers. Figure 2.20 shows the probabilities of breakdowns induced by streamers of both polarities at various pressures. At high pressures, the breakdowns can be induced by positive streamers [109] and the velocity of positive streamers is about 50 km/s [110]. Typical streamer structure in the semi-uniform field is shown in Figure 2.21 (a). Compared with that in the divergent field shown in Figure 2.21 (b), the streamer structure in the semi-uniform field under impulse voltage has more branches and the shape is more spherical [25].

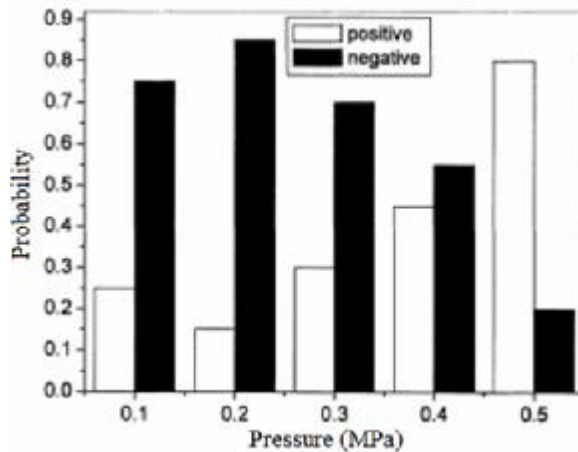
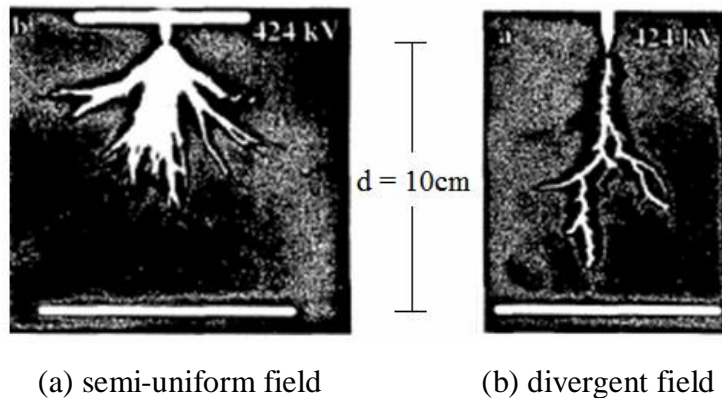


Figure 2.20 Breakdowns induced by positive and negative streamers under AC voltage in semi-uniform field [109]



(a) semi-uniform field

(b) divergent field

Figure 2.21 Streamer structure of mineral oil in semi-uniform and divergent field [25].

It is generally accepted that the streamer propagation in uniform fields is prompted by

high average electric fields (0.5MV/cm). Even a small streamer would be able to propagate and bridge the whole oil gap. Therefore, the liquid breakdown in uniform fields is determined by streamer inception where the liquid quality plays an important role. For contaminated liquid under AC voltage, the movements of the weakest-links favour the inception and propagation of streamers and lead to breakdowns at lower voltage.

2.4 Breakdown of Mineral Oil in Divergent Fields

2.4.1 Introduction

With the recognition of the streamer nature in liquid breakdowns, many investigations have been carried out using high-speed photographic to study streamer performances. Most of the investigations used a highly divergent field and impulse voltage [109, 111-113], which favours the photographic and oscilloscopic recordings due to the predictable time of the streamer occurrences. The application of impulse voltage also offers the possibility of studying the streamer propagation at over-voltage [114]. The main findings of the streamer properties under impulse voltage are summarized as follows.

- | Under negative impulse voltage, negative streamers are produced.
 - ∅ The negative streamers appear at a relatively lower voltage than the corresponding voltage for positive streamers, usually in bush-like structures.
 - ∅ They propagate continuously towards the opposite electrode, and are accompanied by periodic illumination.
 - ∅ The propagation velocity of negative streamers under voltages below the breakdown voltage is less than 1 km/s.
 - ∅ Both the inception and propagation of negative streamers is inhibited by high hydrostatic pressure, indicating the gaseous nature of streamers.

- | Under positive impulse voltage, positive streamers are produced.
 - ∅ They could be classified into 4 modes depending on their velocities, as shown in

Figure 2.22. At low voltage, the slowest streamer mode ('1st mode') rarely leads to breakdown. Breakdown usually occurs due to the '2nd mode' streamer with moderate velocity around 2 km/s. When large over-voltage is applied, a sudden increase of positive streamer velocity ('3rd mode' and '4th mode') is observed at a threshold voltage, around 2 times that of breakdown voltage [115]. The velocity of '4th mode' positive streamer could be up to 140 km/s in mineral oil [116, 117].

- Ø The positive streamers propagate much more easily than negative streamers, and independent of the hydrostatic pressure.
- Ø The positive streamers propagate in step ways with a time interval of several μ s between steps. Breakdown occurs when a positive streamer fully spans the liquid gap.
- Ø The breakdown voltage under positive impulse voltage is much lower than that under negative impulse voltage.

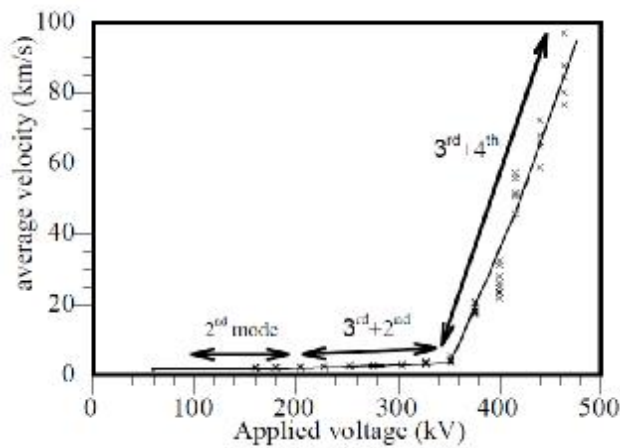


Figure 2.22 Average propagation velocity of positive streamer in mineral oil [118].

Generally speaking, the streamer initiation in divergent fields is caused by the field enhancement (MV/cm) around a sharp point electrode. Nevertheless, the streamers do not necessarily propagate after initiation due to the lower average fields (kV/cm) between electrodes. They can propagate and span the liquid gap only if the applied voltage is further increased. Therefore, the liquid breakdown in divergent fields is determined by the streamer propagation. The streamer propagation is affected by the applied voltage and the transformer liquid, rather than the liquid quality.

2.4.2 Definitions of Pre-breakdown Phenomena

Compared to impulse voltage, only a few investigations were carried out to study the streamer performances in mineral oil under AC voltage [114, 119, 120]. Although the streamer behaviours under AC voltage are similar to those under impulse voltage, differences have been discovered. For example, space charges deposit in mineral oil more easily under AC voltage than under impulse voltage due to longer voltage durations, and the streamers behaviours will be affected by these space charges [114].

In order to clarify the pre-breakdown phenomena, the definitions of ‘streamer’ and ‘streamer channel’ are provided below. It should be noted that the ‘streamers’ are also referred to as ‘leaders’, ‘partial discharges’ or ‘local breakdowns’ in the literature.

- 1 **The Streamer** refers to the gaseous nature of the pre-breakdown phenomena. It is related to the cavities developed around the point electrode during the initiation phase, or related to the ionized material within the ‘streamer channel’ during the propagation phase. The streamer propagation is governed by the electric field around the tip of the streamer channel. Current and light signals usually accompany the streamers.

- 1 **The Streamer Channel** refers to the gaseous channel inside which the streamer exists. The diameter of a streamer channel is in the range of a few μm and tens of μm . The streamer channel extends when an existing streamer channel combines with a gaseous bubble produced at the channel tip. Usually, two types of streamer channels are observed in mineral oil under AC voltage, namely weakly conducting streamer channel and highly conducting streamer channel (leader) [19]. The highly conducting streamer channels were only observed at applied voltage around the breakdown voltage.

2.4.3 Streamer Initiation

2.4.3.1 Pre-initiation

The streamer initiation is characterized by a small cavity in the region surrounding the highly stressed electrode. The pre-initiation, however, is characterized by a small current pulse injected from the electrode into the bulk liquid.

This current was first noticed by Nosseir in the 1960s as a current pulse superimposed on the conductive leakage current [121]. It was attributed to the injection of electrons into the liquid from the cathode and dissociation of the liquid molecules by energetic electrons. The fluorescence accompanying by the current indicates that the emitted electrons attain some energy, which might be used to dissociate the chemical bonds in the liquid molecules or to vaporize the liquid. This might give rise to the formation of a small cavity and transfer the pre-initiation current to streamer initiation [122]. However, it was not until 1987 that the question was answered whether the streamer is the cause or the consequence of the current pulse [123]. The optical time-resolved study of the streamer and current showed that the streamer always appears after the pre-initiation current. Calculation also showed that a bubble of a few μm might be produced if all the energy in the current is transferred into heat [20]. This further confirms that the streamer is produced by heating and vaporizing the local liquid due to the pre-initiation current.

2.4.3.2 Streamer Occurrence

The most widely accepted model to interpret streamer initiation was proposed by Chadband [48]. It suggested that the positive streamers are caused by electrons absorption, while the negative streamers are caused by local heating of surrounding liquid.

Under positive voltage, the electric field around the sharp anode tip is greatly enhanced, and the liquid molecules ahead of the tip might be ionized. The electrons will be absorbed by the anode tip, leaving behind positive charges which become the new tip.

This process will continue until the field at the tip is not high enough to ionize liquid molecules. The essential feature of the model is that positive charges are left in the bulk liquid to maintain the high field at the streamer tip [48]. This indicates the electronic nature of positive streamers. Since high field is a crucial factor of positive streamer initiation, the inception voltage of positive streamers is affected by the electric field around the tip electrode. As shown in Figure 2.23, either increasing the tip radius or increasing the distance L (tip electrode extended from the plane electrode) reduces the electric field, thus increases the streamer inception voltage.

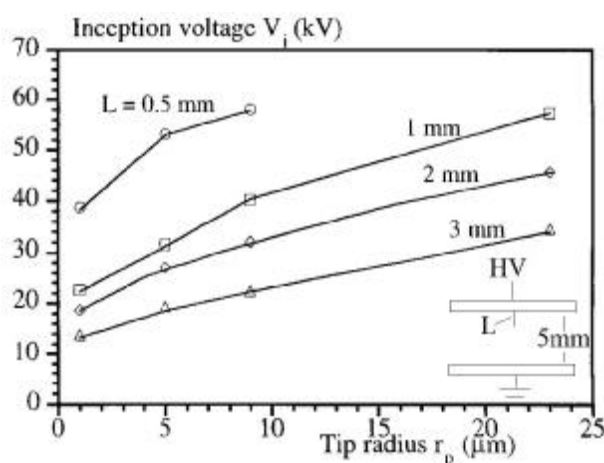


Figure 2.23 Inception voltage of positive streamer versus tip radius [119].

Under negative voltage, a somewhat different model was proposed to interpret the streamer initiation. The pre-initiation current heats and vaporizes the local liquid, forming a vapour bubble attached to the electrode. The electrons emitted from the cathode point after the formation of the bubble will accumulate on the surface of the vapour bubble [111, 122]. Mutual repulsion between the cathode point and the negative charge will push the charge away from the bubble surface, resulting in a hemispheric volume of negative charge. The injection of negative charge from this area will further vaporize the local liquid, gradually enlarging the gas bubble. This model shows the gaseous nature of the negative streamers and agrees well with the dependence of negative streamers on hydrostatic pressure [48].

2.4.3.3 Post-initiation

After the occurrence of positive streamers, there is an inevitable voltage drop on the

streamer channel depending on the conductivity of the streamer [124]. At relatively low voltage, the field at the streamer tip might not be enough to ionize liquid molecules and the streamer disappears in a few μs . If the voltage is high, the liquid molecules around the streamer tip can be further ionized and the streamer starts to propagate.

For negative streamers, the gas bubble will expand slightly after its occurrence [123]. With a low average field $E < 20 \text{ kV/cm}$, the bubble detaches from the cathode point and sweeps into the liquid, as shown in Figure 2.24. The negative charge attached to the bubble surface will gradually disappear, and the field around the cathode tip is rebuilt, leading to the formation of the next streamer. With a high average field $E > 20 \text{ kV/cm}$, more energy will be provided to create the vapour bubble. Therefore, the bubble will experience a high pressure. If the bubble expansion rate exceeds the bubble dispersion rate from the cathode point, it will remain in contact with the tip electrode. The gas bubble produced at the negative streamer tip might be integrated with the streamer channel, and the negative streamer starts to propagate.

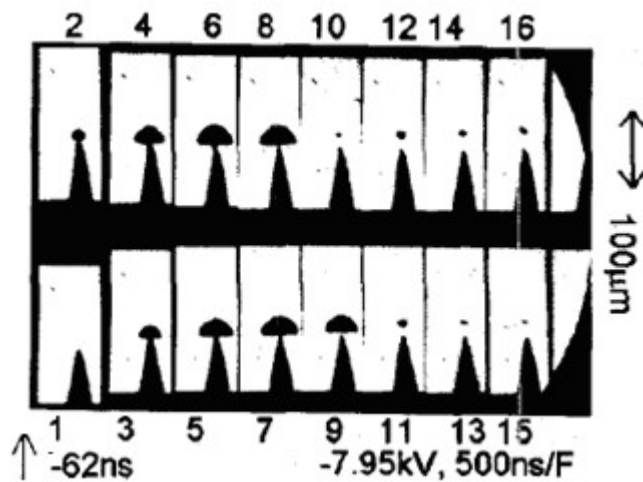


Figure 2.24 Bubble growth, detachment, and disappearance of a negative streamer [111].

2.4.4 Streamer Propagation

2.4.4.1 General Features

The propagation process of streamers is the same as the initiation process. The propagation of positive streamers is an electronic process, through the ionization and

attraction of electrons from bulk oil. However, the propagation of negative streamers is an electrodynamic process, through the expansion of the gaseous channel.

Near the high potential electrode, the positive streamers propagate in a ‘bush-like’ structure. A branch of positive streamers might divide into several sub-branches when conditions are equally favourable for the streamer to grow in several alternative directions [48]. For the propagation of a positive streamer, the required minimum charge at the streamer tip is about 3 to 4 pC [48] and the typical current is about a few mA [125]. When a ‘bush-like’ streamer propagates close to the ground electrode, a fast streamer might be produced at the tip of the ‘bush-like’ streamer without distinct branches. The fast streamer propagates in a ‘filamentary-like’ structure with a much higher velocity (around 20 km/s) than that of the ‘bush-like’ streamer (around 2 km/s) [114].

On the other hand, the negative streamers propagate in the ‘bush-like’ structure with a much slower velocity of 0.5 km/s [123]. During the propagation, mutual repulsion ensures the negative charge is trapped at the streamer channel tip, enhancing the electric field within the channel. A discharge might occur within the gaseous channel when the field is large enough. The discharge energy would further vaporize surrounding liquid and sustain the expansion of the streamer channel [122].

2.4.4.2 Polarity Effect

The most significant difference between positive and negative streamers is that positive streamers propagate much more easily than negative streamers in mineral oil. At the same voltage, positive streamers propagate faster and further into the liquid than negative streamers. This could be generally attributed to two factors.

- 1 Firstly, the diameter of negative streamers is larger than that of positive streamers. A negative streamer channel is about 50 μm in diameter, 5 to 10 times that of a positive streamer channel [126]. Therefore, the tip radius of a positive streamer is small and field enhancement is high [122]. This favours the ionization of surrounding liquid and the propagation of positive streamers [26]. However for negative streamers, the

field at the streamer tip is not as high as that of positive streamers due to larger streamer diameter.

- Secondly, the ionization zone and energy exchange surface is more dispersed for negative streamers [126]. Due to the electron absorption nature, the energy exchange of positive streamers occurs inside the ionization zone. However for negative streamers, the energy exchange occurs at the far end of the ionization zone due to the electron ejection nature, as shown in Figure 2.25. Since the energy injected into the surrounding liquid is more dispersed, the propagation of negative streamers is less effective than that of positive streamers.

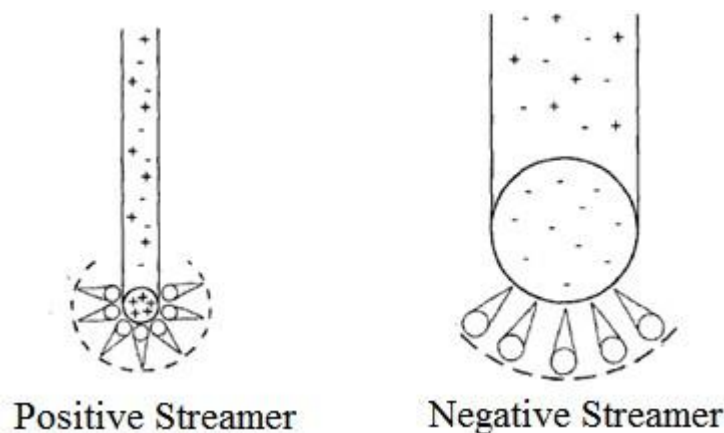


Figure 2.25 Ionization zone of negative and positive streamers [126]

In divergent fields, the electric field ahead of a streamer channel ensures the streamer propagation, and the propagation of negative streamers is less effective than positive streamers. This fact agrees with the conclusion that positive streamers are decisive in the breakdown process of mineral oil. However, recent research under impulse voltages shows that the propagation of negative streamers is significantly promoted in esters than in mineral oil [127].

2.4.4.3 Streamer Channel Types

The streamer channels are generally classified as weakly conducting channels and highly conducting channels, depending on the conductivity of the streamers [19]. Both channels start from high field areas (usually the sharp electrode) and extend into liquid gaps discontinuously with an interval of a few microseconds between steps [114].

The weakly conducting channel usually occurs in small gaps at relatively low voltages, corresponding to the ‘bush-like’ shape streamer. There is a high voltage drop on this type of channel due to the low conductivity. It is suggested that the discharge current passing through the streamer is relatively low and the heat dissipated in the channel is relatively small. Consequently, liquid vapour in the channel is only partially ionized, leading to the high resistivity of this type of channel [19]. As the streamers propagate into the liquid gap, a high voltage drop on the streamer channel reduces the electric field at the channel tip. Thus, the streamer usually stops at a certain length before touching the other electrode.

The highly conducting channel, on the other hand, usually occurs in large gaps at higher voltages near breakdown. It extends from the tip of weakly conducting channels. The transition from weakly conducting channels into highly conducting channels occurs when liquid vapour inside the channel is fully ionized under the high streamer current [19]. The high conductivity of this type of channel indicates that the voltage drop on the channel is minute. The high field on the streamer tip is maintained, which allows the streamer to propagate continuously toward the ground electrode until breakdown.

2.4.4.4 Streamer Re-illumination

During the streamer propagation, the streamer channels are periodically re-illuminated by bright flashes over an increasing length at each step. The re-illuminations are correlated both in time and magnitude with current pulses from mA to A, depending on the applied voltage [128]. Figure 2.26 shows a typical recording of synchronized light and current during the propagation of a streamer.

The illumination is produced by an intensive discharge current passing through the streamer channel. The liquid molecules inside the channels are ionized into small radicals by the discharge current, such as H⁻ and CH₃⁻ [129]. Consequently, the conductivity of the channels is high and the streamer propagates some length into the bulk liquid during the period of the current in about 100 ns. When the current is extinct, the streamer illumination disappears, but the gaseous streamer channels remain due to the pressure

inside the channels. However, the ions of opposite polarities might be recombined into new molecules. The released energy of the electron transition during the recombination will be emitted in the form of quanta, resulting in small light pulses between two successive re-illuminations, as shown in Figure 2.26.

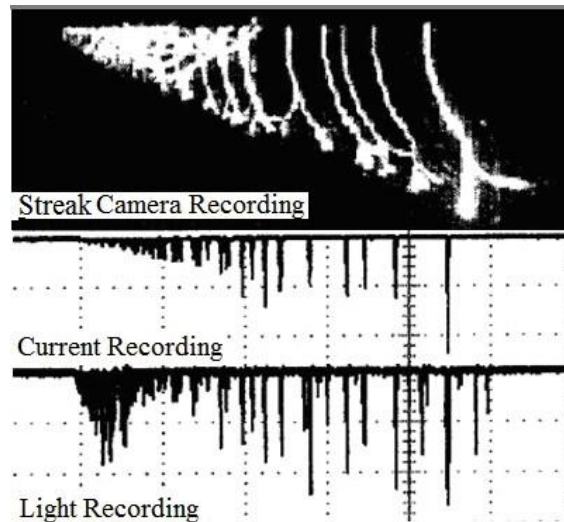


Figure 2.26 Re-illumination of a positive streamer with current and light recordings [120]

After recombination, the streamer channel regains its resistivity, and is subjected to an increasing voltage drop [125]. At some point, another discharge occurs when the voltage drop exceeds the withstand ability of the streamer channel. The discharge current will re-illuminate the same streamer channel and promote the streamer propagation. In this way, the streamers propagate step-by-step with re-illuminations, until the streamer stops propagating at some length depending on the applied voltage.

2.4.5 Streamer-led Breakdown

The breakdowns in mineral oil under AC voltage could be classified into ‘direct’ breakdown and ‘burst’ breakdown [120]. The ‘direct’ breakdown is caused by a single streamer occurring in an AC cycle, while the ‘burst’ breakdown is caused by several streamers occurring in several cycles.

2.4.5.1 Direct Breakdown Mode

Direct breakdowns usually occur at small liquid gaps. During streamer propagation, the

voltage at the streamer tip is the remainder of the high voltage potential minus the voltage drop at the streamer channel. Under high applied voltage, streamers will propagate into the liquid gap until breakdowns. As the streamer travels the last quarter of the gap, the field in the remaining gap begins to increase rapidly and a ‘final jump’ can be observed. The existence of the ‘final jump’ is evidenced by the discontinuity between the streamer stopping length and the gap length, as shown in Figure 2.27 [124].

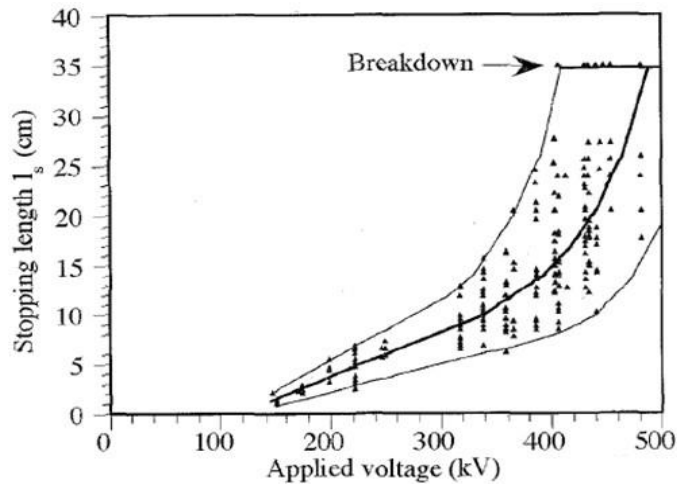


Figure 2.27 Streamer stopping length of positive streamers with applied voltage [124]

When a positive streamer approaches the ground electrode, a fast filament will originate from the head of the bush-like streamer and bridge the remaining gap. Breakdown usually occurs when the fast filament touches the ground electrode [26]. However in some cases, the filament could not lead to breakdown due to the discontinuity of the streamer, as shown in Figure 2.28. For negative streamers, the fast filament could also originate from the ground electrode (return stroke) since the positive streamer is easier to propagate than negative streamers [130]. Breakdown will occur when the ‘return stroke’ propagates back to the negative high potential electrode following the same channel as the negative streamers, as shown in Figure 2.29.

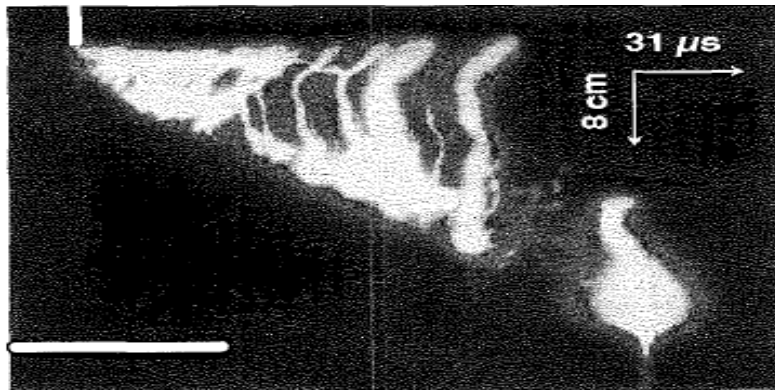


Figure 2.28 Positive streamer propagating to the plane without causing breakdown [114]

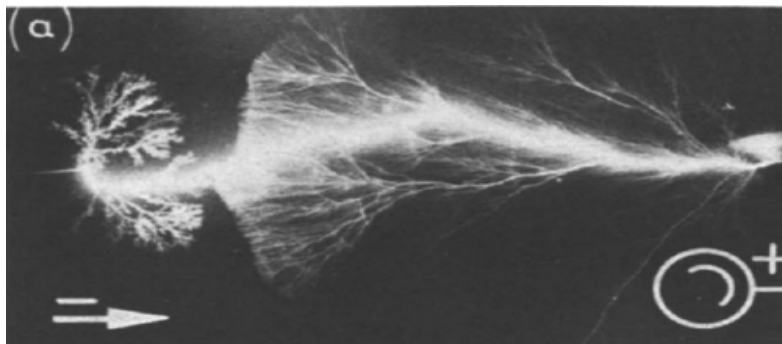


Figure 2.29 Return streamer channel developed from sphere electrode[130]

2.4.5.2 Burst Breakdown Mode

Burst breakdowns usually occur at large liquid gaps, when an AC cycle does not give enough time for the streamer to fully span the gap [120]. The current and voltage recording of a typical burst breakdown are shown in Figure 2.30.

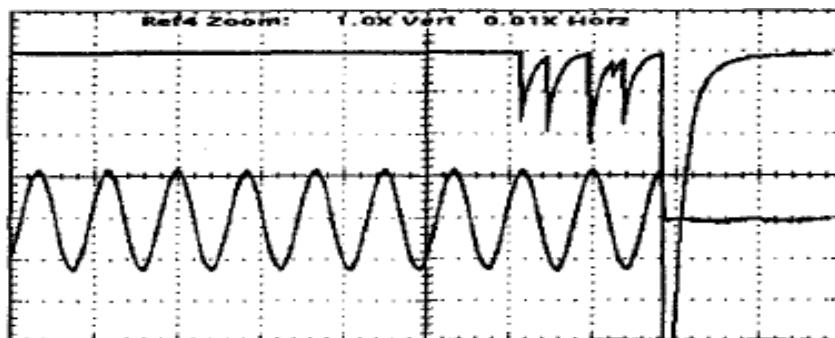


Figure 2.30 Current and voltage signal for streamer burst breakdown [120]

The ‘burst’ means the breakdown is preceded by a streamer ‘burst’ produced at previous cycles, and only the last streamer leads to breakdown. The streamers within a ‘burst’ usually follow the same streamer channel. This indicates that the gaseous channel

produced by a previous streamer remains until the next streamer, leaving a preferential track for the next streamer to follow.

2.4.6 Influence of Some Factors

In divergent fields under AC voltage, the liquid breakdown is mainly determined by streamer propagation. The general feature of streamer propagation is the extension of streamer channels due to the heating and vaporization of local liquid, either by emitting or absorbing electrons around the channel tips. Therefore, any factors affecting the streamer propagation would affect the dielectric strength of mineral oil.

2.4.6.1 Influence of Liquid Structure

The influence of liquid structure is commonly studied by introducing additives into pure insulating liquids and determining the streamer performances [131]. Two types of additives are usually introduced, including low ionization potential additives, such as N-dimethylaniline (DMA), or high electron affinity additives, such as sulphur hexafluoride (SF_6) and ethylchloride ($\text{C}_2\text{H}_5\text{Cl}$).

For positive streamers, the streamer properties are affected by additives with low ionization potentials. In the presence of these additives, the propagation velocity of positive streamers is significantly promoted and the streamer structure is more emenative [117]. Since the positive streamers propagate by abstracting electrons from the liquid, additives with low ionization potential could promote the propagation efficiency by providing more electrons in the liquids under the same voltage [132].

For negative streamers, on the other hand, the streamer properties are affected by additives with high electron affinities [133]. These additives could greatly accelerate the streamer propagation velocity, and increase the number, duration and amplitude of the streamer current [134]. Since the negative streamers propagate by emitting electrons from streamer tips, electrons would be emitted more easily and the energy would be concentrated in a more confined volume in the presence of high electron affinity additives [134]. Consequently, the propagation of negative streamers is more efficient.

2.4.6.2 Influence of Electrode Configuration

Generally speaking, the streamer initiation is affected by the local electric field surrounding the point electrode, while the streamer propagation is governed by the local field surrounding the streamer tip. Therefore, the electrode configuration affects the streamer properties mainly through its influence on the field distribution between electrodes.

Rain investigated the streamer properties in divergent fields under AC voltage using point-plane electrode arrangements with various point electrodes, plane electrodes and gap distances [135]. It was concluded that the effect of electrostatic coupling between point electrode and plane electrode is quantitatively similar to that between streamer tip and plane electrode. Shown in Figure 2.31 as an example, the voltage difference between the initiation voltages and breakdown voltages are similar for two electrode arrangements. This indicates that the geometry arrangement has a similar influence on the streamer initiation and streamer propagation assuming the distances between tip electrode/ plane electrode and streamer tip/ plane electrode are the same. Furthermore, no detectable difference was found when comparing the streamer performances with and without an insulating paper covering the plane electrode [136].

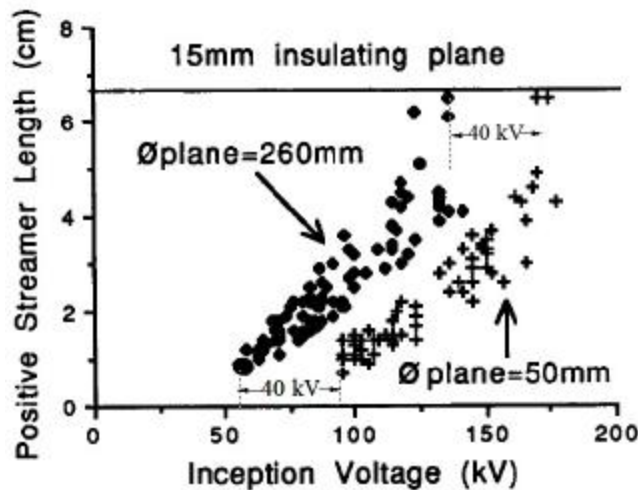


Figure 2.31 Influence of electrode configuration on positive streamer properties [135]

2.4.6.3 Influence of Water Content

In divergent fields, the dielectric strength of mineral oil is hardly affected by water content since only a small volume of liquid is stressed. There is almost no change of the PDIV and breakdown strength of mineral oil for water content up to saturation [137]. After saturation, the liquid breakdown strength is sharply reduced in the presence of free water droplets.

2.4.6.4 Influence of Particles

In divergent fields, a limited number of particle contaminations have almost no effect on the dielectric strength of mineral oil under AC voltage [114]. As shown in Figure 2.32, although some particles significantly reduce the streamer inception voltage, the streamer propagation is hardly affected, and thus the dielectric strength of the liquid will not be affected. The stopping length l_s is the length of a streamer when it stops propagation.

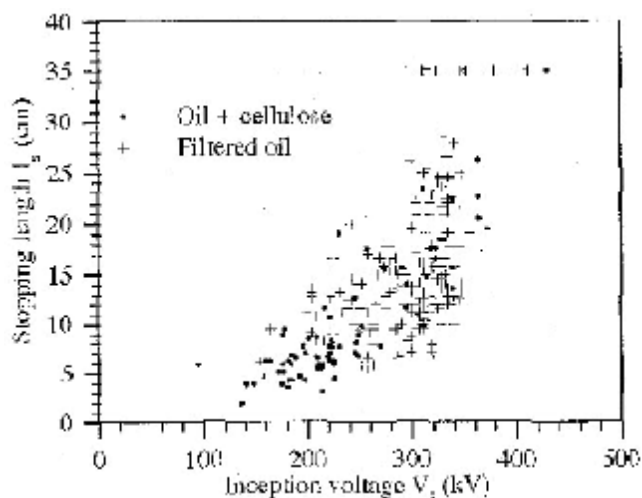


Figure 2.32 Positive streamer propagations in clean and cellulose contaminated oils [114]

On the contrary, the presence of some particles improves the dielectric behaviours of mineral oil [73, 74, 128]. As shown in Figure 2.33, carbon particles of 416 mg/l could elevate the breakdown strength of mineral oil by approximately 45% [74]. In divergent fields, the carbon particles are charged by space charges and move along the field lines. These carbon particles are gradually gathered at sites of maximum field strength around the point electrode, virtually enlarging the radius of the electrode tip [74]. Consequently,

local electric field is reduced and the streamer inception is increased. The same process would occur during streamer propagation, and as a result, the dielectric strength of contaminated mineral oil is improved.

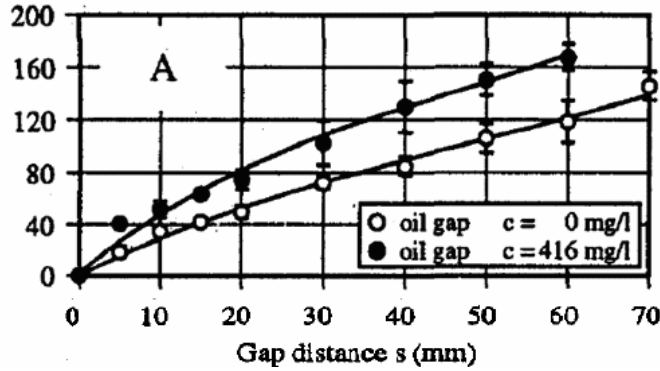


Figure 2.33 Breakdown voltage with oil gaps for new and carbonized mineral oil [74]

It should be noted that the particle motion is critical to interpret the improvement effect of carbon particles on the liquid dielectric strength. Particles without movement would not elevate the liquid dielectric strength [138]. For example under impulse voltage, the voltage duration is too short for the particles to move. The carbon particles are evenly distributed in the bulk liquid when a negative impulse voltage is applied. Therefore, the liquid dielectric strength is greatly reduced due to the high electron affinity of the carbon element [75].

Too many carbon particles would, however, reduce the dielectric strength of mineral oil in divergent field under AC voltage [73]. The particles might partly bridge the liquid gap in the form of carbon chains, which would lead to a smaller streamer inception voltage and a decreased breakdown voltage as shown in Figure 2.34. The carbon particles in this graph were produced by carbonizing liquid samples with controlled energy. This conclusion is further confirmed by cellulose particles and needle/plane electrodes [139].

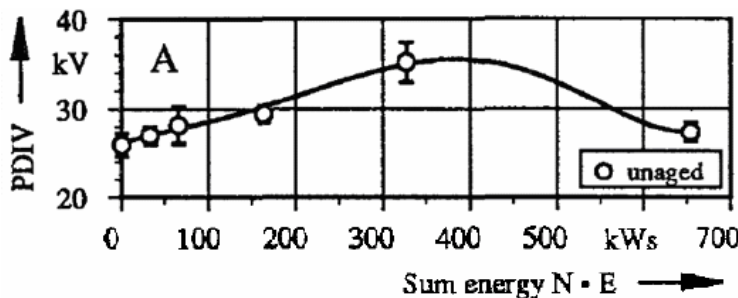


Figure 2.34 PD inception voltage of carbonized samples with controlled energy [73]

2.5 Comparison between Breakdown in Uniform and Divergent Fields

Despite a variety of factors that influence liquid breakdowns, the breakdown mechanisms in uniform fields and in divergent fields are similar in the sense that they are triggered by the occurrence of a streamer, and a breakdown will occur when the streamer fully spans the liquid gap.

However, there are also differences between the breakdown mechanisms in uniform fields and in divergent fields. In uniform fields, almost every streamer will propagate to breakdown due to a high average field. Therefore, the liquid breakdown is determined by streamer inception, and the breakdown voltage is the same as the streamer inception voltage [119]. On the other hand, the liquid breakdown in divergent field is determined by streamer propagation due to a low average field. Thus, the breakdown voltage is much higher than the streamer inception voltage.

Using impulse voltage, an almost linear relationship exists between the logarithm of streamer inception field and the logarithm of the liquid scale, as shown in Figure 2.35. The breakdown strength in uniform field in Figure 2.35 (b) is the same as the inception field. Although ‘stress oil volume’ was used in Figure 2.35 (a) and ‘stressed electrode area’ was used in Figure 2.35 (b) as the liquid scale, similar conclusions were obtained. The number of weakest-links in both the electrode surface and bulk liquid increases with the increase of the liquid scale, leading to a decreased streamer inception field [140].

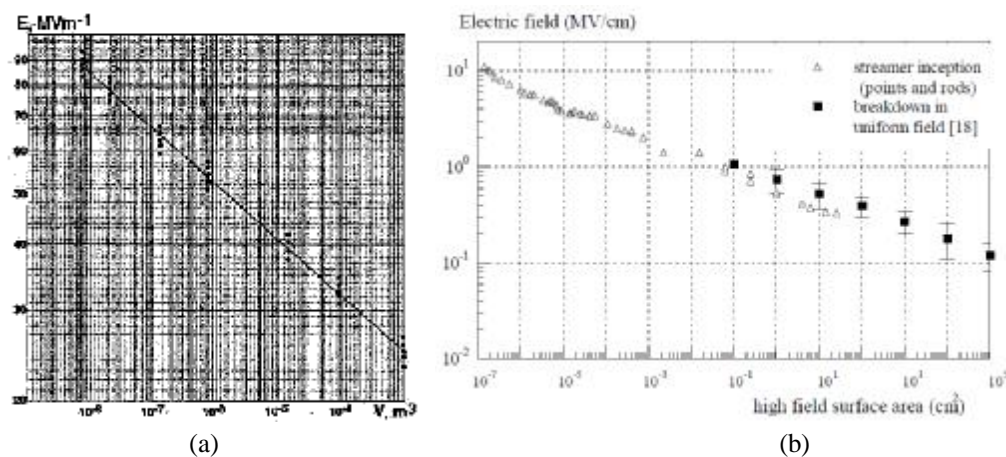


Figure 2.35 Impulse streamer inception field of mineral oil versus stressed liquid scale (a) Torshin [140], (b) Lesaint [141]

Under AC voltage, the relationship between streamer inception field and the liquid scale in Figure 2.36 is slightly different. In uniform fields ($>10^{-1} \text{ cm}^2$), the streamer inception field of filtered oil (equal to breakdown field) under AC voltage is lower than that under impulse voltage. This is attributed to longer voltage application duration, and thus a higher chance of streamer initiation at lower voltage [142]. For polluted oil, the streamer inception voltage is further decreased due to movement of contaminants. In highly divergent fields ($<10^{-3} \text{ cm}^2$), the AC streamer inception field become higher than impulse streamer inception field. This effect is due to larger space charge injection under AC voltage compared to impulse voltage. The space charge reduces the field on the point electrode, thus increases the AC streamer inception field, whereas it has almost no influence on the impulse streamer inception field due to a short duration [140].

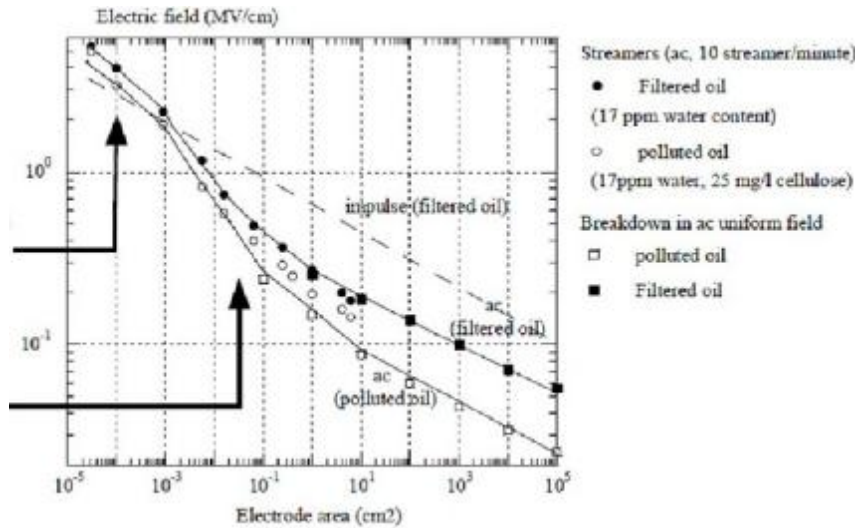


Figure 2.36 AC streamer inception field of mineral oil versus electrode area [142].

2.6 Summary

Starting with a review of the history of breakdown theory, this chapter provides literature review about the breakdown process in uniform and divergent fields. In both fields, the ‘streamer’ theory and the ‘weakest-link’ theory are proved to be correct. The ‘streamer’ theory is developed to interpret the gaseous nature of liquid breakdown, which is regarded as the consequence of streamer initiation and propagation. The ‘weakest-link’ theory is developed to interpret the origin of streamer initiation, especially in uniform fields.

In uniform fields, the breakdown strength provides data related to streamer initiation. Due to a relatively high average field, every streamer propagates into breakdown. The breakdown voltage is therefore the same as the streamer initiation voltage. The initiation is highly sensitive to the liquid quality, such as water content, gas content, particle content and additives. Consequently, a comparison of transformer liquid properties is difficult by applying breakdown tests in uniform field, unless the oil quality is strictly controlled to an identical condition. The breakdown strength in uniform field is quite essential to the high voltage application of transformer liquid, especially for application in high voltage transformers, where the electric field is relatively low and the stressed oil surface/volume is relative large.

On the other hand, in divergent fields, the streamer inception is determined by the field enhancement around the point electrode, which is independent of the liquid quality. Not every streamer propagates to breakdown, and the liquid breakdown is determined by streamer propagation. Therefore, the AC breakdown voltage of transformer liquid in divergent fields is much higher than the streamer inception voltage.

Chapter 3. Experimental Study on Breakdown in AC Uniform Fields

3.1 Introduction

The AC dielectric strength test is generally used as one of the quality check and acceptance tests for transformer liquids before filling new transformers or during routine maintenance. The mean breakdown voltage is commonly reported, and used to evaluate the ability of a transformer liquid to withstand the electrical stress. Transformer liquid manufacturers have reported that the dielectric strengths of esters (Midel 7131 and FR3) are comparable to that of mineral oil (Gemini X), as shown in Table 3.1.

Table 3.1 AC breakdown voltages of transformer liquids reported by manufacturers

	Breakdown voltage (kV)	Standard	Comment
Gemini X	40-60	IEC 60156	Before treatment
	>70	IEC 60156	After treatment
Midel7131	>75	IEC 60156	2.5 mm gap
FR3	28-33	ASTM D1816	1 mm gap
	56	ASTM D1816	2 mm gap

However, the reported AC breakdown voltages are measured using different standards, and the qualities of transformer liquids, such as the water content and the particle content, are not specified in detail. In order to make a reliable comparison between the AC breakdown voltages of different liquids, their qualities should be controlled to a similar level, and furthermore, the same test procedure should be followed.

In this chapter, Section 3.2 reports on measurements of the breakdown voltages and breakdown voltage distributions of three transformer liquids with carefully controlled qualities. Section 3.3 extrapolates the withstand voltages of these liquids from their distributions using the Weibull function. Section 3.4, section 3.5 and section 3.6 investigate the influences of some extraneous factors on the breakdown strengths of

transformer liquids. The extraneous factors studied in these sections are water content, particle content and electrode surface area. Section 3.7 gives an example on how to estimate the withstand voltages of transformer liquids in the scale and quality encountered in practice from small scale laboratory tests. Finally, a summary of the dielectric breakdown properties of mineral oil and esters in AC uniform fields is given in section 3.8. The test equipment and measurement methods used in this chapter are provided in Appendix I.2.

3.2 Breakdown Strengths of Transformer Liquids

3.2.1 Introduction

The purpose of this investigation is to measure the dielectric strengths of mineral oil and esters, and compare their breakdown voltages at a low failure rate (i.e. withstand voltage). In order to achieve the purpose, the qualities of transformer liquids should be controlled at the same level. A suitable procedure of sample preparation and breakdown voltage measurement method should be used for both mineral oil and esters. Since the breakdown voltage of a transformer liquid is a statistically distributed parameter, it is necessary to find a suitable function to model the breakdown voltage distribution, and to estimate the withstand voltage based on this distribution function.

3.2.2 Sample Preparation

During the manufacturing process, the qualities of transformer liquids are carefully controlled. Thus, both the water content and particle content in newly produced transformer liquids are relatively low. However, their qualities may gradually deteriorate during long-term storage or during transportation, due to slow ageing or contamination from the atmosphere. To prevent the deterioration, the transformer liquids used in our tests are sealed in non-transparent tanks and stored in oil sheds. Before any test, the liquid samples are filtered, dehydrated and degassed. The liquid processing procedures are described in Appendix I.3.

Table 3.2 compares the liquid qualities of mineral oil and esters. Typical values of water content and particle content of transformer liquids in as-received condition, long-term stored condition and processed condition are listed. Since the contamination levels are usually classified by the number of particles with a diameter larger than 5 μm per 100 ml according to CIGRE working group 12.17 [53], we only list the number of particles larger than 5 μm per 100 ml liquid sample. The processed transformer liquids (purified, dehydrated, and degassed) are in good condition with relative water content of less than 3% and particle number of less than 500 ($> 5 \mu\text{m}$ per 100 ml). Therefore, the qualities of various transformer liquids are the same. The water saturation levels of transformer liquids at ambient temperature are also listed in Table 3.2, and the definition of relative water content was provided in section 2.3.2.1.

Table 3.2 Comparisons of liquid qualities of mineral oil and esters

Liquid condition	Parameter	Gemini X	Midel7131	FR3
New stock (as-received)	Water (ppm)/ RH	8/ 14.5%	80/ 3.1%	60/ 5.5%
	Particle ($>5 \mu\text{m}$)	2803	1830	2150
Old stock (long-term stored)	Water (ppm)/ RH	15/ 27.3%	210/ 8.1%	180/ 16.5%
	Particle ($>5 \mu\text{m}$)	6530	3235	4333
Processed (purified, dehydrated, degassed)	Water (ppm)/ RH	$<2/ <3.6\%$	70/ 2.7%	30/ 2.7%
	Particle ($>5 \mu\text{m}$)	470	350	320
Water saturation level at 25 °C (ppm)		55	2600	1100

3.2.3 AC breakdown Voltages

The AC breakdown tests were carried out following the standard ASTM D1816 with several improvements described as follows. Firstly, the degassing of the liquid samples is carried out in a vacuum oven. Secondly, the time interval between two successive breakdowns is increased from 1 minute to 5 minutes. Thirdly, the sample size of the breakdown tests is increased from 10 to 40, and the electrode conditioning is carried out by successive breakdowns. The detailed test procedure is provided in Appendix I.4.

Figures 3.1 to 3.3 represent the breakdown voltage results of processed transformer liquids. Before and after the tests, the water and particle contents of the liquids were measured and nearly no change was found, which could be attributed to the short test duration. Therefore, we can conclude that the qualities of the samples did not deteriorate during successive breakdowns.

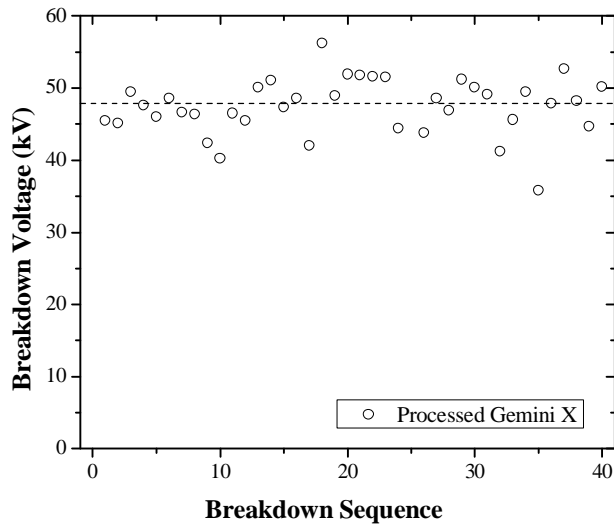


Figure 3.1 AC breakdown voltages of processed Gemini X

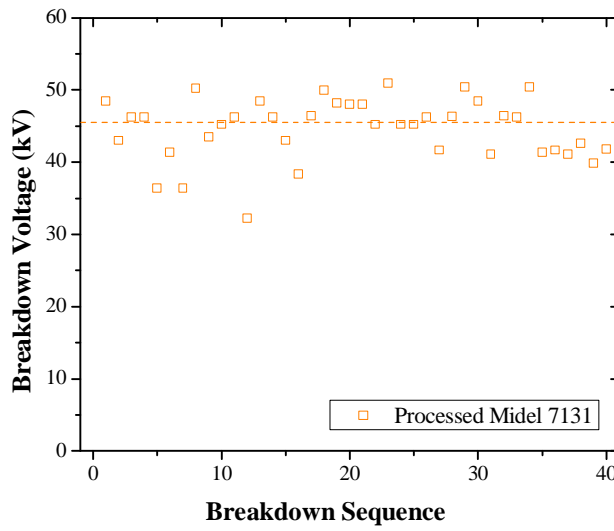


Figure 3.2 AC breakdown voltages of processed Midel 7131

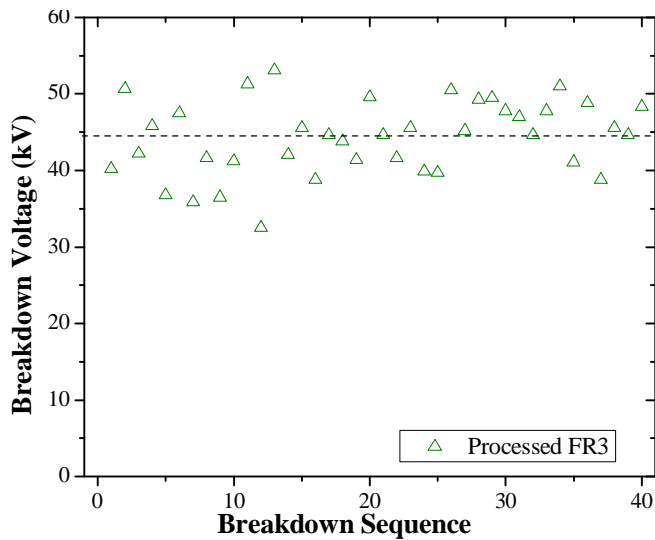


Figure 3.3 AC breakdown voltages of processed FR3

The mean and standard deviation of the breakdown voltages of transformer liquids are calculated and shown in Figure 3.4. It was reported in [143] that the mean breakdown voltage of Gemini X is about 10% lower than that of esters before processing. After processing, the mean breakdown voltages of both mineral oil and esters are increased and the standard deviations are reduced, due to the removal of moisture and particles from liquids. The mean breakdown voltage of Gemini X is 47 kV, which ranks the highest among the investigated liquids. Moreover, the standard deviation of Gemini X is the smallest among all the liquids.

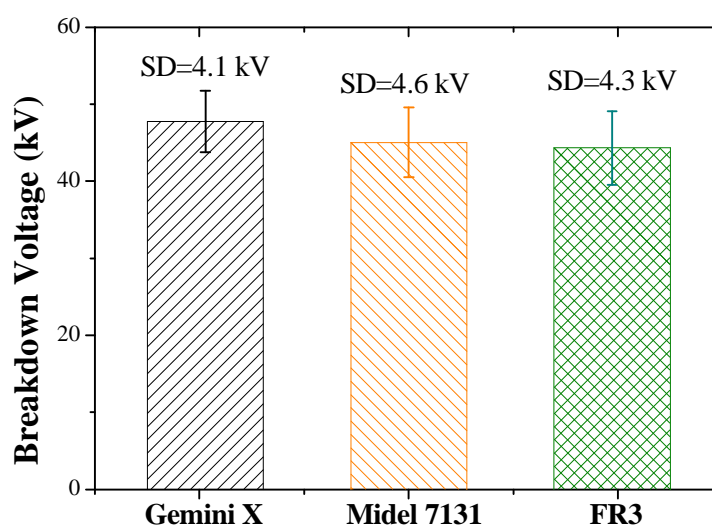


Figure 3.4 Comparison of AC breakdown voltages of processed transformer liquids

Existing international standards [144-146] have already specified the breakdown voltage requirement of new insulating liquids used in power transformers. The minimum breakdown voltage of unused mineral oil for usage in transformers (all voltage ratings) required by IEC 60296 is 70 kV/2.5 mm [144]. The minimum breakdown voltage of untreated synthetic esters required by IEC 60199 for transformer (all voltage ratings) use is 50 kV/2.5 mm [146]. The breakdown voltage of natural esters should be higher than 30 kV/mm as required by IEEE 57.104, for usage in power transformers with a nominal voltage higher than 234 kV [145]. Therefore, the mean breakdown voltages of Gemini X, Midel 7131, and FR3 fulfill the specifications required by these standards. Although the mean breakdown voltage of Gemini X is slightly higher (about 2-3 kV) than those of esters, they can be regarded as similar when considering the safety margins used in transformer insulation design. It should be noted that the transformer liquids used in the

tests are in processed conditions.

3.2.4 Breakdown Voltage Distributions

Under AC voltage, the breakdown process might be triggered by particles, free water or gas bubbles. Thus, the breakdown voltage of a transformer liquid is a statistically distributed quantity. Usually, the mean breakdown voltage and standard deviation are used to represent the breakdown voltage distribution, based on the assumption that the liquid breakdown voltage follows the normal distribution.

Parametric and non-parametric statistical techniques have been widely applied to study the breakdown voltage distribution of transformer liquids [143, 147]. Commonly studied distributions include normal distribution, minimum Gumbel distribution (Double Exponential distribution), and Weibull distribution, whose accumulative functions are given in Equations 3.1 to 3.3 [148]. The Gumbel distribution and Weibull distribution are extreme-value distributions considering the asymmetry between the low and the high failure rates. Although previously published papers concluded that Weibull distribution is the best distribution to model the breakdown voltage of mineral oil [149], it has not yet been determined which distribution is the best to model the breakdown voltages of esters.

$$P_N(E; m, s^2) = \frac{1}{\sqrt{2ps^2}} \int_{-\infty}^E e^{-(t-m)^2/2s^2} dt \quad (\text{Normal}) \quad \text{Equation 3.1}$$

$$P_G(E; m, b) = 1 - e^{-e^{(E-m)/b}} \quad (\text{Gumbel}) \quad \text{Equation 3.2}$$

$$P_W(E; k, l) = 1 - e^{-(E/l)^k} \quad (\text{Weibull}) \quad \text{Equation 3.3}$$

3.2.4.1 Non-parameter Method

The quantile-quantile plot (Q-Q plot) is a graphical method for determining whether two data sets come from the same distribution. If the two data sets come from the same distribution, the points in the Q-Q plot will approximately overlap [150].

Supposing one data set is generated by a theoretical distribution, the Q-Q plot then

become a non-parameter method to study the similarity between a set of data and an expected theoretical distribution [150]. If the breakdown voltage results can be fitted by an expected distribution, they will be approximately overlapped with each other in the Q-Q plot. Figures 3.5 to 3.7 represent the Q-Q plots of the breakdown voltage results and the expected distributions. In these graphs, the measurement results of breakdown voltages are shown as points, and the expected distributions are shown as solid lines.

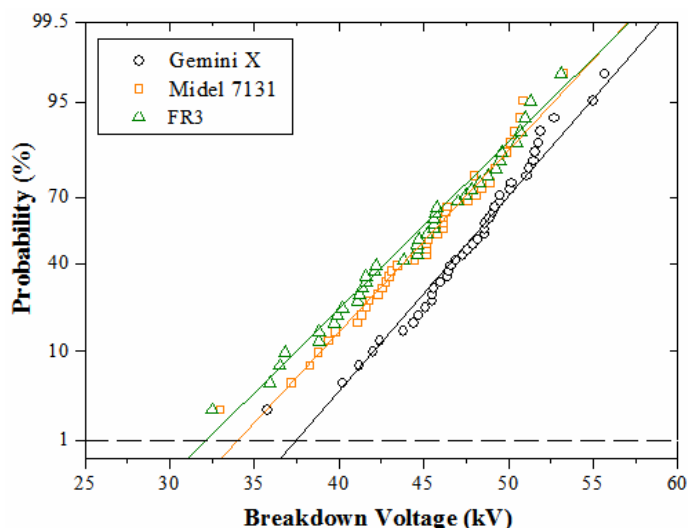


Figure 3.5 Normal distributions of breakdown voltages of transformer liquids

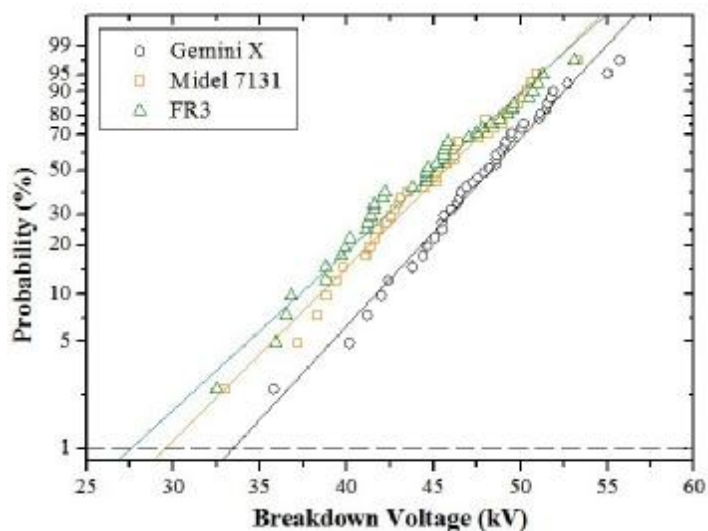


Figure 3.6 Gumbel distributions of breakdown voltages of transformer liquids

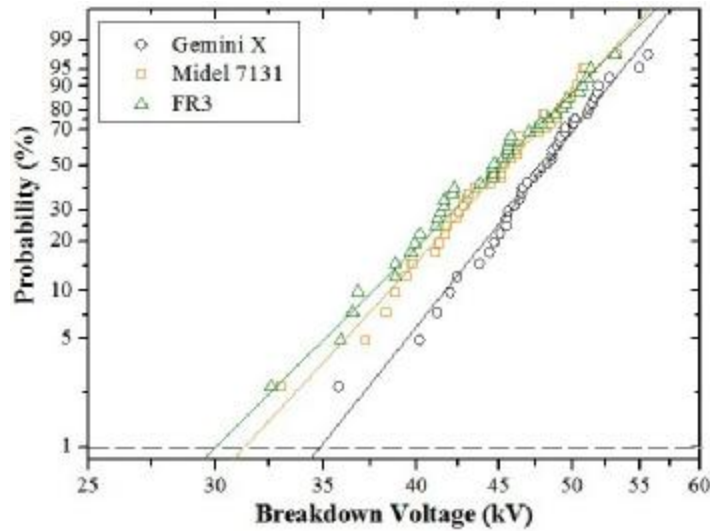


Figure 3.7 Weibull distributions of breakdown voltages of transformer liquids

Between failure rates of 10 % and 90 %, all three distributions give relatively similar fittings of the measurement results of the breakdown voltages for both mineral oil and esters. However at low failure rates (<10 %) and high failure rates (>90 %), the normal distribution gives larger prediction values than the measurement results of the breakdown voltages. The Gumbel distribution gives smaller prediction values than the measurement results of the breakdown voltages. In other words, the normal distribution tends to overestimate the breakdown voltages, and the Gumbel distribution tends to underestimate the breakdown voltage. On the other hand, for Weibull distribution, it seems that the measurement results overlapped well with the prediction values at the whole failure rate range. This indicates that Weibull distribution might be a better function to fit the breakdown voltages of mineral oil and esters than normal distribution and Gumbel distribution.

3.2.4.2 Parameter Methods

In order to confirm the results of non-parameter method, a parameter statistical method, goodness of fit test, is applied to determine best function to fit the breakdown voltage distribution. The idea behind the goodness of fit test is to see whether or not a set of observation data (here are the measurement results of breakdown voltage) comes from an expected distribution [151]. The first step of the goodness of fit test is to make a hypothesis that the observation data come from an expected distribution. Then, each type

of goodness of fit test will define a suitable *Test Statistic*, which is a measurement of the goodness of fit for the expected distribution. The test statistic should be calculated based on the observation data and compared to a pre-tabulated list. The comparison will derive a *Critical p-value*, which is an estimation of the likelihood of the hypothesis. Therefore if the p-value is near to 100%, the hypothesis can be accepted, but if the p-value is near to 0%, the hypothesis should be rejected. At the same time, it is also possible to rank the distributions by comparing their critical p-values.

The Shapiro-Wilk Test for Normality

The Shapiro-Wilk (S-W) test is the most reliable test to determine whether the observation data come from the normal distribution. The W statistic, as defined in Equation 3.4, is used in the S-W test. Table 3.3 lists the statistic values and critical p-values of normal distribution for mineral oil and esters. If the significance level to accept the hypothesis is chosen as 95 %, the results indicate that the hypothesis of normal distribution should not be accepted. Therefore, the breakdown voltages of transformer liquids are not normally distributed, but belong to extreme type distributions. This conclusion can be further confirmed by extending the sample size from 40 breakdowns to 100 breakdowns, when the critical p-values of both mineral oil and esters reduce to 2% [143].

$$W = \frac{(\sum_{i=1}^n a_i x_i)^2}{\sum_{i=1}^n (x_i - \bar{x})^2} \quad \text{Equation 3.4}$$

Table 3.3 Summary of S-W test results of normal distributions for transformer liquids

	Statistic W	P-Value (%)	Accepted (?)
Gemini X	0.9768	57.4	NO
Midel 7131	0.9791	65.6	NO
FR3	0.9798	68	NO

The Kolmogorov-Smirnov Test

The Kolmogorov-Smirnov (K-S) test is commonly used to determine whether the

observation data come from a specified distribution. Firstly, this test assumes that the observation data come from an expected distribution, of which the parameters are estimated from the observation by maximum likelihood. Then it statistically quantifies a distance D between the observation data and the expected distribution as shown in Equation 3.5. An attractive feature of this test statistic is that its distribution always follows normal distribution, and does not depend on the type of the expected distribution. This feature allows an effective comparison of the goodness of fit between various expected distributions. Table 3.4 lists the statistic values and critical p-values of three distributions for mineral oil and esters.

$$D = \max_{1 \leq i \leq N} \left| F(x_i) - \frac{i}{N+1} \right| \quad \text{Equation 3.5}$$

Table 3.4 Summary of K-S test results of various distributions for transformer liquids

Distribution	Oil	Statistic D	P-Value (%)	Accepted (?)
Normal	Gemini X	0.0768	94.81	NO
	Midel 7131	0.0992	78.99	NO
	FR3	0.1029	75.20	NO
Gumbel	Gemini X	0.0818	92.16	NO
	Midel 7131	0.0961	81.98	NO
	FR3	0.1231	53.83	NO
Weibull	Gemini X	0.0705	98.05	YES
	Midel 7131	0.0756	96.30	YES
	FR3	0.0809	95.71	YES

Therefore, the comparison of the K-S test results in Table 3.4 indicates that Weibull distribution gives the best fittings of the breakdown voltages of mineral oil and esters among all the expected distributions, since the p-value of Weibull distribution is the largest among all the expected distributions.

To summarize, the S-W test shows that the breakdown voltage distributions of both mineral oil and esters are extreme type distributions, rather than normal distribution. The K-S test was used to compare the goodness of fit for three expected distributions, and the results show that Weibull distribution is better than normal and Gumbel distributions to fit the breakdown voltage distributions of transformer liquids.

3.3 Withstand Strengths of Transformer liquids

3.3.1 Introduction

Rather than considering the withstand voltage to be a value where the transformer liquids will not fail as a dielectric, the withstand voltage could be considered as a level where the risk of failure is acceptably low [152]. Usually, the failure rate of 1% is regarded as the acceptable level [153, 154], and the dielectric withstand voltage is the breakdown voltage of 1% probability.

During the insulation design of a transformer, the withstand voltage value of transformer liquids should always be used with a sufficient margin to fulfill the safety requirements. It also determines the amount of insulation material used in the transformer, thus determining the scale/size of the transformer [155]. If the withstand voltage of an insulating liquid is small, larger bulk oil gaps and creepage distances should be given to fulfill the safety requirements of a transformer. This will increase both the scale and the overall cost of the transformer. For in-service transformers, the withstand voltages of the transformer liquids might be gradually decreased during the ageing and deterioration process. Thus, transformer liquids with high withstand voltages will ensure the safety operation of a transformer.

3.3.2 Prediction of Withstand Voltages

The most straightforward approach to determine the withstand voltage is to carry out numerous breakdown tests. The withstand voltage should be the breakdown voltage corresponding to the 1% accumulative probability, above which 99% of the breakdowns will occur. The more breakdown tests are carried out, the more accurate the withstand voltage will be determined. However, this method is rather expensive and time-consuming, and is only valid when the breakdown voltage of the test liquid is not influenced by the by-products of frequent breakdowns.

Therefore, it would be of great advantage if the experimental work could be helped by

statistical calculations. The basic concept of the statistical calculation is to find an expected distribution, and the withstand voltage can be then predicted using the distributions based on a limited number of breakdown voltage results.

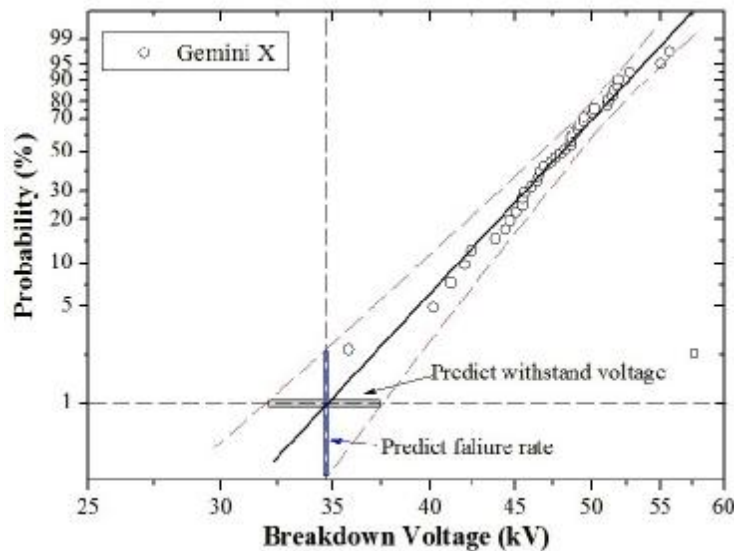


Figure 3.8 Prediction of withstand voltage from breakdown voltage distribution of Gemini X using Weibull fitting

Taking the Weibull distribution as an example, Figure 3.8 shows how to predict the withstand voltage from the breakdown voltage distribution of Gemini X. The solid line is the Weibull fitting of 40 breakdown voltage results and the dash lines represent the 95% prediction confident bounds. Since the withstand voltage is the breakdown voltage with 1% probability, the dielectric withstand voltage of Gemini X can be obtained from the intersection of the Weibull fitting curve and the 1% failure rate. The graph shows that the withstand voltage of Gemini X is 34.6 kV. However, the prediction result always comes with an inevitable uncertainty, which can be evaluated by the 95 % *Confidence interval*. In this graph, the 95 % confidence interval indicates that the actual value of the withstand voltage of Gemini X might not be exactly 34.6 kV, but around this value. There is 95 % probability that the actual withstand voltage is between 32.1 kV to 37.8 kV. Thus, the withstand voltage of Gemini X is 34.6 kV, with 95 % confidence interval from 32.1 kV to 37.8 kV.

For Midel 7131 and FR3, similar predictions can be made. Table 3.5 lists the prediction results of the withstand voltages of mineral oil and esters using Weibull distribution, and

the corresponding 95 % confidence intervals. It can be seen that the withstand voltages of Midel 7131 and FR3 are significantly lower than that of Gemini X. If we consider the confidence interval, it might be more reliable to use the lower limit of the confidence interval as the criterion for insulation design than the predicted withstand voltage.

Table 3.5 Prediction of withstand voltages using Weibull distribution

	Gemini X	Midel 7131	FR3
$U_{1\%}$ (kV)	34.6	31.4	30.2
95% Confidence interval (kV)	[32.1, 37.8]	[30.2, 34.9]	[27.6, 33.5]

From Figure 3.8, we can also obtain the failure rate of Gemini X at a given voltage using Weibull distribution. At 34.6 kV, the failure rate of Gemini X is 1 %, with 95 % confidence interval from 0.29 % to 2.61 %. Use the same method, the failure rates of transformer liquids at specified voltage can be estimated using Normal distribution and Gumbel distribution. Table 3.6 lists the 95 % confidence intervals of the failure rates for transformer liquids at specified voltages. The confidence intervals are predicted by Weibull distribution, normal distribution and Gumbel distribution respectively.

Table 3.6 Prediction results of failure rates and 95% confidence intervals at specified voltages using three distributions

	Weibull	Normal	Gumbel
Gemini X (34.6 kV)			
Failure rate	1.00%	0.07%	1.07%
$P_{up95\%}$	2.61%	0.41%	2.95%
$P_{low95\%}$	0.29%	0.02%	0.49%
Midel 7131 (31.4 kV)			
Failure rate	1.00%	0.12%	1.34%
$P_{up95\%}$	1.95%	0.55%	2.95%
$P_{low95\%}$	0.20%	0.007%	0.49%
FR3 (30.2 kV)			
Failure rate	1.00%	0.23%	1.75%
$P_{up95\%}$	2.45%	2.83%	0.99%
$P_{low95\%}$	0.27%	0.41%	0.17%

3.3.3 Examination of Withstand Voltages

Although the statistical method confirms Weibull fitting as the best fitting to model the breakdown voltage distribution, it is not known for sure whether the predicted withstand voltages using Weibull distribution are the actual values. The most straightforward method to the examinations of the prediction results can be achieved by carrying out numerous tests. If the failure rates at the predicted withstand voltages are around 1 %, the prediction results can be accepted. Otherwise, the prediction results should be rejected.

3.3.3.1 Experiments

500 withstand tests were carried out for each type of transformer liquid to examine the prediction results. The same test configuration and the same time interval between successive tests were used as described in Appendix I.4. The applied voltage is increased continuously from 0 kV up to the predicted withstand voltage at a rate of $0.5 \text{ kV/s} \pm 5 \%$. The prediction results of withstand voltages using Weibull distribution are 34.6 kV for Gemini X, 31.4 kV for Midel 7131 and 30.2 kV for FR3.

3.3.3.2 Results and Analysis

During the tests, the by-products from a previous breakdown, such as carbon particles or gas bubbles, might reduce the breakdown voltage of later breakdowns. Therefore, it is necessary to ensure that the qualities of transformer liquids were similar before and after the withstand tests. In order to remove the gas bubbles by-products from the liquid gap between electrodes, a magnetic stir worked continuously. During the tests, no visible bubble was observed when the voltage was stressed on the liquid gap. Table 3.7 shows the comparison between the water contents and particle contents of transformer liquids before and after the withstand tests. It can be seen that the water and particle contents were only increased slightly after the withstand tests, even considering possible contaminations during the test. The similarity indicates that the withstand tests are independent of each other, and thus the test results are credible.

Table 3.7 Water and particle contents of transformer liquids before and after tests

Oil	Water (ppm)		Particle (> 5µm per 100ml)	
	Before	After	Before	after
Gemini X	<2	4.5	427	1230
Midel 7131	70	98	350	980
FR3	30	138	320	1450

Figures 3.9 to 3.11 represent the results of the withstand tests for both mineral oil and esters. The solid dots stand for the tests with no breakdown, and the hollow dots show the tests in which the breakdown occurs. In the 500 withstand tests, Gemini X failed 7 times, Midel 7131 failed 3 times, and FR3 failed 5 times. Thus, the failure rates at the applied voltages could be calculated as the number of breakdowns divided by the number of tests (n=500), which is 1.4 % for Gemini X, 0.6% for Midel 7131 and 1.0 % for FR3. Since the failure rates of transformer liquids at the withstand voltages (predicted) are near to 1 %, the prediction of withstand voltages using Weibull distribution seems to be credible.

However, it should be noted that the calculated failure rates values from 500 withstand tests are not precise. This is because the withstand tests have random features, thus the calculated values only give a rough idea about what the failure rates are at the applied voltages. In order to more precisely evaluate the failure rates and examine the credibility of the predicted withstand voltages, the confidence intervals of the failure rates at the predicted withstand voltages should be calculated.

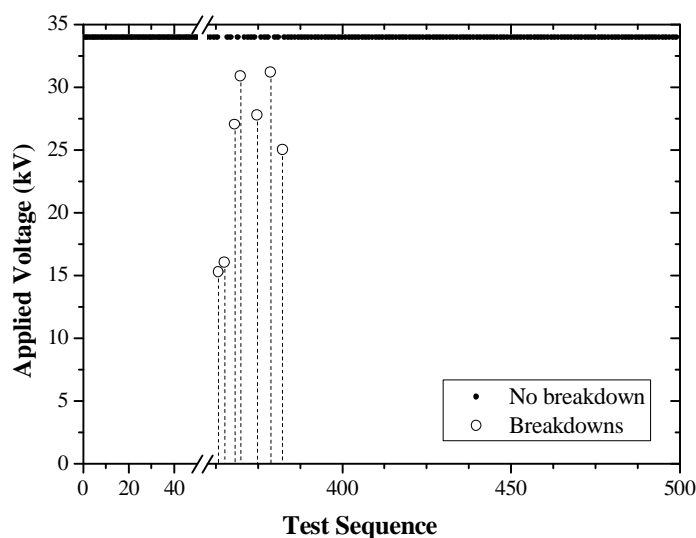


Figure 3.9 Results of 500 withstand tests for Gemini X

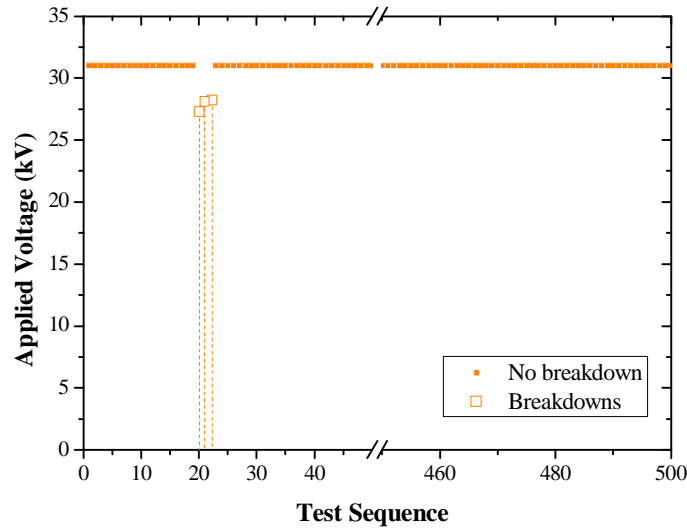


Figure 3.10 Results of 500 withstand tests for Midel 7131

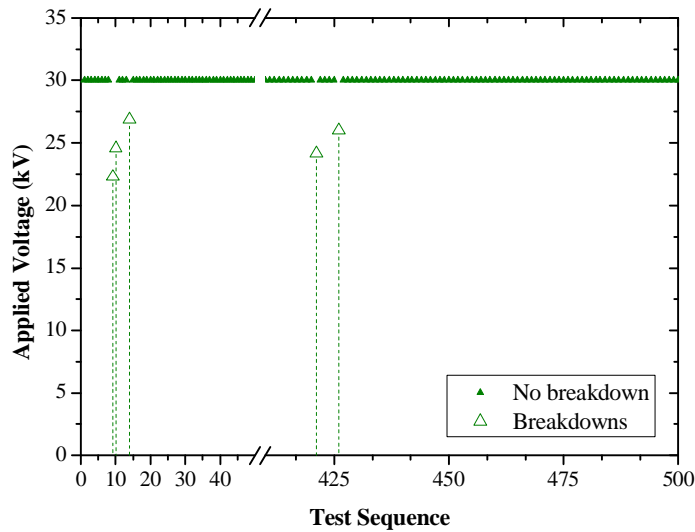


Figure 3.11 Results of 500 withstand tests for FR3

3.3.3.3 Estimation of Confidence intervals

From a statistical point of view, it is impossible to obtain the exact value of the failure rate based on a limited number of withstand tests. For example, Figure 3.12 shows the probability distribution of breakdown numbers in 500 withstand tests. If 5 breakdowns occurred in 500 withstand tests, the failure rate might be 0.5 % or 1 %, or any values between 0 % and 100 %. However, the graph indicates that the failure rate is likely to be between 0.5 % and 2 %, and nearly impossible to be larger than 5%. Therefore, the failure rate is all about probabilities. In order to estimate the failure rate based on the test results, the most suitable way is to calculate a range in which the failure rate is most likely to be. This range is called the confidence interval of the failure rate, and usually the confidence interval level is chosen as 95 %, which indicates that the actual failure

rate has a 95 % probability to be within this confidence interval.

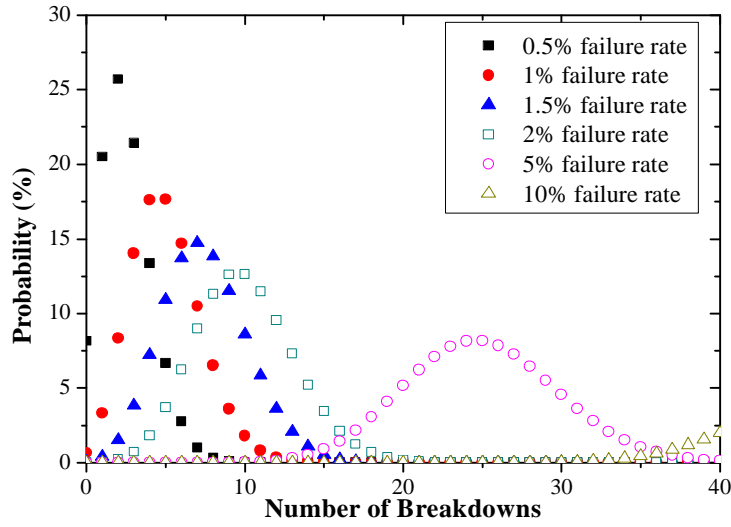


Figure 3.12 Probability distributions of breakdown numbers in 500 withstand tests

The estimations of the failure rates of transformer liquids at predicted withstand voltages could be obtained using Bayes’ theorem, as shown in Equation 3.6. Bayes’ theorem is used to calculate the aim conditional probability (i.e. the failure rate at a given voltage when the number of breakdowns is known) based on the original conditional probability (i.e. the number of breakdowns at a given voltage when the failure rate is known), which is the reverse of the previous one. In Equation 3.6, the $P(A=x/n)$ is the desired aim function of the failure rate based on the withstand test results (n breakdowns occurred in m withstand tests, known). The $P(n/A=x)$ is the original probability of the breakdown numbers based on the failure rate (the failure rate is x , known). The $P(A)$ is the expected occurrence probability of a specified failure rate without carrying out the withstand tests.

$$P(A = x | n) = \frac{P(A = x, n)}{P(n)} = \frac{P(n | A = x)P(A)}{\int_{-\infty}^{+\infty} P(n | A = x)P(A)dx} = \frac{C_m^n x^n (1-x)^{m-n} P(A)}{\int_{-\infty}^{+\infty} C_m^n x^n (1-x)^{m-n} P(A)dx} \quad \text{Equation 3.6}$$

Based on the test results, Bayes equations could be rewritten into Equations 3.7 to 3.9 for Gemini X, Midel 7131 and FR3 respectively. Their probability density and accumulative probability are plotted in Figures 3.13 to 3.15.

$$P(A = x | n = 7) = \frac{C_{500}^7 x^7 (1-x)^{493} P(A)}{\int_0^1 C_{500}^7 x^7 (1-x)^{493} P(A)dx} = \frac{x^7 \cdot (1-x)^{493}}{1.3431 \cdot 10^{-18}} \quad (\text{Gemini X}) \quad \text{Equation 3.7}$$

$$P(A = x | n = 3) = \frac{C_{500}^3 x^3 (1-x)^{497} P(A)}{\int_0^1 C_{500}^3 x^3 (1-x)^{497} P(A) dx} = \frac{x^3 (1-x)^{497}}{9.6386 \cdot 10^{-11}} \quad (\text{Midel 7131}) \quad \text{Equation 3.8}$$

$$P(A = x | n = 5) = \frac{C_{500}^5 x^5 (1-x)^{495} P(A)}{\int_0^1 C_{500}^5 x^5 (1-x)^{495} P(A) dx} = \frac{x^5 (1-x)^{495}}{7.8199 \cdot 10^{-15}} \quad (\text{FR3}) \quad \text{Equation 3.9}$$

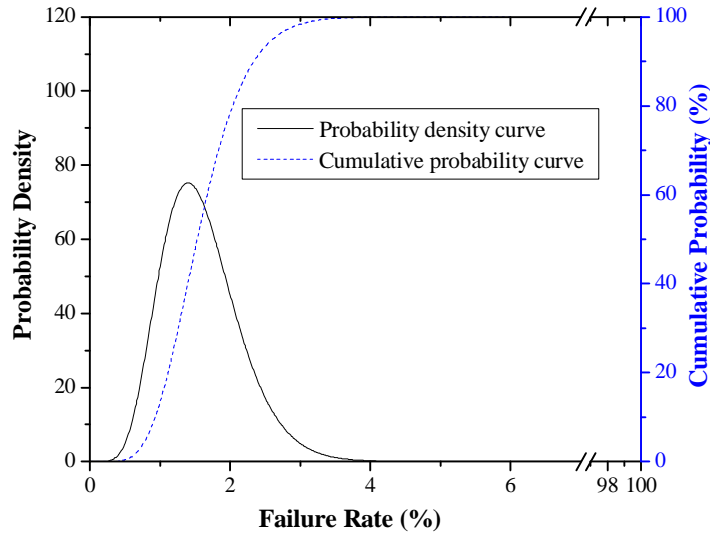


Figure 3.13 Probability density and cumulative probability of failure rate for Gemini X

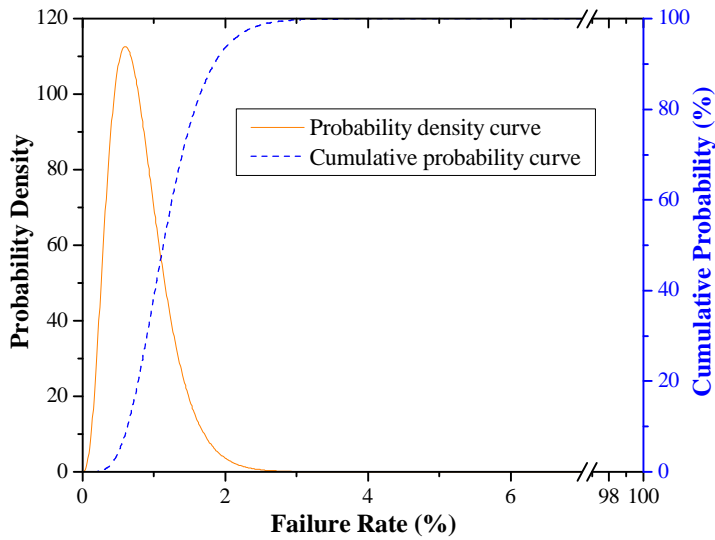


Figure 3.14 Probability density and cumulative probability of failure rate for Midel 7131

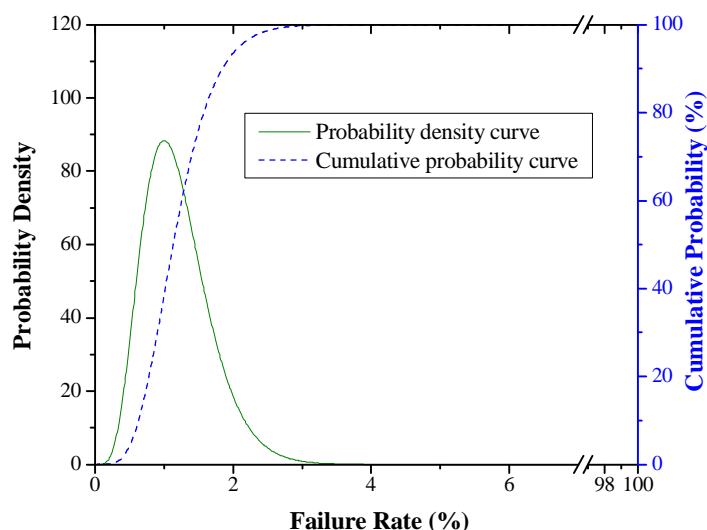


Figure 3.15 Probability density and cumulative probability of failure rate for FR3

The results show that the probability density curves of the failure rates of both mineral oil and esters are distributed from 0 % to 100 % following the extreme distributions. Their location of the peak values on the x-axis correspond to the ratio of the breakdown number and the total test number. These peak values only represent the failure rate of the maximum probability, without showing their confidence intervals. In the graphs, the cumulative probabilities of the failure rates are calculated as the integration of the probability density, and the confidence intervals can be determined. Therefore, the failure rates and the 95 % confidence intervals at the predicted withstand voltages for transformer liquids (34.5 kV for Gemini X, 31.4 kV for Midel 7131, 30.2 kV for FR3) could be obtained, as shown in Table 3.8.

Table 3.8 95% confidence intervals of failure rate for transformer liquids

	Gemini X	Midel 7131	FR3
Predicted withstand voltage (kV)	34.6	31.4	30.2
Failure rate (%)	1.4	0.6	1.0
95% confidence interval (%)	[0.79, 2.53]	[0.28, 1.53]	[0.51, 2.08]

3.3.4 Comparison of Prediction Results and Measurement Results

Since Table 3.6 shows the prediction results of the failure rates and confidence intervals at withstand voltages using three distributions while Table 3.8 shows the actual test results, a comparison of Table 3.6 and Table 3.8 will confirm which distribution can be used to fit the breakdown voltage distribution and to predict the withstand voltage.

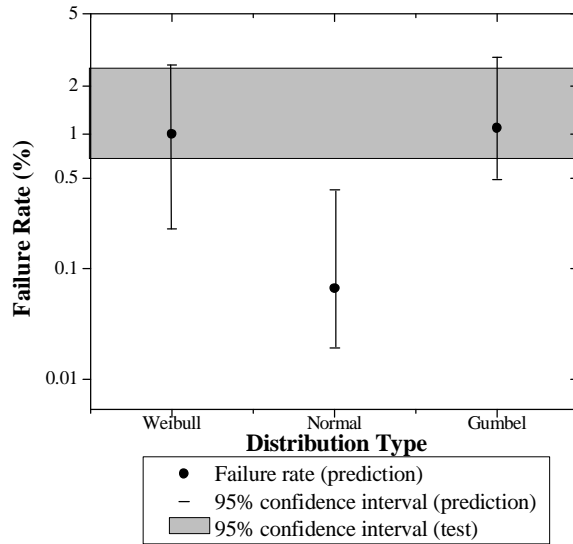


Figure 3.16 Evaluations of prediction results for Gemini X using various distributions

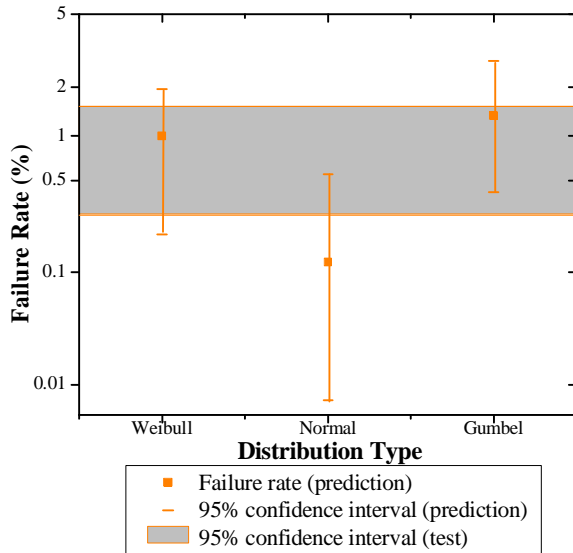


Figure 3.17 Evaluations of prediction results for Midel 7131 using various distributions

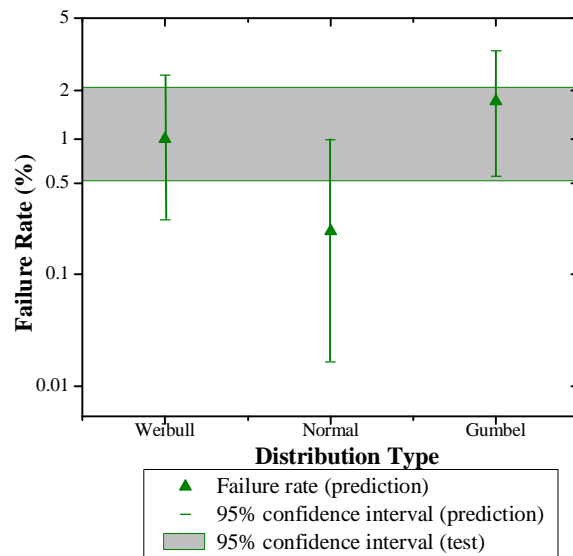


Figure 3.18 Evaluations of prediction results for FR3 using various distributions

Figures 3.16 to 3.18 represent comparisons for Gemini X, Midel 7131 and FR3 respectively. For Weibull distribution, the prediction confidence intervals include the test confidence intervals for both mineral oil and esters. This indicates that the prediction using Weibull distribution will provide correct results, although not completely accurate. Therefore, Weibull distribution can be used to fit the breakdown voltage distribution and to predict the withstand voltage of transformer liquids. For normal distribution, the prediction confidence intervals do not include (for Gemini X) or only include a part of (for Midel 7131 and FR3) the test confidence intervals. This indicates that the prediction using normal distribution would or might provide wrong results. Therefore, normal distribution should not be used. Similarly, neither should Gumbel distribution.

3.4 Particle Effect on Breakdown Voltages

For in-service power transformers, the presence of particles in the transformer liquids is unavoidable but can be controlled by purification. The particles have a detrimental effect on the dielectric strengths of transformer liquids, and they account for one of the main failure mechanisms in large power transformers [53]. Although numerous research studied the particle effect on the dielectric strength of mineral oil [11, 62, 156], there is a lack of information regarding the particle effect on the breakdown voltage of esters. Since the chemical compositions and physical properties of esters are significantly different from those of mineral oil, it is expected that the particle effect on the AC breakdown voltage of transformer liquids may differ. In this section, the breakdown voltages of transformers liquids are comparatively studied with different particle materials at various particle amounts.

3.4.1 Contaminations in Power Transformers

The absorption spectroscopy analysis and microscopic observation indicate that the majority of particles presented in transformer liquids are pressboard dusts or cellulose fibres. Besides, metallic particles such as iron, aluminium, and copper, can be found in the transformer liquids as well, but in relatively smaller amounts [53]. Based on the reports of in-service transformers by various countries, the CIGRE working group 12.17

has recommended a classification method of the contamination levels encountered during the operation of power transformers [53]. The contamination levels are classified by the particle content in 100 ml transformer liquid samples, and the classification criteria are listed in Table 3.9. The corresponding contamination levels of NAS and ISO classifications and typical occurrence situations of these contamination levels are also listed in the same table.

Table 3.9 Contamination levels recommended by CIGRE working group 12.17 [53]

Levels	Particle content		NAS	ISO	Occurrence
	>5 μm	>15 μm			
Nil	250	32	00	1-8	IEC cleanness for sampling bottles
Low	1000	130	1-2	9-10	Factory oil cleanliness in acceptance test
Normal	32000	4000	3-7	11-15	Typical value for new transformers
Margin	130000	16000	8-9	16-17	Long-term in service transformers
High	>130000	>16000	>10	>17	Transformers of abnormal operation

3.4.2 Experimental Description

Previous research has indicated that the existence of both water and particles in the transformer liquids can reduce their breakdown voltages significantly. In order to study the particle effect without the influence of water, well-dehydrated transformer liquid samples were investigated in this section. At first, the transformer liquids were purified, dehydrated, and degassed as described in Appendix I.3. The relative water contents were less than 5 % for both mineral oil and esters after processing. The particle contaminations were cellulose powder (product code: 4021050) and copper powder (product code: C712050) purchased from Fisher Scientific Ltd in UK, and they were dried overnight in an air-circulating oven at 80 °C. Then, the processed liquid samples were artificially contaminated by the particles and stirred for at least 15 minutes to ensure the even distribution of particles in liquids. The particle contents in the contaminated samples were measured using the HIAC particle counting system as described in Appendix I.2.3. Table 3.10 lists the typical size distributions of cellulose and copper particles in contaminated liquid samples. In this experiment, the contamination level is expressed in terms of the number of particles with diameters larger than 5 μm per 100 ml volume liquid, which is the same as that used in the CIGRE report [53].

Table 3.10 Size distributions of cellulose and copper particles in artificially contaminated liquid samples of 100 ml

Particle size (μm)	1-5	5-15	15-25	25-50	50-100	100-200	>200
Number (cellulose particles)	16536	6706	1163	286	26	0	0
Number (copper particles)	29490	15480	3590	3300	720	10	0

The measurements of the breakdown voltages were carried out using the same configurations and the same test procedures as described in Appendix I.4. At least 40 breakdown voltages were measured for each liquid sample to obtain their mean breakdown voltages and standard deviations. An electromagnetic stir worked constantly to ensure the even distribution of particles and avoid the agglomeration of particles at the bottom of the test container. When changing the liquid samples, the test container was carefully cleaned to avoid contamination from the previous liquid sample.

3.4.3 Experimental Results

3.4.3.1 Influence of Cellulose Particles

Figure 3.19 plots the mean breakdown voltages and the standard deviations as a function of the cellulose particle contents in both mineral oil and esters. In the graph, the contamination levels are represented by the shaded areas from light to dark. The results show that the breakdown voltages of both mineral oil and esters are decreased with the increase of the cellulose particle contents. However, the breakdown voltage of mineral oil seems to be more sensitive to the cellulose particle content than those of esters. For example, the breakdown voltage of clean Gemini X exceeds that of clean FR3, but it drops quickly and takes up only 70 % of the breakdown voltage of FR3 at a particle content of 10,000 per 100 ml liquid sample.

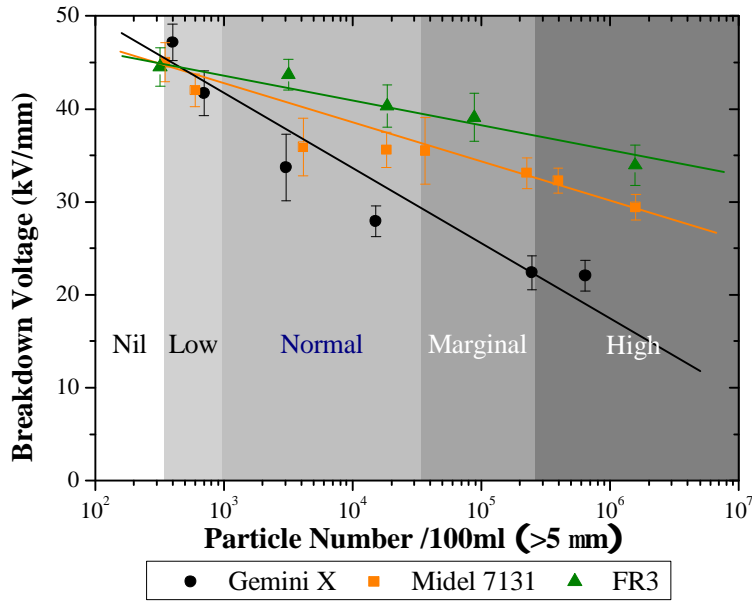


Figure 3.19 Breakdown voltages and standard deviations of transformer liquids contaminated by cellulose particles

The IEC and IEEE have published standards for the maintenance of transformer liquids, in which the satisfactory criteria of the breakdown voltages for continuous use are defined [145, 157, 158]. For mineral oils used in power transformers with a nominal voltage above 170 kV, the satisfactory criterion of the breakdown voltage is 50 kV/2.5 mm. For natural esters used in power transformers with a nominal voltage above 230 kV, the criterion of breakdown is 50 kV/2 mm. For synthetic esters, the breakdown voltage above 45 kV/2.5 mm is considered to be satisfactory to be used in power transformers with all voltage ratings. Although slightly different, their criterion values are in the range of 18 - 25 kV/mm.

The contamination levels defined in Table 3.9 by CIGRE are based on conventional mineral oils. The criterion value of the particle content between the normal state and the marginal state of an in-service power transformer is 130,000 particles (>5 μm) per 100 ml sample. For Gemini X as shown in Figure 3.19, this criterion value corresponds to a breakdown voltage of 22.5 kV/mm, which is in good agreement with the IEC regulation of the breakdown voltage criterion. However, since the influence of cellulose particles on the breakdown voltages of esters are different from those of mineral oil, the classification of the contamination levels used for mineral oil might not be suitable for esters. As an example, the criterion value (45 kV/2.5 mm) of the breakdown voltage for Midel 7131

corresponds to a cellulose particle content above 10,000,000 (>5 μm per 100ml sample). Therefore, it is suggested that the classification criterion of the cellulose particle content should be increased for esters. Since cellulose is the main contamination type in transformer liquids of in-service qualities, this conclusion indicates that the breakdown performances of esters are relatively superior to those of mineral oil in the presence of cellulose particles. The esters might be able to maintain good dielectric performances even being contaminated during transformer operation.

3.4.3.2 Influence of Metallic Particles

The metallic particles exist in the transformer liquids of in-service qualities in relative smaller amounts, but they have more detrimental effect on the breakdown voltages compared with cellulose particles. Figure 3.20 plots the mean breakdown voltages and standard deviations as the function of the copper particle content in both mineral oil and esters. The copper particles are chosen to be investigated because they are one of the commonly found metallic particles in transformer liquids, and they will not be attracted to the magnetic stir used in breakdown voltage tests like the iron particles. In the graph, the contamination levels are expressed as a reference by the shaded areas from light to dark.

The results show that the presence of copper particles will reduce the breakdown voltages of both mineral oil and esters. The breakdown voltage of Gemini X reduces faster than those of Midel 7131 and FR3 with the increase in copper particle content. For example, a particle content of 3,000 (>5 μm per 100 ml liquid) reduces the breakdown voltage of Gemini X by 60 %, but it will only reduce the breakdown voltage of Midel 7131 by 30 %. Compared with cellulose particles, the reduction of breakdown voltages in the presence of copper particles is more significant than that of cellulose particles.

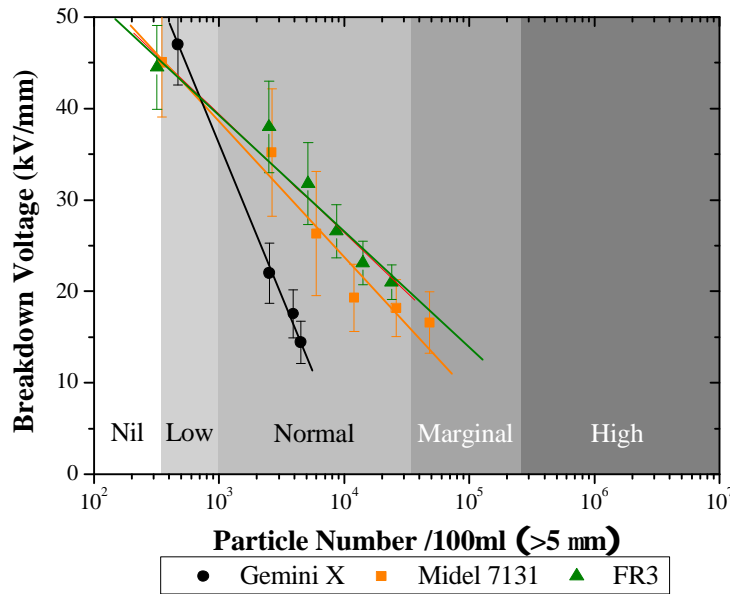


Figure 3.20 Breakdown voltages and standard deviations of transformer liquids contaminated by copper particles

Since the majority of particles presented in transformer liquids are pressboard dusts or cellulose fibres, the contamination classification recommended by CIGRE might not be suitable for transformer liquids contaminated by pure copper particles. For example, the cellulose particle content of 130,000 (>5 μ m per 100ml sample) will lead to the unacceptable breakdown voltage less than 50 kV/2.5 mm for Gemini X, but the copper particle content of only 2,500 will lead to the unacceptable breakdown voltage for Gemini X. For Midel 7131 and FR3 contaminated by copper particles, the unacceptable breakdown voltages correspond to particle contents (>5 μ m per 100 sample) of 10,000 and 20,000 respectively.

Therefore, the metallic particles will harm the dielectric performances of the transformer liquids the most among all the contaminations encountered in transformer liquids of in-service qualities. Since the metallic particles are mainly from the transformer manufacturing process or from the auxiliary components such as the pumps or coolers, it is suggested that when the transformer tanks are filled with insulating liquids, the transformer liquids should be circulated and purified for several passes in order to remove the metallic particles within transformer tanks. The results also indicate that esters are able to maintain higher breakdown voltages during transformer operations when insulating liquids are contaminated, and thus provide better dielectric performances

and more operation safety than conventional mineral oil.

3.4.4 Influence of Viscosity on Breakdown Voltages

It is well-known that the breakdown voltages of transformer liquids are related to their viscosities. In the presence of particles, research has confirmed that the breakdown voltage of a transformer liquid with high viscosity is relatively higher than that with low viscosity. Pompili compared the dielectric performances of two transformer liquids with similar chemical structures and physical properties [159], and the breakdown voltage of the liquid with a viscosity of 13.0 cts is about 20 % higher than that with 9.0 cts viscosity at ambient temperature. For the same type of transformer liquid, Clark found that the breakdown voltage reduces with an increase of environmental temperature in the range of 20 °C and 80 °C, as shown in Figure 3.21 [83]. This reduction is attributed to the decrease in viscosity at higher temperature. However, Nelson found that the breakdown voltage of mineral oil increases at first and then decreases, with the increases of temperature [160]. It is concluded that although the reduction of viscosity at elevated temperatures increases the breakdown voltage, the reduction of the relative water content, due to higher water saturation level at higher temperatures, increases the breakdown voltages of transformer liquids.

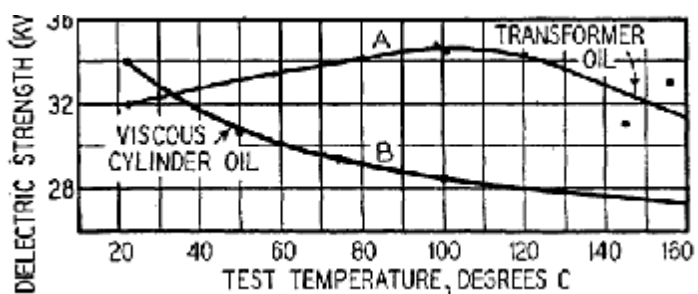


Figure 3.21 Dielectric strengths of transformer liquids with temperature [83]

In order to summarize the particle effect, the relationships between the breakdown voltages and the particle contents are fitted using the function as shown in Equation 3.10, in which N is the number of particles, and d is the maximum particle size [80].

$$E(N) = a \cdot \ln(N \cdot d) + b \quad \text{Equation 3.10}$$

Since the same type of particles was added into liquid samples, the maximum particle sizes were the same for all the tests. Therefore, Equation 3.10 could be written as Equation 3.11, in which a' and b' are determined by the liquid type.

$$E(N) = a' \cdot \ln(N) + b' \tag{Equation 3.11}$$

Table 3.11 lists the curve fitting parameters between the breakdown voltages and the particle contents for both mineral oil and esters. The parameter a' stands for the reduction rate of the breakdown voltage with the increase of the particle content. It is noticed that a' is inversely proportional to the viscosity of the transformer liquid, and a' can be approximated by the division of an arbitrary value and the viscosity of the transformer liquid. The arbitrary values are -90 and -400 for cellulose particles and copper particles respectively. Therefore, the particle effect on the breakdown strength of transformer liquids seems to be related to their viscosities.

Table 3.11 Curve fitting parameters for particle effect on liquid breakdown voltages

Particle	Parameter	Mineral oil	Synthetic ester	Natural ester
	Viscosity (Cst)	12	28	32
Cellulose	b'	62.91	52.60	53.22
	a'	-7.45	-3.71	-2.98
	-90/viscosity	-7.5	-3.22	-2.82
Copper	b'	133.87	78.12	76.72
	a'	-32.60	-13.55	-12.96
	-400/viscosity	-33.33	-14.29	-12.50

The relation between the breakdown voltages of transformer liquids and their viscosity can be expressed by Equation 3.12, in which N is the number of particles ($>5\mu\text{m}$) per 100 ml sample, η is viscosity of the transformer liquid, K is a value determined by the particle material (90 for cellulose, and 400 for copper), and V is a constant value determined by the type of the transformer liquid.

$$E(N) = -\frac{K}{h} \cdot \ln(N) + V \tag{Equation 3.12}$$

For a transformer liquid, the reduction of the viscosity results in the ‘loosening up’ of the liquid molecules, which favours the mobility of charge carriers and thus favours the breakdown process in the liquid [60, 64, 159, 161]. When the liquid is stressed in an electric field, the particles will be polarized and will function as charge carriers. When a charge carrier approaches an electrode, the local field will be enhanced, and small partial discharges might be produced between the particle and the electrode. In a transformer liquid with low viscosity, the mobility of the charge carriers is relatively high due to a smaller viscous drag force. This will result in a higher probability of producing partial discharges [162], and thus a lower breakdown voltage. In the same electric field, the metallic particles contain more charge than the cellulose particles of the same size. Thus, a higher electrical force will be applied on the metallic particles, resulting in higher mobilities and higher probability to breakdown. Consequently, the breakdown voltages of transformer liquids are reduced more significantly in the presence of metallic particles than cellulose particles.

3.4.5 Particle Movement in Transformer Liquids

To confirm the influence of viscosity on the breakdown strengths of transformer liquids, the motion of a single conductive particle and its effect on AC breakdown voltages of the liquids was investigated. It was confirmed that the motion of particles in a transformer liquid is closely related to its viscosity, thus the breakdown voltage of the transformer liquid is also dependent on its viscosity.

3.4.5.1 Test Setup

The test setup is schematically illustrated in Figure 3.22. Two parallel brass electrodes of 45 mm in diameter were utilized and the separation between them was set at 10 mm. This electrode system was placed in a transparent glass container filled with transformer liquids. The AC voltage was provided by a single phase transformer up to 70 kV. A 500 k Ω resistor was connected between the high voltage supply and the test container to limit the current when a breakdown occurs.

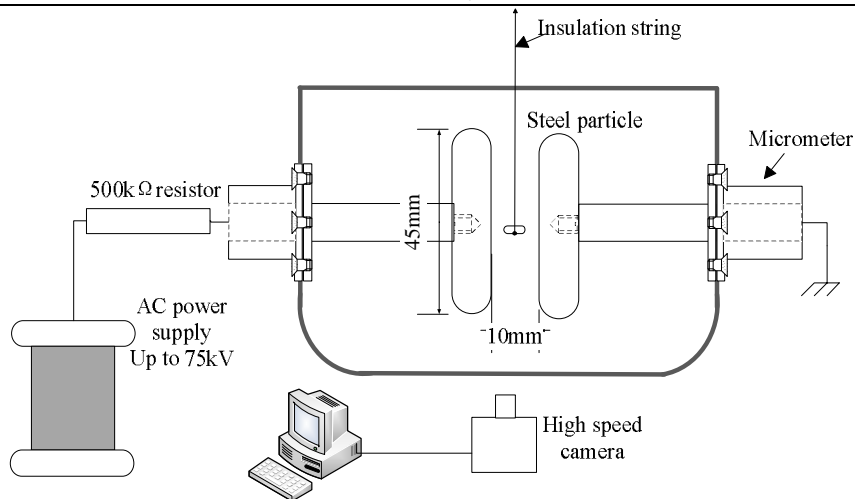


Figure 3.22 Schematic diagram of experimental setup for particle movement test

A steel cylinder particle was suspended by an insulation string between the electrodes. This particle is 0.8 mm in diameter and 3 mm in length. It can move freely in horizontal direction. During the experiment, the particle motion was recorded by a high speed CCD video camera, which worked at 3000 fps.

3.4.5.2 Results and Discussions

During the tests, the applied voltage was increased from 0 kV at a constant speed of 0.5 kV/s until the breakdown occurs. The particle motion between electrodes was recorded. It is found that the particle motion can be divided into three stages.

- Applied voltage $\leq V_{\text{threshold}}$

When the steel particle is placed between the electrodes, the particle will be charged since it is exposed to the electric field [56]. If the applied voltage is low, the electrostatic force applied on the charged particle is so small that no motion is observed. If the applied voltage reaches a certain threshold value ($V_{\text{threshold}}$), the electrostatic force will exceed the resistance force, and the particle starts to move toward the electrode. It is observed that the $V_{\text{threshold}}$ depends heavily on the position of the particle. Figure 3.23 depicts the threshold voltages for the steel particle in various transformer liquids versus its position. The threshold voltage is the highest when the particle is suspended in the central line between the electrodes. The results also show that the threshold voltage is independent of the type of liquid. This probably means that the viscous resistance has little influence on

the particle motion at the moment when it starts to move.

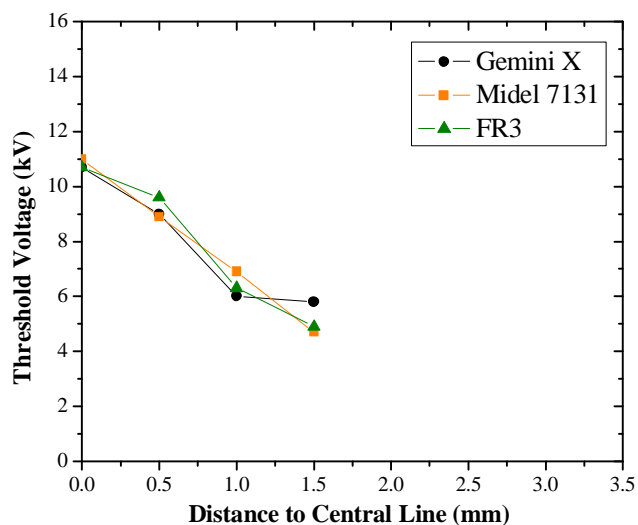
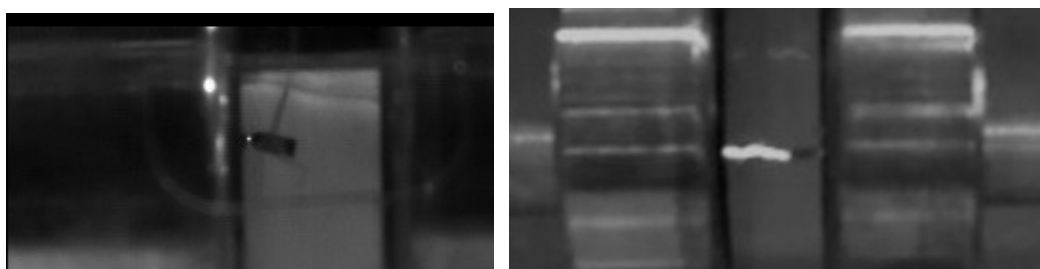


Figure 3.23 Threshold voltages of particle motions in transformer liquids

$$- V_{\text{threshold}} < \text{Applied voltage} < V_{\text{swing}}$$

When the applied voltage exceeds the threshold voltage, the steel particle starts to move back and forth between the electrodes. At relatively low voltages, the particle touches with only one electrode. When the particle approaches the electrode, small discharges might be produced between the particle and the electrode in the form of sparks, as shown in Figure 3.24 (a). The small sparks will not go across the particle, so no breakdown is developed between the electrodes.



(a) Spark

(b) Breakdown

Figure 3.24 Phenomena of spark and breakdown during particle motion

The particle motion was recorded by a high speed video camera. Its position was measured from each frame of the video clips. Figure 3.25 depicts the typical motions of particle in various transformer liquids at the applied voltage of 20 kV. The x-axis is the frame number of the recording, with the inter-frame interval of 0.33 ms. The y-axis is the

horizontal distance between the particle edge and the electrode. It seems that the motion of particle depends heavily on the type of liquid. The particle moves faster and travels further in Gemini X than in Midel 7131 and FR3. Since Midel 7131 and FR3 are more viscous than Gemini X, the viscous drag forces provided by Midel 7131 and FR3 are larger than those of Gemini X. Thus, the motions of particle in Midel 7131 and FR3 face more resistance, so the speeds are slower and the travelling distances are shorter.

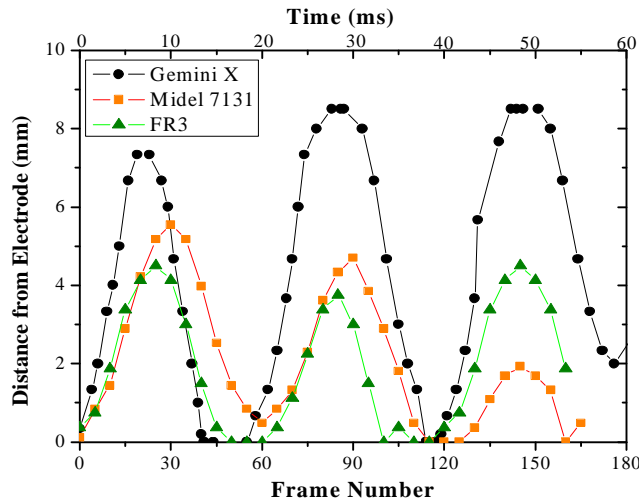


Figure 3.25 Particle motions in transformer liquids at 20 kV

- Applied voltage $\geq V_{swing}$

When the applied voltage is further increased and reaches a certain level (V_{swing}), the particle swings in the oil gap, touching with both electrodes. The V_{swing} values of particle motion in various transformer liquids are shown in Figure 3.26.

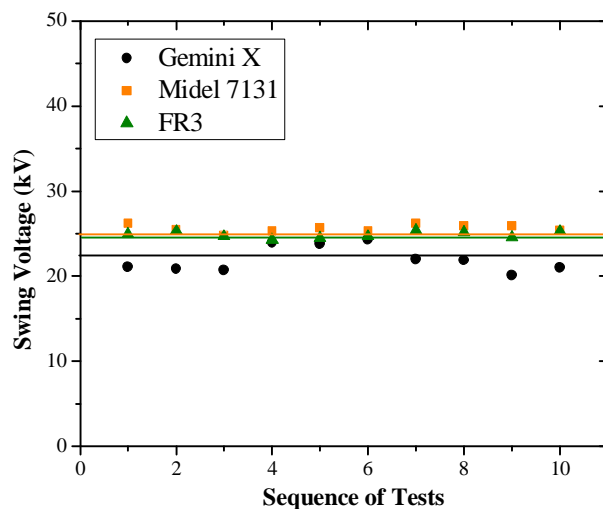


Figure 3.26 Swing voltages of particle motion in transformer liquids

As particle motion is dependent on the viscosity of the liquid, so is the swing voltage. Thus, the swing voltage of Gemini X is about 2 kV lower than that of Midel 7131 and FR3.

When the particle swings between electrodes, breakdowns might occur when the particle touches the electrodes, usually the one with positive potential. The particle acts like the extension of the electrode, which is similar to forming a rod plate electrodes system, and the arc is then developed between the steel particle and the opposite electrode, as shown in Figure 3.24 (b). For Gemini X, the breakdown occurs shortly after the applied voltage reaches its swing voltage, usually during the first few cycles of the swing motion. However for Midel 7131 and FR3, the breakdowns only occur when the applied voltages exceed their swing voltages much further. Sometimes if the voltage is too high, the steel particle might just rest on the electrode without any motion and the breakdown will not occur up to the maximum supply voltage of 75 kV. As shown in Figure 3.27, the breakdown voltage of Gemini X is similar to its swing voltage, around 22 kV. This value is 40% lower than the breakdown voltages of Midel 7131 and FR3, probably due to the influence of viscosities.

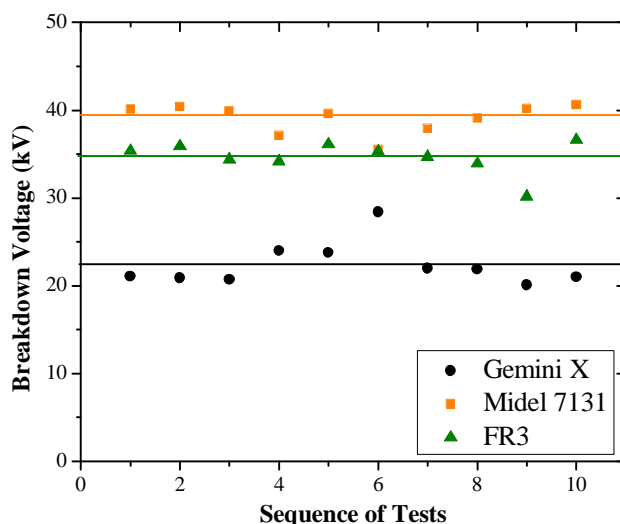


Figure 3.27 AC breakdown voltages of transformer liquids with a steel particle

Table 3.12 lists the comparison of the threshold voltages, swing voltages and breakdown voltages of Gemini X, Midel 7131 and FR3 with the presence of a steel particle. Although the threshold and swing voltages of mineral oil are similar to those of esters,

the breakdown voltage of mineral oil is much smaller than those of esters.

Table 3.12 Threshold voltages, swing voltages and breakdown voltages of transformer liquids with a steel particle

	Gemini X	Midel 7131	FR3
Threshold Voltage (kV)	10.7	11.0	10.8
Swing Voltage (kV)	22.0	25.6	24.9
Breakdown Voltage (kV)	22.4	39.4	34.7

Note: Gap distance between electrodes is 10 mm and initial position of particle is at the center. The steel particle is 0.8 mm in diameter and 3 mm in length.

The experimental results show that the conductive particles will significantly reduce the dielectric strengths of the transformer liquids. Due to the higher viscosities of esters, the motions of the conductive particles in esters are much slower than those in mineral oil, which is the reason why the breakdown strengths of esters are higher than that of mineral oil in the presence of particles.

3.5 Water Effect on Breakdown Voltages

3.5.1 Introduction

It is widely accepted that the breakdown voltages of transformer liquids depend on the water content in the liquids. Chadband studied the breakdown process of a wet transformer liquid and suggested that water acts as the charge carrier when it is dissolved in the liquid and absorbed by the hygroscopic particles, which function as weakest-links and reduce the breakdown voltage [48]. It is also observed that the water influences the breakdown voltages of mineral oil and esters to different degrees [10]. A small increase in the water content of mineral oil leads to a sharp decrease in the breakdown voltage. However, the breakdown voltages of esters keep quite stable when the water in the liquids increases. Since most of the papers reported the results without specifying the qualities of the transformer liquids, it is hard to obtain a correct comparison between them. In this section, the qualities of the transformer liquids are carefully controlled, and the water effects on the breakdown voltages of mineral oil and esters are comparatively investigated.

3.5.2 Sample Preparation

The transformer liquids are purified, dehydrated, and degassed as described before. Since the relative water contents in processed samples are less than 2 %, they could be directly used as dry samples. To obtain liquid samples with a relative water content larger than 10 %, water is added back into processed samples using equilibrium method [163]. The detailed procedure of sample preparation is described in Appendix I.5.

3.5.3 Tests and Results

The liquid samples were prepared with various water contents. The breakdown voltage tests were carried out using the same configuration and procedure as described in Appendix I.4, and 40 breakdown voltages were measured for each sample to obtain the mean breakdown voltage and the standard deviation. Special care should be taken during the tests to avoid contamination from the environment. The water contents before and after the breakdown voltage tests were measured using Karl Fischer method, and they were almost the same due to relative short durations. This indicated that there is little influence from the environment on the breakdown voltage results.

Figure 3.28 represents the mean breakdown voltages and the standard deviations of both mineral oil and esters with the absolute water content in the unit of ppm. The results show that the breakdown voltage of purified Gemini X is slightly larger than those of Midel 7131 and FR3 when they are in a dry condition. But it suffers from a steep drop when Gemini X is moisturized. However, the comparison is not fair to Gemini X since the water saturation level of Gemini X is much smaller than those of Midel 7131 and FR3. It is more reasonable to compare their breakdown voltages using relative water content instead of absolute water content.

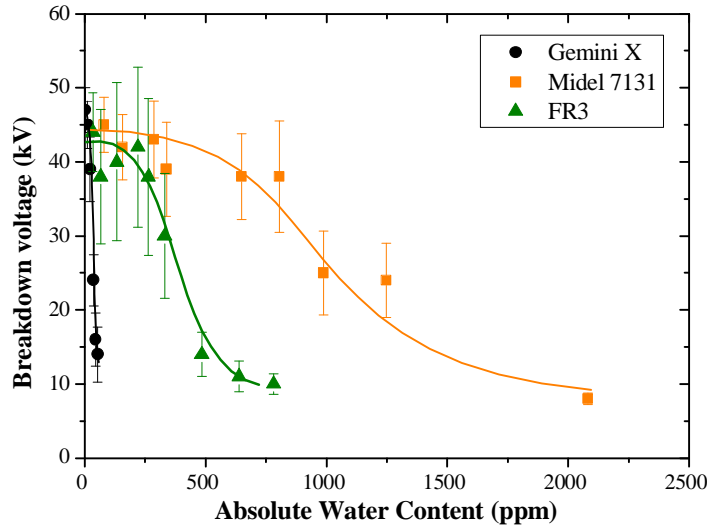


Figure 3.28 Breakdown voltages and standard deviations with absolute water content for transformer liquids

Figure 3.29 shows the mean breakdown voltages and the standard deviations of both mineral oil and esters with relative water content in the unit of percentage. In terms of the relative water content, the influence of water seems to be similar for both mineral oil and esters. It is clearly seen that the breakdown voltages of both mineral oil and esters are not affected by the moisture up to 20% RH. When the relative water contents are above 20% RH, their breakdown voltages are gradually reduced with the increase of the relative water contents. The breakdown voltage of Gemini X decreases to 20 kV/mm at 70% RH, while the breakdown voltages of Midel 7131 and FR3 decrease to about 10 kV/mm at 70% RH. After that, their breakdown voltages are gradually stabilized with the increase of the relative water content due to water saturation.

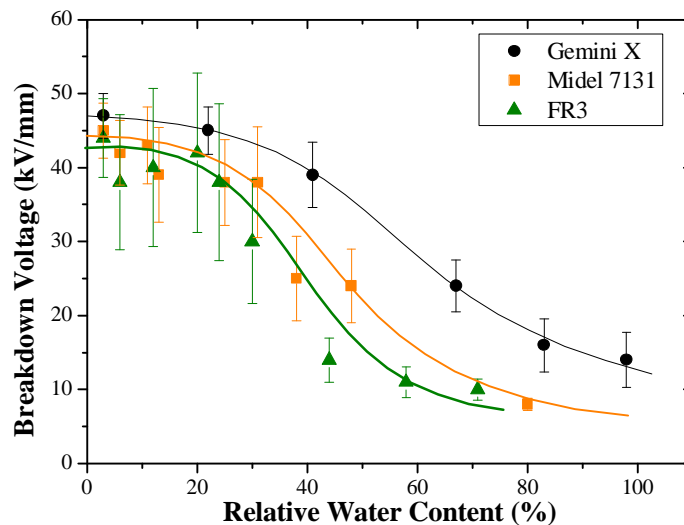


Figure 3.29 Breakdown voltages and standard deviations with relative water content for transformer liquids

The graph also shows that the standard deviations of Midel 7131 and FR3 are much higher than those of Gemini X when the relative water content is smaller than 40 % RH. Therefore, the withstand voltage of mineral oil should be higher than those of esters in the presence of water.

3.5.4 Discussion and Further Work

3.5.4.1 Water Effect of Clean Liquids

As described in Chapter 2, the water dissolves in transformer liquids in two forms as the associated water and the dissociated water [36]. In clean liquids at low relative water content, most of the water exists as associated water [33]. The mobility of the water molecules is restricted since the water molecules are combined with large liquid molecules by weak H-H bonds [164]. This is further enhanced when the associated water act as intermolecular bridges and connect two or more hydrocarbon molecules together [165]. Therefore, the breakdowns voltages are relatively high and the water effect on liquid dielectric strength is not obvious.

However at high water content, some of the water molecules will exist as dissociated water in the form of free water or water clusters. These dissociated water might function as charge carrier when electrons, whether induced by cathode electrons emission or by collision ionization processes, are trapped by the water molecules due to their high polarization. Therefore, the liquid conductivities are usually increased with the water content [38], and the liquid breakdown voltages are reduced when the relative water contents exceed certain limits.

3.5.4.2 Water Effect in the Presence of Impurities

If the transformer liquids contain particle contaminations, the water content will affect their breakdown voltages more significantly. Figure 3.30 represents the comparison of the breakdown voltages with relative water content for clean and dirty Gemini X. The dirty Gemini X is produced by exposing clean oil to atmosphere. It is naturally

contaminated, with a particle content of about 24,000 (>5 μm per 100ml sample). The results clearly show that the breakdown voltage of dirty Gemini X drops quickly as soon as water appears in the transformer liquid.

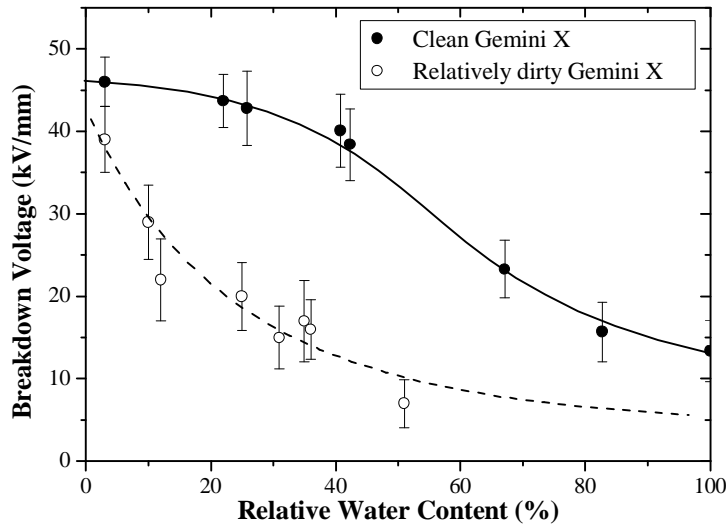


Figure 3.30 Water effect on breakdown voltages of clean and relatively dirty Gemini X

Gemini X is a type of mineral oil which is mainly composed of saturated hydrocarbons, and only a small amount of water can dissolve in Gemini X due to the existence of polar structures materials such as aromatics or additives. When Gemini X is contaminated with particles, the water molecules are easier to combine with the particles due to their polar structures. Thus, a significant number of conductive particles are produced and these conductive particles will function as the charge carriers. These charge carriers act as weakest-links, and reduce the breakdown voltages of mineral oil. On the other hand, esters are mainly composed of molecules with polar structures due to the ester parts. Thus, the water molecules will be more easily combined with ester molecules by H-H bonds. Even though the liquids are contaminated, a large amount of water is still in combination with the oil molecules. Therefore, the water content has little effect on the breakdown voltage of Midel 7131 and FR3 [43].

3.6 Area Effect on Breakdown Voltages

3.6.1 Introduction

Insulating oils are used as one of the main insulation materials in power transformers and

are used in large volumes, usually tens of tons. To ensure their optimum utilization, an understanding of the breakdown strengths of the liquids in full scale in power transformers is of great importance. However, it is neither economical nor necessary to carry out such a test. A reasonable estimation of the breakdown strengths of transformer liquids in full scale can be obtained by extrapolation from a series of small scale tests following parallel/series breakdown probability models, which represent the area effect or the volume effect.

It is well known that the AC breakdown strength of mineral oil is decreased with the increase of the electrode surface area or the liquid volume subjected to high electric field stresses [103, 166]. Thus, the area effect or the volume effect should be considered in the design of the insulation systems. Since the area effect is closely related to the contamination in the transformer liquids [65], the liquid qualities should also be considered. The weakest-links will reduce the liquid breakdown strengths and influence the breakdown voltage distributions, thus affecting the area effect.

3.6.2 Theoretical Analysis of Area Effect using Weibull Distribution

It is generally accepted that the breakdowns of transformer liquids in uniform AC fields are caused by the ‘weakest-links’, existing both in the bulk oil or on the surface of the electrodes [122]. With the enlargement of the electrode area, the number of ‘weakest-links’ will increase due to the increase of the electrode surface area and the increase of the stressed oil volume. Therefore, the breakdown voltage is reduced consistently with the increase of the electrode surface area.

Considering the ‘weakest-links’, a reasonable assumption is that the ‘weakest-links’ distribute evenly in the transformer liquids and on the surfaces of the electrodes. Thus, the number of ‘weak links’ increases linearly with the increase of the electrode surface area. Following the parallel breakdown probability model [167], an electrode with **Effective Stressed Area** (ESA) S can be regarded as n pieces of basic element S_0 connected in parallel, as shown in Figure 3.31.

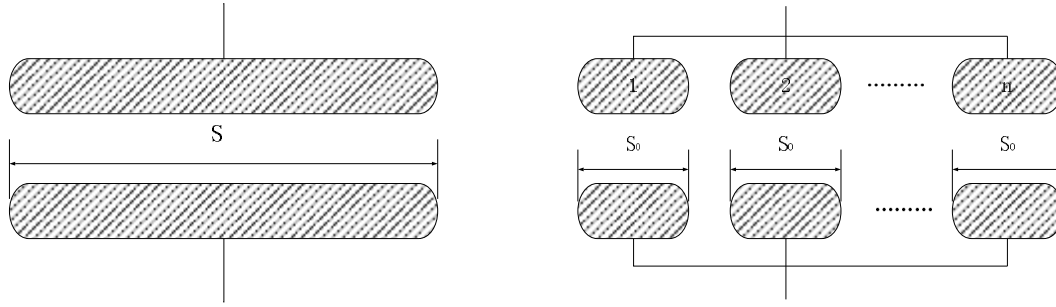


Figure 3.31 The parallel breakdown probability model for electrode area effect

For a transformer liquid, the breakdown voltage distributions of electrode S (P) and basic element S_0 (P_i) should follow Weibull distribution, as shown in Equation 3.13 and Equation 3.14. Where $P(E)$ is the failure rate of the test liquid at the applied voltage of E . α is the scale parameter, indicating the breakdown voltage at a failure rate of 63%. β is the shape parameter, measuring the dispersion of the breakdown voltage distribution.

$$P(E) = 1 - e^{-\left(\frac{E}{a}\right)^\beta} \quad \text{Equation 3.13}$$

$$P_i(E) = 1 - e^{-\left(\frac{E}{a_i}\right)^{\beta_i}} \quad \text{Equation 3.14}$$

Since the basic elements were connected in parallel, the breakdown probability of P and P_i follows Equation 3.15.

$$1 - P = \prod_i^n (1 - P_i) \quad \text{Equation 3.15}$$

$$\ln(1 - P) = \sum_i^n \ln(1 - P_i) \quad \text{Equation 3.16}$$

The S_0 is the basic element of electrode S , and the applied voltage on each element is the same. Thus P_i is the same for all the basic elements and Equation 3.15 can be written as:

$$\left(\frac{E}{a}\right)^\beta = \sum_i^n \left(\frac{E}{a_i}\right)^{\beta_i} = \frac{S}{S_0} \left(\frac{E}{a_i}\right)^{\beta_i} \quad \text{Equation 3.17}$$

To solve this equation, we have:

$$b = b_i \quad \text{Equation 3.18}$$

$$a = a_i \left(\frac{S}{S_0} \right)^{\frac{1}{b}} \quad \text{Equation 3.19}$$

Equation 3.18 indicates that the shape parameter of the breakdown voltage distributions is independent of the electrode *ESA*. From Equation 3.19, we have:

$$\log(a) = -\frac{1}{b} \log(S) + \left(\frac{1}{b} \log(S_0) + \log(a_i) \right) \quad \text{Equation 3.20}$$

The S_0 , α_i and β are the area, scale parameter and shape parameter of the basic electrode element, which can be regarded as constants. Thus, Equation 3.20 can be written as Equation 3.21, in which α and β are scale and shape parameters of the breakdown voltage distribution under electrode S , and k is a constant determined by the liquid.

$$\log(a) = -\frac{1}{b} \log(S) + k \quad \text{Equation 3.21}$$

Equation 3.21 can be further written as Equation 3.22 **Error! Reference source not found.**, in which a , b are constants depending on the type of insulating liquid. Since α is the breakdown voltage at a failure rate of 63%,

$$\log(a) = a - b \cdot \log(S) \quad \text{Equation 3.22}$$

Error! Reference source not found. shows the area effect on the breakdown voltage of an insulating liquid. Three conclusions can be obtained from the analysis, and experiments will be carried out to confirm if these three conclusions are correct.

- ı There is a linear relationship between the logarithmic scale parameter α and the logarithmic electrode *ESA*.
- ı Comparison of Equation 3.21 and **Error! Reference source not found.** shows that the reduction rate b of the scale parameter is in reverse relationship with the shape

parameter β . This indicates the breakdown voltage will reduced more significantly with the increase of electrode ESA if the breakdown voltage distributes wider.

- The shape parameter β of the breakdown voltage distribution is independent of the ESA of the electrode, if parallel breakdown probability model is ideally followed.

3.6.3 Experimental Description

To study the scale effect on the breakdown voltages of transformer liquids, breakdown voltages test for Gemini X, Midel 7131 and FR3 were carried out using seven pairs of electrodes with various surface areas. Figure 3.32 shows seven types of electrodes employed for the breakdown voltage measurement in the tests. Electrode 1 is a sphere type electrode with a diameter of 12.5 mm, and electrode 2 is a VDE type electrode with a diameter of 35 mm. Electrodes 3 to 7 are circular, flat electrodes with different diameters, whose edges are curved away with a radius of 1 mm.

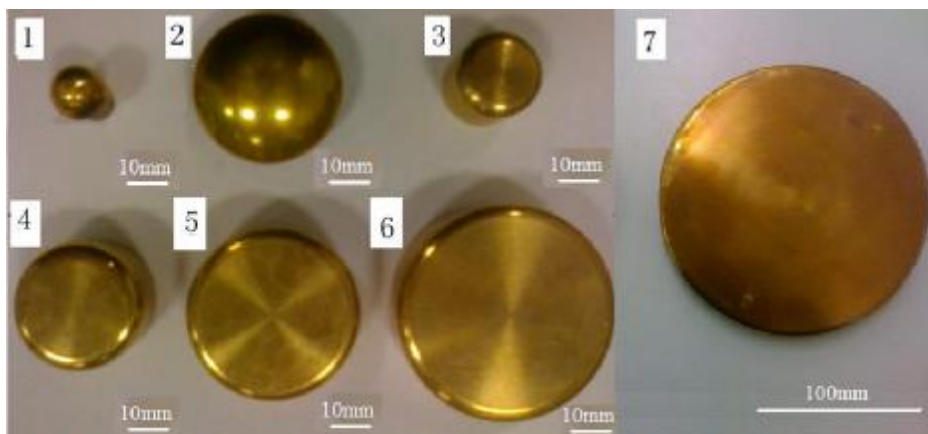


Figure 3.32 Electrodes used in scale effect test

Table 3.13 lists the diameters of the electrodes and their corresponding **Effective Stressed Areas (ESA)**. The ESA is the electrode area which is stressed under an electric field larger than 90 % value of the maximum electric field. It is found that the breakdown strength of a transformer liquid depends on the ESA rather than the total electrode area [168]. To confirm the field distributions, the field calculation shows that the electric field near the electrode edge does not affect the uniform field between the flat portions of the electrodes.

Table 3.13 Effective stressed areas of electrodes used in scale effect test

Electrode number	1	2	3	4	5	6	7
Diameter (mm)	12.5	35	20	30	40	50	150
Effective stressed area (mm ²)	2.17	5.22	283	660	1194	1885	17671

In the tests, the samples of transformer liquids are purified, dehydrated and degassed as described in Appendix I.3. The breakdown voltage tests were carried out using the same procedure as described in Appendix I.4. For electrodes 1 to 6, the AC breakdown voltages of the processed liquids were measured by a Baur DPA75 tester. Since electrode 7 is too large to fit into the DPA 75, the breakdown voltage was measured using a different setup described as follows. The AC voltage was provided by a single phase transformer up to 70 kV. A 500 k Ω resistor was connected between the high voltage supply and the test container to limit the current when a breakdown occurred. The gap distance between parallel electrodes was set at 1 mm.

In the tests, the testing electrodes were fitted into the test container filled by Gemini X, Midel 7131 and FR3, respectively. The applied AC voltage was increased from 0 kV at a speed of 0.5 kV/s until a breakdown occurred. For electrode 1 to 6, at least 40 breakdown voltages were measured for each setup and the time interval between two successive breakdowns was at least 5 minutes. For electrode 7, since the released energy by each breakdown is quite large, no more than 20 breakdown voltages were measured for each setup to reduce the deteriorations, and the time interval was increased to 15 minutes.

3.6.4 Results and Discussions

Figure 3.33 shows the Weibull plots of the AC breakdown voltages of transformer liquids for various electrodes. The Weibull plots of both mineral oil and esters give generally straight lines, which indicate that Weibull distribution can be applied to fit the breakdown voltage of both mineral oil and esters.

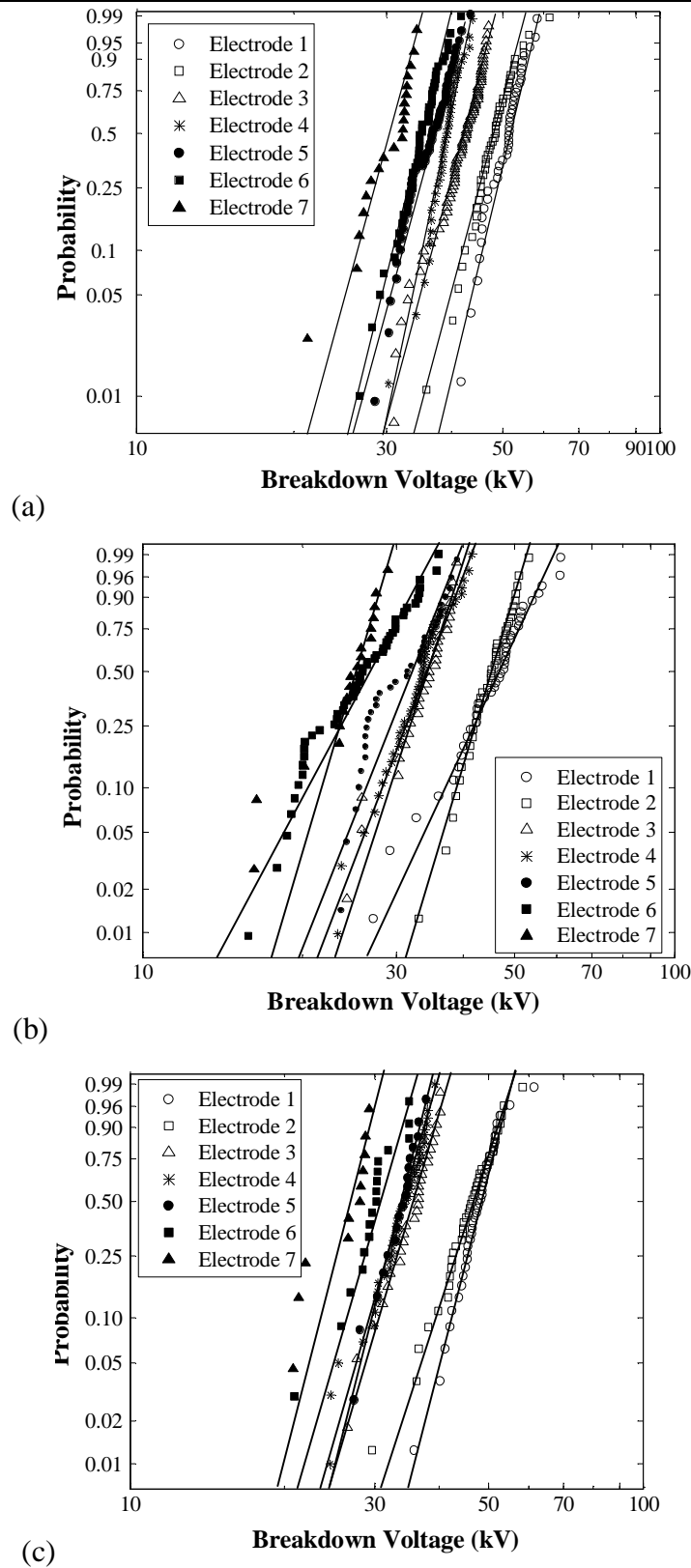


Figure 3.33 Weibull plots of breakdown voltage distributions using various electrodes
 (a) Gemini X, (b) Midel 7131, (c) FR3

Table 3.14 lists the Weibull scale parameters (α) and shape parameters (β) estimated from the Weibull plots of the breakdown voltages using various electrodes. The results indicate that the scale parameters of all the liquids are decreased with the increase of the

electrode *ESA*, which shows the electrode area effect.

Table 3.14 Weibull parameters of transformer liquids using various electrodes

Electrode	Gemini X		Midel 7131		FR3	
	α	β	α	β	α	β
1	52.4	15.2	49.1	7.19	49.3	12.9
2	50.3	13.7	47.4	10.4	49.1	10.6
3	43.6	14.4	35.0	9.22	36.9	13.0
4	40.0	17.9	35.6	12.1	35.3	13.0
5	38.1	12.6	33.1	7.72	34.8	15.6
6	36.3	13.5	28.1	6.02	31.3	10.2
7	31.8	12.5	25.7	10.0	27.5	12.2

Table 3.14 also shows that the shape parameters of a test liquid are not the same under different electrode areas. Table 3.15 lists the calculated average values and standard deviations of the shape parameters for transformer liquids from the experiment results. It is clearly seen that the shape parameters vary within a range. Generally speaking, the shape parameters of Gemini X are larger than those of Midel 7131 and FR3. This indicates that the breakdown voltages of Gemini X distribute narrower than Midel 7131 and FR3. Similar results were also obtained in [152].

Table 3.15 Average shape parameters, standard deviations and 90% confidence intervals of transformer liquids

Liquids	Average β	Standard deviation	90% confidence interval
Gemini X	14.3	1.9	[11.2, 17.3]
Midel 7131	9.0	2.1	[5.5, 12.4]
FR3	12.5	1.8	[9.5, 15.5]

Figure 3.34 plots the relationship between the scale parameter and *ESA*. The solid lines are the fitting curve of the scale parameters by the least square method. The results support the conclusion from the theoretical analysis that the logarithmic scale parameter (α) reduces linearly with the increase of the logarithmic electrode *ESA* (Equation 3.22). The breakdown voltages of Midel 7131 and FR3 reduce more significantly with the increase of electrode area than that of Gemini X.

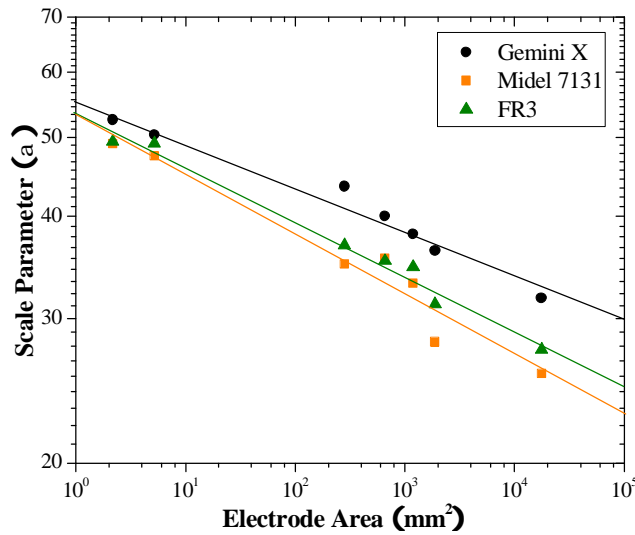


Figure 3.34 Scale parameters of transformer liquids as a function of electrode area

From Figure 3.34, the area effect for transformer liquids can be derived. Table 3.16 lists the parameters a and b used in **Error! Reference source not found.** Equation 3.23 shows the final equation of the area effect for mineral oil and esters. This equation can be used to extrapolate the scale parameters of transformer liquids stressed under electrodes with large ESA .

Table 3.16 Parameters used in area effect equations for transformer liquids

Liquids	a	b
Gemini X	1.7391 ± 0.0096	0.0508 ± 0.0034
Midel 7131	1.7195 ± 0.0140	0.0697 ± 0.0056
FR3	7.7274 ± 0.0140	0.0666 ± 0.0055

$$\begin{cases} \log(a_{\text{GeminiX}}) = 1.7391 - 0.0508 \cdot \log(S) \\ \log(a_{\text{Midel7131}}) = 1.7195 - 0.0697 \cdot \log(S) \\ \log(a_{\text{FR3}}) = 7.7274 - 0.0666 \cdot \log(S) \end{cases} \quad \text{Equation 3.23}$$

Therefore, the breakdown voltage distribution of a clean transformer liquid can be derived by putting the scale parameter extrapolated from Equation 3.23 and the average shape parameter listed in Table 3.15 back into Equation 3.13. Equation 3.24 shows the breakdown voltage distribution for Gemini X, Midel 7131 and FR3 respectively when they are stressed under electrode S . In this equation, the unit of electrode area S is mm^2 , and the unit for applied voltage E is kV/mm . Based on Equation 3.24, the breakdown voltage at specified probability can be obtained.

$$\left\{ \begin{array}{l} P_{\text{GeminiX}}(E) = 1 - \exp\left(-S^{0.73} \left(\frac{E}{54.8}\right)^{14.3}\right) \\ P_{\text{Midel7131}}(E) = 1 - \exp\left(-S^{0.63} \left(\frac{E}{52.4}\right)^{9.0}\right) \\ P_{\text{FR3}}(E) = 1 - \exp\left(-S^{0.83} \left(\frac{E}{53.4}\right)^{12.5}\right) \end{array} \right. \quad \text{Equation 3.24}$$

3.7 Withstand Voltages of In-service Transformer Liquids

For in-service transformers, the transformer liquids are usually used in large volumes and with contaminants. Therefore to estimate their withstand voltages, all the influences, such as the particle effect, water effect and scale effect should be taken into consideration. The estimation can be roughly achieved by several stages described as follows.

- Firstly, the breakdown voltage distribution of a processed transformer liquid based on small scale tests should be extrapolated to that of full scale.
- Then, a safety margin should be taken into consideration, and the withstand strength can be obtained from the breakdown voltage distribution at 1% failure rate.
- Finally, the realistic liquid qualities encountered for in-service transformers should be considered, in terms of particle content and water content.

Example

Considering for an 11 kV distribution transformer, the height of the winding is about 1000 mm, and the diameter of the winding is about 600 mm. Thus, the equivalent electrode area can be calculated, around $1.88 \times 10^6 \text{ mm}^2$.

- Equation 3.23 shows the electrode area effect of clean transformer liquids; hence the scale parameters used in the breakdown voltage distributions can be extrapolated from small to large scales using this equation. Considering the shape parameters listed in Table 3.15, the breakdown voltage distributions of clean transformer liquids at a electrode area of $1.88 \times 10^6 \text{ mm}^2$ and 1 mm gap are shown in Equation 3.25, in which E is the breakdown strength of transformer liquids in kV/mm.

$$\begin{cases} P_{\text{GeminiX}}(E) = 1 - \exp\left(-\left(E/26.3253\right)^{14.3}\right) \\ P_{\text{Midel7131}}(E) = 1 - \exp\left(-\left(E/19.1501\right)^{9.0}\right) \\ P_{\text{FR3}}(E) = 1 - \exp\left(-\left(E/20.3958\right)^{12.5}\right) \end{cases} \quad \text{Equation 3.25}$$

Taking into consideration of a safety margin, the withstand strengths of clean transformer liquids could be obtained from Equation 3.25 at 1% failure rate. The withstand strengths are 19.1 kV/mm, 11.7 kV/mm and 13.9 kV/mm for clean Gemini X, Midel 7131 and FR3.

Then the withstand strengths of the clean transformer liquids should be revised by the particle contamination. For in-service transformers, the main contamination in the insulating liquids is cellulose particles, and the normal number is around 20,000 to 30,000 (>5 μm per 100 ml). Thus, the reduction factors derived from Figure 3.19 are 0.64 for Gemini X, 0.81 for Midel 7131 and 0.87 for FR3, respectively. The withstand strengths are 12.3 kV/mm for Gemini X, 9.3 kV/mm for Midel 7131 and 12.1 kV/mm for FR3.

Furthermore, the withstand voltage should be revised by the water content. Since the relative water content of in-service transformer liquids are around 5%, the reduction factor are about 0.66 for mineral oil calculated from Figure 3.30. For Midel 7131 and FR3, the water has little influence on their breakdown voltages due to their polar molecular structures, and the reduction factors are 1.0. Therefore, the withstand voltage are 8.1 kV/mm for Gemini X, 9.3 kV/mm for Midel 7131 and 12.1 kV/mm for FR3.

The above calculation shows that the withstand strengths of transformer liquids of in-service qualities and under large size of electrode are much smaller (only about 1/4) than the breakdown voltages derived from small scale tests using clean liquids. The withstand strengths of transformer liquids of any transformer geometry can be estimated by above calculation. For the transformer geometry given in the example, the withstand strengths of in-service esters are expected to be slightly higher than that of mineral oil.

3.8 Summary

The AC dielectric strengths of Gemini X, Midel 7131 and FR3 were comparatively studied in this chapter. The effect of particle content, water content and the electrode scale effect on the breakdown voltages were investigated. The results indicate that the esters might be used as substitutes to conventional mineral oil in terms of dielectric strengths.

▮ The breakdown voltages of transformer liquids in ‘processed’ qualities are compared. Weibull distribution is the best fitting to model the breakdown voltage distribution and can be used to predict the withstand voltage. The predicted results are confirmed by 500 withstand tests.

▮ The breakdown voltage of Gemini X is sensitive to particle contamination. However, the breakdown voltages of Midel 7131 and FR3 are less sensitive to particles than Gemini X. The particles effect probably depends on the liquid viscosities. The breakdown voltage of a contaminated transformer liquid can be estimated using the equation below, in which N is particle number, η is the viscosity, K is a constant determined by the particle material, and V is a constant determined by the transformer liquid.

$$E(N) = -\frac{K}{h} \cdot \ln(N) + V$$

▮ In terms of the relative water content, the water effect on the breakdown strengths are similar for clean mineral oil and esters. For clean transformer liquids, their breakdown voltages only decrease when the relative water contents exceed a certain value. It is concluded that the dissociated water plays a decisive role in the breakdown processes of transformer liquids.

▮ The breakdown voltage of Gemini X distributes much narrower than those of Midel 7131 and FR3, resulting in the relatively small reduction of breakdown voltage with the

increase of electrode ESA. The scale parameter α of breakdown voltage distribution can be predicted from laboratory small scale tests to large scale using the following equation, in which a , b are constants depending on the type of insulating liquid.

$$\log(a) = a - b \cdot \log(S)$$

- The withstand voltages of transformer liquids of in-service qualities can be predicted from small scale tests, taken in consideration of the particle effect, the water effect, and the electrode scale effect.

These conclusions could help the application of esters in power transformers. Since the dielectric strengths of esters are reduced much less than mineral oil with increased water and particle content, esters might be able to provide better insulation than mineral oil when the liquids are contaminated. Since the dielectric strengths of esters are reduced more significantly with increased electrode area than mineral oil, esters might be more applicable in distribution transformer with smaller electrode area than high voltage power transformer with large electrode area.

Chapter 4. PD Measurement and PD Performances of Transformer Liquids

4.1 Introduction

Post-failure analysis shows that there are mainly two causes of insulation failures in power transformers: partial discharges in large oil gaps [169] and creepage discharges along liquid (transformer liquids) – solid (transformer paper/ pressboard) interfaces [170]. Partial discharges are generally attributed to the inappropriate design or poor manufacturing craftwork.

Material defects, such as protrusions or particle contaminations from manufacturing procedure or material ageing, could enhance local electric field, and lead to the inception of partial discharges near these areas [171-173]. Once the discharges are initiated, they can further degrade the surrounding insulation materials, allowing their propagation from the local areas into the bulk liquids, and eventually leading to breakdowns [142]. The process of discharge induced insulation failures, developing from discharge inception to breakdown, can take years, months, minutes or just seconds, depending on which area the local field concentrations are located at and under what condition the transformer is operated. Thus, the insulating liquids in power transformers are required to withstand high electrical stresses without the inception of partial discharges [174].

Partial Discharge Inception Voltage (PDIV) test is one of the most important tests to determine the intrinsic dielectric characteristics of transformer liquids [175], and experience has been accumulated to measure the PDIV of conventional mineral oil [175, 176]. As esters have been considered as alternatives to mineral oil for larger power transformers in recent years, it is essential to ensure that the PDIV test method used for mineral oil can still yield correct measurements for esters, considering the different chemical compositions of esters from mineral oil.

This chapter discusses the suitability of applying the conventional PDIV measurement method to esters. Some additional procedures are suggested in order to yield a correct comparison between the PD characteristics of mineral oil and esters. In this chapter, section 4.2 briefly introduces the IEC 61294 test procedure and the existing knowledge related to the PDIV. Section 4.3 introduces the test arrangement used in this chapter. Section 4.4 discusses the shortcomings of IEC 61294 and gives suggestions to improve IEC 61294 to measure the PDIV values of esters. Section 4.5 compares the PDIV measurement results of Gemini X, Midel 7131 and FR3, following the IEC 61294 and the suggested new procedure. Section 4.6 studies the PD performances of these transformer liquids at overstressed voltage, and it is found that overstressing these liquids using the suggested new procedure provides more information about their dielectric properties, and can better differentiate the liquids.

4.2 Knowledge Related to PDIV Measurements

4.2.1 IEC 61294 Test Procedure

The standard test procedure of IEC 61294 (Insulating Liquids – Determination of the Partial Discharge Inception Voltage (PDIV) – Test Procedure) is designed with the purpose of characterizing the ability of insulating liquids to prevent or suppress the inception of partial discharges when they are subjected to high electrical stresses [177]. The current version of IEC 61294 has existed for about two decades without revision. At present, PDIV is considered as a parameter which is mostly related to the chemistry compositions of the insulating liquids, and is relatively less affected by their quality. For many transformer users, the PDIV test is a more applicable test related to the application of the liquids than conventional tests, such as AC dielectric strength test or lightning impulse breakdown strength test, because the PDIV test is virtually non-destructive [137]. Thus, the IEC 61294 provides a standardised method of assessing the PD inception voltages of transformer liquids for the purpose of quality assurance, specification, and condition monitoring.

The PDIV measurement results are heavily dependent on the field configurations. The IEC 61294 utilizes a highly divergent electric field provided by a needle to sphere electrode configuration. It requires the usage of a needle electrode with 3 μm tip curvature as the high

potential electrode, and a sphere electrode with 12.5 mm or 13 mm diameter as the opposite ground electrode. In the appendix of IEC 61294, the needle electrodes, from batches supplied by Ogura Jewel Industry Co. Ltd, are suggested for use in the PDIV measurements. Since the PD inception depends on the local high electric field near the needle tip, and only a small volume of the liquid sample is under high stress, the PDIV measurement using the point-sphere electrode configuration is relatively independent of the qualities of the liquids, such as the moisture and particle contaminations.

The test cell used in the PDIV measurement contains a vertical gap of 50 ± 1 mm. The volume of this cell is about 300 ml. The discharge detection equipment required by the IEC 61294 is commercially available, with frequency response typically in the range of 10 kHz to 300 kHz. The background PD noise should be less than 50 pC at the maximum applied voltage.

The outline of the test procedure in IEC 61294 is described as follows. The liquid sample is poured into the test cell first, and the sample is allowed to stand for at least 15 minutes after filling the cell and before applying voltage. The occurrence of the discharges is monitored by an appropriate PD detector. A power frequency voltage is applied to the cell, increasing at a constant rate of 1 kV/s from 0 kV until a partial discharge occurs of apparent charge equal to or greater than 100 pC. The voltage is recorded as the PDIV results. At least 10 PDIV measurements need to be carried out on each of two different fillings of the cell. The mean value of 20 PDIV measurement results is taken as the reported PDIV result.

4.2.2 Definitions of PD Inception Voltage

Partial discharges (PD) have certain numbers of random features, thus an accurate and precise measurement of the PDIV value is difficult. The determination of PD inception seems to be more or less arbitrary, depending on the definition of the PDIV [178, 179]. Usually, two types of inception definitions are adopted in previous studies: one is widely used for industrial purposes, and the other is commonly used in laboratory researches.

4.2.2.1 Industrial Definition of PDIV

The definitions of PDIV in high voltage tests for industrial purposes have been published in IEC 60270 and IEC 61294 respectively.

In IEC 60270, the PDIV is defined as '*the applied voltage at which repetitive partial discharges are first observed in the test object*'. However, there is no further definition of the '*repetitive*' partial discharges. It is totally arbitrary for the individual test operator to determine at what repetition rate the partial discharge can be regarded as '*repetitive*'. Therefore in practice, the inception voltage is usually regarded as the lowest applied voltage at which the magnitude of a PD pulse becomes equal to or exceeds a specified threshold [180]. In this type of definition, only partial discharges with an apparent charge higher than the threshold value are regarded as the actual partial discharges in the test object. Thus, the PDIV measurement results depend heavily on the choice of the threshold value.

The PDIV definition in IEC 61294 avoids the use of '*repetitive*'. In IEC 61294, the background level is required as less than 50 pC. Thus, the threshold is chosen as twice that of the background level, and the PDIV of an insulating liquid is defined as '*the lowest voltage at which a partial discharge occurs of an apparent charge equal to or exceeding 100 pC when the sample is tested under the specified condition*' [177]. Since the threshold of PDIV is twice of the maximum allowed background PD noise, separation of the actual PDs in the test cell from the background noises can be easily achieved. For this condition, a choice of threshold higher than 100 pC gives no apparent merit.

In principle, these PDIV definitions involve the detection of electric pulses produced by charge displacements within the test objects [181]. The charge displacement is believed to be the result of an electric field induced ionization process in the dielectric [179]. Due to the randomness of this process and the self-recovery ability of the liquid dielectrics, partial discharges usually appear in the form of PD pulse bursts that consist of a series of discrete current pulses occurring over a finite time interval of a few μs [182]. The reported PD charge is the apparent charge measured by commercially available PD detectors, being proportional to the integration of all the charges contained in a PD pulse burst. Test experiences (section

4.6.2.1) show that the charge of partial discharge increases almost linearly with the increase of applied voltage around the inception voltage, while it increases nonlinearly when the applied voltage exceeds a certain level.

4.2.2.2 Academic Definition of PDIV

In the academic research, the study of partial discharge was usually carried out together with streamer study using electro-optical techniques [175]. The streamers were produced by the injection of charge carriers from high potential electrodes into the transformer liquids, and the charge injection processes were always accompanied by current pulses. Therefore, the streamer study usually involves the electrical recording of the streamer currents and the photographic recordings of the streamer structures.

In the streamer studies, there is a definition of the ‘*streamer inception voltage*’ based on the first optical/ electric evidence of streamer appearances [181]. In fact, the inception of streamer and inception of partial discharge manifest the same physical process: one concerns streamer formations and one concerns partial discharge formations. When streamers occur, the charge injections and field-enhanced ionizations within low density regions produce current pulses (charge displacements), whose charges are detected as partial discharges by an external measuring system [175]. Since the streamers and partial discharges refer to the same phenomena, the ‘*streamer inception voltage*’ is regarded as ‘PDIV of academic definition’ in this thesis.

The academic definition of PDIV has two main differences from the industrial definition of PDIV. Firstly, the background noise in the academic study can be well-controlled to less than 2 pC. Thus, the PD inception investigates the first detectable PD either measured by the electrical method (current measurement) or the optical methods (structure measurement). Therefore, the academic definition of PDIV is less dependent on the background noise, but more dependent on the detection limit and the resolution level of the measuring device of high specifications. Secondly, since the charge of the first detectable partial discharges is small, it is more practical to use the repetition rate other than the charge of partial discharges in the academic definition of PDIV. Up to now, there is still no agreement on the threshold of

the repetition rate to define the PDIV, and different thresholds based on the PD repetition rate are used to study the inception of partial discharges in transformer liquids [175, 179, 183]. In this thesis, the threshold of PDIV is chosen as 1 PD per minute, and thus the academic definition of PDIV is defined as ‘the lowest voltage at which the repetition rate of PD above the noise level reaches 1 PD per minute’.

4.3 Experimental Description

As shown in Figure 4.1, a traditional PD test circuit was used to determine the PDIV values of transformer liquids. A discharge-free transformer was used to provide AC voltages of 50 Hz up to 70 kV. The corona shields were used in the connections of the test container in order to reduce the background partial discharge noises. Before the test, the point electrode was removed and the maximum test voltage of 70kV was applied to the test samples for 5 minutes. During this period, the maximum apparent charge of the background noise was registered as less than 10 pC. A small series resistor R_3 of 50Ω was connected between the test container and the ground as a current shunt for measuring the partial discharge current. This resistor R_3 was connected only when it was necessary to detect the current. Since the resistance of R_3 is far smaller than the impedance of the test samples, the voltage drop on this resistor can be ignored.

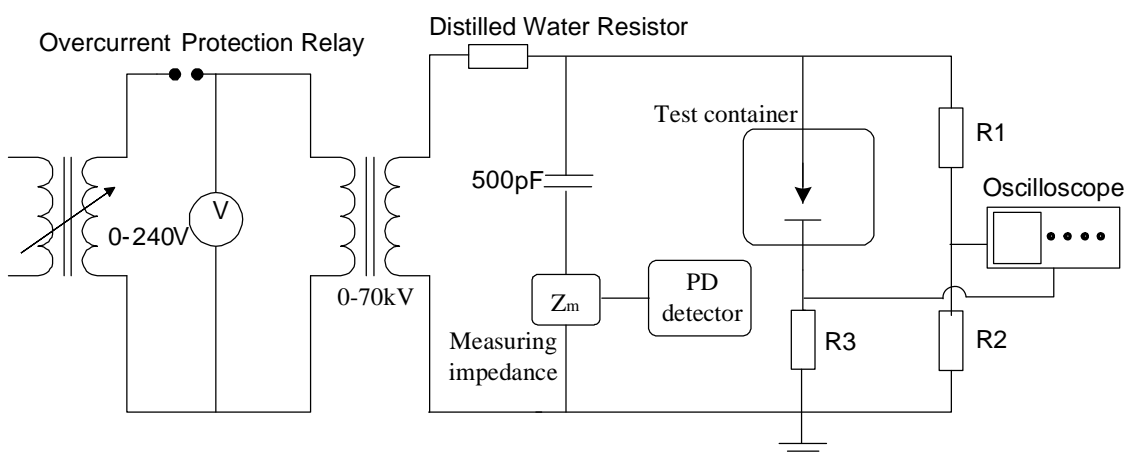


Figure 4.1 Traditional test circuit for PD detection

The test container shown in Figure 4.2 was manufactured following the specifications in IEC 60897. The structure of the test container fulfilled the requirements of IEC 61294 test

procedure. Suitable needle electrodes of 50 mm in length were obtained from Ogura Jewel Industry Co Ltd. The extension of the needle from the hold is set at 25 ± 1 mm. The sphere electrodes were made of copper with a diameter of 12.5 mm. The distance between electrodes was set at 50 ± 1 mm. It should be noted that a small error in the gap length does not affect the PDIV but a small change of tip radius may affect the result significantly. To avoid the erosion of the needle tip by continuous discharges, new needle electrodes were used for every test. Microscopic photos of the needle tip before and after the tests showed no sign of erosion of the needle tip during the tests.

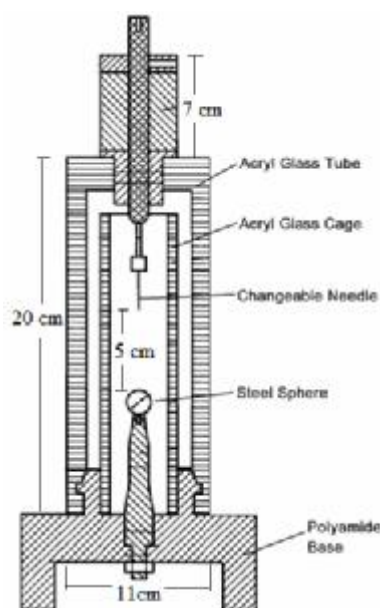


Figure 4.2 Structure of partial discharge test cell

A commercially available PD detector LEMKE LDS-6 was used in the tests. This wide bandwidth PD detector has a bandwidth of 900 kHz, with an upper frequency limit of 1 MHz and a lower frequency limit of 100 kHz. The single pulse resolution of this detector is 100 kHz, which means that successive PDs within $10 \mu\text{s}$ will be detected as a single PD.

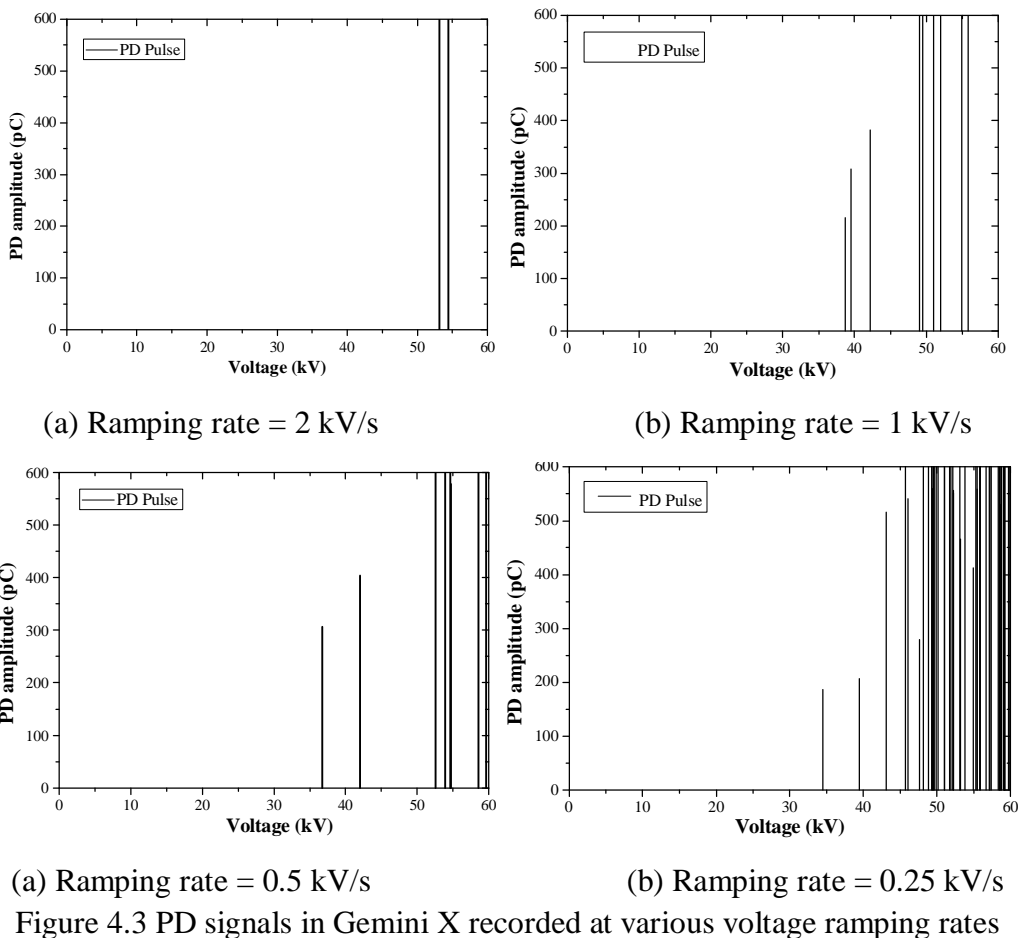
4.4 Suggestions relating to IEC 61294

IEC 61294 has been established for nearly two decades to measure the PDIV of insulating liquid based on industrial definition, and no revision has been made ever since. With the application of esters in power transformers, this test procedure suffers from some shortcomings, leading to unfairness when it is used to compare the dielectric properties

between different insulating liquids. This section discusses these shortcomings and suggests possible improvements.

4.4.1 Ramping Speed

In the IEC 61294 test procedure, the voltage ramping rate is required at 1 kV/s. However, it was found that different voltage ramping rates may affect the PDIV measurement results. Taken Gemini X as an example, Figure 4.3 shows the charge amplitudes of all the PD signals recorded during the ramp-up of applied voltage up to 60 kV, when the ramping rates are 2 kV/s, 1 kV/s, 0.5 kV/s and 0.25 kV/s. Since only the PD about 100 pC is of interest, the auto-ranging setting on the detector is prohibited and the maximum PD amplitude is manually fixed at 600 pC.



The results clearly show that the measurements give smaller PDIV values for lower voltage ramping rates. The PDIV measurement results are 53.0 kV at 2 kV/s, 38.5 kV at 1 kV/s, 36.5 kV at 0.5 kV/s and 34 kV at 0.25 kV/s. The lower ramping rate indicates a longer duration of

voltage application at each level; hence there is a higher probability of discharges being initiated. Since the PD repetition rate of Gemini X is low (as shown in section 4.6.2.2), the inception voltage can only be measured correctly when the voltage ramping rate is small enough to give sufficient time for a partial discharge to be produced.

For esters, similar tests at different ramping rates were also carried out to measure the PDIV values when they were stressed under AC voltages. The measured PDIV results show no significant differences under various ramping rates. Since the PD repetition rates of esters are high (as shown in section 4.6.2.2), more partial discharges will be produced for the same time duration in esters than in mineral oil, thus giving more consistent PDIV measurement results.

The above discussion shows that the ramping voltage method gives advantages to transformer liquids with low repetition rates in measuring their PDIVs. Thus, a comparison of the PDIV values between transformer liquids with different PD repetition rates can not be achieved by an arbitrary chosen ramping rate of 1 kV/s in IEC 61294. In practice, power transformers are stressed under rated voltages for most of their operation time. In order to simulate the practical situations, the PDIV may be measured more precisely using step voltage than ramping voltage. A commonly used method is to increase the applied voltage step by step (step voltage) with an interval of 1kV per step [183].

4.4.2 Voltage Duration

The step voltage method of 1 kV per step can be used to better measure the PDIV values of transformer liquids with higher precision. In each step, the maximum PD amplitude is specified as a parameter to evaluate the intensity of partial discharges. However, there is argument about the voltage duration staying in each step. Previous researches used voltage duration from 2 minutes [175] to 10 minutes [183]. In general, the voltage duration should satisfy two requirements: long enough to record a sufficient number of PDs, and not too long to damage the needle tip by continuous discharge erosion.

Figure 4.4 shows an example of all the PD signals recorded in Gemini X for a duration of

two minutes at 26 kV (2 kV above PDIV). The maximum PD amplitude at this voltage step is about 170 pC. From the enveloping line shown in Figure 4.4, one minute seems to be a suitable duration which is sufficiently long enough to have the maximum PD amplitude produced. For esters, one minute duration should be more than enough due to the high PD repetition rates. Therefore, one minute is suggested as the duration for each voltage step. All the PD signals during a step should be recorded, and the step with the lowest voltage value to generate a partial discharge with amplitude larger than 100 pC is regarded as the PDIV.

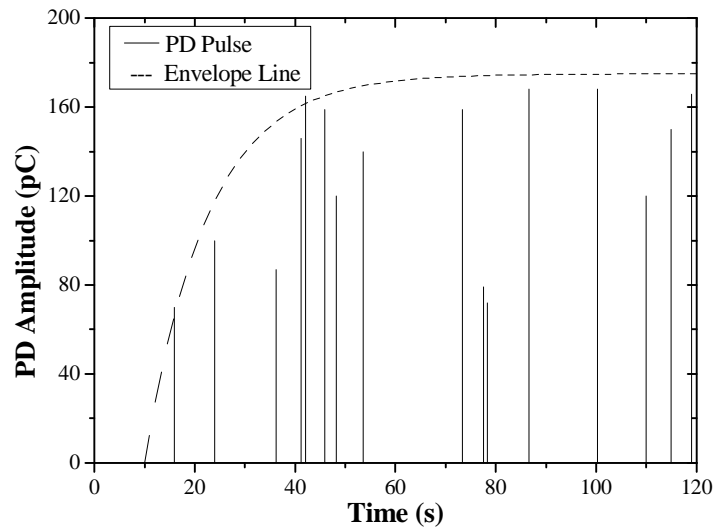


Figure 4.4 PD pulses in Gemini X recorded at 26 kV for two minutes

Note that a setting time of a few seconds should be given after the applied voltage reaches the required value when recording the PD signals, in order to avoid disturbance signals from the variac. In the tests, a setting time of 15 seconds or more was used. After the setting time, the PD signals were recorded continuously for 1 minute at each step.

4.4.3 PD Detector

To study the dependence of PDIV measurements on the PD detection device, three types of PD detectors were used to measure the PDIV values of transformer liquids. One is an analogue PD detector, the Model DD-5 discharge detection system produced by Robinson Instrument. The other two are digital PD detectors, the LDS-6 PD detection system produced by LEMKE DIAGNOSTICS GmbH and the digital MPD 540 PD detection system produced by OMICRON. Table 4.1 lists PDIV measurement results of mineral oil and esters using these discharge detection systems.

In Table 4.1, the analogue Robinson detector gives relatively higher PDIV values than the digital LDS-6 detector, probably due to different display patterns. The analogue detector displays the PD pulses on the screen. There is an inevitable delay between PD occurrence, display on the screen, reading by the operator and recording voltage. Therefore, the measured PDIV values are always higher than the actual values. However for the computer-aided LDS-6 detector, the PD signals were recorded in the computer simultaneously avoiding the time delay.

Table 4.1 PDIVs of transformer liquids using various discharge detection systems

Configuration	Ramping voltage, needle/sphere		Step voltage, needle/plane	
	DD-5	LDS-6	LDS-6	MPD540
Gemini X	45.4 kV	38.5 kV	19.1 kV	16.9 kV
Midel 7131	N/A	28.2 kV	N/A	N/A
FR3	34.5 kV	34.0 kV	18.0 kV	16.5 kV

For digital PD detectors, the measurements using the LDS-6 detector give PDIV results about 2 kV higher than those using the Omicron MPD 540 detector, although both PD detectors were calibrated by the same calibrator (50 pC) before carrying out the tests and the same test procedure was used.

Therefore, the PDIV tests for the same liquid using different PD detectors will give different results. For a more reliable comparison between PDIV values of different transformer liquids, the same PD detector should be used in the tests.

4.4.4 Outline of Suggested Revisions

As discussed before, the IEC 61294 test procedure suffers from several shortcomings. An accurate comparison between PDIV values of different transformer liquids can only be achieved when the test method is improved with the following modifications. The ramping voltage at 1 kV/s is suggested to be replaced by step voltage method with 1 kV increase per step; the voltage duration of each step is suggested to be 1 minute; and the same PD detector should be used for the PDIV measurements of transformer liquids.

The outline of the proposed method is described as follows. The liquid sample is poured into the test cell first, and the sample is allowed to stand for at least 15 minutes after filling the

cell and before applying voltage. Then, a power frequency voltage is applied to the test cell, increasing step by step (1 kV per step) from a voltage level significantly lower than the PDIV value. The PD signals are recorded by a wide bandwidth PD detector. For each step after the voltage reaches the required value, at least 15 seconds resting time is given before the PD signals are recorded continuously for 1 minute. The lowest voltage at which the maximum amplitude of PD signals reaches 100 pC is defined as the PDIV. Since the maximum amplitude of PD signals increases linearly with the increase of applied voltage around the PDIV level, linear fitting can be applied to determine the PDIV more precisely. It should be noted that the proposed method uses the threshold value of 100 pC, the same as the one used in IEC 61294.

4.5 PDIV Measurements

4.5.1 Industrial PDIV Definition

Based on the proposed method, the PDIV values of Gemini X, Midel 7131 and FR3 were measured using the test configuration described in section 4.3. The computer-aided LEMKE LDS-6 detector was used to record the PD signals as the wide bandwidth PD detector. Figure 4.5 shows the relationship between the maximum PD amplitudes and the applied voltages for mineral oil and esters. In this graph, linear fittings of the PD amplitudes versus applied voltage are used to determine the PDIV values from the cross-points of the fitting curves and the measurement threshold of 100 pC.

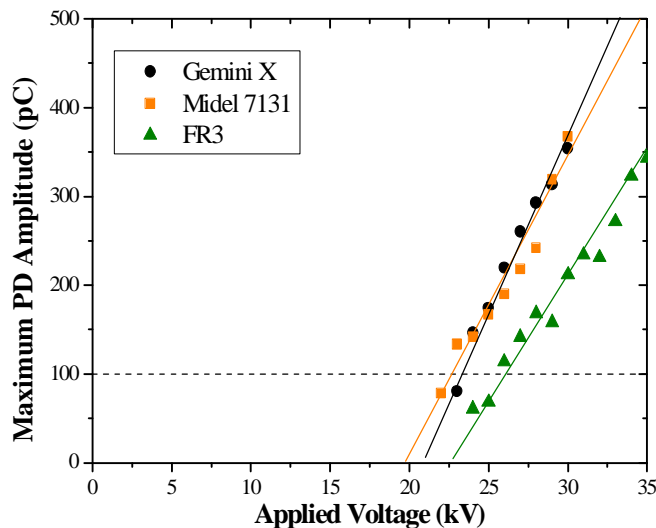


Figure 4.5 Maximum PD amplitudes with applied voltage in transformer liquids

Table 4.2 lists the comparison of PDIV values of transformer liquids measured using the proposed method and IEC 61294 method. The PDIV values determined using the proposed method are lower than those determined using the IEC 61294 method. The PDIV value of Gemini X is influenced the most by the test methods, and is reduced by 40% when using the proposed method. The PDIV values of esters are less influenced by the test methods, and are reduced by 21% and 24% for Midel 7131 and FR3 when using the proposed method.

Table 4.2 PDIVs of transformer liquids using IEC 61294 and proposed method

	Gemini X	Midel 7131	FR3
PDIV _{IEC 61294} (kV)	38.5	28.2	34.0
PDIV _{Proposed} (kV)	23.2	22.3	25.6

When using the proposed method, the PD signals were recorded continuously for 1 minute at each voltage step. Considering there are 3000 AC cycles in one minute, the measurement of PDIV is almost independent of the PD repetition rate. However when using the IEC 61294 method, the voltage is increased continuously. When the PD repetition rate of the transformer liquid is low, there is a good chance that no PD occurs within the short duration of applied voltage staying at the inception level. Therefore, measurements using the proposed method should obtain PDIV values with higher precision than the measurements using IEC 61294. The PDIV values of mineral oil and esters are similar, with a variation of less than 3 kV.

In this test, care must be taken not to damage the tip of the needle. It is noticed that a small variation of the tip curvature of the needle may significantly affect the PDIV result, as shown in Appendix I.6. The measured PDIV values depend on the compositions of transformer liquids as well as the needle tip used in the measurement. Therefore, repetitive tests were carried out to confirm the PDIV values of different transformer liquids.

4.5.2 Academic PDIV Definition

To measure the PDIV of academic definition, the PD current was collected by a sample resistor of 50 Ω connected between the test container and the ground, as shown in Figure 4.1. The current signal was monitored by an oscilloscope with bandwidth of 500 MHz. The occurrence of a partial discharge near the PDIV level is characterized by a small current

signal with amplitude above the background noise. The rising time of the small current is usually a few nanoseconds and the duration is hundreds of nanoseconds. During the test, the applied voltage is increased step by step (1 kV/step) with each step lasting 5 minutes. The number of PD pulses was counted in each step, and the PD repetition rate (PD number per minute) was calculated by the overall PD number divided by the time duration.

Figure 4.6 shows the PD repetition rates in both mineral oil and esters. The results show that the PD repetition rates (including both positive and negative partial discharges) increase exponentially with the increase of applied voltage. In order to determine the PDIV more accurately, linear fitting between the applied voltage and the logarithm of the PD repetition rate is applied. Thus the PDIV can be determined from the cross-points of the fitting curves and the measurement threshold of 1 PD/minute.

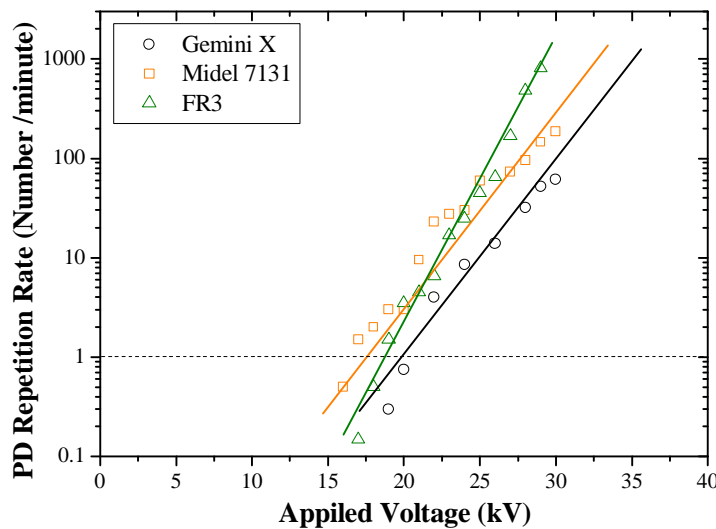


Figure 4.6 PD repetition rates with applied voltage in transformer liquids

Table 4.3 compares the PDIV values of the industrial definition and the academic definition for transformer liquids measured in this chapter. It can be clearly seen that the PDIV values of the academic definition are lower than the PDIV values of the industrial definition for both mineral oil and esters. The PDIV values of mineral oil and esters are similar.

Table 4.3 PDIVs of transformer liquids using industrial and academic definitions

	Gemini X	Midel 7131	FR3
PDIV _{industrial} (kV)	23.2	22.3	25.6
PDIV _{academic} (kV)	19.6	17.5	18.8

The lower PDIV values of the academic definition than those of the industrial definition might be attributed to two reasons. Firstly, the academic definition uses the first PD pulse which exceeds the background noise level, while the industrial definition uses the PD signals with amplitude of 100 pC. Since the background noise in laboratory condition is well-controlled, the PD signals with amplitudes of 100 pC occur at higher voltages than the first PD pulses exceed background noises. Thus, the PDIVs of the academic definition give relatively lower values than those of the industrial definition. Secondly, the oscilloscope is much more sensitive to PD signals than the LDS-6 PD detectors, as it does not use a band-pass filter which partly attenuates a pulse.

The PDIV measurement results using both definitions suggest that mineral oil and esters have similar PDIV results. However, this does not indicate that mineral oil and esters have similar PD characteristics. In order to compare the abilities of transformer liquids to suppress the development of partial discharges, the PD performances of transformer liquids should be studied at overstressed voltages.

4.6 PD Performances at Overstressed Voltages

Pre-breakdown studies show that there are two stages of partial discharges, initiation and propagation, leading to the ultimate breakdowns of transformer liquids. The comparison of PDIV values between mineral oil and esters in the previous section only shows the properties of transformer liquids during the PD initiation stage, offering no information on the PD behaviours during the propagation stage.

In order to differentiate various transformer liquids and to comprehensively evaluate their dielectric properties, their PD performance should be investigated at overstressed voltage.

4.6.1 Experimental Description

The same test configuration and procedure, as described in section 4.3, were adopted to investigate PD behaviours in mineral oil and esters at overstressed voltage. The applied voltage was increased from a level lower than the inception voltage at 1 kV/step. After PD

inception, the applied voltage was increased at 5kV/step until the maximum voltage 70 kV. The duration of each step is 1 minute.

4.6.2 Experimental Results

In IEC 60270, several parameters are defined to evaluate the PD performances of the test object [180]. The minimum requirement for a digital PD instrument is to show the value of the maximum repetitive PD amplitude. Additionally, one or more of the following parameters may be evaluated and recorded, including the apparent charge Q , instantaneous value of the voltage, and phase angle Φ . Derived parameters which show the PD behaviours include PD repetition rate, equivalent discharge current, and equivalent discharge power.

Among these parameters, commonly used ones are maximum PD amplitude, PD repetition rate, Φ - Q - N pattern, equivalent current and equivalent power. These parameters are compared for mineral oil and esters as follows.

4.6.2.1 Maximum PD Amplitude

Figure 4.7 shows the maximum PD amplitudes for mineral oil and esters occurring in each step at overstressed voltages up to 70 kV. The maximum PD amplitude indicates, to some extent, the propagation ability of partial discharges at a voltage level before a breakdown occurs. From 25 kV to 45 kV, the maximum amplitudes of partial discharges in all three liquids are similar, normally lower than 1000 pC. However, at overstressed voltage, the maximum PD amplitude of ester liquids increases dramatically. At 70kV, the maximum PD amplitude of Midel 7131 reaches 7000 pC, and breakdowns appear at this voltage level. The results of the maximum PD amplitudes indicate that partial discharges propagate more easily in esters than in mineral oil.

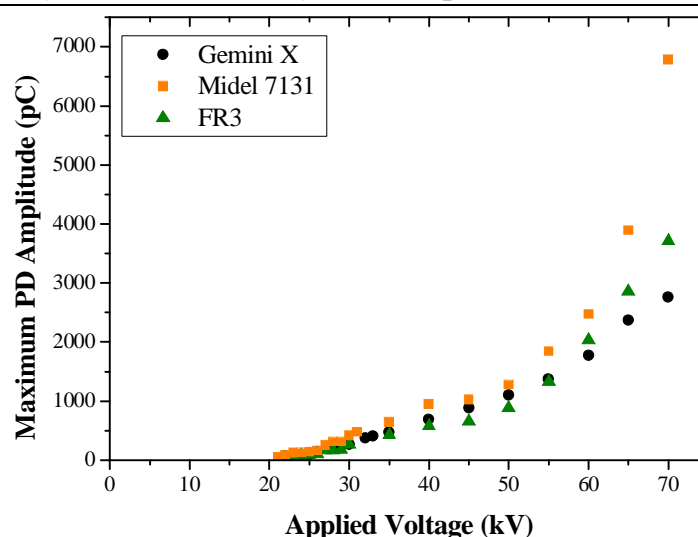


Figure 4.7 Maximum PD amplitudes with applied voltage in transformer liquids

4.6.2.2 PD Repetition Rate

The PD repetition rate is the total number of PD pulses recorded in a selected time interval, usually in one minute. IEC 61294 states that ‘further classification of liquids in terms of the increase in discharge number with voltage may be performed with the same test arrangement’ [177]. Thus the PD repetition rate is another important parameter to characterize the PD behaviours of various insulating liquids.

Figure 4.8 shows the PD repetition rates with applied voltage for all three liquids. The PD repetition rates were measured by the LDS-6 detector, counting all the PDs with apparent charge larger than the 1/10 of the maximum charge amplitude. Clearly, more partial discharges are produced in esters than in mineral oil, which indicates that the PD activities are much more intensive in esters than in mineral oil. It should be noted that the recordings normally include some level of continuous noise, which can be caused by background noise or by a large number of partial discharges whose amplitude is so small compared with the maximum amplitude to be measured. Thus in order to prevent such background noise and yield correct calculations, threshold levels of 5% of the maximum detected PD amplitudes are used to remove the background noise. The PD repetition rates reported in Figure 4.8 are calculated after removing all the background noise using the threshold levels. It is clearly seen that the PD repetition rate is an effective parameter for differentiating various insulating liquids and evaluating their PD properties.

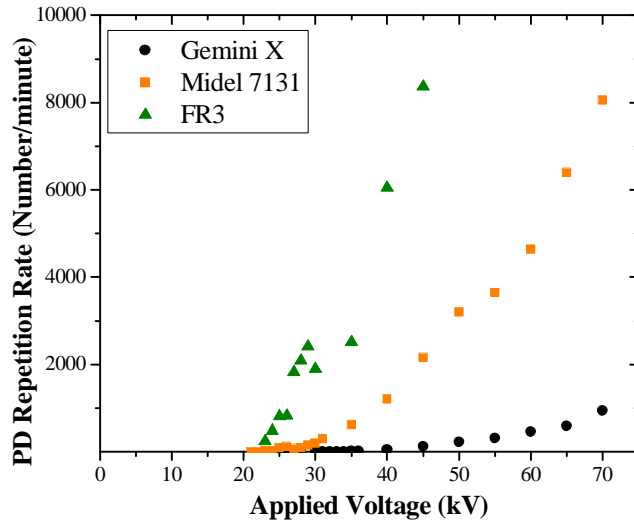


Figure 4.8 PD repetition rates with applied voltage for transformer liquids

4.6.2.3 Φ -Q-N Pattern

Since partial discharges are statistically distributed, the Φ -Q-N PD pattern might be a good parameter for differentiating various liquids. It considers all the PD activities in a defined period of time, in terms of both the individual apparent charge Q_i , and the corresponding phase angle Φ_i of occurrence. Figure 4.9 gives the Φ -Q-N patterns of mineral oil and esters at the applied voltage of 55 kV.

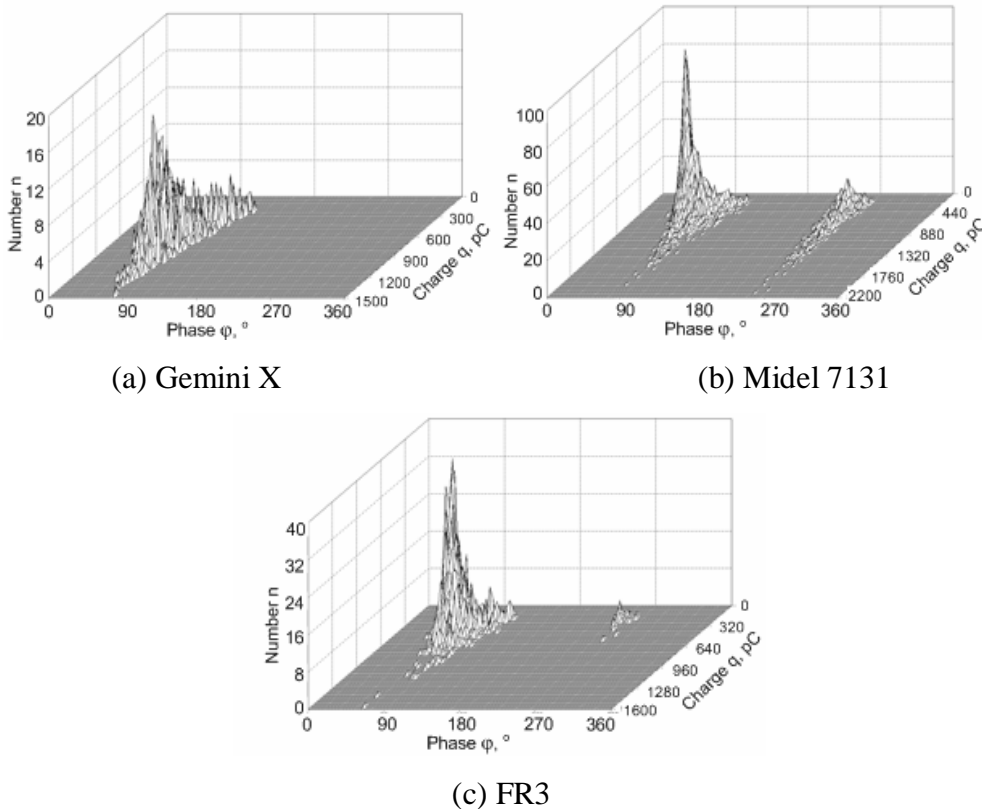


Figure 4.9 Φ -Q-N patterns at applied voltage of 55 kV in transformer liquids

Generally speaking, the partial discharges at positive half cycle (Φ from 0° to 180°) are more intensive than those at negative half cycle (Φ from 180° to 360°) in terms of both PD amplitudes and PD repetition rates. This is probably because positive partial discharges propagate easier, faster and further than negative partial discharges in transformer liquids.

At the voltage of 55 kV, negative partial discharges have been already observed in Midel 7131 and FR3 at the negative half cycle with high amplitudes and significant numbers. However, partial discharges in Gemini X only occur in positive half cycle with lower amplitude and smaller repetition rate. Therefore, the Φ -Q-N pattern can be used as an effective parameter to compare the PD behaviours of various transformer liquids at overstressed voltages.

4.6.2.4 Equivalent Current

The intensity of partial discharges can be evaluated from two aspects: the amplitude and the repetition rate. The equivalent current is derived by the sum of the absolute values of all individual apparent charge divided by the chosen reference unit interval, usually in one minute. It is a combined parameter considering both the PD amplitude and PD repetition rate. The calculation equation is shown in Equation 4.1.

$$I = \frac{1}{T} (|q_1| + |q_2| + \dots + |q_i|) \quad \text{Equation 4.1}$$

Figure 4.10 shows the PD equivalent currents for mineral oil and esters with applied voltages up to 70 kV. The partial discharges in esters have higher amplitudes and larger repetition rates than those in mineral oil. Consequently, the equivalent currents of PD activities in esters are larger than those in mineral oil. From Figure 4.7 and Figure 4.8, it is clearly seen that the PD amplitudes in Midel 7131 are higher than those in FR3, but the PD repetition rates are smaller. As a combined parameter, the equivalent currents in Midel 7131 are similar to those in FR3. Therefore, the equivalent current might be a better parameter to comprehensively evaluate the PD properties of various transformer liquids considering both aspects of PD intensity.

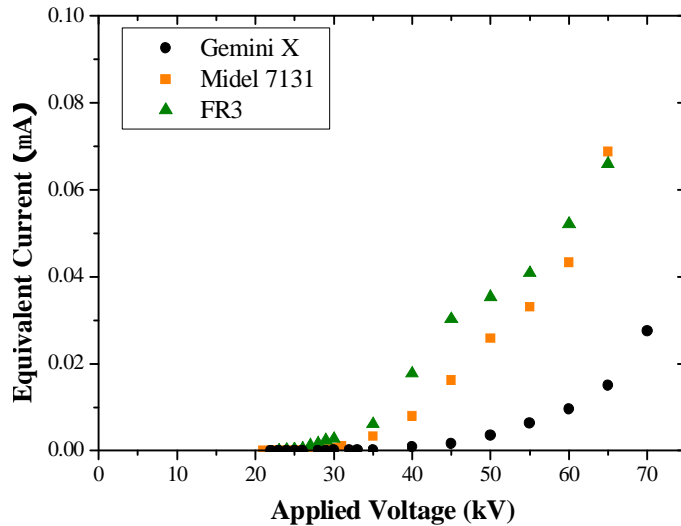


Figure 4.10 PD equivalent currents with applied voltage in transformer liquids

4.6.2.5 Equivalent Power

The equivalent power of partial discharges is defined as the average pulse power fed into the terminals of the test object due to charge transfer during a chosen reference unit interval. It considers not only the PD amplitude and the PD repetition rate, but also the instantaneous applied voltage when an individual partial discharge occurs. The equivalent power can be calculated from Equation 4.2.

$$E = \frac{1}{T} (q_1 u_1 + q_2 u_2 + \dots + q_i u_i) \quad \text{Equation 4.2}$$

Figure 4.11 shows the PD equivalent powers for mineral oil and esters with applied voltage up to 70 kV. It is seen from the results that Midel 7131 and FR3 dissipate similar powers into the test object, but much higher than Gemini X. Since the equivalent current and equivalent power are both combined parameters considering the PD amplitude and the PD repetition rate, the conclusions derived from the test results of the equivalent power are similar to those of the equivalent current. However, the equivalent power indicates the degree of damage that PD activities might cause to transformer liquids. Therefore, it is a more useful parameter to evaluate the intensities of the PD activities. In transformer liquids, the energy dissipated by partial discharges are used to produced light, heat, and to generated fault gases, which will be discussed in detail in Chapter 6.

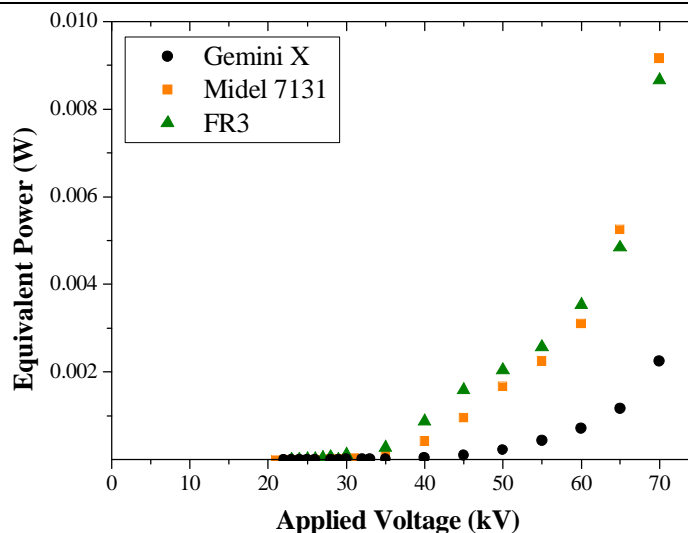


Figure 4.11 PD equivalent powers with applied voltage in transformer liquids

Generally speaking, the PD activities in esters are more intensive than in mineral oil at overstressed voltage levels. The PD properties of Midel 7131 and FR3 are found to be relatively inferior to that of Gemini X in terms of higher maximum PD amplitude, higher PD repetition rate, higher equivalent current, higher equivalent power, and more negative partial discharges. Considering IEC 61294, it is suggested that the PD behaviours at overstressed voltage should be provided as complements to PDIV results, in order to better differentiate between transformer liquids and evaluate their dielectric behaviours.

4.7 Summary

Considering the existing knowledge in literature and the experiment results in this chapter, several additional improvements are suggested as complements to IEC 61294.

- I Step increased voltage is suggested to replace ramping voltage in the PDIV test method, which can provide more stable and reliable results. This replacement also allows building up the Φ -Q-N patterns at given voltages.
- I The voltage application duration is proposed as 1 minute/step, allowing enough PD signals to be recorded without damaging the needle tip. A time gap of 15 seconds should be given after the applied voltage reaches the required value and before recording PD pulses, in order to avoid background noise and disturbances.

- I The PD behaviours at overstressed voltages are recommended as a complement to PDIV measurement results, to comprehensively evaluate the properties of transformer liquids. Commonly used parameters to evaluate the PD behaviours include the maximum PD amplitude, the PD repetition rate, the Φ -Q-N patterns, the equivalent current and the equivalent power.

- I It should be noted that for the same liquid, different PDIV measurement results might be obtained when employing different PD detectors. Therefore, comparisons of PDIV results are not always reliable unless they are determined by the same PD measuring system.

Based on the proposed PDIV test method, the PDIV values of Midel 7131 and FR3 are found to be similar to that of Gemini X. However, the test results of PD behaviours at overstressed voltages indicate that Midel 7131 and FR3 are relatively inferior to Gemini X, in terms of higher maximum PD amplitude, higher PD repetition rate, higher equivalent current, higher equivalent power, and more negative partial discharges.

Chapter 5. Experimental Study on Breakdown in AC Divergent Fields

5.1 Introduction

Up to now, esters have been utilized mainly in medium-voltage transformers due to their environmental features. The suitability of applying esters in high-voltage power transformers is being researched worldwide. Most work involves only the measurements of conventional parameters, such as the breakdown voltage, using standard test methods [5, 14], and few data are currently available which characterize the insulating properties of esters at high voltages and large gaps under AC voltage.

A large amount of data has been obtained over the past decades concerning the pre-breakdown and breakdown properties of mineral oil under high voltages and large gaps [111, 119, 141]. Since the first observation of streamers in mineral oil, a fair correlation has been established between the streamer phenomena and the breakdown strength, from reproducible events and similar observations. However for esters, the streamer study has only been carried out in recent years, usually under impulse voltage or step voltage, which are more convenient conditions for steamer observation [127]. Only a few studies have been carried out to investigate the pre-breakdown phenomena in esters at large gaps under AC voltage.

This chapter comparatively studies the pre-breakdown phenomena of mineral oil and esters in AC divergent fields. Different electrode configurations are used in this chapter with gap distances from 5 mm to 100 mm, and electrode tip curvatures from 1 μm to 700 μm . Section 5.2 introduces the experimental techniques and explains how to synchronize the measurement methods. Section 5.3 studies the features of streamer initiation at relatively low voltage, concluding that the streamer initiations are similar for various transformer liquids. Section 5.4 studies the behaviours of streamer propagation under AC voltage for both positive streamers and negative streamers, and it shows that the propagation of negative

streamers depends heavily on the compositions of the transformer liquid. Section 5.5 measures the breakdown voltages of transformer liquids, and attributes the breakdowns to streamers of different polarities. Finally, section 5.6 provides a summary of the main conclusions.

5.2 Experimental Description

5.2.1 Experimental Setup

The schematic view of the experimental setup is shown in Figure 5.1. The cylinder shaped test cell (4.5 L in volume) was made of transparent Perspex, containing the needle-sphere/needle-plane electrode system. The needle electrode was connected to the high voltage, and the sphere/ plane electrode was connected to the ground. The tip curvatures of the needle electrodes were in the range between 1 μm and 700 μm . The diameter of the sphere electrode was 12.5mm, and the diameter of the plane electrodes were in the range between 40 mm and 100 mm. During the test, the gap distance between the electrodes was adjustable from 1 mm to 100 mm. Although some previous investigations used covered plate electrodes [123, 135], bare electrodes were used in this test to study the streamer properties.

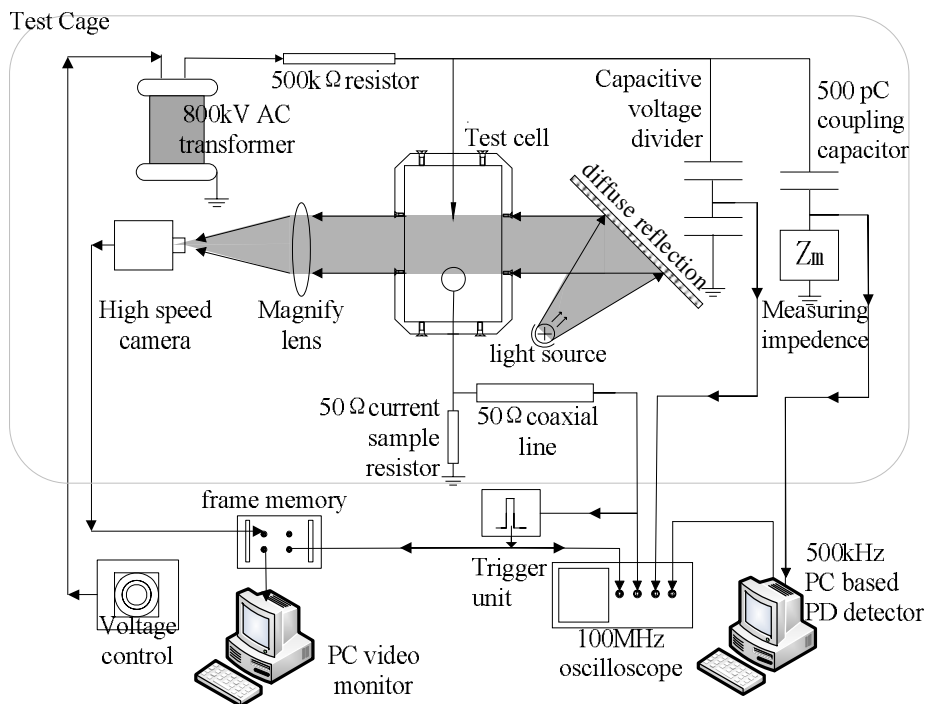


Figure 5.1 Schematic view of experimental Setup

Two types of AC supply were used in the tests. For gap distances < 50 mm, a 70 kV single phase transformer was used to provide the high voltage. For gap distances ≥ 50 mm, in order to provide enough voltage for liquid breakdowns, an AC resonance test set with 800 kV maximum voltage output was used. The highest voltage used in the tests was 150 kV, above which flashovers would occur on the outside surface of the test cell. In order to limit the current when a breakdown occurs, a 500 k Ω resistor was connected between the high voltage output and the test cell. The applied voltage on the point-sphere electrodes was measured by a capacitive voltage divider connected in parallel with the test cell.

5.2.2 Measurement Methods

In this chapter, several methods were used to measure the streamers: a high speed video camera to record the streamer structure, an oscilloscope to measure the streamer current, and a PD detector to measure the apparent charge of a streamer.

5.2.2.1 Streamer Structure Measurement

A high speed CCD video camera, Photron SA-1, was employed to record the streamer structure. This camera has a digital memory of 16 Gigabits, which is able to save a video of, for example, 1.2 seconds in length at a speed of 20,000 **frames per seconds** (fps) and a resolution of 512×512 pixels. The maximum speed of the camera is 40,000 fps, and the quickest shutter speed (smallest exposure time for each frame) is 1 μ s.

In order to record the streamer structure, the **Shadowgraph** technique was used in the tests. A strong light source provided carrier light from one side of the test cell, and the high speed camera recorded the streamer structure from the opposite side. When the carrier light passes through areas with different densities, the carrier light was refracted and the areas were shown as dark shadows in the shadowphotos of streamer structures. By continuously recording the streamer structures, the process of the streamer initiation and propagation could be observed.

However, it should be noted that the photos obtained by this technique only show the structures of streamer channels, rather than the self-irradiated light. Although previous

research reported the self-irradiated light of streamers under impulse voltage [184, 185], it is difficult to obtain those under AC voltage, because the energy released by the streamers under AC voltage is much less than those under impulse voltage, hence the light irradiation under AC voltage is weak. In order to observe the self-irradiated light, more than one light intensifier is required [135].

5.2.2.2 Current Measurement

A 50 Ω sampling resistor was connected between the ground electrode and the ground to measure the streamer current. The current signals were recorded by a 500 MHz-bandwidth digital oscilloscope with sampling capability of 1 G/s. The current was measured at voltages below the breakdown level to protect the oscilloscope from damage.

5.2.2.3 Charge Measurement

The streamer charges were measured by a commercially available PD detector LEMKE LSD-6 with a bandwidth of 900 kHz from 100 kHz to 1 MHz. The computer aided PD detector was calibrated by a 50 pC calibrator, following IEC 60270. The streamer charges can be measured in two different ways, which are described as follows.

- | The PD detector can measure the charge of an individual streamer. After data acquisition, sampling, digitizing and processing, the PD detector has a data interface to output the charge signal. The charge signal was also displayed on the same oscilloscope which measured the current signal, as shown later in Figure 5.3 (a). A comparison with the current signal shows that a charge pulse is the integration of all the streamer current pulses occurred within a period of 10 μ s, and this 10 μ s is called the response resolution time.
- | The PD detector also can summarize all the charge recordings within a period of time, and report them in the Φ -Q-N pattern. In this chapter, the recording duration is set at 1 minute.

5.2.2.4 Synchronization of Measurement Methods

To study the streamer characteristics of transformer liquids, it is of great importance to relate

each streamer to its current and charge. Therefore, much effort was devoted to synchronizing different observation methods. Figure 5.2 shows the time configuration of the synchronization of the streamer structure recording, current recording and charge recordings.

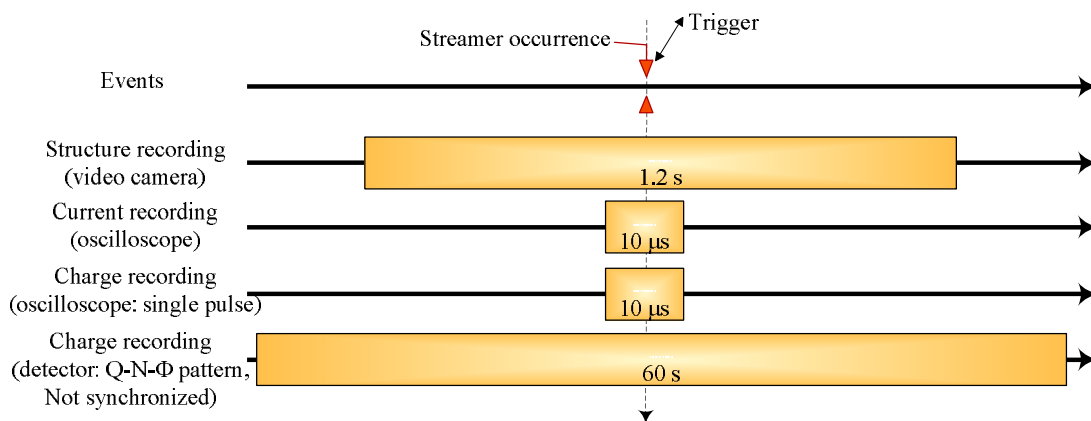


Figure 5.2 Synchronization of measurement methods

When the AC voltage was applied on the electrodes, the high speed video camera and oscilloscope were working continuously, but their measurement signals would not be saved before the detection of a streamer. Once a streamer was produced, a small current pulse with amplitude higher than the background noise would be detected. This current pulse would act as the trigger signal to trigger both the video camera and oscilloscope, and then the recordings before and after the trigger signal, each having duration of 0.6 s for video camera and 5 μs for oscilloscope, were saved, so the overall recording durations were 1.2 seconds for the video camera and 10 μs for the oscilloscope.

Example

Figure 5.3 shows an example of the synchronized recordings. The positive streamer occurred at the positive half cycle of the AC voltage. The streamer current in Figure 5.3 (a) lasted for 1.5 μs , and the stopping length of this streamer was about 2.8 mm as shown in Figure 5.3 (b). Since the duration of the streamer current is almost the same as the duration of the streamer propagation [120], the average propagation velocity of this streamer could be calculated as the ratio of the streamer length and the current duration, about 2 km/s. The streamer charge recorded by the oscilloscope in Figure 5.3 (a) was about 85 pC. The Φ -Q-N pattern recorded by the PD detector in Figure 5.3 (c) showed that only a few streamers were produced at this

voltage level in 1 minute duration, and the maximum apparent charge is about 150 pC.

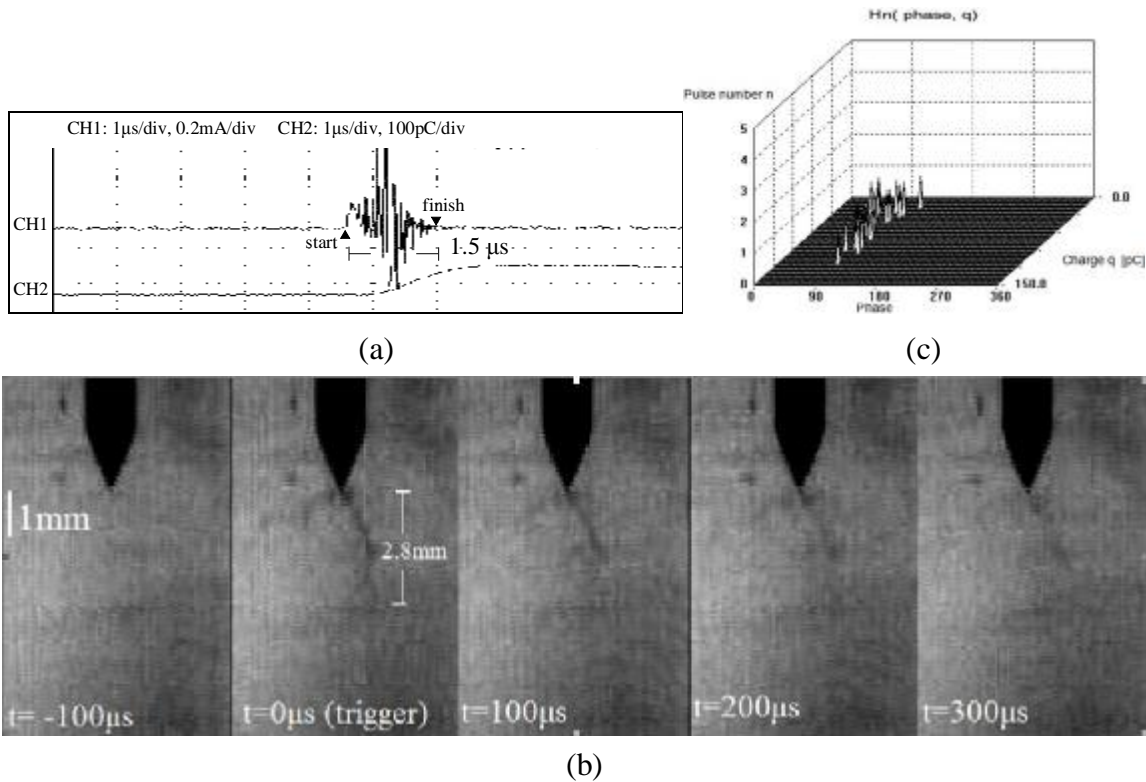


Figure 5.3 The structure, current and charge recordings of a positive streamer in FR3 Point curvature = $1 \mu\text{m}$, $V_{\text{rms}}=24 \text{ kV}$, apparent charge = 85 pC , (a) Streamer current (CH1) and apparent charge (CH2), (b) Streamer structure, (c) Φ -Q-N pattern

5.3 Streamer Initiation

In this section, the generation features of streamer initiation are described at first. Then, the streamer inception voltages and Φ -Q-N patterns in mineral oil and esters are compared. The results show that the streamer characteristics in mineral oil and esters are similar at the initiation stage. However, small differences on such as the streamer repetition rate can still be found. In the discussion, the streamers are classified into positive streamers and negative streamers, depending on their current directions.

5.3.1 General Features

5.3.1.1 Initiation of Negative Streamers

The first observed negative streamer was a small spheroid shadow produced at the electrode tip, occurring at the negative crest of AC voltage. The shadow is caused by a significant change of the refractive index at this area, indicating a density change. Similar phenomenon

was also documented in [123], where the small shadow was regarded as a gaseous bubble.

Figure 5.4 gives an example of a negative streamer in FR3 at 20 kV, using needle (1 μ m tip curvature) to sphere (12.5 mm diameter) electrode configuration with a 50 mm gap. The negative streamer is in a spherical structure and the diameter is about 100 μ m as shown in Figure 5.4 (a). It is associated with a current pulse with magnitude of less than 100 μ A (Figure 5.4 (b)), lasting for no more than 200 ns. At 20 kV, the charges of negative streamers are usually less than 1 pC.

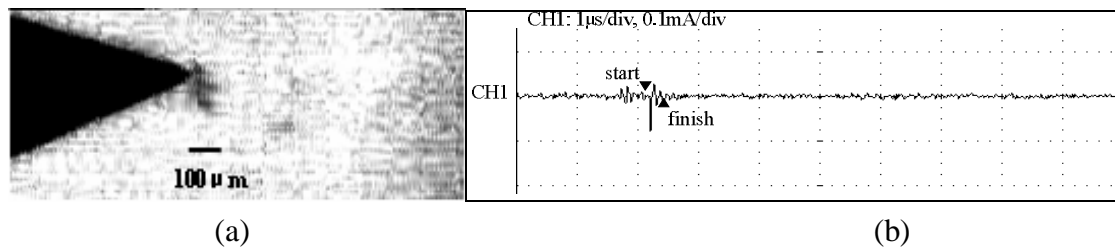


Figure 5.4 Initiation of a negative streamer in FR3 at 20 kV

Point curvature =1 μ m, sphere electrode diameter =12.5 mm, gap distance =50 mm, (a) shadow graph, bubble diameter =80 μ m, (b) associated current

After the occurrence, the negative streamer detaches from the electrode at low voltages (<20 kV at 50 mm gap) and dissolves into surrounding liquid. Figure 5.5 shows the detachment process of the same negative streamer as in Figure 5.4. The negative streamer leaves the electrode tip at a velocity (**detachment velocity**) of about 1.0 to 1.5 m/s, and dissolves in the liquid in the next 400 μ s. After 400 μ s, there is no trace of the streamer in the shadowgraph recordings.

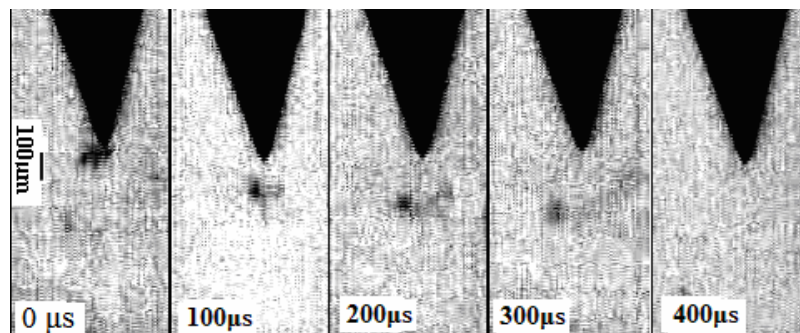


Figure 5.5 Detachment of a negative streamer from electrode tip in FR3 at 20 kV
Point curvature =1 μ m, sphere electrode diameter =12.5 mm, gap distance =50 mm

On the other hand, when the applied voltage is higher (\geq 20 kV at 50 mm gap), the main features of negative streamers stay the same, but the associated current might be higher

(about 500 μA) and last longer (about 300 ns), and the streamer diameter might be increased up to 300 μm . The streamers might continuously expand while still touch with the needle electrode. Then, the negative streamers will grow into bush-like structures, and start to propagate.

5.3.1.2 Initiation of Positive Streamers

The positive streamers appear at the positive crest of AC voltage and at a slightly higher (10 %) voltage than negative streamers, which is in agreement with the results in [123]. As soon as they are detected, the positive streamers were characterized by longer streamer lengths than negative streamers, probably because they expand more easily than negative streamers.

Figure 5.6 shows an example of a positive streamer in Midel 7131 at 24 kV, using needle ($1\mu\text{m}$ tip curvature) to sphere (12.5 mm diameter) electrode configuration with a 50 mm gap. As shown in Figure 5.6 (a), this streamer is composed of many thin branches with an average length of 1 mm, forming a bush-like structure. In the tests, the bush-like structure was only observed in highly divergent fields when the needle tip curvature is less than 5 μm . For less divergent fields, the positive streamers are characterized by filamentary structures with a few long, thin branches [111]. Figure 5.6 (b) shows the associated current with the positive streamer. It is composed of a continuous component, superimposed by several fast pulses. At the initiation stage, the apparent charges of the positive streamers are about 10 pC, much higher than those of negative streamers.

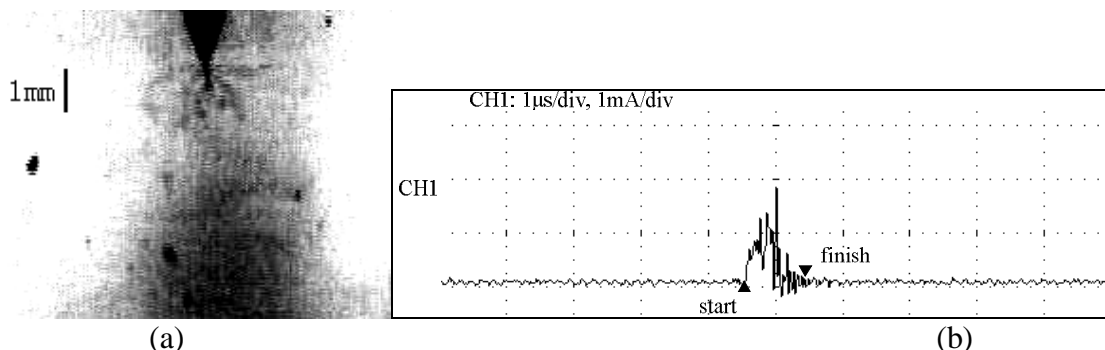


Figure 5.6 Generation of a positive streamer in Midel 7131 at 24 kV
 Point curvature = 1 μm , sphere electrode diameter = 12.5 mm, gap distance = 50 mm, (a) shadow graph, streamer length = 1.3 mm, (b) associated current

After the occurrence, the positive streamer detaches following a similar process to that of a

negative streamer, in terms of detaching from the electrode tip, sweeping away into the bulk liquid and dissolving. Figure 5.7 shows the detachment process of a positive streamer in FR3 at 22 kV. The positive streamer leaves the electrode at a velocity (detachment velocity) of 0.2 to 0.3 m/s, which is much smaller than that of a negative streamer. A possible reason is that the mobility of positive ions in a positive streamer is much lower than the mobility of electrons in a negative streamer.

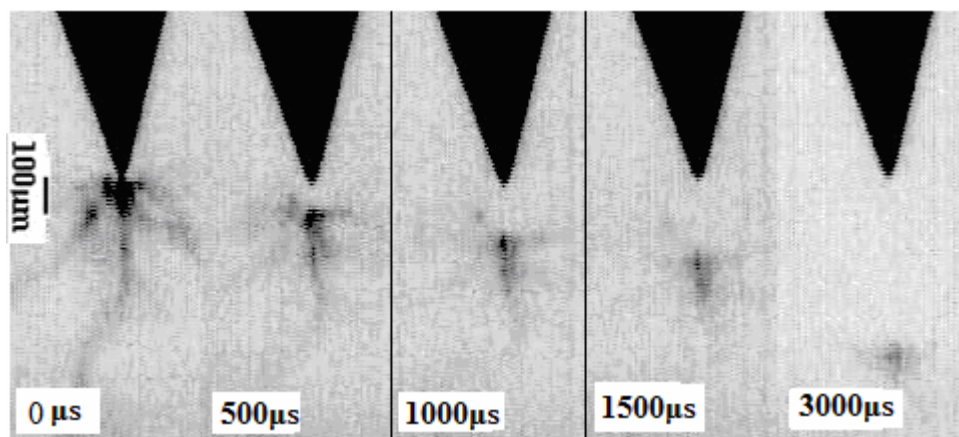


Figure 5.7 Detachment of a positive streamer from electrode tip in FR3 at 22 kV
Point curvature =1 μm, sphere electrode diameter =12.5 mm, gap distance =50 mm

5.3.2 Inception Voltages

Using the needle (1 μm tip curvature) to sphere (12.5 mm diameter) electrode configuration with a 50 mm gap distance, the streamer inception voltages for mineral oil and esters are similar, as shown in Table 4.3. A possible reason is that the streamer inception is caused by the enhancement of local electric field near the needle electrode tip, which is determined by the tip curvature of the needle electrode.

For different electrode configurations, different streamer inception voltages are obtained. Figure 5.8 shows the streamer repetition rates with applied voltage in Midel 7131 using two different electrode configurations, with the same ground sphere electrode (12.5 mm diameter) and gap distance (50 mm). The streamer repetition rates were measured by counting the number of streamer current pulses in the oscilloscope. When the tip curvature of the needle electrode is increased from 1 μm to 50 μm, the streamer inception voltage of Midel 7131 is increased by 2 kV.

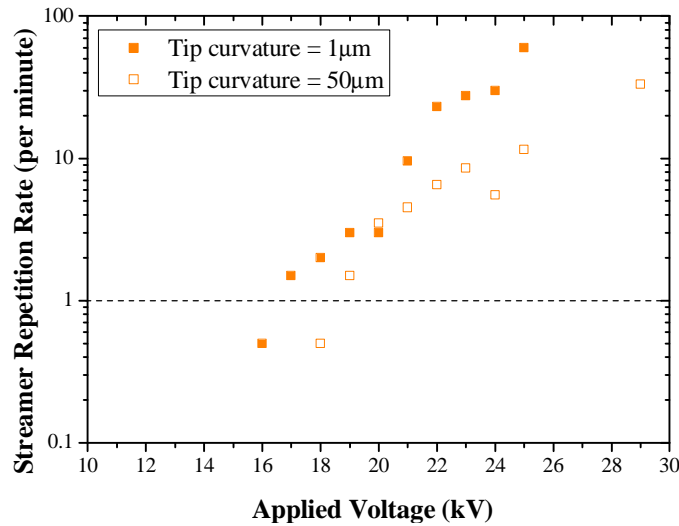


Figure 5.8 Streamer repetition rates versus applied voltage in Midel 7131 using two needle electrodes

Nevertheless, since the streamer inception is determined by the needle electrode, Gemini X and FR3 should have similar inception voltages using the same electrode configuration, as shown in Appendix I.6. A similar conclusion was also documented in [186].

5.3.3 Φ -Q-N Patterns

Figure 5.9 shows the Φ -Q-N patterns of all the streamers recorded by the PD detector during a 1-minute period in both mineral oil and esters at the initiation stage. The applied voltages are 5 kV above the streamer inception voltages of transformer liquids. Although mineral oil has a similar maximum apparent charge (100 pC) to those of esters, the streamer repetition rates of mineral oil is much lower.

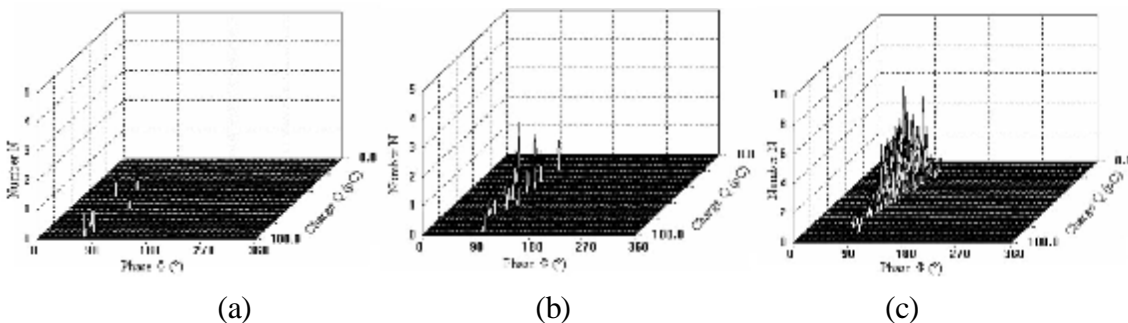


Figure 5.9 Φ -Q-N patterns during 1 minute period recorded by a digital PD detector Point curvature = 1 μm , sphere electrode diameter = 12.5 mm, gap distance = 50 mm, in (a) Gemini X, $V_{\text{rms}} = 24$ kV, (b) Midel 7131, $V_{\text{rms}} = 23$ kV, (c) FR3, $V_{\text{rms}} = 24$ kV.

At this stage, streamers of both polarities can be detected using a high speed camera and

shadowgraph technique. However, the PD detector only shows the existence of positive streamers, without any trace of negative streamers. A possible reason is that the charge contained in the negative streamers at the initiation stage is too small to be recognized by the PD detector.

At higher voltages when negative streamers start to propagate, their durations increase and there are the more charges contained in the negative streamers. Therefore, negative streamers can be recognized correctly at higher voltages.

5.4 Streamer Propagation

In the propagation stage, significant differences exist in the streamer behaviours of mineral oil and esters. This section describes the streamer behaviours in terms of streamer structure, associated current, stopping length, velocity and Φ -Q-N patterns. The streamers are discussed as positive streamers and negative streamers respectively. After that, the space charge effect on the streamer inception voltage and streamer structure is investigated.

5.4.1 Streamer Structures and Associated Currents

5.4.1.1 Positive Streamers

When the applied voltage exceeds the streamer inception voltage, the positive streamers start to propagate. Previous work attributes the propagation of positive streamers to the field enhancement at the streamer tips [26], which is high enough to ionize surrounding liquid molecules [187, 188]. The electrons produced from the ionization process are absorbed into the streamer tips, leaving positive ions as the extension of the streamer channels. The streamer current is caused by electrons moving in the streamer channels, showing the overall effect of ionization and electron absorption process at all streamer tips [123].

Figure 5.10 shows the positive streamer structures of both mineral oil and esters in the propagation stage at 50 kV, using needle (1 μ m tip curvature) to sphere (12.5 mm diameter) electrode configuration with a 50 mm gap distance. The positive streamers in mineral oil and

esters have similar structures. At the roots of the streamers, small streamer branches extend from the needle electrode to many directions; but only several branches can propagate deeply into the bulk oil and develop into long filaments, forming filamentary structures. When they reach certain lengths, the filaments will divide into sub-branches, and the streamer propagation will stop soon afterwards

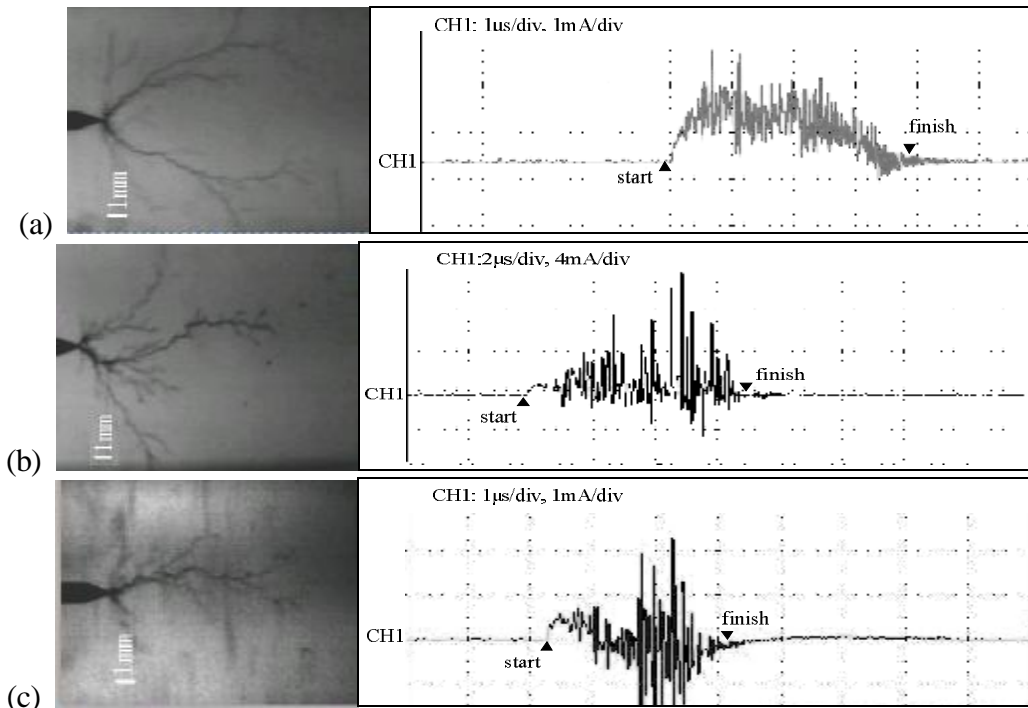


Figure 5.10 Structures and associated currents of positive streamers propagation Point curvature = $1 \mu\text{m}$, sphere electrode diameter = 12.5 mm , gap distance = 50 mm , $V_{\text{rms}} = 50 \text{ kV}$, in (a) Gemini X, (b) Midel 7131, (3) FR3

Figure 5.10 also shows the associated currents of positive streamers in mineral oil and esters. The associated current is composed of a continuous component superimposed by a train of high frequency pulses, which is also documented in [123]. For Gemini X, the continuous component of the streamer current remains quasi-constant for $3 \mu\text{s}$, and then the current signal gradually disappears. The high-frequency pulses are superimposed on the continuous component. On the other hand, the continuous component of the streamer current of esters lasts for a shorter time and reduces soon. Afterwards, the current signal is mainly composed of high-frequency component of higher amplitude than mineral oil. [125] related this type of current to hybrid streamers, in which the filamentary streamers appear at first and propagate until a certain length, and then they slow down and transform into a slow streamer with periodic reillumination, represented by discrete current pulses.

5.4.1.2 Negative Streamers

Within a large voltage range above the streamer inception voltage, the negative streamers are still near to the HV electrode. They only start to propagate when the applied voltage exceeds a certain threshold voltage. In [123], the propagation of negative streamers was attributed to the expansion of the gaseous streamer channels, as a result of high temperature and high pressure inside the channels caused by streamer currents.

Figure 5.11 shows the negative streamer structures and the associated currents of both mineral oil and esters at 50 kV, using needle (1 μm tip curvature) to sphere (12.5 mm diameter) electrode configuration with a 50 mm gap. At 50 kV, the negative streamers in esters have an average length of 2 mm, but the negative streamer in mineral oil is still gathered around the needle electrode as a faint shadow. For this configuration, mineral oil has a much higher threshold voltage of 65 kV for negative streamers to propagate than those of ester (about 40 kV), which probably indicates that esters are relatively inferior to mineral oil in terms of the ability to suppress the propagation of negative streamers.

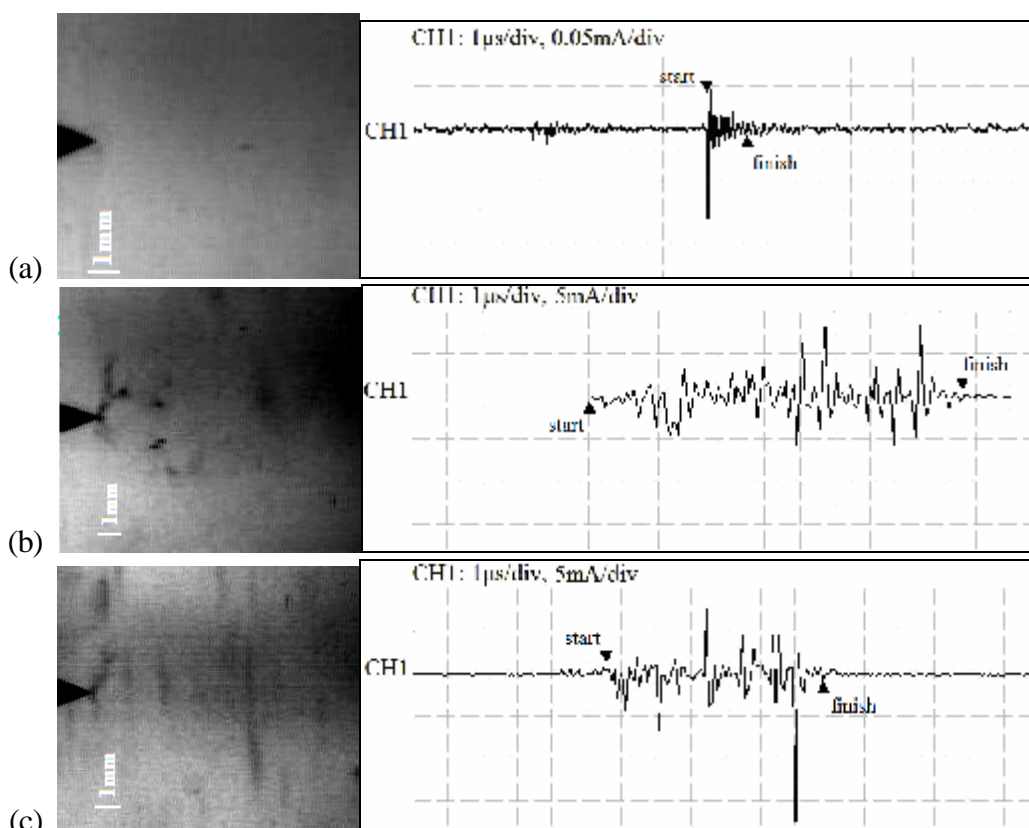


Figure 5.11 Structures and associated currents of negative streamers propagation Point curvature = 1 μm , sphere electrode diameter = 12.5 mm, gap distance = 50 mm, V_{rms} = 50 kV, in (a) Gemini X, (b) Midel 7131, (3) FR3

Significant differences of the associated current of negative streamers also exist between mineral oil and esters. In Figure 5.11, the current signal of mineral oil is mainly a single pulse of 0.15 mA in amplitude and 300 ns in duration, but the current signals of negative streamers in esters have higher amplitudes (6 mA for Midel 7131, and 15 mA for FR3) and longer durations (5 μ s for Midel 7131, and 3 μ s for FR3) than mineral oil. Compared to the positive streamer current, the negative streamer current is only composed of the high-frequency component, without the continuous component.

When the applied voltage is further increased, the negative streamers in both mineral oil and esters will start to propagate. Figure 5.12 shows the negative streamer structures in transformer liquids at the breakdown voltage levels, using needle (1 μ m tip curvature) to sphere (12.5 mm diameter) electrode configuration with a 75 mm gap. Although they have similar filamentary structures, the negative streamers propagate much further in esters than in mineral oil. Compared with the positive streamers in Figure 5.10, the diameter of the negative streamer channels are larger than positive streamers, similar to the results in [126].

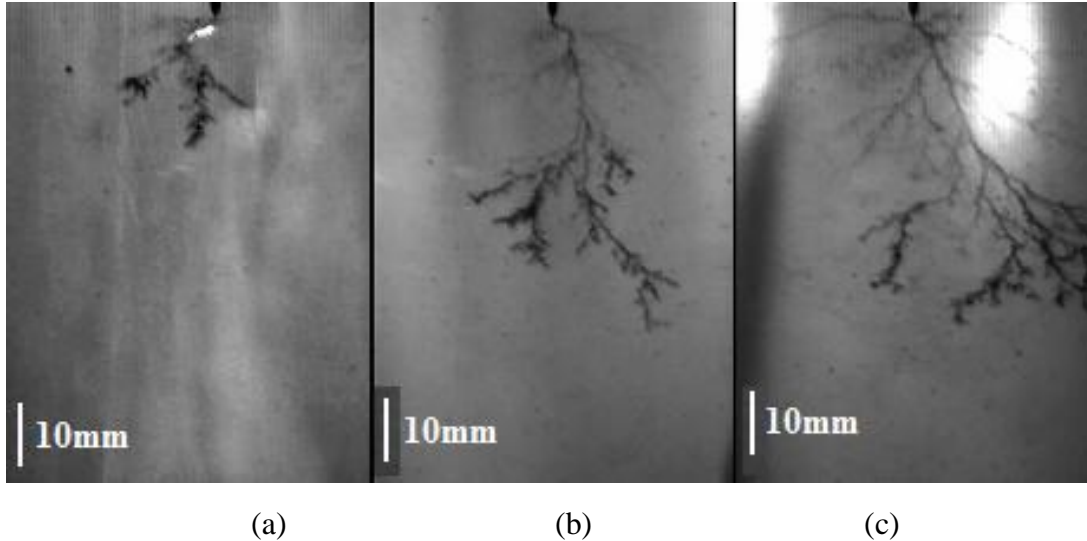


Figure 5.12 Structures of negative streamers at breakdown voltage levels
Point curvature =1 μ m, sphere electrode diameter =12.5 mm, gap distance =75 mm, in (a)
Gemini X, $V_{\text{rms}} =130$ kV (b) Midel 7131, $V_{\text{rms}} =100$ kV (c) FR3, $V_{\text{rms}} =110$ kV

5.4.2 Maximum Stopping Lengths

Below the breakdown voltage, the streamers will not cross the entire gap between the electrodes. They usually stop at certain lengths, which mainly depend on the applied voltage.

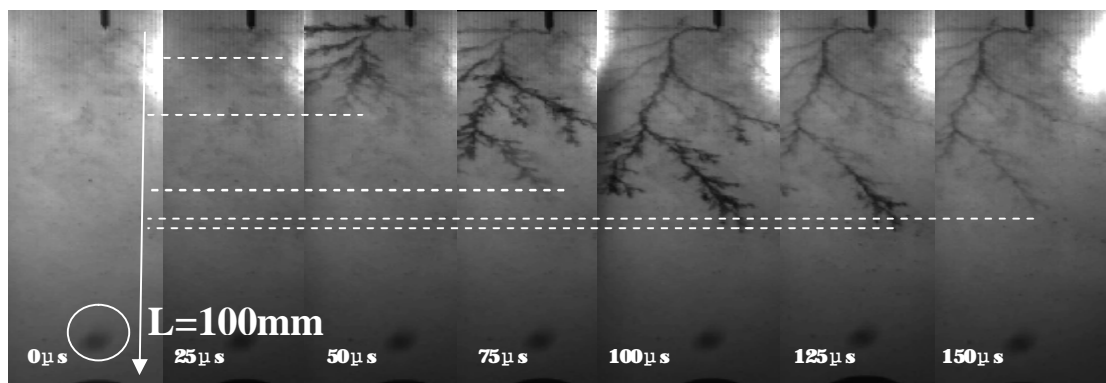
The higher the applied voltage, the further the streamers propagate into the bulk liquids.

5.4.2.1 Definitions

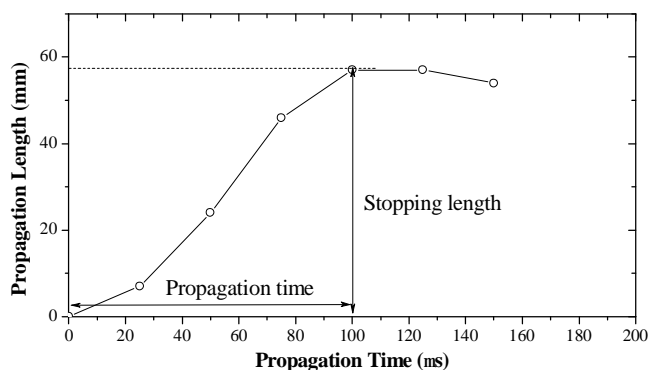
Streamer Stopping Lengths

The ‘**stopping length**’ of a streamer is the length of the streamer projection along the axis (from the tip electrode to the ground electrode) when the streamer stops propagation. The streamer stopping lengths can be determined from the shadowgraph recordings of the streamer structures. The measurement accuracy of the stopping length is about 0.2 mm, limited by the quality of the shadowgraph photos.

Figure 5.13 shows an example of how to determine the streamer stopping length, based on the shadowgraph recordings of a negative streamer in Midel 7131 at 90 kV, using needle (1 μm tip curvature) to sphere (12.5 mm diameter) electrode configuration with a 100 mm gap.



(a) Streamer propagation recorded by a high speed camera



(b) Streamer propagation length versus propagation

Figure 5.13 Propagation of a negative streamer in Midel 7131 at 90 kV
 Point curvature = 1 μm , sphere electrode diameter = 12.5 mm, gap distance = 100 mm

The 1st photo of Figure 5.13 (a) shows the electrode configuration and the negative streamer

has not propagated at the moment. **The black shadow near to the ground electrode marked by a circle is caused by a defect in the camera lens, which will also appear in later graphs.** From the 2nd to the 5th photos, the streamer starts to propagate and reaches a length of 57 mm (projection length) after 100 μ s. Afterwards, the streamer gradually fades out and disappears in the following photos. Figure 5.13 (b) shows the streamer propagation length versus propagation time, obtained from the shadowgraph recordings. It is clearly seen that the stopping length of this streamer is 57 mm.

Maximum Stopping Lengths

The ‘**maximum stopping length**’ is the maximum value of streamer stopping lengths during a period of time (100 AC cycles) at a certain voltage. The streamer with the maximum stopping length represents the most dangerous streamer under this voltage.

When the applied voltage is higher than the streamer inception voltage, the streamers do not necessarily appear at the crests (phase angle $\theta = \pm 90^\circ$) of the AC voltage. The instantaneous voltage ($V_{\text{instantaneous}} = V_{\text{peak}} \times \sin(\theta)$) is the voltage applied on the HV electrode when a streamer occurs. The relationships between V_{peak} , V_{rms} and $V_{\text{instantaneous}}$ are expressed in Figure 5.14.

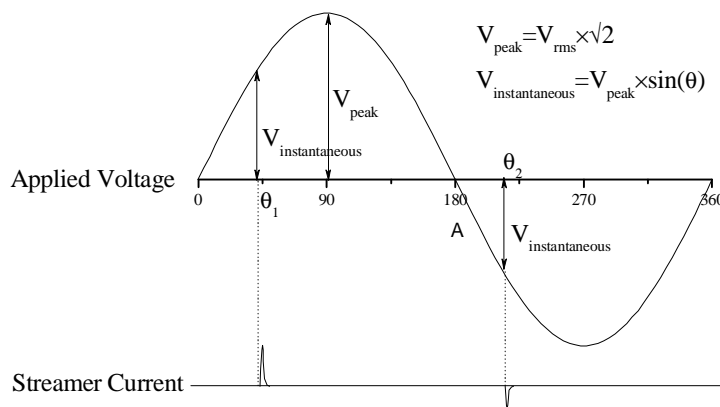


Figure 5.14 Interpretation of V_{peak} , V_{rms} and $V_{\text{instantaneous}}$ for streamers under AC voltage

In AC divergent field, the reproducibility of the streamer stopping lengths at a certain voltage is rather poor, and a large scattering of the streamer stopping lengths is observed. Figure 5.15 shows the streamer stopping lengths versus instantaneous voltage in Gemini X at 80 kV, using needle (1 μ m tip curvature) to sphere (12.5 mm diameter) electrode configuration with

a 50 mm gap. All the positive and negative streamers occurred in 100 AC cycles are measured and plotted in the graph versus their corresponding instantaneous voltages. It shows that the stopping lengths of positive streamers distribute widely from 10 mm to 50 mm at this voltage, and those of negative streamers distribute from 0 mm to 3 mm.

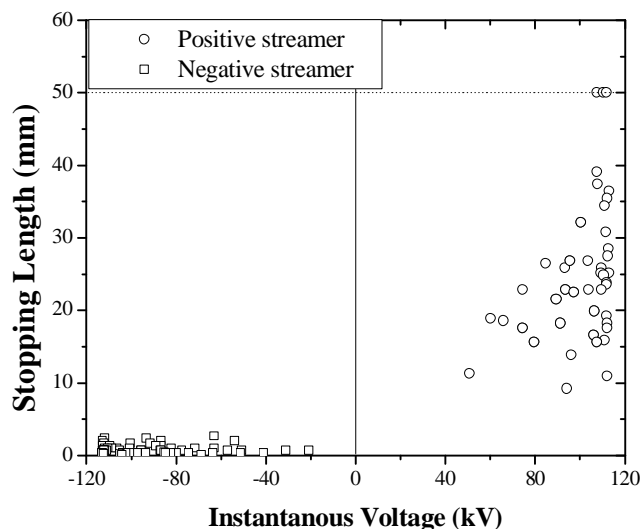


Figure 5.15 Streamer stopping length versus instantaneous voltage in Gemini X at 80 kV
Point curvature = 1 μ m, sphere electrode diameter =12.5 mm, gap distance =50 mm

Since the streamer with the maximum stopping length represents the most dangerous streamer at a certain voltage, the ‘maximum stopping length’ might be a good parameter to evaluate the streamer characteristics. In this chapter, a period of **100 AC cycles** is regarded to be long enough to record enough streamers for determining the ‘maximum stopping length’ at this voltage.

5.4.2.2 Positive Streamers

Figure 5.16 shows the maximum stopping lengths of positive streamers in transformer liquids versus applied voltage (rms value), using needle (1 μ m tip curvature) to sphere (12.5 mm diameter) electrode configuration with a 50 mm gap. In the graph, V_{b-G} , V_{b-M} and V_{b-F} , standing for the 50 % breakdown voltages of Gemini X, Midel 7131 and FR3, are provided as references. The maximum stopping lengths of mineral oil and esters behave similar, increasing in an almost linear relationship with applied voltage. A ‘final jump’ might occur when a streamer reaches a certain length (**critical length**) near to the breakdown voltage, which is evidenced by a non stopping area between the lengths of 40 mm and 50 mm.

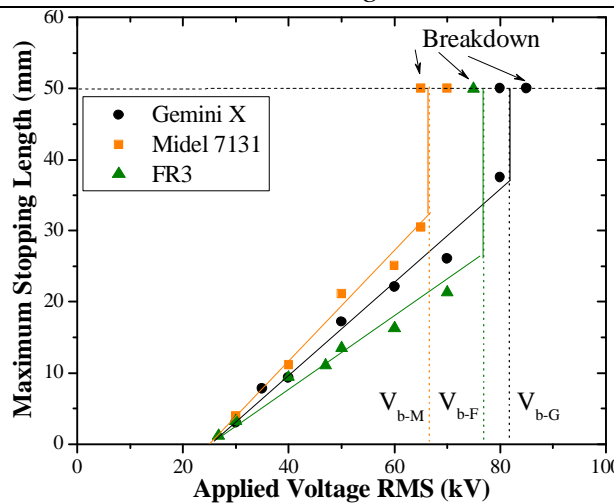


Figure 5.16 Maximum stopping lengths for positive streamers in transformer liquids
Point curvature = $1\mu\text{m}$, sphere electrode diameter = 12.5 mm , gap distance = 50 mm

Two differences on the maximum stopping lengths of positive streamers are found between mineral oil and esters. Firstly, Midel 7131 has a higher increasing rate of 0.73 mm/kV than those of Gemini X (0.60 mm/kV) and FR3 (0.45 mm/kV). Usually a higher increasing rate corresponds to a lower breakdown voltage [189], thus, the breakdown voltage of Midel 7131 is the lowest (68 kV). However, it is surprising to find that FR3 has the lowest increasing rate but a lower breakdown voltage than Gemini X. This might be attributed to the fact that the final jump occurs from a shorter length (critical length) in FR3 (25 mm , 50% of the gap length) than in Gemini X (40 mm , 80% of the gap length). Critical length is the second difference we observed from the results. The smaller critical lengths in Midel 7131 (30 mm , 60% of the gap length) and FR3 than Gemini X might be explained by two possible reasons, described as follows.

- 1. The voltage drop on a streamer channel is dependent on the streamer current [26]. The high streamer current in esters results in a low voltage drop on the streamer channels. Hence, more voltage is applied on the streamer tips in esters, enhancing the local field around the streamer tips and promoting the occurrence of ‘final jumps’ at smaller lengths.
- 2. Esters have higher viscosities than Gemini X. The diameters of streamer channels could be thinner in esters than in Gemini X due to higher expansion resistances (the image quality can not ascertain this point). Hence, the electric field at the streamer tip might be higher in esters than Gemini X, favouring the occurrence of ‘final jumps’ at smaller lengths.

5.4.2.3 Negative Streamers

Figure 5.17 shows the maximum stopping lengths of negative streamers in transformer liquids versus applied voltage (rms value), using the same configuration as in Figure 5.16. For negative streamers, a significant difference of the maximum stopping lengths exists between mineral oil and esters. In Midel 7131 and FR3, the negative streamers start to propagate at 35 kV and 45 kV. Their maximum stopping lengths increase rapidly afterwards, and the streamers fully span the liquid gap at 70 kV and 84 kV, only a little higher than the 50 % breakdown voltages. Therefore, the breakdowns in esters are sometimes triggered by negative streamers.

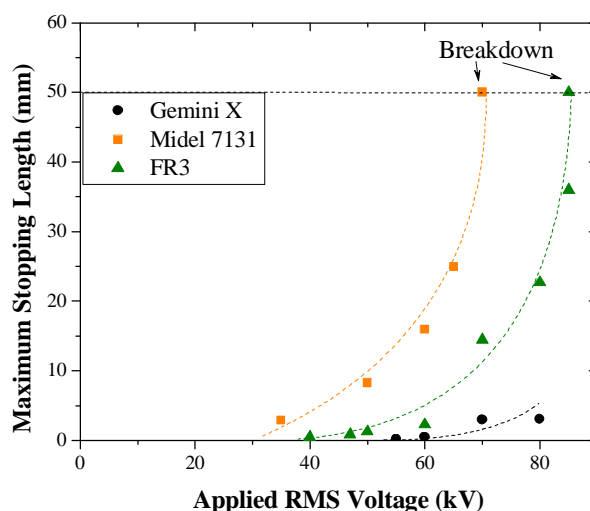


Figure 5.17 Maximum stopping lengths for negative streamers in transformer liquids
Point curvature = $1\mu\text{m}$, sphere electrode diameter = 12.5 mm, gap distance = 50 mm

However, the negative streamers in Gemini X do not propagate below 65 kV. Above 65 kV, the maximum stopping length of negative streamers increases very slowly, and the negative streamers only reach 5 mm at the 50 % breakdown voltage, which indicates the breakdown in Gemini X can be only triggered by positive streamers. Similar behaviours were also documented in [135] using mineral oil and needle to plane configuration. The fact that negative streamers propagate much easier in esters than in Gemini X confirms that Gemini X has a higher ability to suppress the propagation of negative streamers than Midel 7131 and FR3.

5.4.3 Average Propagation Velocities

It is generally accepted that the streamers propagate at a constant velocity before a breakdown occurs. Therefore, the average propagation velocity of a streamer can be calculated as the ratio of the stopping length and the propagation time. The stopping length can be determined from the shadowgraph recordings of the streamer structures, and the propagation time can be determined from the current recordings, because the propagation time of a streamer is the same as the duration of the streamer current [120].

5.4.3.1 Positive Streamers

Figure 5.18 shows the stopping lengths of positive streamers versus propagation time in transformer liquids at various voltages, using needle (1 μm tip curvature) to sphere (12.5 mm diameter) electrode configuration with a 50 mm gap. The corresponding regression lines are plotted in the graph, whose slopes are the propagation velocities. For positive streamers, mineral oil and esters have similar propagation velocities. Their regression lines are nearly overlapped, giving propagation velocities of about 1.5 km/s. This value is similar to previously documented results in [114]. Classification by their velocities shows that the positive streamers belong to the 2nd mode streamers [127], which are characterized by a similar propagation velocity over a wide range of applied voltage.

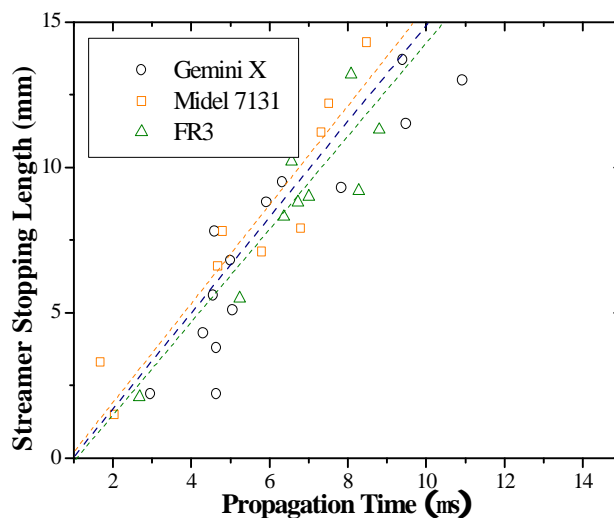


Figure 5.18 Propagation velocities of positive streamers in transformer liquids
Point curvature = 1 μm , sphere electrode diameter = 12.5 mm, gap distance = 50 mm

5.4.3.2 Negative Streamers

Figure 5.19 shows the stopping lengths of negative streamers versus propagation time, using the same configuration as in Figure 5.18. Since too few negative streamers were captured in Gemini X at a 50 mm gap and their stopping lengths are too short to determine the propagation velocity, negative streamers captured at a 85 mm gap and higher voltages were also used in Figure 5.19 to aid the average velocity calculation and these streamers are marked out, this is reasonable since the streamer propagation velocities are similar at applied voltages lower than the breakdown voltage [127].

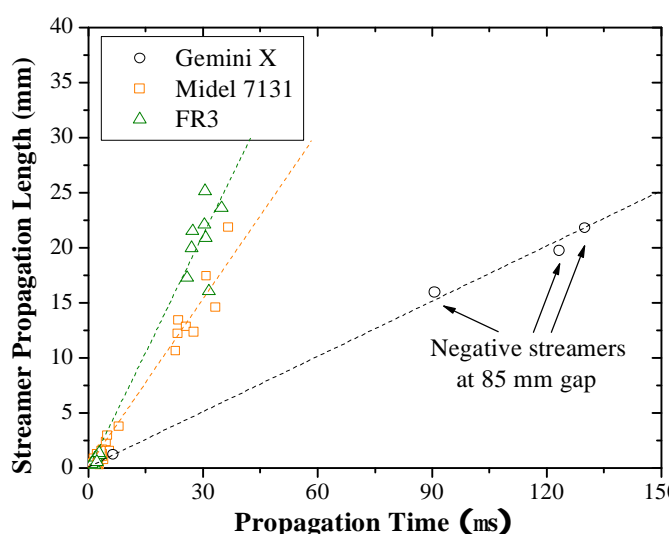


Figure 5.19 Propagation velocities of negative streamers in transformer liquids
Point curvature = $1\mu\text{m}$, sphere electrode diameter = 12.5 mm , gap distance = 50 mm

A significant difference of the propagation velocity of negative streamers exists between mineral oil and esters. The propagation velocity of negative streamers in FR3 and Midel 7131 is 0.7 km/s and 0.55 km/s , much higher than that in Gemini X at about 0.2 km/s . In previous publications, the high velocity of negative streamers was attributed to the high electronic affinity of liquid molecules [190]. Hence, the higher velocity of negative streamers in Midel 7131 and FR3 than in Gemini X might be attributed to their high electronic affinities due to the ester ($-\text{COO}-$) parts in their molecular structures. For FR3, the carbon-carbon double and triple bonds might further increase the electronic affinity, further promoting the negative streamer velocity.

The streamer velocities might give us clues to the possible physical nature of streamer

propagation. The positive streamers propagate at a speed of kilometres per second, whose nature is clearly electronic. The negative streamers propagate at a lower speed of hundreds meters per second, whose nature might be electro-hydrodynamic [48].

5.4.4 Φ -Q-N Patterns

Figure 5.20 shows the Φ -Q-N patterns of mineral oil and esters at the streamer propagation stage of 40 kV, using needle (1 μm tip curvature) to sphere (12.5 mm diameter) electrode configuration with a 50 mm gap. The positive streamers in esters have higher apparent charges and higher repetition rates than in Gemini X. In Midel 7131, the negative streamers have already developed to an apparent charge of 200 pC, but in FR3 and Gemini X, there is no trace of negative streamers in the Φ -Q-N patterns, which agrees with previous observation that the negative streamers in Midel 7131 start to propagate at 35 kV, and the negative streamers in FR3 and Gemini X start to propagate at 45 kV and 60 kV.

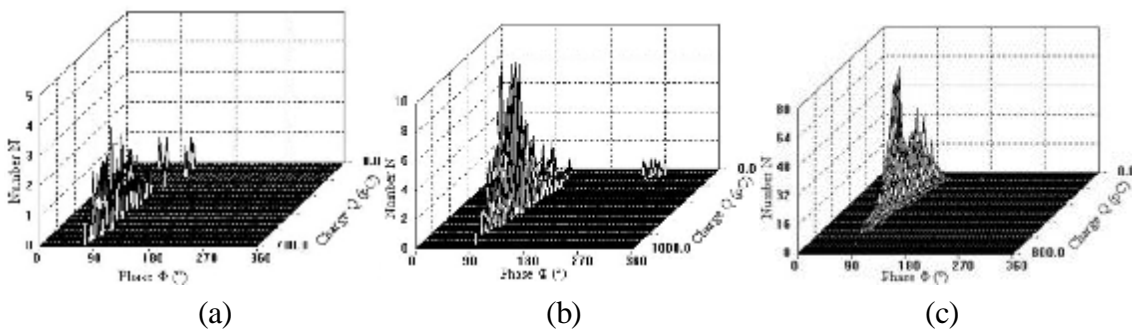


Figure 5.20 Φ -Q-N patterns of transformer liquids at 40 kV

Point curvature = 1 μm , sphere electrode diameter = 12.5 mm, gap distance = 50 mm, in (a) Gemini X, (b) Midel 7131, (c) FR3

Figure 5.21 shows the Φ -Q-N patterns of mineral oil and esters at higher voltage of 70 kV, using the same configuration as in Figure 5.20. In Midel 7131 and FR3, the apparent charges and repetition rates of negative streamers are similar to or even exceed those of positive streamers. However, the negative streamers in Gemini X have much smaller apparent charges and repetition rates than positive streamers, further confirming that Gemini X has a higher ability to suppress the propagation of negative streamers.

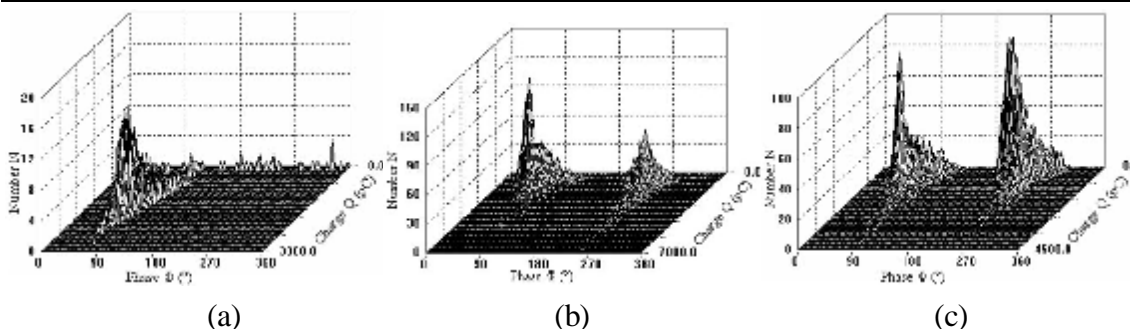


Figure 5.21 Φ -Q-N patterns of transformer liquids at 70 kV

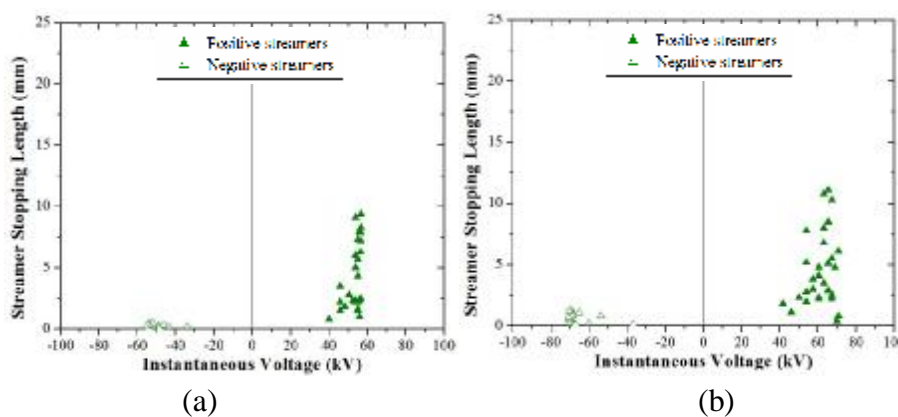
Point curvature = 1 μ m, sphere electrode diameter = 12.5 mm, gap distance = 50 mm, in (a) Gemini X, (b) Midel 7131, (c) FR3

5.4.5 Space Charge Effect

Under AC voltage, the HV electrode will inject space charge into the bulk liquid surrounding the electrode [142]. The injected space charge accumulates in the bulk liquid and disturbs the field distribution, thus affecting both the streamer inception voltage and the streamer structures [114]. Since the duration of voltage application under AC voltage is longer than under impulse voltage, more space charge will be injected and thus the space charge effect is more significant under AC voltage [142].

5.4.5.1 Effect on Inception Voltages

Under AC voltage, the space charge effect on streamer inception voltage is similar between Midel 7131 and FR3. Taken FR3 as an example, Figure 5.22 depicts the relationships between the streamer stopping length and the instantaneous voltage in FR3 at various applied voltages, using needle (1 μ m tip curvature) to sphere (12.5 mm diameter) electrodes with a 50 mm gap.



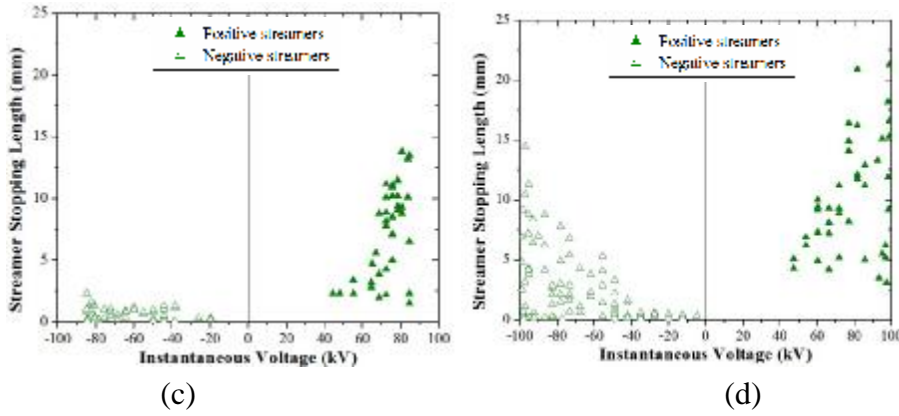


Figure 5.22 Streamer lengths versus instantaneous voltages in FR3

Point curvature = 1 μm , sphere electrode diameter = 12.5 mm, gap distance = 50 mm, (a) $V_{\text{rms}} = 40$ kV, (b) $V_{\text{rms}} = 50$ kV, (c) $V_{\text{rms}} = 60$ kV, (d) $V_{\text{rms}} = 70$ kV

It is clearly seen that when the applied AC voltage (rms) is increased from 40 kV to 70 kV, the inception voltage of positive streamers is increased from 38 kV as in Figure 5.22 (a) to 44 kV as in Figure 5.22 (d), but the inception voltage of negative streamer is increased to 38 kV at first and then decreased to 0 kV as shown in Figure 5.22 (d). In order to show this tendency more clearly, the streamer inception voltages versus the applied voltage are plotted in Figure 5.23 for both positive streamers and negative streamers, and the space charge effect is suspected as the key mechanism dominating the trend.

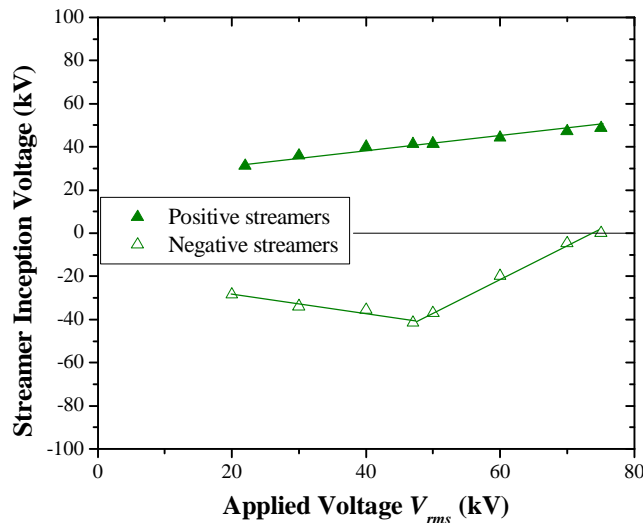


Figure 5.23 Streamer inception voltages versus applied voltage in FR3

Point curvature = 1 μm , sphere electrode diameter = 12.5 mm, gap distance = 50 mm

Likewise, the space charge effect on the streamer inception voltage of Gemini X can be determined and is shown in Figure 5.24. Since too few negative streamers were recorded at 50 mm gap, only the positive streamers are plotted. The space charge has similar effect on

the inception voltage of positive streamers in Gemini X to that in FR3. However, Gemini X has a higher increase rate of the inception voltage than that of FR3.

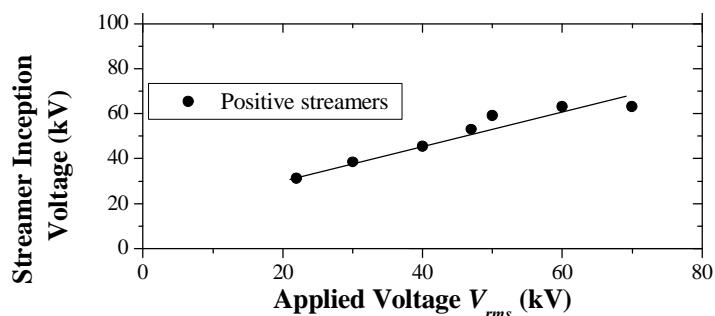


Figure 5.24 Streamer inception voltages versus applied voltage in Gemini X
Point curvature = 1 μm , sphere electrode diameter = 12.5 mm, gap distance = 50 mm

Although the quantity and distribution of the space charges cannot be determined from the test results, it is obvious that the space charge effect occurs and influences the streamer inception voltages. It is also clear that, in a point-sphere gap under AC voltage, the space charge effect on streamer inception voltages can be classified into two situations.

When the HV electrode is positive (negative) polarity, positive (negative) space charge will be formed in the vicinity of the electrode (homo-charge). The homo-charge will reduce the local field around the electrode as shown in Figure 5.25 (a), thus increasing the streamer inception voltages. The effect of homo-charge on the field distortion was also documented in [191] under DC voltages.

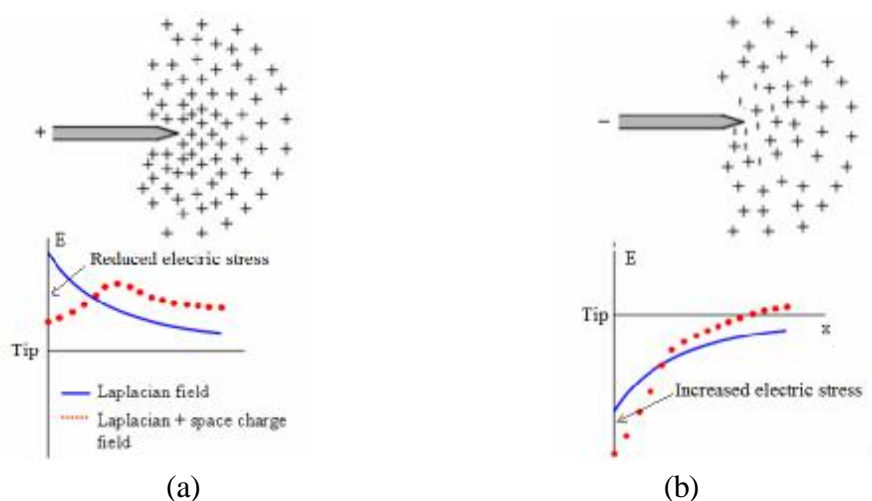


Figure 5.25 Space charge disturbance on field distribution near HV point electrode
(a) homo-charges, (b) hetero-charges

Reversely, the space charge with opposite polarity (hetero-charge) to the HV electrode will reduce the streamer inception voltage. For example, when the HV point electrode changes from positive polarity to negative polarity due to AC voltage alternation, the electrode starts to inject negative charges. At this moment, the bulk liquid surrounding the HV electrode is filled by positive space charges from the previous positive half cycle because the drift velocity of positive ions is slow, only a few mm/s as documented in [19]. When the amount of the positive space charges is small, the injected negative charges will neutralize them soon, and the streamer inception voltage will not be reduced. However, when there is a large amount of positive charge in the liquid (i.e. left by a large positive streamer in the previous positive half cycle), the injected negative charges only neutralize a part of the positive ions, but some positive ions further away from the point electrode will remain in the liquid. The hetero-charge will enhance the local field around the electrode tip as shown in Figure 5.25 (b), thus reducing the streamer inception voltage.

5.4.5.2 Effect on Streamer Structures

The space charge not only affects the streamer inception voltage, but also affects the streamer structures. The effects of space charge on streamer structures are similar between Midel 7131 and FR3.

Taking Midel 7131 as an example, Figure 5.26 shows a streamer sequence in Midel 7131 at 65 kV (rms value), using needle (1 μm tip curvature) to sphere (12.5 mm diameter) electrodes with a 50 mm gap. The instantaneous voltage was recorded by the oscilloscope, and the streamer structures were recorded by a high speed camera. The oscilloscope and the video camera are synchronized by a trigger signal, taken as the start point as shown in the graph. The streamer occurrences can be observed in the shadowgraph photos and used to determine the instantaneous voltage.

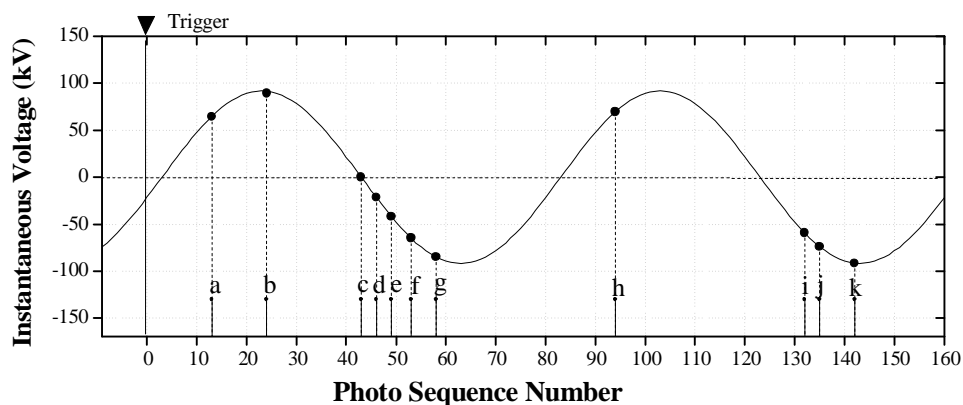


Figure 5.26 Streamer sequence versus instantaneous voltage in Midel 7131 at 65 kV
Point curvature = 1 μm , sphere electrode diameter = 12.5 mm, gap distance = 50 mm

In this graph, streamers a, b and h occur at the positive AC half cycle, classified as positive streamers. Streamers d, e, f, g, i, j and k occur at the negative AC half cycle, classified as negative streamers. Although streamer c occurs at the zero-crossing point when the AC voltage changes from positive polarity to negative polarity, it could be also classified as a negative streamer due to the influence of hetero-charge as described in previous section.

Figure 5.27 shows the shadowgraph photos of streamer structures in time sequence. The polarity of the HV electrode when a streamer occurs is marked by a circle, and the polarity and position of a previous streamer are marked by triangles in each graph. It seems that the streamer structures depend on their polarities as well as their positions in the streamer sequence. Assuming the space charge is left by the previous streamer and has the same polarity, the propagation of current streamers is clearly affected by the space charge. The space charge effect on the streamer structures can also be classified into two situations.

For streamers a, c, h and i, the space charge is in the opposite polarity to the HV needle electrode when the streamer occurs. The hetero-charge increases the field distribution, thus promoting the occurrence of streamers. These streamers propagate from the HV needle electrode to the residuals of a previous streamer, possibly due to the ‘attraction’ of the hetero-charges. Since the space charge generally drifts in the direction from the point electrode to the ground electrode, the streamers also propagate along this direction.

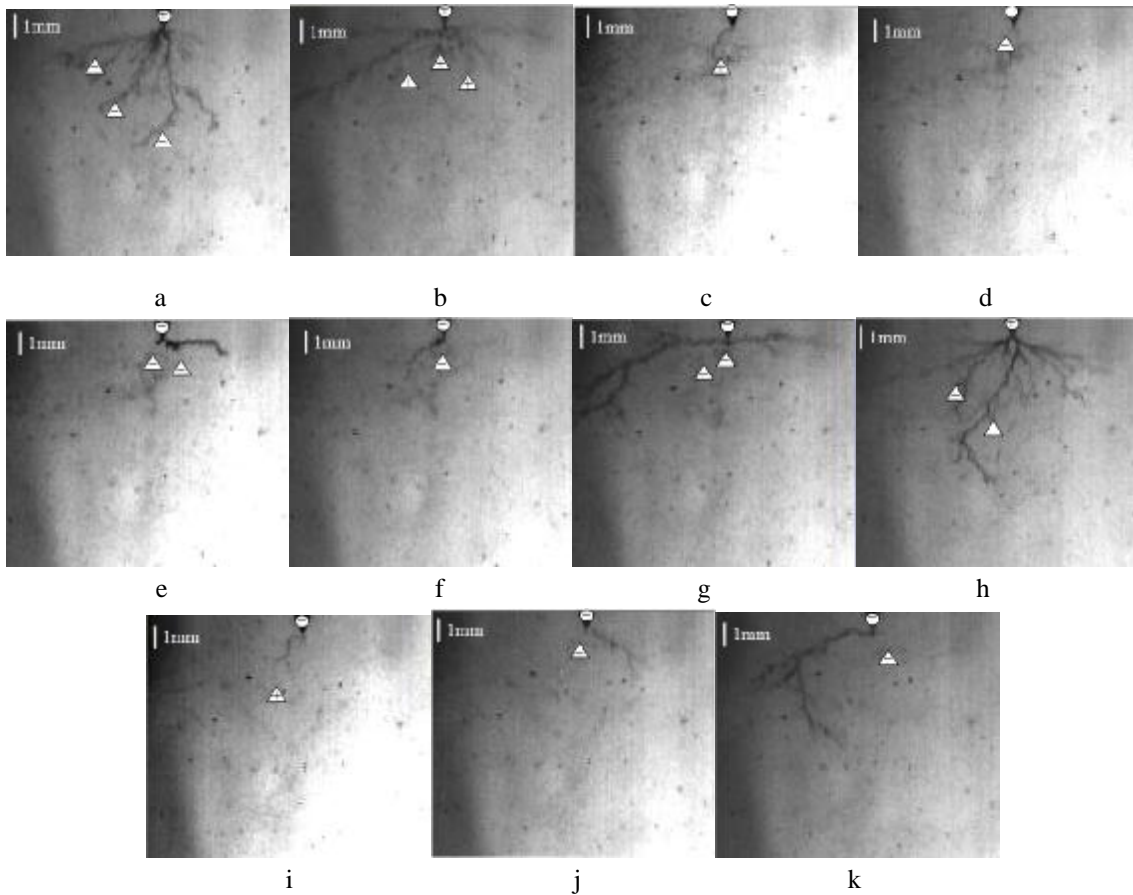


Figure 5.27 Shadowgraph recordings of streamer structures in time sequence

On the other hand, for streamers b, d, e, f, j and k, the space charge is in the same polarity as the HV electrode when the streamer occurs. The homo-charge reduces the field distribution, and these streamers avoid the residual of a previous streamer during their propagation, possible due to the ‘expulsion’ of the homo-charges. Therefore, the streamers mainly propagate to the side directions.

For Gemini X, the effect of the homo-charge on the streamer structures is similar to that in esters. However, since Gemini X has a higher ability to suppress the propagation of negative streamer, less amount of negative space charge could be formed in the liquid gap, and the effect of hetero-charge is not significant.

5.5 Streamer Lead to Breakdown

In AC divergent field, a breakdown is the consequence of the initiation and propagation of a streamer touching both electrodes [114], independent of its polarity [192]. This section

investigates the breakdown strengths of transformer liquids in AC divergent field, and the influence of electrode configuration on their breakdown strengths.

5.5.1 Breakdown Modes

Previous investigations have attributed the liquid breakdown of mineral oil in divergent AC field to the positive streamers [123, 135]. However, the liquid breakdown in esters can be induced by both positive streamers and negative streamers, because the negative streamer propagate easily in esters and the stopping lengths of negative streamers are similar to those of positive streamers near to the breakdown voltages.

The liquid breakdown usually occurs at the positive or negative crest of the AC voltage, thus the polarity of the streamer could be determined by the polarity of applied voltages. During the experiments, three types of breakdowns were observed.

5.5.1.1 Breakdown Induced by Positive Streamers

The breakdown induced by positive streamers is the most common situation occurring in both mineral oil and esters. Figure 5.28 shows the shadowgraph recording of a breakdown induced by a positive streamer in FR3 at 135 kV, using the needle (1 μm tip curvature) to sphere (12.5 mm diameter) electrode configuration with a 100 mm gap.

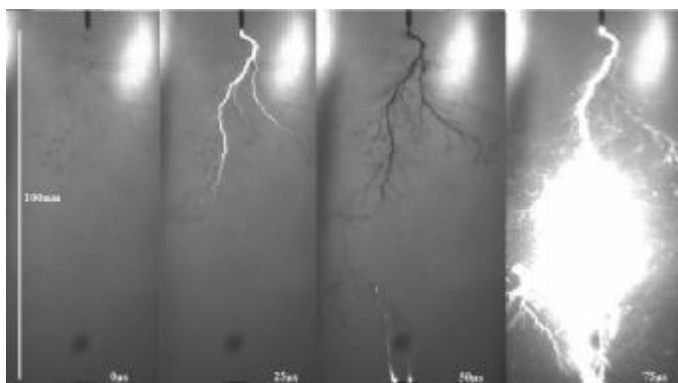


Figure 5.28 A breakdown induced by a positive streamer in FR3 at 135 kV
Point curvature =1 μm , sphere electrode diameter =12.5 mm, gap distance =100 mm

The first graph shows the electrode configuration before the streamer is produced, and this moment is regarded as the start point. After 25 μs , a positive streamer is produced

and reaches a length of 50 mm, characterized by illuminous channels. This streamer touches the ground electrode after 50 μ s. The illumination at the streamer tip is probably the result of the high current associated with the ‘final jump’. The breakdown occurs shortly after the streamer connects both electrodes as shown in the fourth graph. Intensive light is released when the breakdown occurs.

5.5.1.2 Breakdown Induced by Negative Streamers

The breakdown induced by negative streamers is similar to breakdown induced by positive streamers, but is only observed in esters at gap distances ≥ 50 mm. Figure 5.29 shows the shadowgraph recordings of a breakdown induced by a negative streamers in Midel 7131 at 68 kV, using the needle (1 μ m tip curvature) to sphere (12.5 mm diameter) electrode configuration with a 50 mm gap.

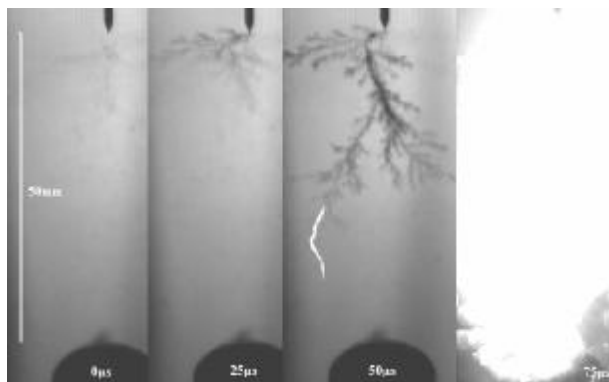


Figure 5.29 A breakdown induced by negative streamer in Midel 7131 at 68 kV
Point curvature =1 μ m, sphere electrode diameter =12.5 mm, gap distance =50 mm

The first graph in Figure 5.29 also shows the electrode configuration before the negative streamer is produced. After 25 μ s, the negative streamer reaches a length of 15 mm as shown in the second graph. In the third graph, the streamer has a length of 40 mm and the luminous channel at the streamer tip probably shows the ‘final jump’. Breakdown occurs in the fourth graph when this negative streamer touches the ground electrode, characterized by an intensive light emission and high current. Similar process of negative streamer induced breakdown is documented in [122].

5.5.1.3 Breakdown Induced by Restroke Streamers

A third type of breakdown process was also observed in esters, relating to both a positive streamer and a negative streamer. This type of breakdown occurs at the positive crest of the AC voltage. It starts with a positive streamer produced from the HV needle electrode, and finishes with a negative streamer (restroke) produced from the ground electrode.

Figure 5.30 shows the development of a restroke streamer in Midel 7131 at 125 kV, using the needle (700 μm tip curvature) to sphere (12.5 mm diameter) electrode configuration with a 100 mm gap. A positive streamer occurs after the first graph, and propagates to the ground electrode in the second and third graphs. In the third graph, the positive streamer is close to the ground electrode, but no breakdown occurs. Instead, a restroke negative streamer is produced from the ground electrode probably due to the field enhancement. The negative streamer propagates continuously to the needle electrode in the next few graphs, generally following the trace of the previous positive streamer. As shown in the last graph, the restroke streamer stops propagation and gradually disappears without leading to a breakdown.

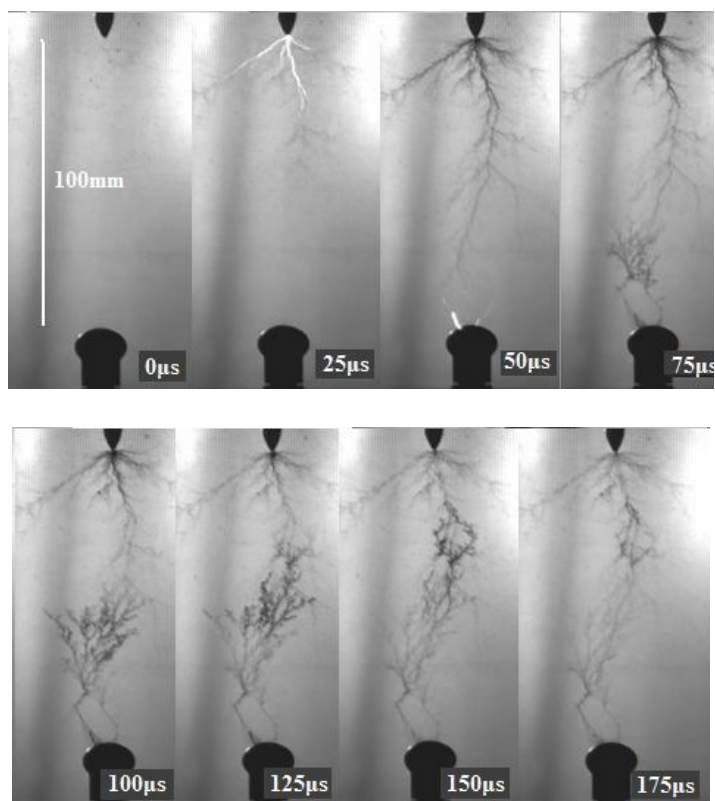


Figure 5.30 A re-stroke pre-breakdown in Midel 7131 at 125 kV
Point curvature = 700 μm , sphere electrode diameter = 12.5 mm, gap distance = 100 mm

However, the restroke negative streamer might fully span the gap and lead to a liquid breakdown. Figure 5.31 shows the shadowgraph recordings of such a breakdown in Midel 7131 at 125 kV, using needle (1 μm tip curvature) to sphere (12.5 mm diameter) electrode configuration with a 100 mm gap. It is clearly seen that a breakdown occurs when the restroke negative streamer fully spans the gap, accompanied by intensive illuminations.

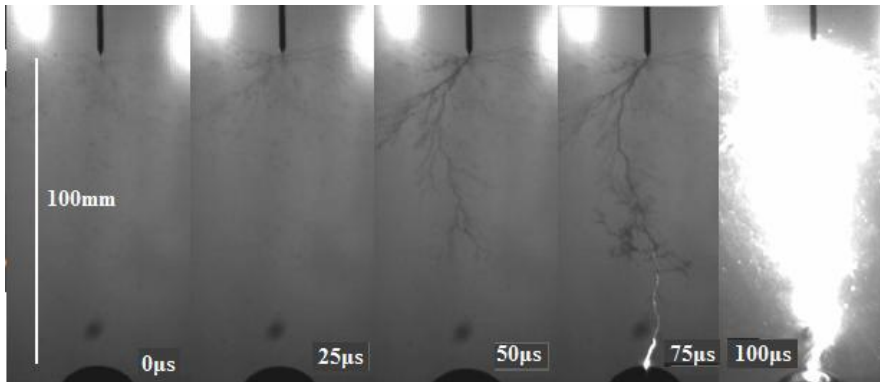


Figure 5.31 A re-stroke breakdown in Midel 7131 at 125 kV
Point curvature = 1 μm , sphere electrode diameter = 12.5 mm, gap distance = 100 mm

5.5.2 Influence of Gap Distance

The AC breakdown tests were carried out for both mineral oil and esters at various gap distances, using the needle (1 μm tip curvature) to sphere (12.5 mm diameters) electrode configuration. The applied voltage is increased at a constant speed of 2 kV/s until a breakdown occurs. Figure 5.32 shows the relationship between the 50% breakdown voltages and the gap distances from 2 mm to 100 mm for both mineral oil and esters. For each electrode configuration, at least 10 breakdown tests were carried out to obtain the 50% breakdown voltages, and the error bar is the standard deviation of the breakdown voltages.

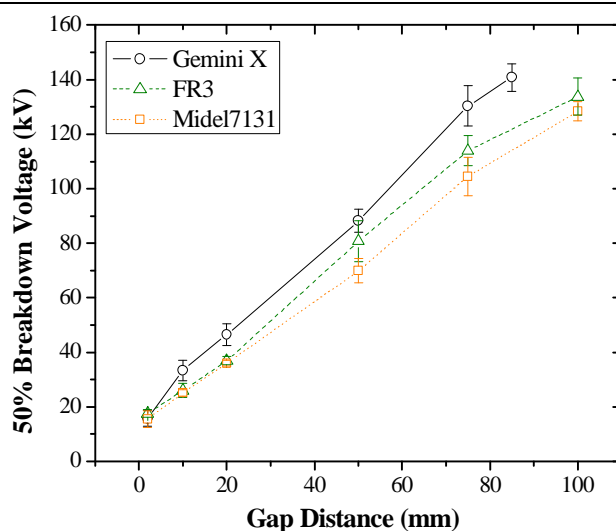


Figure 5.32 50 % breakdown voltages of transformer liquids versus gap distance
Point curvature = 1 μ m, sphere electrode diameter = 12.5 mm

When the gap distance is 2 mm, the breakdown voltages are almost identical for both mineral oil and esters. At this stage, the electric field in the liquid gap is semi-uniform, and the breakdowns are mainly dominated by the streamer initiation. Since the streamer inception voltages of transformer liquids are similar, their breakdown voltages are also similar.

When the gap distance is increased, the breakdown voltages of esters are lower than that of mineral. The lower breakdown voltages of esters than mineral oil can be explained by the following reasons.

- 1. As shown in Figure 5.16, Midel 7131 has a higher increasing rate of maximum stopping length than FR3 and Gemini X, leading to a lower breakdown voltage. Although FR3 has a lower increasing rate than Gemini X, it has a shorter critical length (50 % of the gap length) than Gemini X (80 % of the gap length), indicating the ‘final jump’ and breakdown will occur at a lower voltage.
- 1. As shown in Figure 5.20 and Figure 5.21, the streamer repetition rates in Midel 7131 and FR3 are much higher than in Gemini X. At the same voltage, more streamers are produced in Midel 7131 and FR3 than in Gemini X during the same period, indicating higher chance of breakdown at low voltages.
- 1. At gap distances larger than 50 mm, the breakdown in Gemini X is only induced by positive streamers, but the breakdown in Midel 7131 and FR3 can be induced by both

positive streamers and negative streamer, further increasing the chance of breakdown at low voltages.

The AC breakdown voltages of transformer liquids at large gaps are of great importance in their application in large power apparatus. Since the liquid breakdown in AC divergent field is determined by streamer propagation, a good power law relationship exists between the breakdown voltage and the gap distance, as shown in Figure 5.33. For Gemini X, the breakdown voltage results agree well with the results documented in [128] and [99], using the rod-plane electrode configuration and large gaps up to 1000 mm. For Midel 7131 and FR3, the relationships should be further examined due to lacking of sufficient data.

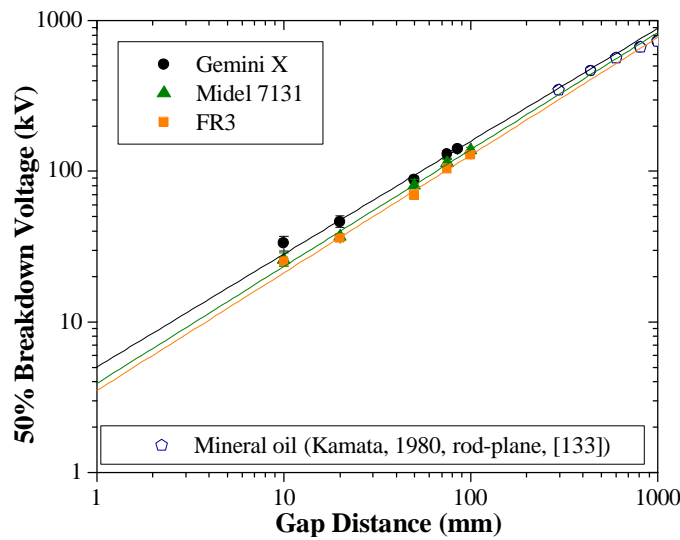


Figure 5.33 50 % breakdown voltage logarithms versus gap distance logarithms
Point curvature = 1 μ m, sphere electrode diameter = 12.5 mm

Based on the results, the empirical formula of the 50 % breakdown voltages of transformer liquids at large gaps are listed in Equation 5.1, in which BDV is the 50 % breakdown voltage in kV, and d is the gap distance in mm.

$$\begin{cases} BDV_{\text{GeminiX}} = 5.01539 \times d^{0.74953} \\ BDV_{\text{Miel7131}} = 3.49098 \times d^{0.78222} \\ BDV_{\text{FR3}} = 4.389751 \times d^{0.777659} \end{cases} \quad \text{Equation 5.1}$$

5.5.3 Influence of Needle Electrode

The breakdown process of transformer liquids is dependent on the field distribution between

the electrodes. For a **semi-uniform field**, the streamer inception voltage is relatively high. When a streamer occurs, the average field between electrodes is high, and the streamer can propagate easily into the bulk liquid. Therefore, the liquid breakdown is determined by the streamer initiation. Since negative streamers are produced at lower voltages than positive streamers, the breakdown of transformer liquids is mainly induced by negative streamers.

For **highly divergent fields**, such as needle-plane electrode configurations, the streamer inception voltage is relatively low. When a streamer occurs, the average field is low, and then the liquid breakdown is determined by the streamer propagation. Since positive streamers propagate more easily than negative streamers, the breakdown of transformer liquids is mainly induced by positive streamers.

At a certain voltage, the electric field distribution is determined both by the needle electrode and by the gap distance between the electrodes. A sharper electrode tip or a larger gap distance will transfer the electric field from semi-uniform field to divergent field.

The influences of HV needle electrode are similar between mineral oil and esters. Taking Midel 7131 as an example, Figure 5.34 shows the 50 % breakdown voltages of Midel 7131 with various point electrodes and gap distances up to 100 mm. Figure 5.35 shows the corresponding probabilities of the breakdowns induced by negative streamers.

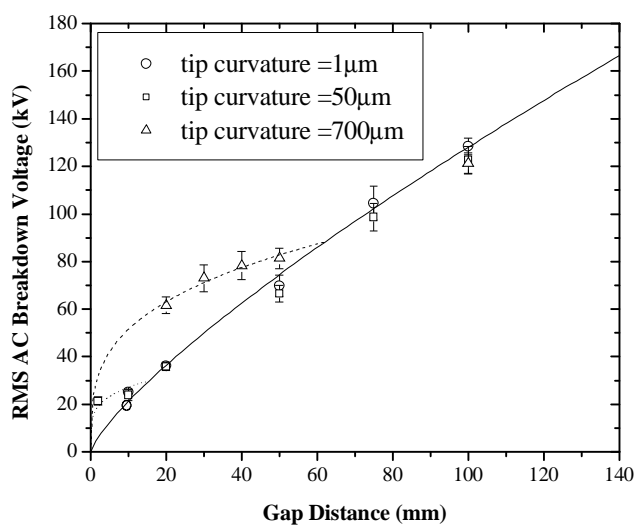


Figure 5.34 50 % breakdown voltages of Midel 7131 versus gap distance Point curvature =1 μm, 50 μm and 700 μm, sphere electrode diameter = 12.5 mm

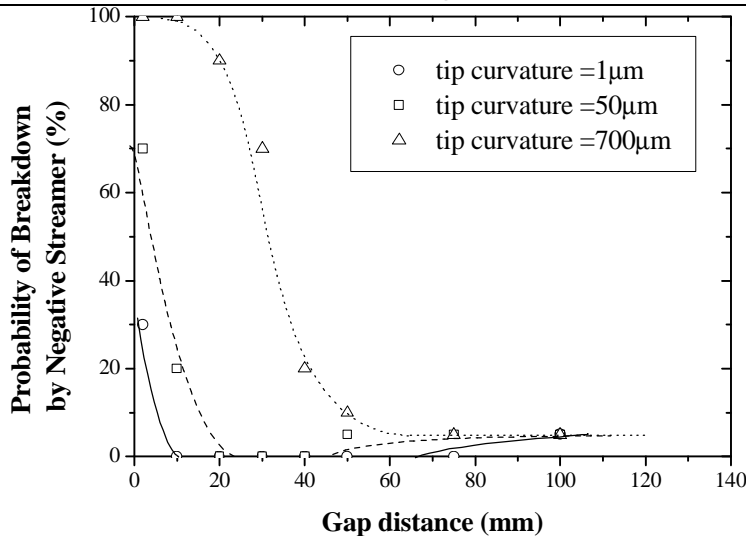


Figure 5.35 Probabilities of breakdowns induced by negative streamers in Midel 7131
Point curvature = 1 μm, 50 μm and 700 μm, sphere electrode diameter = 12.5 mm

When the tip curvature of the needle electrode is 700 μm, three zones can be distinguished from the graphs. At small gaps (<10 mm), the electric field is semi-uniform. The liquid breakdowns are determined by the initiation of negative streamers, thus the breakdown strength (>5 kV/mm) is relatively high. At large gaps (>60 mm), the electric field is highly divergent. The liquid breakdowns are mainly determined by the propagation of the positive streamers, and only a few breakdowns are induced by the negative streamers, thus the breakdown strength (<1.3 kV/mm) is relatively low. At intermediate gaps (10 mm<d<60 mm), the electric field is moderately divergent. The liquid breakdowns are transferred from streamer generation controlled to streamer propagation controlled. Therefore, the breakdowns can be induced by the streamers of both polarities, as shown in Figure 5.35.

When the tip curvature of the needle electrode is 1 μm or 50 μm, similar features are also observed. The transition gap distance from a semi-uniform field to a divergent field is decreased. Therefore, the ‘semi-uniform field’ zone and ‘moderate divergent field’ zone might be too small to be observed.

In Figure 5.34, there seems to be a universal power law relationship between the breakdown voltage and gap distance when the electric field is a highly divergent field. This relationship is independent of the tip curvature of the needle electrode at large gaps. Based on the test results, the relationship of the breakdown voltages of Midel 7131 and the gap distances when the tip curvatures of the needle electrode are 1 μm, 50 μm, and 700 μm are listed in Equation 5.2, in which BDV is the 50 % breakdown voltage in kV, and d is the gap distance in mm.

$$BDV_{\text{Midel7131}_{1\mu\text{m}}} = 3.49098 \times d^{0.78222}$$

$$BDV_{\text{Midel7131}_{50\mu\text{m}}} = \begin{cases} 20.3583 \times d^{0.06929} \mathbf{L} & (d < 20\text{mm}) \\ 3.49098 \times d^{0.78222} \mathbf{L} & (d > 20\text{mm}) \end{cases} \quad \text{Equation 5.2}$$

$$BDV_{\text{Midel7131}_{700\mu\text{m}}} = \begin{cases} 26.0486 \times d^{0.29538} \mathbf{L} & (d < 60\text{mm}) \\ 3.49098 \times d^{0.78222} \mathbf{L} & (d > 60\text{mm}) \end{cases}$$

As shown in Equation 5.2, the breakdown voltage of Midel 7131 can be expressed by a two-section equation. The first section is a power law equation for small gaps, corresponding to the semi-uniform field and the moderate divergent field. The second section is the universal equation for large gaps, corresponding to the highly divergent field.

5.5.4 Influence of Ground Electrode

It is concluded in Appendix I.7 that the streamer propagation in a transformer liquid is determined by the distribution of the overall electric field. Since the breakdown of a transformer liquid is the consequence of the streamer initiation propagation, the ground electrode will affect the breakdown voltage of the liquid by affecting the distribution of the overall electric field. Figure 5.36 represents the breakdown voltages of Midel 7131 versus the surface areas of ground electrode at different gap distances. The results show that the breakdown voltages of Midel 7131 are decreased with the increase of the surface area of the ground electrode, in agreement with the scale effect documented in [135]

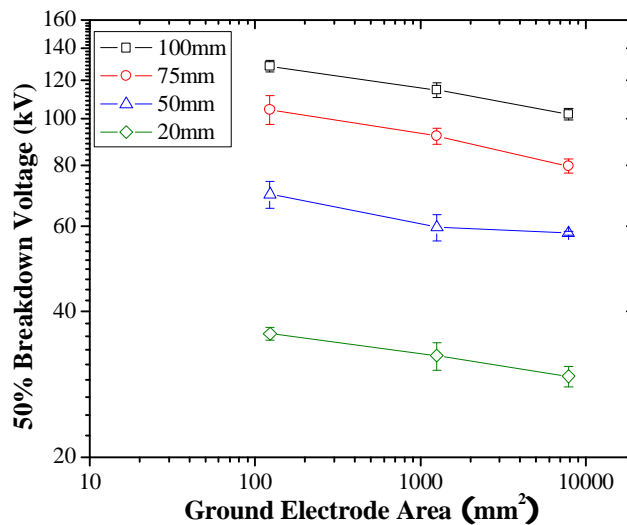


Figure 5.36 50% breakdown voltages versus electrode area in Midel 7131 at various gaps
Point curvature = 1 μm, ground electrode area = 122mm², 1256 mm² and 7854 mm²

5.6 Summary

By synchronizing several measurement methods, this chapter has reported studies into the behaviours of both the positive streamers and the negative streamers in transformer liquids in AC divergent field. A large range of electrode configurations are investigated, including various point electrodes, ground electrodes and gap distances.

- | In the initiation stage, the streamers in mineral oil and esters have similar features, in terms of the streamer structure, associated current, streamer inception voltage and Φ -Q-N pattern. The positive streamers appear at a slightly higher voltage than the negative streamers, but propagate more easily. The initiation of the streamers is determined by the local electric field around the tip of the needle electrode.
- | In the propagation stage, significant differences of the streamer behaviours exist between mineral oil and esters. At the same voltage, the negative streamers propagate much further and faster in esters than in mineral oil. Thus, the mineral oil has a higher ability to suppress the propagation of negative streamers than esters. The propagation of streamers is determined by the average electric field between the electrodes.
- | Under AC voltage, the space charge plays an important role in the propagation of the streamers. Due to relatively long duration of voltage application, space charge is accumulated in the bulk liquid. The homo-charge will increase the streamer inception voltages, and the hetero-charge will reduce the streamer inception voltages.
- | The breakdown in transformer liquids is the consequence of streamer fully propagating between electrodes. In mineral oil, breakdowns are mainly induced by the positive streamers, but in esters, breakdowns in esters can be induced by both positive streamers and negative streamers, especially at large gaps. The 50 % breakdown strengths of esters are identical to those of mineral oil at small gaps, but much lower at large gaps.

These conclusions indicate that the dielectric properties of esters are relatively inferior to mineral oil in divergent field. Therefore, the divergent field should be controlled in

transformers using esters. In the design of power transformers filled with esters, more effort should be put to avoid geometries leading to divergent fields. In the operation of power transformers, the esters should be processed (for example filtered) more frequently than mineral oil in order to reduce the particle content in the liquids which might cause local divergent fields in power transformers.

Chapter 6. Dissolved Gas Analysis under PD Faults

6.1 Introduction

Dissolved Gas Analysis (DGA) has been used for many years as the most sensitive and reliable technique which gives an early indication of the abnormal behavior of mineral oil-filled transformers. Since it is can diagnose the health of a transformer without interrupting its normal operation, the information provided by DGA is of great importance to transformer users.

With the application of esters as a substitution to conventional mineral oil in power transformers, it is essential to ensure that the DGA technique can still be used for ester-filled transformers. In order to yield a correct interpretation of the transformer incipient fault, it is necessary to determine the type and the amount of fault gases produced when a fault occurs in transformers filled with ester liquids.

This chapter describes the experiments in which Partial Discharge (PD) faults were produced in both synthetic ester and natural ester, with mineral oil as a benchmark. The DGA results under various PD faults are reported. In this chapter, section 6.2 introduces two types of PD activities in transformer liquid, one is PDs of corona type and the other is PDs of sparking type. Section 6.3 explains the experimental arrangements and procedures. Section 6.4 and section 6.5 show the DGA results under PD faults with various amplitudes and energy levels, and it is found that a large amount of C_2H_6 is produced in natural ester. Section 6.6 proposes the possible mechanisms which could be responsible for the production of C_2H_6 in natural ester using literature of the food industry. Section 6.7 evaluates the suitability of applying the existing interpretation methods currently being used for mineral oil to esters and suggests necessary modifications.

6.2 DGA Techniques

6.2.1 PD Faults in Oil

Transformers in service are subjected to two types of stresses: electrical stress and thermal stress. Inspection of faulty transformers leads to a broad classification of electrical faults into either partial discharge faults or more serious arcing faults [193]. Based on the discharge energy, Duval classified the partial discharges into either ‘PDs of corona type’ or ‘PDs of sparking type’ in [194].

6.2.1.1 PDs of Corona Type

PDs of corona (cold plasma) type usually occur in gas phase of voids or bubbles, during the initiation stage of a streamer. The amplitudes of corona discharge are usually low, no more than 50 pC in mineral oil [193], and it favors the scission of the weakest C-H bonds (338 kJ/mol) through the ionization process. Because the amplitudes of corona discharges are so small, it is hard to recognize this type of fault in an in-service transformer by commercially available PD detectors. However, it is easy to detect this fault by the DGA technique as long as the corona-type PD fault occurs over a long period of time and produces detectable amounts of fault gases.

Under the corona-type PD fault, the main fault gas generated by mineral oil is H₂, with a certain amount of CH₄ [194]. In power transformers with this fault, formation of X-wax (a hydrocarbon polymer) is usually observed in the paper insulation materials near the fault area [194, 195].

6.2.1.2 PDs of Sparking Type

In terms of chemical degradation and DGA results, PDs of sparking type occurring in the oil phase are very different from PDs of corona type occurring in the gap phase. PDs of sparking type is a type of ‘low-energy discharges’ (other low-energy discharges include tracking discharges and small arcing [194]), referring to partial discharges with higher energy and higher amplitude, from 100 pC to thousands PC [194]. For in-service transformers,

uninterrupted sparking-type PD faults are easily detectable by DGA because the gas formation is large enough [195, 196].

Under sparking-type PD fault, a significant amount of C_2H_2 is produced as well as H_2 . It seems that the ratio of the amount of C_2H_2 to H_2 is an indicator of the intensity of partial discharges [197]. When PD intensity increases, more C_2H_2 is produced and the ratio of C_2H_2/H_2 increases. This increase pulls the PD type from ‘low-energy discharges’ towards ‘high-energy discharges’. In power transformers with this fault, small pinholes or carbonized marks have been occasionally observed [198], thus detection of this type of PD faults is important before they become more serious and further damage the paper insulation [194].

6.2.2 Gas Formation under PD Faults

Mineral oils are mixtures of complex hydrocarbon molecules, in the form of long chain (paraffinic) or cyclic (aromatic) structures. These molecules are bonded together by chemical groups of CH_3- , CH_2- , $CH-$, etc. When mineral oil is exposed to electrical faults, scissions of the C-H or C-C bonds will produce various radicals or ionic fragments, such as H^* , CH_3^* , CH_2^* , CH^* or C^* . The recombination of those radicals can lead to chemical degradation of the mineral oil and give rise to the formation of various combustible gases such as H_2 , CH_4 , C_2H_6 , C_2H_4 , and C_2H_2 [198].

Table 6.1 Main fault gases produced by decomposition of mineral oils [129]

Hydrogen	Methane	Ethane	Ethylene	Acetylene
H_2	CH_4	C_2H_6	C_2H_4	C_2H_2

Higher energy is required to produce combustible gases shown in Table 6.1 from left to right. Thus, H_2 , CH_4 , C_2H_6 can be produced at a low energy level, such as partial discharge of corona type. C_2H_4 can be produced at an intermediate energy level. C_2H_2 can be produced at a high energy level, such as arcing. These gases are partly dissolved in the oil, and partly accumulated in the head space as free gases. The DGA technique measures the type and the amount of fault gases, which can be used to determine the severity of the electrical fault in power transformers [199-201].

In the UK, many power transformers are free-breathing transformers, thus oxygen and

nitrogen are presented in the DGA results. In sealed or nitrogen-filled transformers, oxygen and nitrogen can also be dissolved in transformer liquids as residuals during manufacturing and processing stage, or through leaks or maintenance procedures. Although CO or CO₂ are mainly used as indicators of thermal decomposition of cellulose materials, they will be produced in mineral oil under electrical faults due to oxidation process with the presence of oxygen [202].

Therefore, the fault gases reported in the DGA results are usually H₂, CH₄, C₂H₆, C₂H₄, C₂H₂, CO, CO₂, O₂ and N₂.

6.2.3 PD Fault Diagnosis

If the rate of change of the DGA results suddenly increases during a period, the transformer is probably stressed under an internal fault. Then, the DGA diagnostic method can be applied to interpret the fault. Commonly used diagnostic methods are:

- IEEE methods in IEEE C57.104 (Dornenburg, Rogers and key gas methods) [203]
- IEC methods in IEC 60599 (IEC ratio (modified Rogers method) and Duval triangle method) [129]

Dornenburg, Rogers and IEC ratio methods interpret the DGA results by utilizing gas ratios, such as CH₄/H₂, C₂H₆/CH₄, C₂H₄/C₂H₆ or C₂H₂/C₂H₄. Key gas method simply utilises relative percentages of the selected fingerprint gases to identify fault types, and the gas with the most significant proportion of the overall fault gases is called '*Key Gas*'. The Duval triangle method uses three gases (CH₄, C₂H₄ and C₂H₂) to diagnose fault types.

The drawback of gas ratio methods is that this method is not able to give interpretations when the DGA results do not match the available codes. But this does not occur for the key gas method and the Duval triangle method. Table 6.2 shows the accuracy of various DGA diagnosis methods, in which the key gas and Duval triangle methods give better interpretation results than others.

Table 6.2 Accuracies of DGA diagnosis methods [204]

	Doernenburg	Roger	IEC ratio	Key Gas	Duval Triangle
Total Case	92	92	92	92	92
No Prediction	50	47	26	0	0
Correct Prediction (%)	41%	45%	66%	78%	89%

Duval Triangle Method

Duval triangle method interprets the faults in power transformers using three hydrocarbon gases (CH_4 , C_2H_4 and C_2H_2). CH_4 is chosen to identify the faults, rather than H_2 , because it provides more consistent diagnosis results than using H_2 [198]. This is attributed to the fact that H_2 diffuses much more rapidly than the hydrocarbon gases from the oil through gaskets or metal weld. Figure 6.1 shows the Duval triangle used to interpret the faults in mineral oil-filled power transformers [129]. Faults and typical examples which can be recognized by Duval triangle method are listed in Table 6.3 [198]. An intermediate zone DT has been attributed to mixtures of electrical and thermal faults in the transformer.

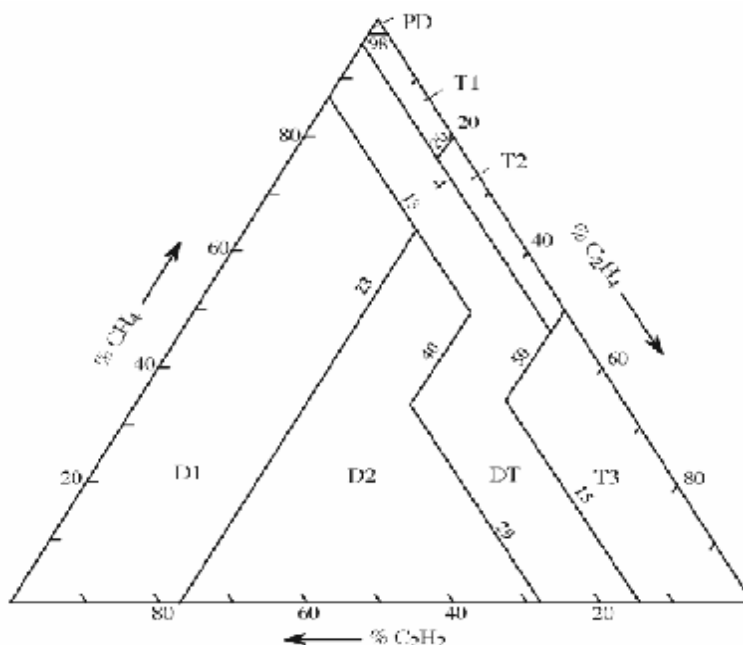


Figure 6.1 Duval triangle graph to diagnosis transformer faults [196]

Table 6.3 Examples of faults detectable by Duval triangle method [198]

	Fault	Examples
PD	Partial discharges	PDs of corona type in gap bubbles or voids, with the possible formation of X-wax in paper
D1	Discharges of low energy	PDs of sparking type, inducing pinholes carbonized punctures in paper. Low energy arcing inducing carbonized perforation or surface tracking of paper, or the formation of carbon particles in oil
D2	Discharge of high energy	Discharges in paper or oil, with power following-through, resulting in extensive damage to paper or large formation of carbon particles in oil, metal fusion, tripping of the equipment and gas alarms.
T1	Thermal fault, $T < 300\text{ }^{\circ}\text{C}$	Evidenced by paper turning brownish or carbonized.
T2	Thermal fault, $300\text{ }^{\circ}\text{C} < T < 700\text{ }^{\circ}\text{C}$	Carbonization of paper, formation of carbon particles in oil.
T3	Thermal fault, $T > 700\text{ }^{\circ}\text{C}$	Extensive formation of carbon particles in oil, metal coloration or metal fusion.

6.3 Experimental Setup and Considerations

As shown in Figure 6.2, a standard PD test circuit was used to generate partial discharges. In the circuit, a single phase 50 Hz test transformer with output voltage up to 70 kV was used as the power supply and a discharge free capacitor of 500 pF was connected in parallel with the test vessel used. The measuring impedance of a LEMKE LDS-6 PD detector was connected in series with the coupling capacitor, and the PD signals were recorded by this detector. The background PD noise level was less than 5 pC at voltages up to 70 kV.

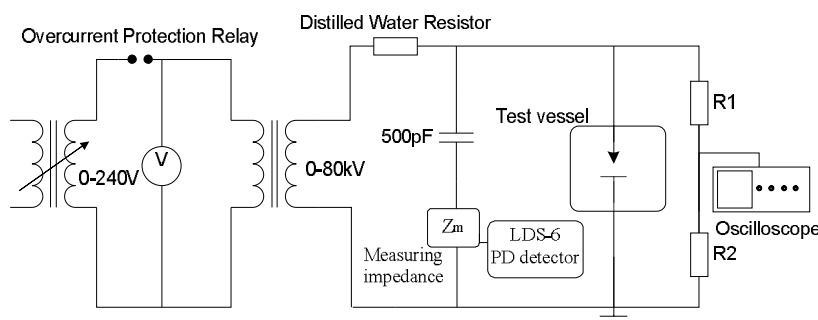


Figure 6.2 Test circuit to generate partial discharge faults

The test vessel used in experiments is shown in Figure 6.3. A 100ml glass vial was filled with the oil sample to be tested, and sealed by an aluminium crimp cap including rubber sealing. The rubber sealing was penetrated by a steel needle, whose tip curvature is 6-7 μm

from the front view and 2-3 μm from the lateral view, acting as high potential electrode. Partial discharges were produced near the tip of the needle electrode at high voltages. The whole assembly of the vial and high potential electrode was immersed inside a container filled with insulating oil. This container was placed on an earthed copper plate with a diameter of 100mm. The distance between the needle and plate electrode was set at 50 mm for all tests.

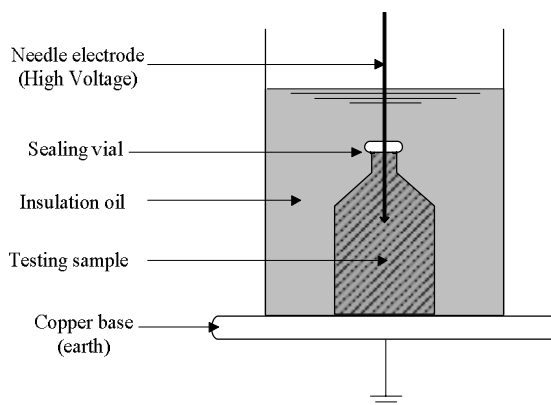


Figure 6.3 Structure of partial discharge test container

A new needle electrode was used for every test to avoid damage to the needle tip by continuous partial discharges. The comparison of microscopic photos before and after the tests showed that the tip curvature of the high potential needle did not change for partial discharges up to 1000 pC lasting for half an hour.

After each test, the needle electrode was pulled out, and the pinhole on the rubber sealing was immediately sealed by an Acrylic-based sealing compound provided by RS Ltd [205]. The sealed vials were sent to TJH2b Analytical Services for DGA analysis, and the DGA results were reported with a resolution of 0.1 ppm. Occasionally, small gas bubbles might appear in the vial due to temperature change. In the DGA analysis, these bubbles were shaken back to dissolve into the oil samples.

Gemini X, Midel 7131 and FR3 were investigated in this chapter after purification, dehydration, and degassing as described in Appendix I.3. The processed new oils were kept as controlled samples for the DGA test to provide a benchmark. The background amounts of dissolved gases in controlled samples for each type of oil are shown in Table 6.4. It can be seen that the processed oils are almost free from hydrocarbon gases. However, large amounts

of O₂, N₂ and CO₂ exist in the controlled samples, which can be attributed to the air re-absorption at the last stage of releasing vacuum during oil processing.

Table 6.4 Dissolved gas contents of controlled samples (ppm)

	Gemini X	Midel 7131	FR3
N ₂	30366	95002	54986
O ₂	5371	9998	15682
H ₂	0	0	0.1
CH ₄	0	0.1	0.2
C ₂ H ₆	0.6	0.2	1.0
C ₂ H ₄	0.3	0.2	0.1
C ₂ H ₂	0.4	0.2	0.2
CO	5.1	7.9	9
CO ₂	247	200	110

6.4 DGA under PD Faults of Controlled Amplitude

Many published studies reported DGA results for various transformer liquids under PD faults, but without specifying the severity of the fault [194, 196, 197, 199, 204, 206-208]. This section correlates the amount of fault gases in both mineral oil and esters with the amplitudes of PD faults.

6.4.1 Experimental Description

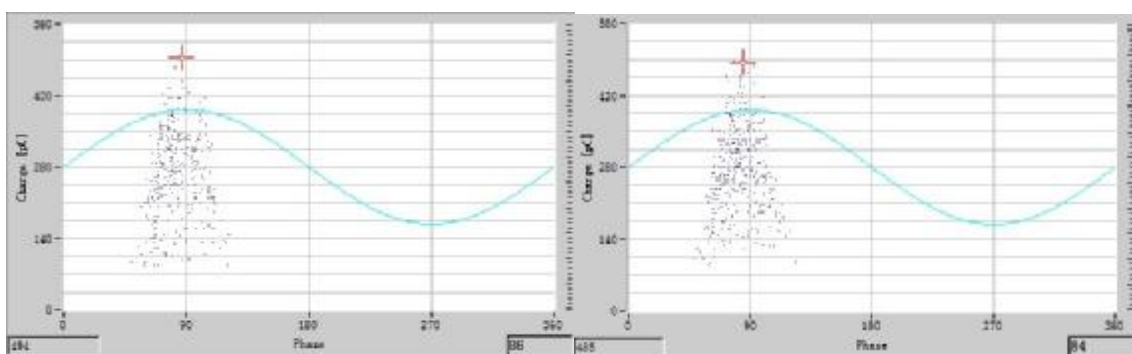
Although partial discharge activity is complex, its severity can be represented to some extent by the maximum amplitude of the charge contained in the partial discharges. To study the gas generation under PD faults of various amplitudes, the PD-DGA experiments on all transformer liquid samples were performed at fixed PD amplitudes (maximum value) of ~200 pC, ~300 pC, ~500 pC and ~1000 pC. The applied voltages to generate partial discharges with amplitudes of these fixed values are given in Table 6.5.

Table 6.5 Applied voltages at controlled discharge amplitude for transformer liquids

Maximum PD amplitude (pC)	Applied voltages (kV)		
	Gemini X	Midel 7131	FR3
200	18.5	19.5	21.2
300	21.0	21.5	25.3
500	25.5	23.5	28.8
1000	34.0	32.0	36.1

For each test, the applied voltage was increased from 0 kV at a rate of 0.5 kV/s until these PD amplitude values were reached. Then the voltage was maintained for half an hour.

Since the needle tip would not be damaged in half an hour, the PD fault was quite stable during the tests. Figure 6.4 compares the PD patterns of the 1st minute and 30th minute in Midel 7131 at 23.5 kV during 30 minutes of voltage application. The results show that both their maximum PD amplitudes and PD repetition rates are similar. The maximum PD amplitudes are 494 pC in Figure 6.4 (a) and 485 pC in Figure 6.4 (b). The PD repetition rates are 336 per minute in Figure 6.4 (a) and 317 per minute in Figure 6.4 (b).



(a)

(b)

Figure 6.4 PD patterns in Midel 7131 at 24.5 kV

(a) 1st minute and (b) 30th minute in 30 minutes voltage application duration

6.4.2 Results and Discussions

The concentrations of dissolved gases in both mineral oil and esters under PD faults of various amplitudes are listed in Table 6.7. For conveniences, the test results are labeled as G1 to G4 for Gemini X, M1 to M4 for Midel 7131, and F1 to F4 for FR3. Due to the possible gas leakage, unexpected results might be obtained in some cases, such as the H₂ amount in G2 is smaller than the H₂ amount in G1, and these results are listed in ***bold and italic*** style. Therefore, it is necessary to study the trend of the results, rather than the detailed values.

Table 6.6 DGA results in ppm under PD faults of various amplitudes

Oil type	Gemini X				Midel 7131				FR3			
Label	G1	G2	G3	G4	M1	M2	M3	M4	F1	F2	F3	F4
Amplitude (PC)	200	300	500	1000	200	300	500	1000	200	300	500	1000
N ₂	43642	29707	28843	28081	24819	17761	20817	30108	32512	45946	30670	46665
O ₂	7303	4202	3361	3847	7647	5195	6198	10472	4118	5658	3223	6508
H ₂	12.4	7.0	62.4	163.0	5.8	11.1	43.5	128.0	29.9	63.7	69.1	140.0
CH ₄	0.9	0.5	0.4	2.9	0.2	0.7	1.0	8.2	1.2	3.9	5.8	11.4
C ₂ H ₆	0.4	0.2	0.3	0.9	0.3	0.4	0.7	1.4	44.7	83.4	46.0	63.4
C ₂ H ₄	0.2	0.2	0.2	1.5	0.2	0.6	0.7	4.5	0.2	2.7	5.5	9.1
C ₂ H ₂	0.2	0.1	0.3	3.5	0.3	0.8	1.0	10.6	0.0	5.0	11.5	22.4
CO	21.7	12.4	13.9	13.6	15.7	15.2	17.0	37.0	20.1	36.2	30.0	49.9
CO ₂	374.0	264.0	408.0	250.0	115.0	242.0	162.0	267.0	305.0	530.0	319.0	275.0
TCG	35.8	20.4	77.5	185.4	22.5	28.8	63.9	202.3	96.1	194.9	167.9	296.2
Note: the bold and italic numbers are unexpected results which might caused by gas leakage.												

Compared with the CO concentrations of controlled samples in Table 6.4, the concentrations of CO were increased in all the tests. Since CO is usually used as an indicator of oxidation [209], there are probably oxidation processes in the liquid samples during the experiments.

Figure 6.5 shows the concentrations of *total combustible gases* (TCG) in mineral oil and esters under various magnitudes of PD faults. Under the same amplitude of partial discharges, Midel 7131 generates similar amounts of combustible gases to those in Gemini X. FR3 generates the highest concentration of TCG in all three liquids, almost twice as much as those in Gemini X and Midel 7131.

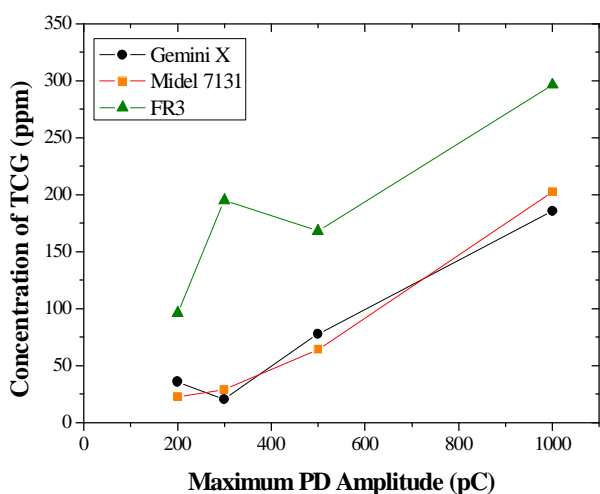


Figure 6.5 Total combustible gases concentrations under PD faults of various amplitudes

Figure 6.6 shows the concentrations of H_2 in mineral oil and esters under various magnitudes of PD faults. H_2 is found in the largest concentrations among all the hydrocarbon gases produced in transformer liquids. The H_2 concentrations increase almost linearly with the increase of maximum PD amplitude. When PD amplitude increases, more energy is released into the surrounding oil to break more C-H bonds, thus a higher concentration of H_2 is produced under larger PD faults. Under PD faults of low amplitude (200 pC and 300 pC), FR3 produces relatively more H_2 than Midel 7131 and Gemini X. Slight variations are found for samples in Gemini X and FR3 under PD faults of 300 pC (G2 and F2), possibly due to the gas leakage. Under PD faults of 1000 pC, Gemini X produced more H_2 than FR3 and Midel 7131.

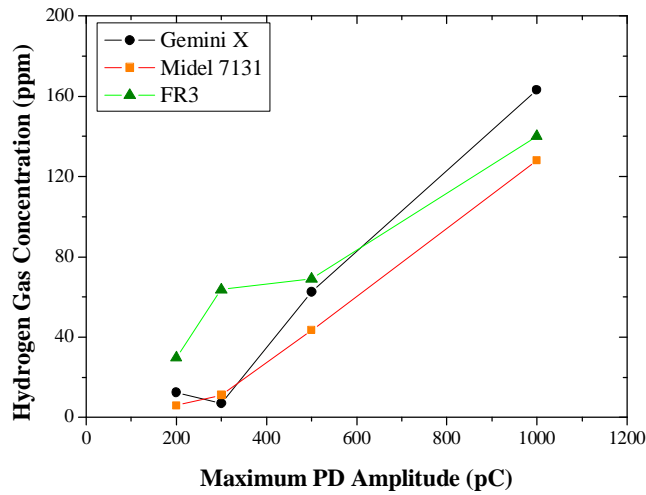


Figure 6.6 H₂ concentrations under PD faults of various amplitudes

Figure 6.7 shows the concentrations of methane, ethylene, ethane and acetylene in mineral oil and esters under PD faults of various amplitudes. The hydrocarbon gases only appear when the amplitude of partial discharges is large enough to breakdown C-C bonds contained in oil molecular structures.

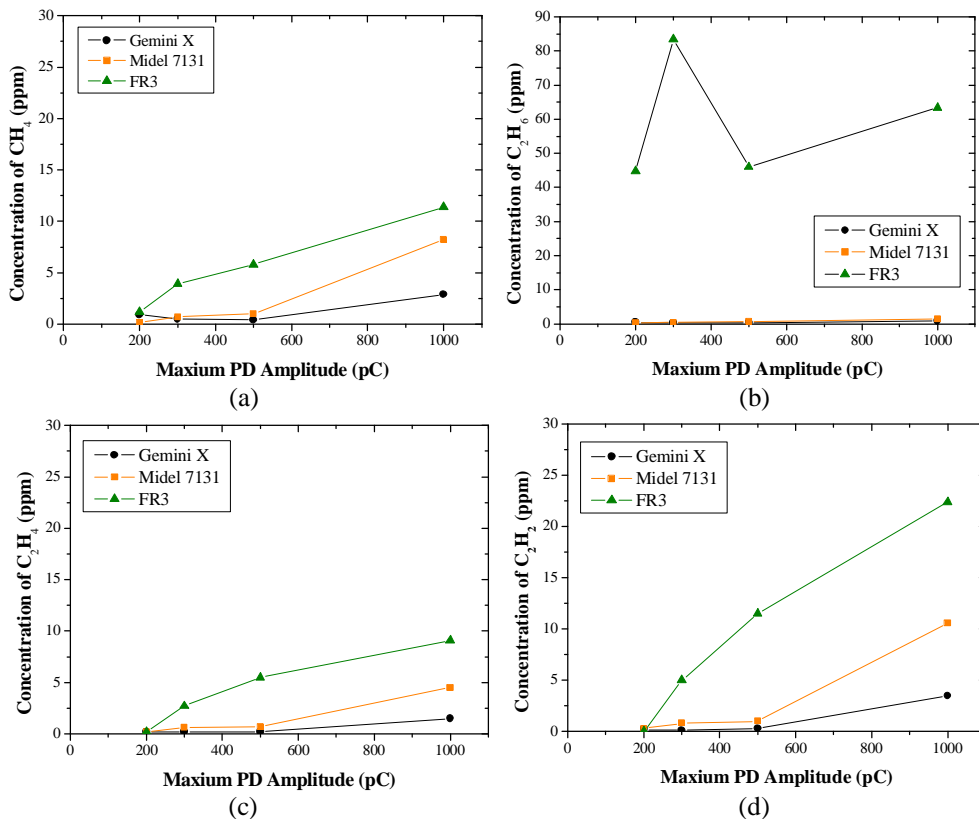


Figure 6.7 Hydrocarbon gases concentrations under PD faults of various amplitudes
 (a) CH₄, (b) C₂H₆, (3) C₂H₄ and (d) C₂H₂

Since it takes more energy to break C-C bonds (607 kJ/mol in mineral oil) than C-H bonds (338 kJ/mol in mineral oil) [129], the concentrations of hydrocarbon gases are increased with

the increase of PD amplitude. Under the same level of PD fault, the concentrations of hydrocarbon gases are higher in FR3 than in Gemini X and Midel7131. For example, under PD fault of 1000 pC, the C₂H₂ concentration in FR3 is about twice that in Midel 7131, and four times that in Gemini X. Taking the gas generation threshold as 1 ppm, the hydrocarbon gases are generated at higher PD amplitudes in Gemini X and Midel 7131 than in FR3. In FR3, hydrocarbon gases start to appear when the maximum PD amplitude exceeds 200 pC, but in Gemini X and Midel7131, the hydrocarbon gases are generated under the PD fault of 500 pC.

However, it should be noted the hydrocarbon gases in Figure 6.7 (except C₂H₆ in FR3) are in small amounts. Considering the possible gas leakage during the test, care should be taken when interpreting the fault type using these results based on ratio methods, because even a small gas leakage from a low gas concentration will significantly increase the uncertainty of the ratio, thus providing unreliable diagnosis [195].

The above results indicate that the FR3 is probably more vulnerable to PDs than Gemini X and Midel7131, in terms of generating hydrocarbon gases under PD fault of smaller amplitude. This can be attributed to the unsaturated bonds in the molecular structure of FR3. It is widely known that the molecule structures of FR3 contain a large amount of C=C double bonds. The C=C double bond consists of one σ bond and one π bond, and is not chemically stable. The scission of the C=C double bond is divided into two steps. The π bond is firstly broken up requiring energy of 264 kJ/mol, and the σ bond is broken up next requiring energy of 456 kJ/mol. Although the total energy required to breakdown C=C double bonds (720 kJ/mol) is larger, the energy consumed in each step to breakdown the C=C double bonds is much smaller than that required to breakdown the σ bond in C-C single bond (607 kJ/mol) [210]. Therefore, the hydrocarbon gases can be generated under PD faults of smaller amplitudes in FR3 than in Gemini X and Midel 7131.

In addition, a high concentration of C₂H₆ is observed in FR3 under PD faults irrespective of their amplitudes, but Gemini X and Midel 7131 have far less C₂H₆. Therefore, it is probably one of the key features of FR3 to produce C₂H₆ even at the PD faults of small amplitudes.

6.5 DGA under PD Fault of Controlled Energy

It was concluded in Chapter 4 that the PD repetition rates are much higher in Midel 7131 and FR3 than in Gemini X. Although each individual PD may contain different levels of energy, more energy in total is released into Midel 7131 and FR3 than into Gemini X under PD faults of the same amplitude and duration. This might be one of the reasons why Midel 7131 and FR3 generate higher concentrations of fault gases than Gemini X.

This test is aimed at determining the relationship between the fault gas concentrations and the total discharge energy which is released into the liquids. The total discharge energy can be calculated as the sum energy of all the PDs occurred in a test, using Equation 6.1, where W is the total discharge energy during a period of time T , Q_i is the apparent charge of a PD pulse, and U_i is the instantaneous voltage applied when the PD pulse occurs.

$$W = \sum_i^T (Q_i \cdot U_i) \quad \text{Equation 6.1}$$

6.5.1 Experimental Description

To study the relationship between fault gas concentrations and total discharge energy, all samples were stressed under PD fault of 500 pC. The applied voltage was increased from 0 kV at a rate of 0.5 kV/s until the PD amplitude reached 500 pC. Then the voltage was maintained for 15 minutes, 30 minutes, 45 minutes and 60 minutes respectively. It was expected that more energy would be released into liquid samples if the voltage was applied for a longer time. A LEMKE LDS-6 PD detector was used to record the PD signals continuously during the experiments, in order to calculate the total discharge energy.

6.5.2 Results and Discussions

The concentrations of fault gases in mineral oil and esters under the PD fault of various durations were listed in Table 6.7. For conveniences, the test results are labeled as G5 to G8 for Gemini X, M5 to M8 for Midel 7131, and F5 to F8 for FR3. This table also lists the number of partial discharges which appeared in each test, and the calculated total discharge energy using Equation 6.1.

Table 6.7 DGA results in ppm under PD faults of 500 pC and various durations

Oil type	Gemini X				Midel 7131				FR3			
Label	G5	G6	G7	G8	M5	M6	M7	M8	F5	F6	F7	F8
Time (mins)	15	30	45	60	15	30	45	60	15	30	45	60
PD Number (k)	0.68	0.88	0.93	1.57	4.00	9.79	22.30	21.90	13.60	25.70	52.60	107.00
Energy (mJ)	7.7	8.1	9.2	15.7	37.4	88.2	151.2	205.1	148.2	161.4	486.6	1020.0
N2	54674	28843	31874	52767	18477	31968	20817	42278	21367	32318	46696	47390
O2	9409	3361	4376	7425	5357	11335	6198	11639	3246	2725	3329	8301
H2	31.3	62.4	70.9	110.0	14.3	12.8	43.5	60.9	46.7	88.4	74.7	138.0
CH4	1.7	0.4	0.9	1.8	1.0	1.0	1.0	0.9	0.7	1.9	3.9	6.6
C2H6	0.2	0.3	0.2	0.3	0.4	0.3	0.7	0.3	12.7	18.2	28.0	63.5
C2H4	0.5	0.2	0.3	0.6	0.7	0.7	0.7	0.6	0.4	1.5	3.3	6.0
C2H2	0.4	0.3	0.5	0.7	1.2	1.2	1.0	0.0	0.6	3.1	7.0	13.6
CO	10.9	13.9	12.5	40.5	16.6	15.2	17.0	24.8	10.1	17.9	29.7	39.6
CO2	200.0	408.0	461.0	819.0	119.0	275.0	162.0	514.0	222.0	305.0	530.0	475.0
TCG	45.0	77.5	85.3	153.9	34.2	31.2	63.9	87.5	71.2	131	146.6	267.3
Note: the bold and italic numbers are unexpected results which might caused by gas leakage.												

The PD number and the discharge energy are two useful parameters to describe the intensity of a PD event. As shown in Table 6.7, under the PD faults with the same amplitude, the PD activities in Midel 7131 and FR3 are more intensive than in Gemini X, in terms of higher PD numbers and higher total discharge energies. For example, when the test voltages are applied for 60 minutes under PD fault of 500 pC, Midel 7131 (M8) and FR3 (F8) released more than 10 times the PD number and the total discharge energy than Gemini X (G8)).

For the same type of liquid, a longer duration of voltage application usually corresponds to a higher PD number and a higher level of total discharge energy, thus more fault gases are produced. However, there is no linear relationship between the duration of voltage application and the total discharge energy, because the needle electrode was replaced by a new one for each test, and the variation of needle tip curvature (6-7 μm from the front view and 2-3 μm from the lateral view) caused different PD intensity for each test. For example, the voltage duration of G6 is twice that of G5, but their total discharge energy are similar.

To better compare the DGA results among different liquids, Table 6.7 is plotted into histogram graphs as shown in Figure 6.8. In all the tests, CO is produced in significant amounts possibly due to the oxidation process. Similar conclusions as described in section 6.4 can also be derived from Figure 6.8.

- | Under PD faults with the same maximum amplitude, FR3 produces more combustible gases than Midel 7131 and Gemini X.
- | H₂ concentration is the highest among all hydrocarbon gases, and it is one of the key indicators of PD faults.
- | The concentration of individual hydrocarbon gas in FR3 is much higher than those in Midel 7131 and Gemini X.
- | FR3 produces a large amount of C₂H₆.

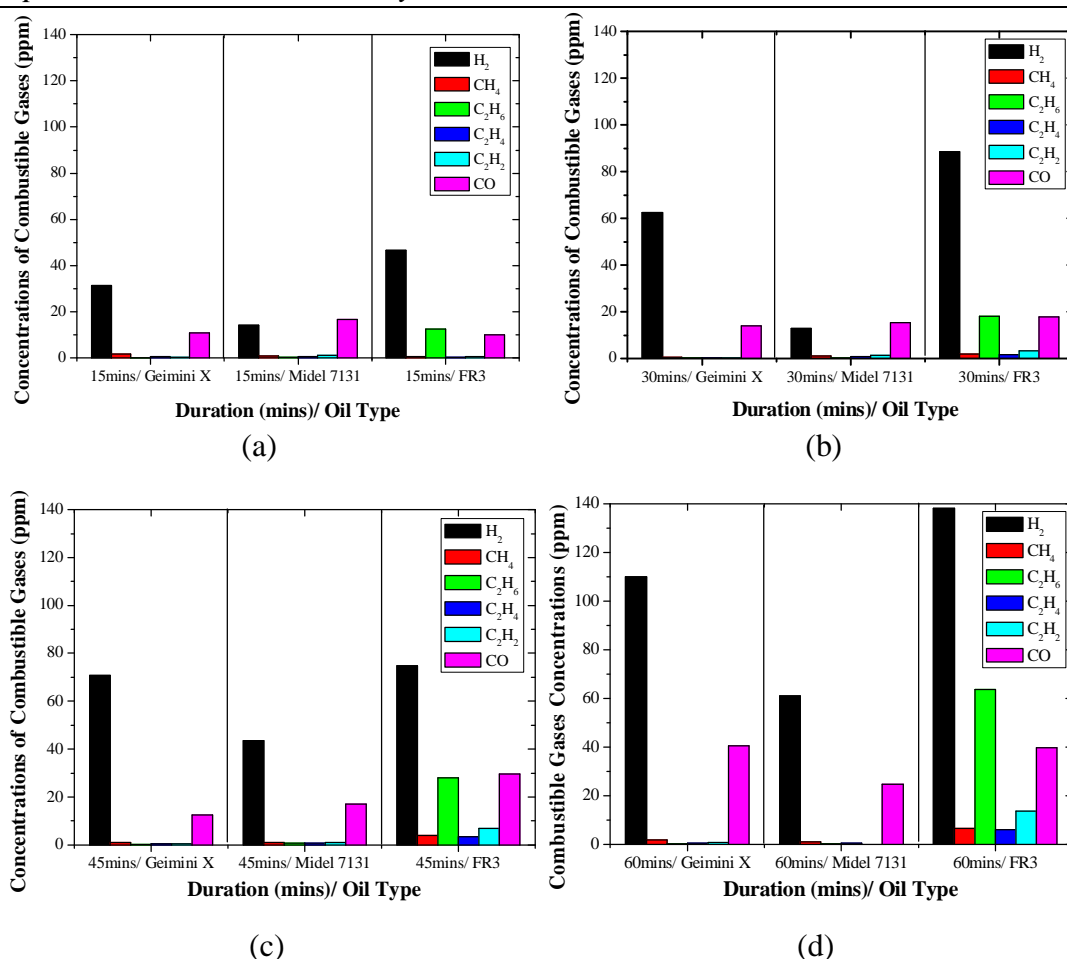


Figure 6.8 Combustible gases concentrations under PD fault of various durations (a) 15minutes, (b) 30 minutes, (c) 45 minutes, and (d) 60 minutes

The higher concentrations of hydrocarbon gases in FR3 can be attributed to two reasons: more vulnerable oil molecular structure and more total discharge energy. In terms of molecular structure, the C=C double bonds and C≡C triple contained in the FR3 molecular structures can be easily attacked under PD faults, thus producing high concentrations of hydrocarbon combustible gases. In terms of total discharge energy, FR3 produces higher levels of total discharge energy than Gemini X and Midel 7131 under PD faults of the same amplitude and duration. For example, Figure 6.9 shows the Φ -Q-N patterns of transformer liquids stressed under PD faults with 500 pC maximum amplitude for 15 minutes (G5, M5 and F5). Although FR3 has similar maximum PD amplitude of 500 pC to Midel 7131 and Gemini X, the PD number in FR3 is much higher than those in Midel 7131 and Gemini X, leading to a higher level of total discharge energy in FR3.

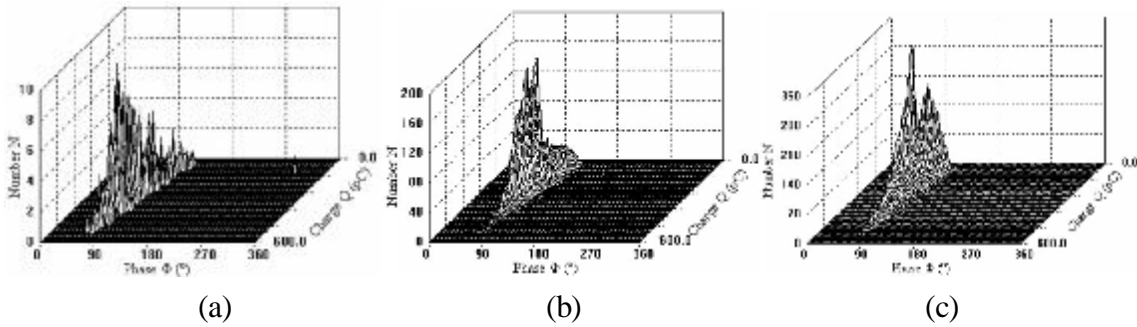


Figure 6.9 Φ -Q-N patterns of transformer liquids under 500 pC PD faults for 15 minutes. Point curvature = 6-7 μ m, sphere electrode diameter = 12.5 mm, gap distance = 50 mm, in (a) Gemini X at 24 kV, (b) Midel 7131 at 23 kV, (c) FR3 at 27 kV

Figure 6.10 shows the concentrations of total combustible gases (TCG) with total discharge energy for both mineral oil and esters under PD faults of 500 pC for various durations. For the same type of liquid, the overall trend is the TCG increases with the increase of total discharge energy. However, it is not true for different types of insulating liquids. For example, Midel 7131 had a much higher level of total discharge energy than Gemini X when stressed for 60 minutes, but less TCG were produced.

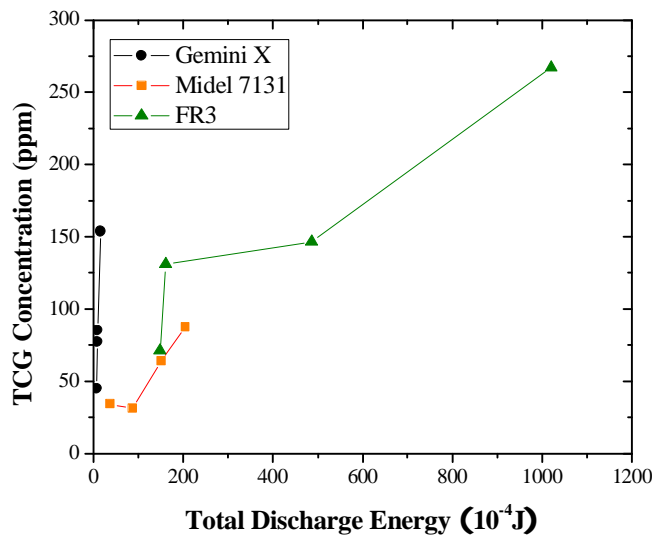


Figure 6.10 Total combustible gases concentrations with discharge energy

Table 6.8 shows the volume of TCG produced in the transformer liquids when unit energy (per Joule) is released. The volume of TCG is calculated by the concentration of the TCG (ppm) multiplied by the volume of the test container (100mL). As shown in the table, the same amount of energy will produce much more TCG in Gemini X than in Midel 7131 and FR3. In [211], the gas volume produced by unit energy (per Joule) is referred to as ‘Gas Generation Rate’. Under PD faults of 500 pC, Gemini X has a gas generation rate of 862 μ l/J,

which is more than 10 times of those in Midel 7131 and FR3. It should be kept in mind that not all the energy released into liquids is consumed to produce fault gases. A part of the energy might be consumed in the oxidation process, or transferred into light or heat.

Table 6.8 TCG amounts produced by unit energy per Joule

Oil	Gemini X				Midel 7131				FR3			
Energy (mJ)	7.7	8.1	9.2	15.7	37.4	88.2	151.2	205.1	148.2	161.4	486.6	1020.0
TCG (μ)	45.0	77.5	85.3	153.9	34.2	31.2	63.9	87.5	71.2	131.0	146.6	267.3
Rate (μ /J)	584.4	956.7	927.2	980.3	91.4	35.3	42.3	42.6	48.0	81.2	30.1	26.2
Average(μ /J)	862.2				52.8				45.6			

6.6 Production of C₂H₆ in Natural Esters

It was observed in the tests that a significant amount of C₂H₆ was produced in FR3 under PD faults as low as 200 pC, and similar results were also reported in [197, 199, 207] under electrical or thermal faults. The food industry has studied the production of alkenes from fatty acids for decades. Since C₂H₆ is a type of alkenes, a review of the literature on flavor chemistry helps to understand the production of C₂H₆ in FR3, which is a type of transformer liquid made mainly from soybeans.

Table 6.9 lists the compositions of new and in-service FR3 [212]. The compositions are listed by individual fatty acids along with their carbon numbers and the double bond numbers (i.e., 18:1 represents 18 carbons and one double carbon bond). The FR3 is comprised of at least 15.5% saturated fatty acids, 23.5% monounsaturated, and 61% polyunsaturated fatty acids.

Table 6.9 Fatty acid compositions in new and in-service FR3

Fatty acid		New FR3 (%)	In-service FR3 (%)
Palmitic	C16:0	10.6	10.6
Stearic	C18:0	4.4	4.03
Oleic	C18:1	23.4	21.8
Linoleic	C18:2	52.4	54.2
Linolenic	C18:3	7.6	8.1
Eicosenoic	C20:1	0.24	0.2
Erucic	C22:1	0	0
Other		1.36	1.07

The mechanism of C₂H₆ formation in mineral oil is explained in [129], using the scission and recombination mechanism. The hydrocarbon molecules of mineral oil are attacked by partial discharges, releasing various **radicals** including CH₃*. The recombination of two CH₃* radicals will produce a C₂H₆ gas molecule. Figure 6.7 shows that PD faults with amplitudes higher than 500 pC can produce C₂H₆ in mineral oil. Since C₂H₆ is produced in FR3 under PD faults as low as 200 pC, there should be another mechanism leading to the formation of C₂H₆ in FR3 except the scission and recombination mechanism.

From literature on the flavor chemistry, the oxidation of unsaturated fatty structures by dissolved oxygen is possibly another mechanism for producing C₂H₆. The unsaturated carbon bonds are critical in this mechanism. Generally speaking, the oxidation process in esters can be classified into two categories: **triplet oxidation** [213] and **singlet oxidation** [214]. Hydro-peroxide, with a carboxyl radical (-COOH) attached to the carbon chain, is formed as a common product of both oxidation processes, which can decompose to alkenes.

The existence of partial discharges will promote both oxidation processes. For triplet oxidation, partial discharges break the chemical bonds in the liquid molecules, producing large amounts of free radicals including H*. Since H* is a necessary component of the triplet oxidation process [215], more H* will promote the triplet oxidation process. For singlet oxidation, a large amount of singlet oxygen atoms might be formed [213] when the dissolved O₂ absorbs the energy provided by partial discharges, promoting the singlet oxidation process by supplying more singlet oxygen atoms as a type of reagent.

In FR3, linolenic composition takes up about 8 % of the total volume. One product from the oxidation of linolenic composition is a type of **hydroperoxide** with carboxyl radical (-COOH) attached to the 16 position carbon. This hydro-peroxide undergoes **β-scission**, producing one **alkoxy** radical and one alkyl (C₂H₅*) radical [216]. The corresponding alkyl radical would be expected to be reactive and unstable. In the presence of a large amount of ionic hydrogen (H*) from the partial discharge, C₂H₆ will be produced by the combination of one C₂H₅* radical and one H* radical [217].

6.7 DGA Diagnosis Methods

For in-service transformers, combustible gases are produced even in the condition of normal operation as a result of oxidation and material ageing. When a fault occurs, higher concentrations of fault gases are produced. Thus, the DGA technique relies on the trend analysis to diagnose the type of faults, and a sudden increase in the concentrations of fault gases would appear to be a clear sign of internal faults in transformers.

With the replacement of esters to mineral oil, it is necessary to determine whether the DGA analysis criteria, which are set for conventional mineral oil, are still correct for esters. Therefore, the DGA results obtained in this chapter are tested as inputs to the DGA diagnosis methods. Two commonly used diagnosis methods are examined, the key gas method and the Duval triangle method.

6.7.1 Criteria for DGA Diagnosis

To perform a DGA diagnosis, IEC 60599 recommends transformer users to calculate gas ratios and diagnosis fault types only when the gas concentrations reach certain criteria [129]. The criteria are defined as the 90% typical values, which indicate that 90 % of gases results in a population of transformers are below these criteria and 10 % are above it. The 90 % typical values recommended by IEC 60599, IEC TC14 and IEC TF11 are listed in Table 6.10 [218].

Table 6.10 90% typical values (ppm) for mineral oil-filled power transformers [218]

	C2H2	H2	CH4	C2H4	C2H6	CO	CO2
<i>IEC60599</i>							
No OLTC	3-50	60-150	40-110	60-280	50-90	540-900	5100-13000
OLTC	80-270	75-150	35-130	110-250	50-70	400-850	5300-12000
<i>IEC TC14</i>							
Transformers	200	500	350	500	800	1000	14000
<i>IEC TF11</i>							
No OLTC	2-20	50-150	30-130	60-280	20-90	400-600	3800-14000
OLTC	60-280	50-150	30-130	60-280	20-90	400-600	3800-14000

The reasons for the criteria are mostly practical: to avoid spending too much money on the

low 90% of the DGA cases where faults are less likely to occur. However, it should be recognized that the DGA diagnosis is not 'simple set of rules', but a technique based on operational experiences. Since the types and amount of fault gases generated in transformers are affected by many factors, the criteria values are influenced by many factors, such as the type of transformers, the voltage ratings, the age and size of the transformers, the operating conditions and so on.

For laboratory studies, the gas concentrations are usually much less than the criteria values, unless a PD fault is intensive or lasts for a long period. Since the criteria are recommended for in-service transformers, not for laboratory studies, the results obtained in this chapter could be diagnosed by the key gas method and the Duval triangle method regardless of the 90% typical values.

6.7.2 Key Gas Method

For mineral oil, it is generally accepted that H₂ is the primary indicator for PD faults, and it usually has the largest concentration in the total combustible gases. According to the key gas method, the relative percentage of H₂ in total combustible gases should be greater than or equal to 85 % [203].

Figure 6.11 shows the relative percentages of combustible gases produced under various PD faults for mineral oil and esters. For each type of oil, the results of eight samples were calculated. The samples are labeled as G1 to G8 for Gemini X, M1 to M8 for Midel 7131, and F1 to F8 for FR3, corresponding to Table 6.6 and Table 6.7.

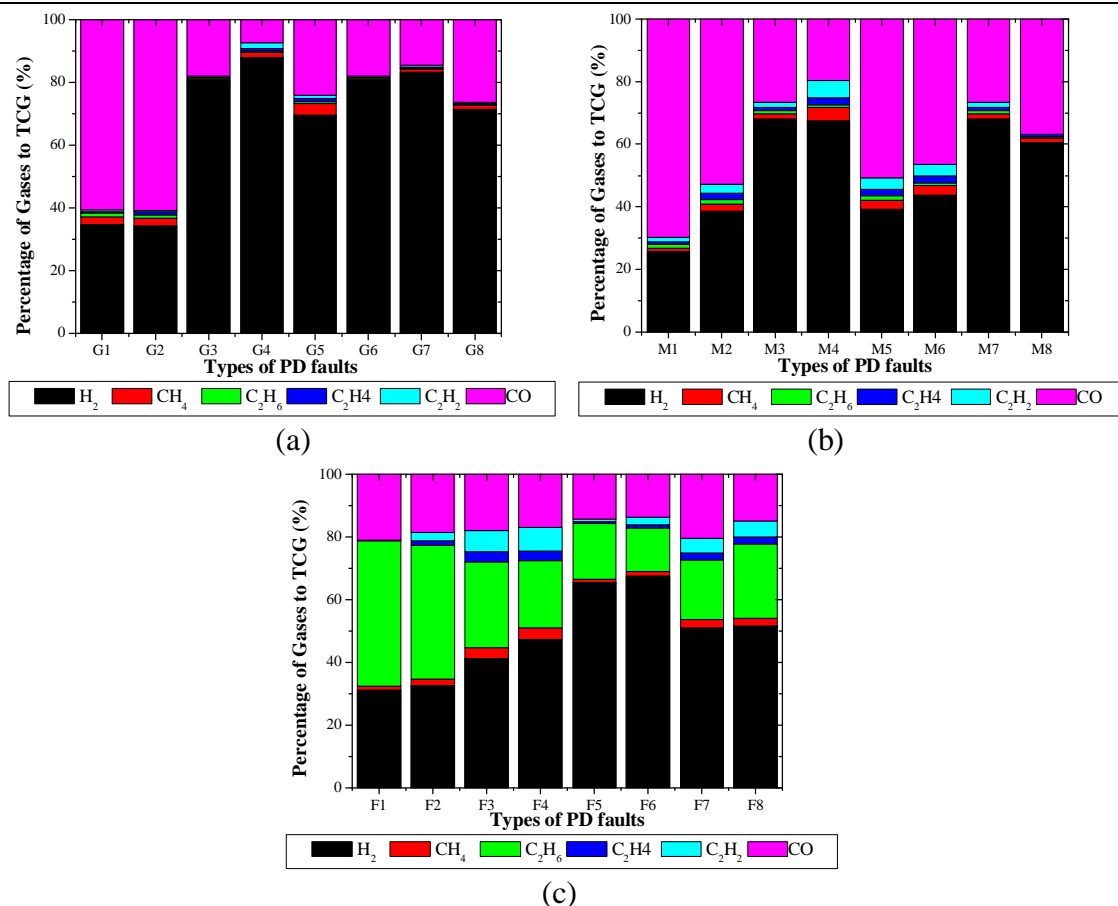


Figure 6.11 Percentages of combustible gases produced under PD faults
(a) Gemini X, (b) Midel 7131, and (c) FR3

The graphs show that H₂ is not always in the largest concentrations in all samples. Large amounts of CO are produced in both mineral oil and esters. As a result, the relative percentage of H₂ in TCG is usually less than 85 %, below the specified criterion for the key gas method to diagnose a fault as PD fault. In FR3, C₂H₆ is produced in significant amounts, which further reduces the relative percentage of H₂ in the TCG. Thus, the PD faults can not be recognized correctly using the key gas method, at least for the results obtained in this Chapter.

It is proposed that some adjustments are needed in order to recognize the PD fault correctly using the key gas method. One possible adjustment is to remove CO from the total combustible gases, since CO is a product of the oxidation process between the liquid molecules and dissolved O₂. Figure 6.12 shows the relative percentages of fault gases (without CO) produced under various PD faults for mineral oil and esters. As shown in Figure 6.12 (a), H₂ takes up more than 85 % of the total gases in Gemini X, indicating the PD faults can be recognized by the key gas method (without CO) for mineral oil. However,

the percentage of H₂ is still lower than 85 % for Midel 7131 and FR3, indicating the 85 % criterion designed for mineral oil is not applicable to esters.

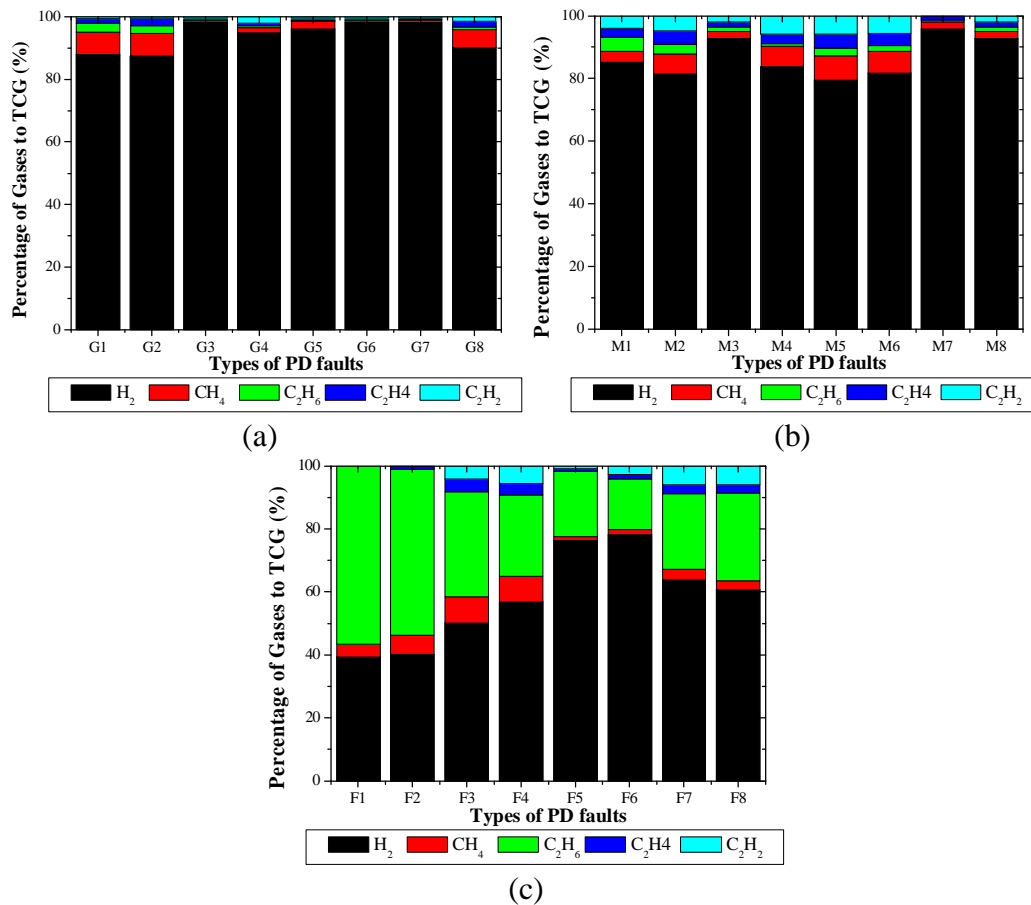


Figure 6.12 Percentages of combustible gases without CO produced under PD faults
(a) Gemini X, (b) Midel 7131, and (c) FR3

A second possible adjustment is to slightly reduce the criterion for diagnosis of PD faults. A percentage of 75 % or 80 % for H₂ might be more appropriate for correct recognition of the PD faults in Gemini X and Midel 7131. In addition, the diagnosis results of PD faults can be enhanced by the ratio of C₂H₂/H₂, which reflects the intensity of discharges [219]. When the discharges are weak, this ratio is usually much smaller than 1. With the increase of discharge intensity, this ratio is gradually increased. When this ratio is close to or more than 1, the discharges are of high energy arcing type.

A third possible adjustment is specified for FR3. The key gas method still can not recognize PD faults correctly in FR3 even considering the above two adjustments, due to the generation of large amounts of C₂H₆ in FR3. Therefore, both H₂ and C₂H₆ should be regarded as the key gases of PD faults, and their amounts should be considered together. Figure 6.13 shows the

percentages of fault gases (without CO) produced under various PD faults in FR3, considering H_2 and C_2H_6 together. The amount of $H_2+C_2H_6$ exceeds 80 % of the total combustible gases (without CO), indicating PD faults in FR3 can be recognized by the key gas method.

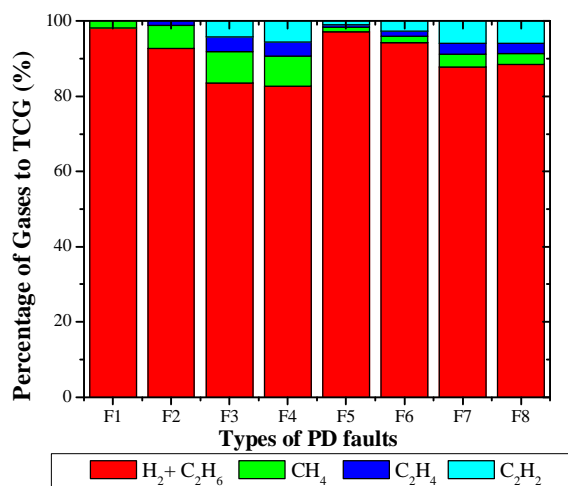


Figure 6.13 Percentages of combustible gases without CO in FR3

6.7.3 Duval Triangle Method

In the tests, the maximum amplitudes of all PD faults were between 200 pC and 1000 pC, thus all the PD faults produced belong to the PD fault of sparking type. Figure 6.14 shows the diagnosis results of fault types using the Duval triangle method.

- 1 For Gemini X, all DGA results fall into the D1 area of Duval triangle graph. The D1 area stands for the PD faults of low energy. Thus, the Duval triangle method is able to recognize the PD fault correctly for Gemini X.
- 1 For Midel 7131, some DGA results fall into D2 area. The PD faults are mistakenly recognized as electrical faults of high energy arcs or breakdowns. Thus, the Duval triangle method fails to diagnosis the PD faults for Midel 7131. It is proposed that the boundary between D1 and D2 areas should be adjusted from $C_2H_4 = 23\%$ to $C_2H_4 = 30\%$ for correct diagnosis of the PD fault in Midel 7131.
- 1 For FR3, most of the DGA results fall on the boundary of D1/D2 area. The severity of PD faults was exaggerated. Therefore, the boundary between D1 and D2 areas also needs to be adjusted from $C_2H_4=23\%$ to a higher value.

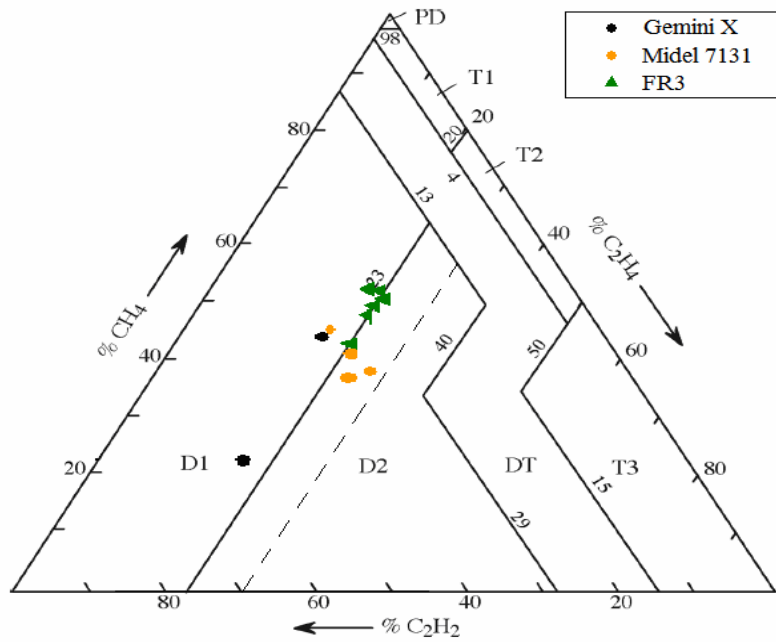


Figure 6.14 Diagnosis of PD faults using Duval triangle method for transformer liquids

This conclusion is similar to Duval’s recent publication in [196], in which the boundaries of D1/D2 area are increased from 23 % to about 27 % for Midel and about 25 % for FR3.

6.8 Summary

The fault gases produced under PD faults for both mineral oil and esters were studied in this chapter. We can conclude from the test results:

- Although their molecular structures are different, mineral oil and esters generate the same type of fault gases under PD faults. Midel 7131 generates similar amounts of fault gases to those of mineral oil under PD faults of the same amplitude, but FR3 generates twice the amounts of fault gases. FR3 is less stable under PD faults than Gemini X and Midel 7131, probably due to the unsaturated carbon bounds in the molecular structures.
- Under PD faults of the same amplitude and the same duration, more energy is dissipated into FR3 than into Gemini X and Midel 7131 due to a higher PD repetition rate in FR3. The same amount of energy will produce much higher amounts of fault gases in Gemini X than in Midel 7131 and FR3.

- | A significant amount of C_2H_6 is produced in FR3 under PD faults, thus C_2H_6 is a feature gas of FR3. The literature from the food industry shows that C_2H_6 is produced mainly due to the linolenic compositions in FR3, through the oxidation process and β -scission of the hydro-peroxide products.
- | Some adjustments should be made for the Key Gas method to diagnose PD faults correctly. The Duval triangle method recognizes the PD faults in Gemini X correctly. However, it needs to be adjusted in order to interpret DGA results in Midel 7131 and FR3. It is suggested that the boundary D1 and D2 areas should be moved from $C_2H_4 = 25\%$ to $C_2H_4 = 31\%$.

Chapter 7. Conclusions and Future Work

7.1 Research Areas

This PhD thesis has provided an extensive study of the breakdown mechanism in transformer liquids under AC voltage, including various transformer liquids and various field configurations. The measurement and diagnosis methods for partial discharge were also discussed and improved for application to esters. Through analytical and experimental researches, the objectives of this thesis were achieved and useful findings were obtained.

In this PhD thesis, the main research areas covered are:

- | **Breakdown mechanism in uniform field under AC voltage**
 - Ø Measurements of the dielectric strengths of transformer liquids
 - Ø Studies of the effect of extraneous factors on the breakdown strengths of esters in comparison to those of mineral oil
- | **Measurement procedure for partial discharge phenomena**
 - Ø Establishment of test procedure for PDIV measurement in esters
 - Ø Experimentations of PD features at full voltage range in mineral oil and esters
- | **Breakdown mechanism in divergent field under AC voltage**
 - Ø Investigation of streamer generation behaviours in various oils
 - Ø Researches on streamer propagation characteristics in various oils, and the influence of electrode configurations
 - Ø Influence of space charge on streamer behaviours
 - Ø Tests of dielectric strengths of various oils, and correlated streamer polarities
- | **Diagnosis technique (DGA) for partial discharge phenomena**
 - Ø Determination of fault gases under partial discharge faults in various oils
 - Ø Examination of DGA interpretation methods for application to esters

7.2 Summary of Main Findings and Results

Through experimental study and analytical modelling, this work has obtained useful results on the breakdowns in AC uniform and divergent fields. Several conclusions are summarized as follows, considering the dielectric properties of esters in comparison with mineral oil.

- | The study of the breakdown mechanism in the uniform field under AC voltage was carried out mainly due to the consideration of whether the dielectric strengths of esters allow their usage in large power transformers.
- Ø Weibull distribution is the best fitting to model the breakdown voltage distributions for both mineral oil and esters. Although the mean breakdown voltages of transformer liquids are similar, the withstand voltages (at 1% failure rate) of esters are 10% lower than those of mineral oil.
- Ø The particle contamination has a detrimental effect on the dielectric strengths of transformer liquids. The breakdown strengths of esters are 30% higher than that of mineral oil when the particle content ($>5 \mu\text{m}$) is 32,000 per 100 ml. This can be attributed to the higher viscosities of esters, and hence the slower motions of a particle in more viscous liquids.
- Ø The water content will only reduce the dielectric strengths of clean transformer liquids when the relative water content is above 30%. However, in the presence of particles, the dielectric strength of mineral oil is reduced more significantly from 47 kV/mm for dry oil to 15 kV/mm for the oil with a relative water content of 30%.
- Ø The breakdown strengths of the transformer liquids are reduced with the increase of electrode area. The calculated withstand strengths of esters are more than 30% lower than that of mineral oil for electrode area of 2 m^2 . This can be attributed to the wider breakdown voltage distributions of esters than that of mineral oil.
- Ø Based on the previous 'single parameter' controlled experiments, the withstand voltages of transformer liquids of in-service qualities can be predicted, taking in consideration of the particle effect, the water effect, and the electrode scale effect.
- | The measurement procedure for partial discharge properties was evaluated for its

application to both mineral oil and esters.

- ∅ The precision of the IEC 61294 test procedure is dependent on the liquid type under testing. Several additional improvements were proposed for applying IEC 61294 to esters. The step increasing method for applying voltage is suggested to replace ramping voltage. The voltage duration of each step is proposed as 1 minute/step, and a time gap of 15 seconds should be given after the applied voltage reaches the required value and before recording PD pulses. To compare the PDIVs of various transformer liquids, the same PD detector should be used.
 - ∅ Using either PDIV of industrial or academic definition, the PDIV values of esters are found to be similar to those of mineral oil. Thus, PDIV might not be an effective indicator to differentiate between transformer liquids. The PD behaviours at overstressed voltage are recommended as a complement to PDIV measurement, to comprehensively evaluate the properties of transformer liquids.
 - ∅ PD behaviours at overstressed voltages indicate that Midel 7131 and FR3 are relatively inferior to Gemini X, in terms of higher maximum PD amplitude, higher PD repetition rate, higher equivalent current, high equivalent power, and more negative partial discharges.
- † The pre-breakdown phenomena and breakdown mechanism in the AC divergent field was investigated with the help of a high-speed camera.
- ∅ Esters have similar performances to mineral oil at the streamer initiation stage. The inception voltage is only determined by the local field near the needle electrode.
 - ∅ The streamer propagation is influenced by the overall field between the needle to sphere/plane electrode configuration. The high electronic affinity of ester molecules favours the propagation of negative streamers in esters. Therefore, mineral oil has a higher ability to suppress the propagation of negative streamers.
 - ∅ The space charge influences the streamer structures. The space charge of opposite polarity will promote the streamer propagation, but the space charge of the same polarity will suppresses streamer propagation.
 - ∅ The dielectric strengths of esters in divergent fields are 10% to 20% smaller than mineral oil. The breakdowns of mineral oil are induced only by positive streamers,

while the breakdowns of esters can be induced by both positive and negative streamers.

- | The DGA diagnosis technique has been investigated under PD faults of various amplitude and energy.
- Ø Although possessing different molecular structures, esters generate the same type of fault gases under partial discharge faults as mineral oil, but in relatively larger amounts. For example, twice the amounts of fault gases are produced in FR3 than in mineral oil.
- Ø The generation of ethane in natural esters can be attributed to two processes. One is the scission of oil molecules and recombination of CH_3^* radicals. Another is the oxidation of linolenic compositions and β -scission of the hydro-peroxide products.
- Ø In order to apply the DGA technique to esters, both the key gas method and the Duval triangle method need to be adjusted, i.e. D1/D2 boundary in the Duval triangle is proposed to move from $\text{C}_2\text{H}_4 (\%) = 25\%$ to around $\text{C}_2\text{H}_4 (\%) = 31\%$.

To sum up, the intrinsic and physical properties of esters, i.e. molecular structure and viscosity, affect their dielectric performance in comparison to mineral oil. In terms of the breakdown mechanism, the breakdown in uniform fields is determined by extraneous factors, but the breakdown in divergent fields is dominated by liquids' intrinsic properties. Conclusions in this thesis suggest that esters are relatively inferior to mineral oil in divergent AC fields in terms of dielectric properties. However, esters have some advantages over mineral oil, such as environmental friendliness, resistance to fire, higher withstand strengths in uniform AC field when in practical qualities and electrode scale, etc. These merits will promote the usage of esters in large power transformers.

7.3 Future Work

This thesis presents a wide range of studies concerning the electrical performances of transformer liquids under AC voltage. The molecular structures of esters are proved to influence their dielectric strengths. However, some studies in this thesis have scope for greater depth and therefore require further investigations.

- | For the streamer study, future work could be carried out considering the following three

aspects.

- ∅ In this thesis, the observation of pre-breakdown phenomena was limited by the magnification factor and speed of the high-speed camera. Thus, the breakdown processes in $\mu\text{s}/\text{ns}$ duration were not recorded, and high quality photographs could not be obtained. Further investigations should be carried out in this area using better experimental designs and better devices, since the formation of streamers in the first few μs might provide valuable information about the differences between esters and mineral oil.
 - ∅ In order to protect the oscilloscope, the streamer currents were only recorded at voltages below the breakdown voltage. The magnitude of the pre-breakdown current might be too high to damage the oscilloscope. More investigations could be carried out to record the pre-breakdown current in transformer liquids at voltages near to the breakdown voltage. This would be helpful to investigate the streamer behaviours prior to breakdown. A possible way is to use wide band current transformers to reduce the current magnitude to a safe value for the oscilloscope.
- ı For the DGA studies, future work could be carried out considering the following two aspects.
- ∅ In this thesis, a study of the DGA diagnosis was carried out only under PD faults of the sparking type. For a better understanding of esters, the investigation of the DGA technique can be carried out under a wide range of thermal faults and electrical faults, i.e. PD of cold corona, arcing, or breakdowns. The energies released by the faults should be calculated and correlated with the amount of the fault gases.
 - ∅ Although the test containers used in the thesis were carefully sealed after the experiments, unfortunately some amount of fault gases could still have leaked during the test or before the container was sealed, due to the pressure difference in and out of the test container. To obtain more credible results of the total fault gases, extended work could be carried out to avoid leakage of the fault gases. This might be achieved by improving the sealing of the test container to avoid gas leakage during the experiments, and using an online DGA analyzer to avoid gas leakage during the oil sample collection.

Appendix I. Additional Information and Further Tests

I.1 Particle Effect on AC Breakdown Strengths of Transformer Liquids

Table I.1 Influence of particles on AC breakdown strengths of transformer liquids

Name	oil	particle	Amount	Effect
Wiegand [72]	Mineral oil	Carbon black	3% in weight	+40%
Krins [73]	Shell diala D, water content = 20 ppm	Carbon particles produced by successive impulse (sum energy)	W=0 W=32.7 kW _s W=65.4 kW _s W=130.8 kW _s	85kV -31% -33% -43%
	Shell diala D, water content =5ppm	Carbon particles produced by successive impulse (sum energy)	W=0 W=32.7 kW _s W=65.4 kW _s W=130.8 kW _s	71kV -22% -27% -36%
Krins [73]	Aged mineral oil	Carbon particles produced by successive impulse (N shots)	N=0 N=5000 N=10000	30kV +33.3% +83.3%
Miyahara [67]	Silicone oil	Natural particles, mostly fibres (n particles in 100ml oil)	n=1000 as clean oil n=10000	-30%
Trinh [65]	Mineral oil	Natural particles (δ is particle content factor)	δ =13,14 δ =15 δ =18	23kV/mm 18kV/mm 11kV/mm%
Kurita [80]	Mineral oil	Natural particles	δ =-3 δ =10	29kV/mm 23kV/mm-21%
Farooq [39]	Mineral oil	Carbon particles (>5 μ m)	n=0	64.7kV
			n=130	59.7kV -7.8%
			n=3,000	47.7kV -26.3%
			n=17,000	38.7kV -40.2%
			n=490,000	32kV -50.4%
			n=1,800,000	31.8kV -50.9%
n=9,600,000	31.3kV -51.7%			
Miners [47]	Mineral oil		n=2000 as clean oil	Unit
		Iron (20 μ m)	n=200,000	-0%
		Iron(45 μ m)	n=200,000	-50%
		Copper(45 μ m)	n=20,000 n=30,000	-40% -50%
		Cellulose (dry) Cellulose (wet)	n=100,000 n=100,000	-10% -40%
Socolov	Mineral oil	Natural particle	n=279,000	-65%

Appendix I. Additional Information and Further Tests

Vincent [220]	Transformer liquid		n=200 as clean oil	
		Aluminium particles	n=100,000	-25%
	(ramp voltage)	Carbon particles	n=20,000	-15%
		Natural particles	n=100,000	-56%
			n=20,000	-9%
		(step voltage)	Carbon particles	n=20,000
Natural particles	n=100,000		-27%	
			n=20,000	-41%
P.Rain [61]	White oil	single tungsten cylinder (ϕ is diameter, l is the length of particle)	($\phi=0.5\text{mm}$, l=3mm) ($\phi=0.5\text{mm}$, l=7mm) ($\phi=0.2\text{mm}$, l=7mm) ($\phi=0.75\text{mm}$, l=7mm)	50kV/cm 32kV/cm 22kV/cm 37kV/cm
Carraz [57]	Mineral oil	Single tungsten Single steel Single copper	($\phi=0.2\text{mm}$, l=2mm) ($\phi=0.2\text{mm}$, l=2mm) ($\phi=0.2\text{mm}$, l=2mm)	46.5kV/cm 46.5kV/cm 45kV/cm
Watson [28]	Mineral oil	Cellulose fibre	Clean oil Fibre-free oil	150kV/cm 400kV/cm

I.2 Equipment and Methods used in Breakdown Voltage Tests

Currently, several test standards are available to measure the qualities of mineral oil, i.e. IEC 60156 to measure the breakdown voltage, IEC 60841 to measure the water content, and IEC 60970 to count the number and measure the size of the particles. However, it might not be suitable to apply these standards to esters without adjustments, because both the physical and chemical properties of esters are different from those of mineral oil. Small changes should be made in order to yield correct results of esters' qualities. This section discusses the test equipment and methods used to measure the AC dielectric strengths, water contents and particle contents for mineral oil and esters.

I.2.1 AC Dielectric Strength

The AC dielectric strengths of transformer liquids are measured by a BAUR Prüf und Messtechnik Fully Automatic Insulating Oil Tester DPA75, as shown in Figure I.1.



Figure I.1 Baur DPA75 automatic transformer liquids tester

The DPA75 tester is designed to automatically test the dielectric strengths of transformer liquids with dissipation factors less than 4.5 and specific volume resistances larger than 30 MΩm. The transformer liquids used in this thesis fulfil this requirement, so their dielectric strengths can be measured by the tester. This tester is capable of supplying 50 Hz AC voltage up to 75 kV with a ramping rate adjustable from 0.5 kV/s to 10 kV/s. The current sensor is set to trip within 10 μs after the breakdown current reaches 4 mA [221], which is found suitable to both avoid a false trip and protect the quality of the transformer liquid from deteriorating. A wide range of pre-programmed standards are provided in the DPA75, among which the most widely used ones are IEC 60156 and ASTM D1816.

I.2.1.1 Comparison of IEC 60156 and ASTM D1816

For manufacturers and users of oil-filled power transformers, different standards are used to check the qualities of transformer liquids when filling new transformers and to diagnose the contaminations from the aging by-products of in-service insulation materials. IEC 60156, ‘Insulating liquids - Determination of the breakdown voltage at power frequency – Test method’ [222], is commonly used by the European transformer manufacturers and users. On the other hand, ASTM D1816, ‘Standard test method for dielectric breakdown voltage of insulating oils of petroleum origin using VDE electrodes’ [223], is usually followed by American transformer manufacturers and users. Table I.2 lists the differences between IEC 60156 and ASTM D1816, including the

Appendix I. Additional Information and Further Tests

electrode shape, the gap distance, the voltage ramping rate, the stirring duration, and the number of required breakdowns.

Table I.2 Differences between IEC 60156 and ASTM D1816

Property	ASTM D1816	IEC 60156
Electrode shape	Brass 36 mm diameter VDE electrode	Brass, bronze or stainless 12.5 mm diameter spherical or 36 mm diameter VDE type
Gap distance	1 or 2 mm	2.5 mm
Voltage ramping rate	0.5 kV/s	2 kV/s
Stirring duration	1 minute	2 minutes (optional)
Number of breakdown	5 or 10	6

For a comparative evaluation of IEC 60156 and ASTM D1816 standard procedures, the breakdown strengths of Gemini X were measured following these two standards. The water content of the liquid sample used in this test was 6.0 ppm, which was corresponded to a relative water content of 12 %. The sample was contaminated by cellulose powder and each 100 ml liquid contained about 1×10^4 particles with diameter equal to or larger than 5 μm . Since the DPA 75 could not provide enough breakdown voltage for a 2.5 mm oil gap required by IEC 60156, the gap distance was reduced from 2.5 mm to 1 m.

Figure I.2 represents the test results of the breakdown strengths using IEC and ASTM standard procedures. The mean breakdown strength using IEC 60156 (solid line) is 22.2 kV, about 1.3 kV higher than that using ASTM D1816 (dash line). This corresponds to a variation of 6%, which is within the tolerance of experimental error. It indicates that the AC dielectric strength tests using IEC and ASTM standard procedures will obtain similar results. Similar tests were also carried out by C. Vicent using Voltesso (a type of mineral oil) purified by a 0.2 μm filter, and five comparisons of the breakdown strengths are listed in Table I.3 [220]. The variations between the breakdown strengths using IEC and ASTM standards are less than 3%, which is the further evidence of similar results using these two standards.

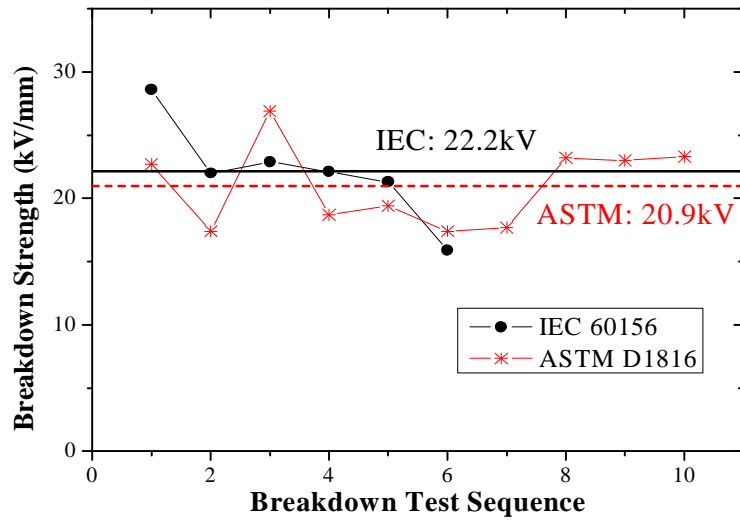


Figure I.2 Breakdown strengths of Gemini X using IEC 60156 and ASTM D1816

Table I.3 Breakdown strengths of Voltesso using IEC 60156 and ASTM D1816 [220]

Breakdown Sequence	1	2	3	4	5
ASTM D1816 (kV/mm)	32.9	32.5	32.4	29.9	30.0
IEC 60156 (kV/mm)	30.2	33.2	31.7	31.7	31.3

Since the gap distance required in IEC 60156 is 2.5 mm, the breakdown voltages of clean transformer liquids using IEC 60156 are usually higher than 75 kV, which exceeds the maximum output voltage of DPA75. Thus, the AC breakdown strengths of transformer liquids are measured using ASTM D1816 standard in this thesis.

I.2.1.2 Test Container

Figure I.3 shows the schematic configuration of the test container used in DPA75 for AC dielectric strength tests. A volume of 0.4 L liquid sample is required to fill the container for each test. The gap distance between the electrodes is set at 1 mm, and two thread gauges located at both sides of the container are used to fine-tune the gap distance. A pair of spherically capped electrodes of the VDE (Verband Deutscher Electrotechniker) specification 0370 type is used to provide uniform field distribution between them.

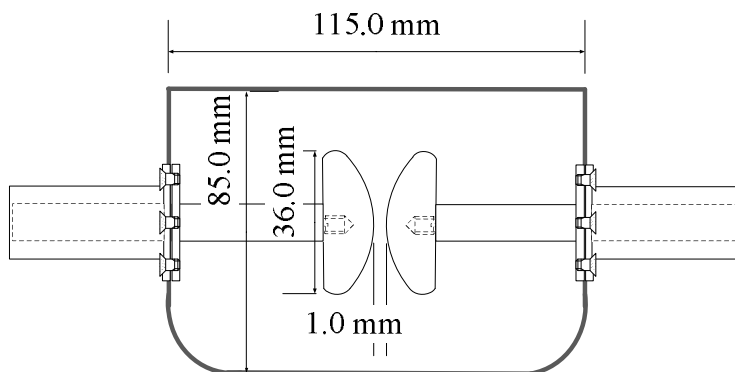


Figure I.3 Schematic configuration of test container used in AC dielectric strength test

I.2.2 Water Content

As shown in Figure I.4, the water contents in the transformer liquids are determined by standard Karl Fischer titration method, following IEC 60814 ‘Determination of water in liquid dielectrics by automatic coulometric Karl Fischer titration’ [34].



Figure I.4 The XB120 scale, 684 Coulometer and 832 Thermoprep of Karl Fischer titration equipment used for water content measurement

The automatic Karl Fischer titration equipment consists of three parts. A Precisa XB120 scale is used to measure the weight of the liquid sample. The accuracy of this scale is less than 0.1 mg. The sample is heated in a 832 Thermoprep oven to 140° C for at least 5 minutes to vaporize all the water in the liquid. The heating will be stopped until the water removal from the sample levels off, indicating that no more water will be released. The vaporized water is then brought into a 684 Coulometer by dry air. The titration is carried

Appendix I. Additional Information and Further Tests

out in this coulometer filled with chemical liquid Hydranal AG-H. During the titration process, an electromagnetic stirrer is driven by a synchronous motor at a constant speed of 300 rpm, to ensure a thorough reaction of water in Hydranal AG-H.

The water content will be reported by the coulometer as absolute weight in the unit of micrograms. This value can be transferred into relative water content in the unit of ppm when the microgram value is divided by the weight of liquid sample. Since esters are much more hygroscopic than mineral oil, it is more reasonable to compare their water content by relative water content rather than absolute water content. The relative water content expresses the water content in percentage as related to the water saturation level in an insulating liquid at a given temperature. Table I.4 lists the saturation levels of water content in the transformer liquids investigated in this thesis at ambient temperature (25 ° C). It is clearly seen that the saturation levels in esters are much higher than that in Gemini X, due to their polar molecular structures.

Table I.4 Saturation levels of water content in mineral oil and esters at ambient temperature of 25° C

	Gemini X	Midel7131	FR3
Water saturation level (ppm)	55	1100	2700

To obtain the real water content, the background water content should be removed from the measurement results. The background water content originates from the small quantity of water which is trapped in the sample vial, either on the wall of the vial or in the air above the liquid surface. Experience shows that the background water content is usually within the range from 50 µg to 100 µg, depending on the relative moisture of the atmosphere. Thus, care need to be taken to determine the precise amount of background water content in the sample vial in order to avoid an error. Especially for mineral oil, an accurate determination of the background water content is of greater importance, since the water saturation level of mineral oil is low and a small measurement error of the background water content will significantly influence the final result. Before the experiments, the background water content is measured three times, and the average value is regarded as the final value, which will be subtracted from the measurement results. In order to reduce the variations between the background water contents in

different sample vials, the Metrohm advises that the sample vials should be exposed to atmosphere for at least 24 hours before measurements.

I.2.3 Particle Content

As shown in Figure I.5, standard automatic particle size analyzer is used to determine the particle content of transformer liquids, following IEC 60970 ‘Insulating liquids – Methods for counting and sizing particles’[66].



Figure I.5 HIAC ABS2 bottle sampler and HIAC 8000A liquid particle counter of particle size analyzer

The automatic particle size analyzer consists of two parts, the HIAC ABS2 bottle sampler and the HIAC 8000A liquid particle counter. The liquid sample is firstly collected in a beaker with a volume of 150 ml. The sample is then degassed under vacuum at a pressure of less than 10 mbar for at least 30 minutes until no visible gas bubbles are observed. After degassing, the beaker is placed on the holder of the HIAC ABS2 bottle sampler, with the inlet pipe dipped into the liquid. The sampler can provide a pressure up to 60 psi to absorb the liquid. The flow rate is adjustable by a thread gauge on the inlet pipe, and the regulated flow rate is 60 ml/min. The particle content of the sample will be measured by the HIAC 8000A particle counter which is operated on the principle of light interruption, and it is capable to measure the number of particles with

Appendix I. Additional Information and Further Tests

diameter larger than 1 μm . During the measurement, an electromagnetic stirrer works continuously to ensure the even distribution of particles in the sample. The results are reported by the analyzer in eight channels classified by the size of the particles. Table I.5 lists the settings of the lower and upper limits of particle diameters for these channels. The accuracy of this particle size analyzer is less than $\pm 10\%$. In order to get a more precise result, the particle content of each sample is usually measured three times. The average value will be reported as the final result.

Table I.5 Settings of lower and upper diameter limits for HIAC 8000A particle counter

Channel	1	2	3	4	5	6	7	8
Lower limit (μm)	1	2	5	15	25	50	100	200
Upper limit (μm)	2	5	15	25	50	100	200	-

It should be noted that the automatic particle analyzer can not recognize the material of the particles. In order to determine the material, the liquid sample should be filtered and the impurities trapped on the surface of the filter paper should be visually checked using microscopic analysis [224]. Figure I.6 shows a typical microscopic photo of impurities trapped on the filter paper from a contaminated transformer liquid [225]. It is clearly seen that many types of particles, including paper fibre, coke, quartz, and copper, might exist in the insulating liquids of in-service power transformers.

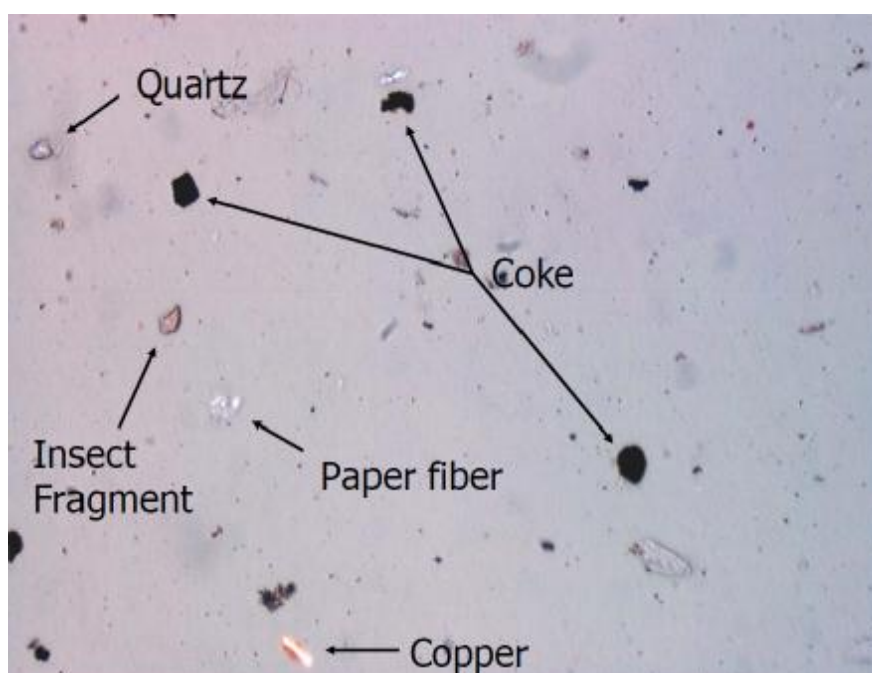


Figure I.6 Microscopic photo of trapped impurities on filter paper from contaminated transformer oil [225]

It is also observed that the particle content analyzer will reach a saturation level when it is used to analyse liquid sample containing particles (diameter $> 5 \mu\text{m}$) more than 1×10^7 per 100 ml. Above this level, the particle analyzer will report incorrect results which are much lower than the expected value. This is because the small particles will accumulate together, forming a large cluster which will be recognized as a large particle. In order to yield correct results, the liquid sample should be diluted by particle-free liquid until the particle content ($> 5 \mu\text{m}$) reduces to less than 1×10^7 per 100 ml, and then, the particle content results should be calculated back.

During the measurement process, care should be taken to avoid contaminations either from the atmosphere or from the container. The contaminations from the container mainly originate from the inside wall of the container, thus it is necessary to clean the sample container. It is recommended that a particle content of less than 200 particles (diameter $> 5 \mu\text{m}$) should be reached in order to consider a container as a clean container [53]. To achieve this requirement, the containers are cleaned following the cleaning procedure described as follows.

At first, a container is washed by a dish washer using detergent at temperature of 40°C . After that, it is rinsed by purified water for several times. To remove the residuals, the container is rinsed by liquid acetone which is filtered by $0.45 \mu\text{m}$ membrane. Then, it is placed upside down and dried in a heating oven with temperature of 50°C for at least an hour. This cleaning procedure should be repeated several times until the container fulfilling the requirement. At last, the prepared container should be rinsed thoroughly by the transformer liquids before collecting the samples.

I.3 Sample Preparation of Breakdown Voltage Tests

The liquid sample is firstly filtered through a membrane filter unit with pore size of $0.2 \mu\text{m}$, usually for three times. Figure I.7 shows the filtration effects of contaminated FR3 up to five cycles. It is clearly seen that the particle content ($>5\mu\text{m}$) of FR3 reduces significantly during the first three filtration cycles from 1×10^4 to 4×10^2 per 100 ml, but changes little for further filtration cycles. After the filtration, the liquid sample will be

dehydrated and degassed in a vacuum oven at less than 10 mbar and 80 °C for two days. Then another day will be given for the sample to cool down to ambient temperature under vacuum condition. The processed liquid samples should be stored in sealed glass containers in dry and clean condition, and ready for use.

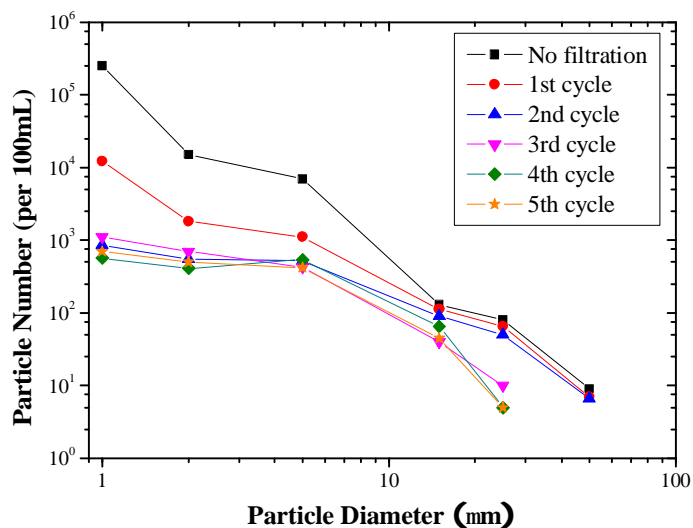


Figure I.7 Particle contents of FR3 up to five filtration cycles

I.4 Experimental Description of Breakdown Voltage Tests

In this thesis, the breakdown voltage tests were carried out following the standard of ASTM D1816. The ASTM D1816 is issued to measure the breakdown voltages of insulating liquids of petroleum origin with low viscosities. However, the IEEE C57.174 found that this test method is not suitable for testing liquids having viscosities of more than 19 cSt at 40 °C, and some improvements were recommended [145]. In order to measure the breakdown strengths of esters which possess high viscosities, these recommendations are adopted in this experiment and some adjustments are made to the ASTM D1816.

Firstly, the degassing method of the liquid samples after filling the test container and before carrying out the experiments is improved. Comparing to mineral oil, the higher viscosities and lower interfacial tensions of esters will result in a slower expulsion of air bubbles out of the samples. Therefore, care must be taken when filling the test container with esters to avoid the air bubbles trapping in the liquid samples. This can be achieved

Appendix I. Additional Information and Further Tests

by pouring the samples along the wall of the tilted container. The IEEE C57.174 recommends that at least 15 minute setting time should be given before starting the test [145]. However in this experiment, the liquid samples were degassed in a vacuum oven at a pressure lower than 10 mbar for at least 30 minutes in order to fully remove the micro-bubbles. Prior to the experiment, the samples should be visually checked to ensure that no bubbles were trapped in the gap or attached on the surface of the electrodes.

Secondly, the time interval between two successive breakdowns is increased. For the same reason, the gaseous by-products of breakdowns take relatively longer time to be expelled from the samples. Thus, IEEE C57.174 recommends that the time interval between two successive breakdowns should be increased from 1 minute (required in ASTM D1816) to at least 5 minutes. Test experience shows that most of the gaseous by-products will be expelled out of the liquid samples in 5 minutes. And an electromagnetic stir should be used to assist the expelling of the gaseous by-products.

Thirdly, the sample size of the breakdown tests is increased. Figure I.8 shows the 95% confident level of the percentage error between the measured breakdown voltage and the actually breakdown voltage as a function of the sample size [10]. This graph clearly shows that the measurement error decreases with the increase of the sample size. Since ASTM D1816 requires 5 or 10 breakdowns to derive the mean value and the standard deviation of the breakdown voltage, a measurement error of 10 % to 15 % will be obtained. This error might be small enough for the measurement of the mean breakdown voltage, but far from the requirement to represent the statistical distribution of the breakdown voltage. Therefore, a sample size of 40 breakdown voltages for each liquid sample will be measured in this experiment, giving a measurement error of less than 5%.

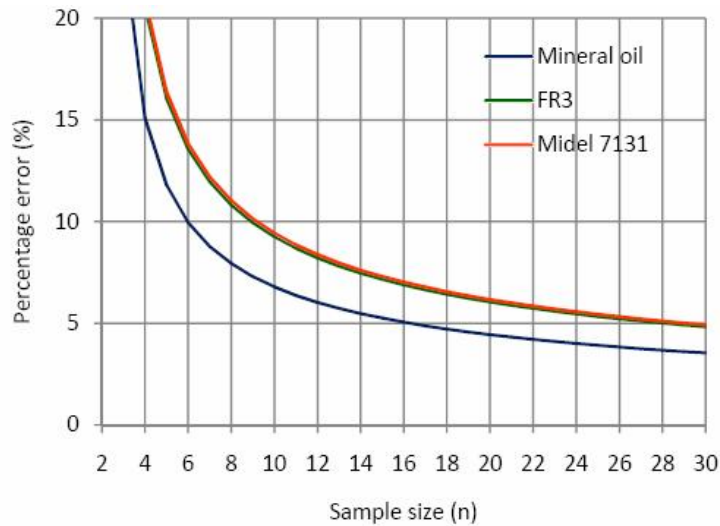


Figure I.8 The 95% confidence levels of the percentage errors between the measurement value and the actual value of the breakdown voltage

The procedure of the electrode conditioning is also improved by preparing the electrodes using 20 breakdowns before carrying out the breakdown tests. It is well-known that the ‘conditioning effect’ affects the measurement results of the breakdown voltage [29]. Thus, ASTM D1816 requires a series of breakdowns to remove the irregularities on the electrode surfaces until the breakdown voltage reaches the anticipated value. After electrodes preparation, a new liquid sample will be filled into the container and the breakdown test will be carried out.

However, it is found that the electrodes need to be re-conditioned after changing new liquid sample. Figure I.9 shows the breakdown voltage results of Midel 7131 up to 80 measurements. The electrodes preparation takes 20 to 30 breakdowns before the breakdown voltage stabilizing. After 50 breakdowns, a new Midel 7131 sample is introduced into the test container, and the vacuum degassing is applied for 30 minutes. It shows that the re-conditioning of the electrodes takes about another 10 breakdowns. Since the small protrusions on the electrode surfaces have already been removed during the first conditioning process, the re-conditioning process probably removes the micro-bubbles which have not been fully removed by the degassing procedure. In this thesis, at least 20 breakdowns are given before recording the breakdown voltage results, in order to avoid the ‘re-conditioning effect’ and yield a correct result.

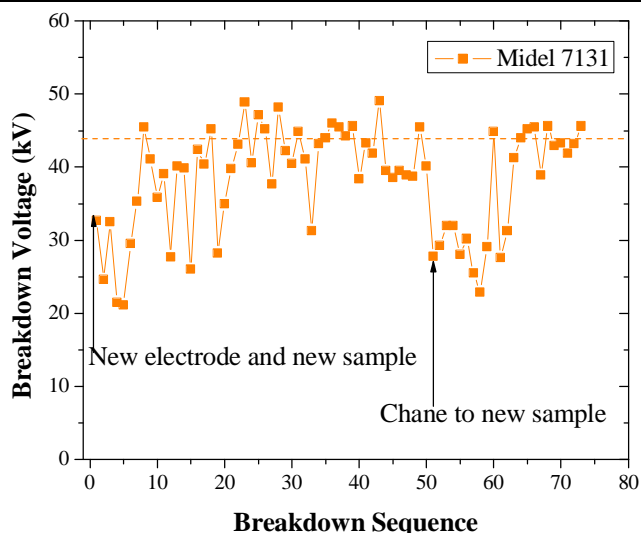


Figure I.9 Conditioning and re-conditioning effect of Midel7131 oil

I.5 Sample Preparation of Water Effect Test

I.5.1 The Water Uptake Method

Water dissolves in the transformer liquids by forming the hydrogen bonds between the water molecules and the polar parts of the liquid molecules. Since most of molecules in mineral oil have non-polar structures, only a small amount of water will dissolve in mineral oil due to the polar components, such as the anti-oxidation additives. However, more water will dissolve in esters because the molecule structures of esters are more polar than mineral oil [2].

In this thesis, the water contents are controlled by moisture equilibrium between the transformer liquids and the wet air. The principle of this method is that when transformer liquids are exposed to wet air, the water in oil will equilibrate gradually with the moisture in air due to the diffusions. Fofana studied the moisture uptake velocities of mineral oil in a closed environment with controlled humidifies [226]. The expected relative humidity in the surrounding atmosphere was controlled by mixing water with certain amount of Glycerine ($C_3H_5(OH)_3$), determined from Figure I.10. Then, the pre-dehydrated sample of the mineral oil was placed in a closed environment and exposed to the atmosphere. The relative water content in the mineral oil was measured from time to time.

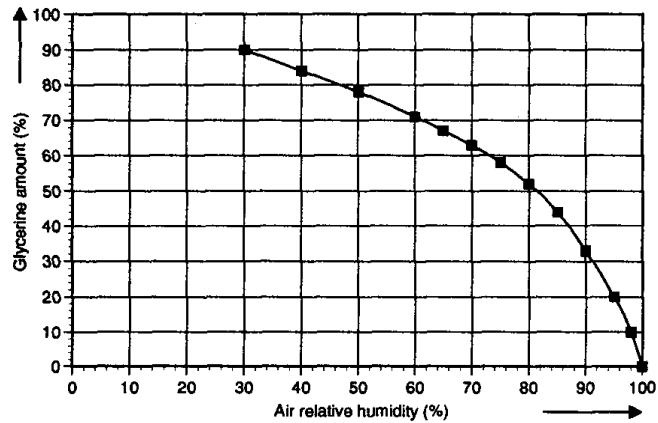


Figure I.10 Relative humidity of air in a closed container using water-glycerine mixture

Figure I.11 shows the water uptake velocity of mineral oil versus the exposure time in the closed environmental with various relative humidity [163]. The results indicate that the equilibrium between the water content in mineral oil and the moisture in air takes 5 to 15 days, depending on the relative moisture in the surrounding air. It was confirmed that this method is also applicable to esters, and is able to control the water content in transformer liquids with an accuracy of 1% [42, 226].

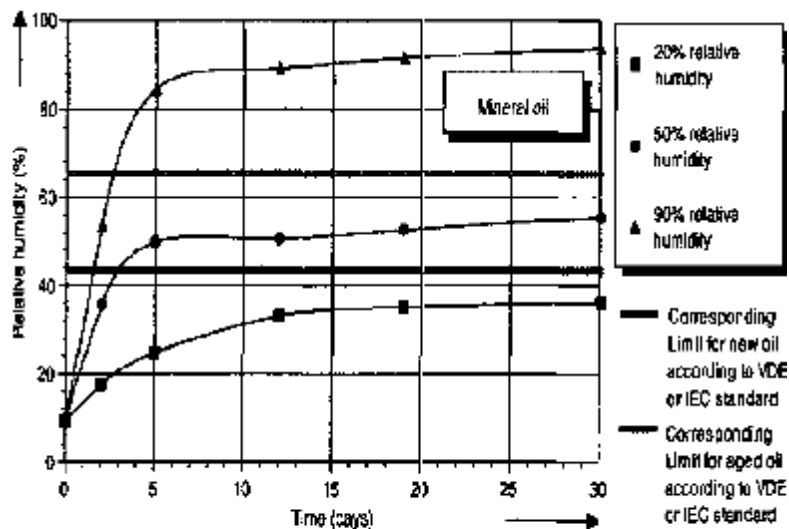


Figure I.11 Moisture uptake of mineral oil exposed to wet air at room temperature [163]

I.5.2 Sample Preparation

The transformer liquids are purified, dehydrated, and degassed as described in Appendix I.3. For both mineral oil and esters, the relatively water contents in the processed samples are less than 2 %, and the particle contents (>5 μm) are less than 500 per 100ml sample. The processed liquids are directly used as dry samples.

To obtain liquid samples with controlled relative water content larger than 10%, the water is added back into the processed samples to the expected relative water content using the equilibrium method proposed by I. Fofana. The procedure of this method is described as follows. Firstly, a mixture of glycerine and water are placed at the bottom of a desiccator in order to control the relative humidity of the air in the desiccator. Then, the dehydrated transformer liquid samples are placed in clean glass dishes in the desiccator. The glass dishes are used to provide large surface area to speed up the moisture uptake procedure. At least two weeks should be given for the samples to absorb moisture from the surrounding air in the desiccator. After the equilibrium between the water in liquids and the moisture in air, the samples are collected and sealed in a clean glass bottled. A further week should be given to ensure the even distribution of water in the samples. Prior to the tests, the exact values of the water contents in the samples should be measured using Karl Fishcher method.

I.6 Influence of Needle Electrode on PDIV

Figure I.12 represents the relationships between the maximum charge of transformer liquids and the applied voltage for four types of needle electrodes, using the procedure described in chapter 4. The criterion level of 100 pC was used to determine the PD inception voltages. The results show that the inception voltage is increased with the increase of the needle tip curvature for both mineral oil and esters, probably due to the reduction of the electric field around the tip of the needle electrodes. It is also observed that the PD inception voltages of transformer liquids are similar for the same needle electrode. This indicates that the PD inception is determined by the local electric field around the needle tip, rather than the compositions of the transformer liquid. Calculations show that the minimum fields required for the PD inception are 5 MV/cm for negative partial discharges and 10 MV/cm for positive partial discharges [111].

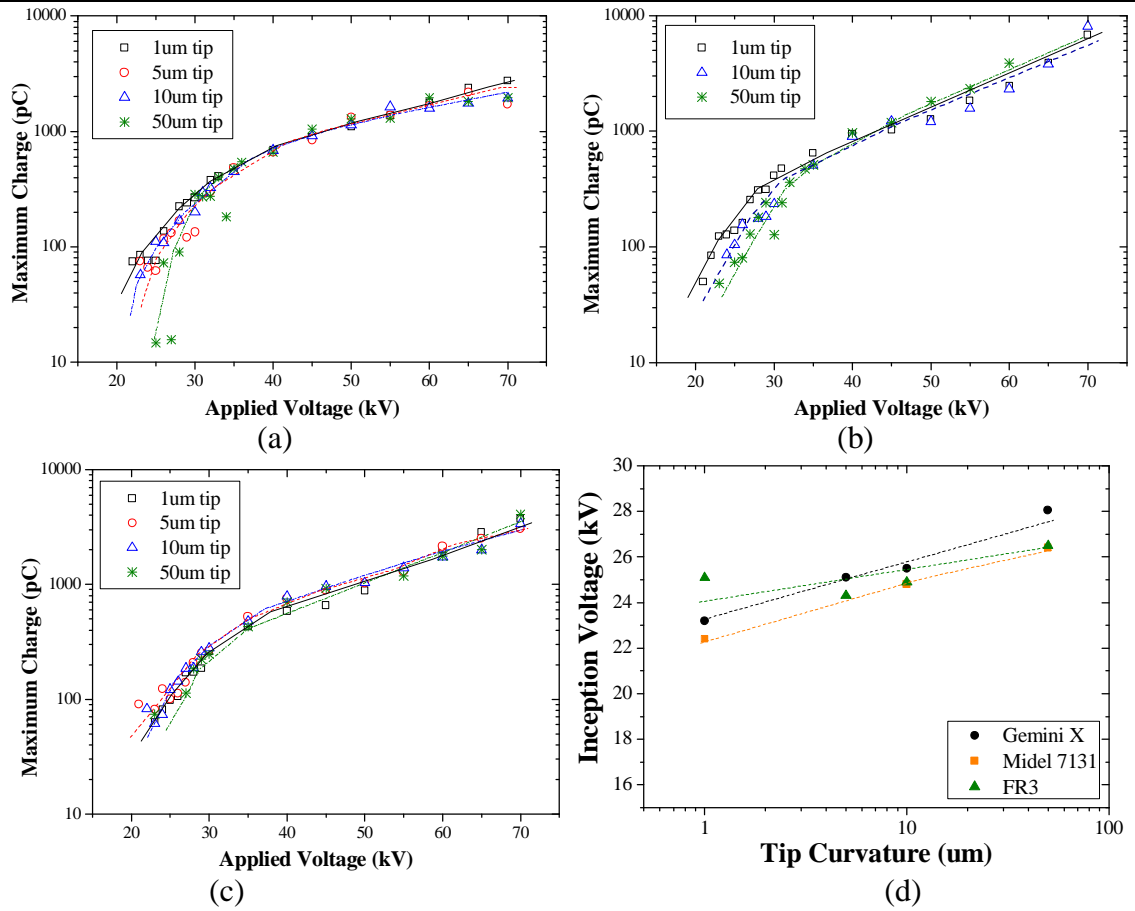


Figure I.12 PD inception voltages using different needle electrodes
 (a) Gemini X, (b) Midel 7131, (c) FR3 and (d) Summary of inception voltages

I.7 Influence of Electrode Arrangement on Streamer Propagation

In this section, the influence of the electric field on the streamer propagation is studied. The electric field is influenced by the tip curvature of the needle electrode, the shape and diameter of the ground electrode, and the gap distances between electrodes. By studying the relationship between the streamer stopping length and the applied voltage at various electrode configurations, it is concluded that the local electric field affects the streamer initiation, and the overall electric field affects the streamer propagation. Whatever the electrode configuration is, the streamer propagation velocities keep quite stable, indicating that the same propagation mechanisms are involved.

I.7.1 Effect of Point Electrode

Figure I.13 and Figure I.14 represent the relationships between the maximum stopping lengths and the applied voltage for both positive and negative streamers in the needle/sphere

Appendix I. Additional Information and Further Tests

electrode configuration with a 100 mm gap distance. The tip curvatures of the needle electrodes used in the tests are 1 μm and 700 μm . It should be noted that changing the point electrode only modifies the local electric field around the electrode tip, without influencing the overall electric field between the electrodes. In the test, Midel 7131 is used as the sample liquid. However, the streamer behaviours are similar in Gemini X and FR3.

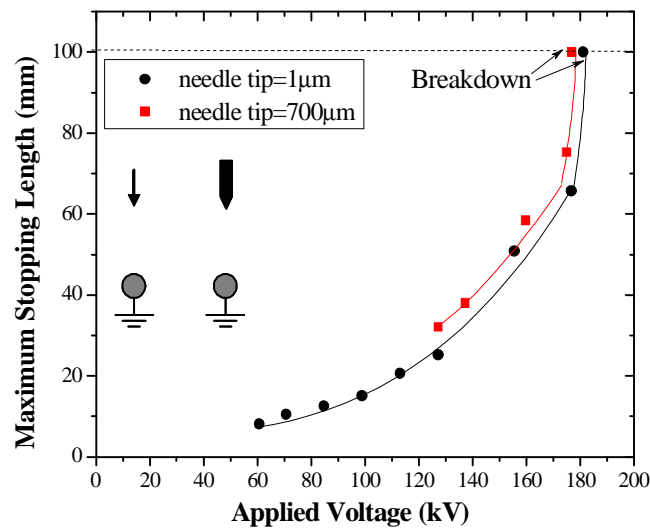


Figure I.13 Stopping length of positive streamers in Midel 7131 for two needle electrodes Point curvature = 1 μm /700 μm , sphere electrode diameter = 12.5 mm, distance = 100 mm

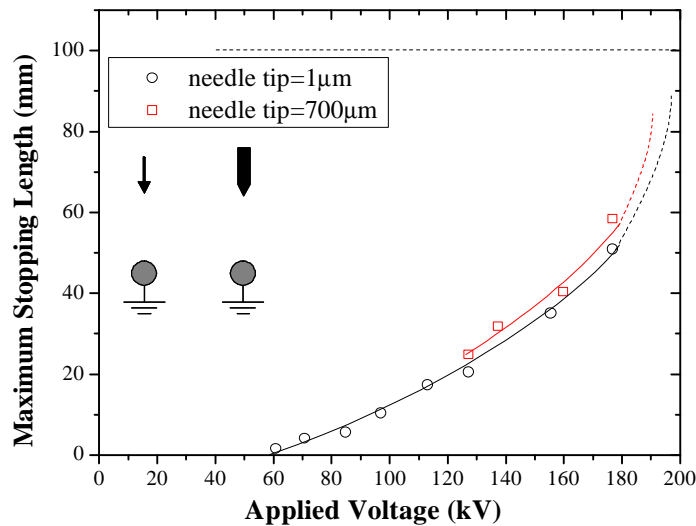


Figure I.14 Stopping length of negative streamers in Midel 7131 for two needle electrode Point curvature = 1 μm /700 μm , sphere electrode diameter = 12.5 mm, distance = 100 mm

The graphs show that the maximum stopping lengths of both positive and negative streamers are almost the same for different needle electrodes. For positive streamers, the average increase slope (at least for streamers shorter than 3 cm) is 24 kV/cm, and the critical length is about 60 % of the total gap distance, which is in agreement with previous result in Chapter 5

using a gap distance of 50 mm. For negative streamers, the average increase slope is similar to that of positive streamers.

However, the streamer inception voltages are significantly different for different needle electrodes. For needle electrode with a tip curvature of 1 μm , the inception voltages for positive and negative streamers are around 60 kV. When the tip curvature of the needle electrode is 700 μm , the inception voltages for positive and negative streamers are much higher, around 130 kV. As soon as the streamers are produced, they will propagate deep into the bulk liquid, and the stopping lengths of these streamers are similar to those streamers when the tip curvature of the point electrode is 1 μm .

Furthermore, it is found that the repetition rates of the streamers are different for different point electrodes. When the point curvature is 1 μm , the repetition rate of streamers is several orders of magnitude higher than that when the point curvature is 700 μm .

I.7.2 Effect of Ground Electrode

Figure I.15 and Figure I.16 represent the relationships between the maximum stopping lengths and the applied voltage for both positive and negative streamers in needle to sphere/plane electrode configurations at a 100 mm gap distance. The tip curvature of the needle electrode is 1 μm . The diameter of the sphere electrode is 12.5 mm, and the diameters of the plane electrodes are 40 mm and 100 mm. It should be noted that the ground electrode affects the overall electric field between the electrodes, without affecting the local field around the needle electrode. In the tests, Midel 7131 is used as the sample liquid. However, similar conclusions could be obtained in Gemini X and FR3.

The result shows that the streamer inception voltages for different ground electrode are almost identical. The inception voltage is about 55 kV for positive streamers, and 60kV for negative streamers. Therefore, the streamer inception voltage only depends on tip curvature of the needle electrode. The critical lengths of positive streamers are 60 % of the total gap distance.

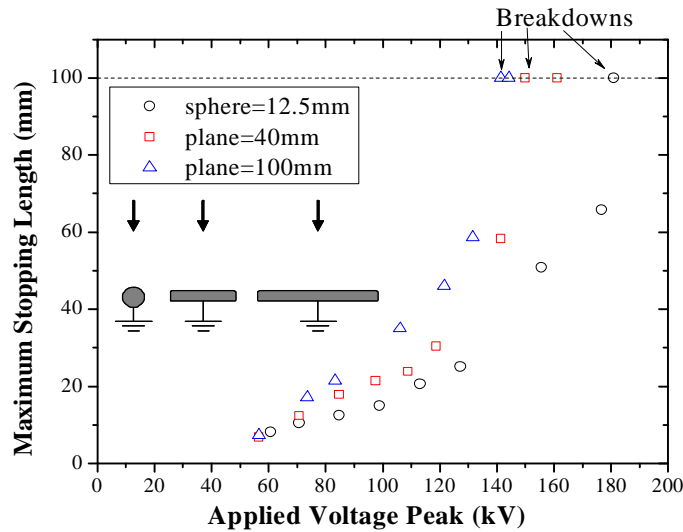


Figure I.15 Stopping length of positive streamers in Midel 7131 for different ground electrodes

Point curvature = 1 μm , gap distance = 100 mm, ground electrode diameter = 12.5 mm (sphere), 40 mm (plane), 100 mm (plane)

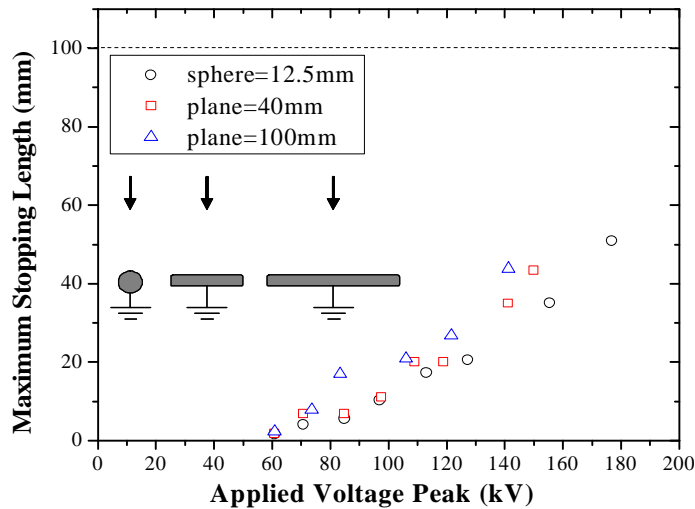


Figure I.16 Stopping length of negative streamers in Midel 7131 for different ground electrodes

Point curvature = 1 μm , gap distance = 100 mm, ground electrode diameter = 12.5 mm (sphere), 40 mm (plane), 100 mm (plane)

At a given voltage, the maximum streamer length is increased with the increase of the diameter of the ground electrode. Calculation shows that the average increase slopes are 24 kV/cm, 18 kV/cm and 13 kV/cm for ground electrode with diameters of 12.5 mm, 40 mm, and 100 mm respectively. Since the critical lengths of streamers are the same, the breakdown voltage is higher when the diameter of the ground electrode is smaller, which is in good agreement of the breakdown voltage measurement reported in [128].

I.7.3 Effect of Gap Distance

Figure I.17 and Figure I.18 represent the relationships between the maximum stopping lengths and the applied voltage for both positive and negative streamers in needle/sphere electrode configuration at gap distances of 50 mm and 85 mm. Both the local electric field around the needle electrode and the overall electric field between electrodes are affected by changing the gap distance. The electric field will be weakened by increasing the gap distance. In the test, Gemini X is used as the sample liquid. However, the conclusions of streamer behaviours could also be found in Midel 7131 and FR3.

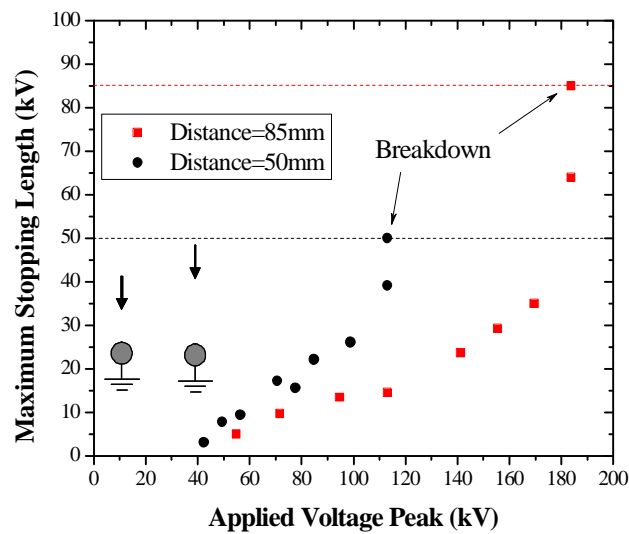


Figure I.17 Stopping length for positive streamers in Gemini X at different gaps
Point curvature = 1 μm , sphere electrode diameter = 12.5 mm, distance = 50 mm/85 mm

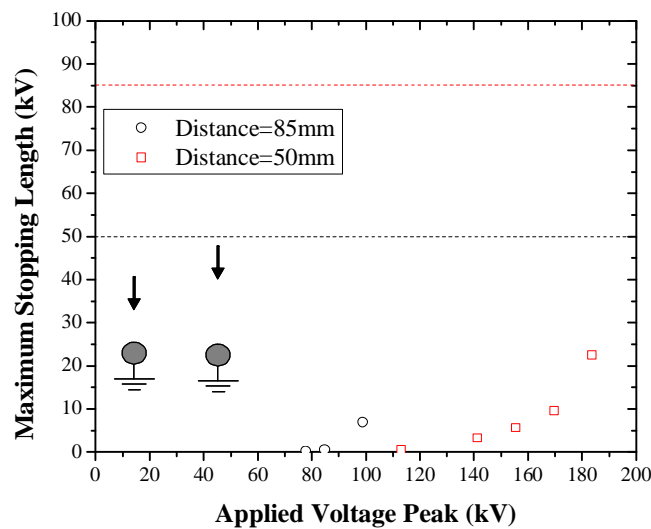


Figure I.18 Stopping length for negative streamers in Gemini X at different gaps
Point curvature = 1 μm , sphere electrode diameter = 12.5 mm, distance = 50 mm/85 mm

The result shows that the inception voltages for both positive streamers and negative streamers are different at different gap distances. When the gap distance is 50 mm, the inception voltages for positive streamers and negative streamers are 40 kV and 80 kV respectively. When the gap distance is 85 mm, the inception voltages for positive streamers and negative streamers are 15 kV and 30 kV higher than those at a 50 mm gap.

On the other hand, the maximum stopping lengths of streamers are significantly reduced when the gap distance is larger. Calculations show that the average increase slopes of positive streamers are 20 kV/cm and 30 kV/cm for 50 mm and 80 mm gaps respectively, while those for negative streamers are 30 kV/cm and 55 kV/cm for 50 mm and 80 mm gaps respectively.

I.7.4 Discussions

This section studies the effect of electrode configuration on the streamer behaviours. It is found that the streamer behaviours are influenced by the electrode arrangement by affecting the electric field distribution. Local electric field around the needle electrode influences the streamer initiation, and the overall electric field between the electrodes influences the streamer propagation.

For the streamer initiation, the local electric field is determined by the tip curvature of the needle electrode and the applied voltage. At a fixed gap distance, a lower voltage is required for the local electric field to reach the threshold value and produce the streamers when the tip curvature is smaller. Thus, the inception voltage is lower when the needle tip curvature is smaller (Figure I.13 and Figure I.14). For the same electrode, the local electric field will be reduced with the increase of the gap distance (Figure I.17 and Figure I.18). Thus, the inception voltage is higher when the gap distance is longer. [122] and [123] reported that a local electric field of 5 MV/cm should be reached in mineral oil for producing streamers. Therefore, it seems that inception voltage of a transformer liquid under specified electrode arrangement can be calculated concerning the threshold of the electric field. However, this calculation is rather difficult and imprecise, because the field calculation should take into consideration of the influence of the space charge accumulated in the bulk liquid under AC

voltage. Since an accurate measurement of the space charge in bulk liquid is nearly impossible, the calculation of the local electric field and thus the prediction of inception voltage are imprecise.

For the streamer propagations, it is determined by the overall electric field between electrodes. When the overall electric field is smaller, the streamer stopping lengths of both polarities are larger. The overall electric field is determined by the size of ground electrode (Figure I.15 and Figure I.16) and the gap distance between electrodes (Figure I.17 and Figure I.18). [26] proposed a theory to explain the dependence of streamer propagation on the overall field distributions. In the theory, the propagation of a streamer is attributed to the electric field around the streamer tips. This electric field is a combination of two fields, one being the remaining field caused by the voltage applied on the streamer tips, and the other being the overall field determined by the electrode configuration. Therefore, a higher overall field will increase the electric field at the streamer tips, promoting the streamer propagation. The streamer will propagate to a longer length until the streamer tip field reduces below a critical value, due to a higher voltage drop in longer streamer channels.

From the above discussion, it is found that the electrode configuration affects the streamer initiation and propagation by influencing the local field and the overall field distributions. The role of the local electric field on the streamer initiation and the role the overall field on the streamer propagation are similar.

Appendix II. Test Results Used in Thesis

Table II.1 AC breakdown voltages of transformer liquids in long-term stored conditions

Sequence	Breakdown voltage (kV)			Sequence	Breakdown voltage (kV)		
	Gemini X	Midel 7131	FR3		Gemini X	Midel 7131	FR3
1	37.9	45.8	42.2	21	42.8	42.7	39.8
2	37.7	45.1	48.4	22	36.4	40.8	47.1
3	26.9	38.9	35.6	23	29.2	39.0	33.6
4	32.5	46.6	40.2	24	38.3	46.0	35.3
5	41.0	44.4	45.2	25	37.7	43.0	35.3
6	46.8	27.9	49.3	26	31.1	39.4	30.1
7	37.9	36.9	25.6	27	29.2	40.2	39.1
8	25.7	44.3	45.5	28	23.7	32.6	45.4
9	33.7	39.8	38.8	29	24.5	43.2	39.5
10	25.9	45.5	34.7	30	40.6	44.4	45.2
11	40.5	40.4	34.7	31	42.2	41.1	47.7
12	39.0	43.1	40.3	32	42.4	36.9	49.9
13	37.3	39.8	47.5	33	48.9	45.5	38.3
14	27.9	48.0	36.3	34	34.3	43.6	30.8
15	36.8	43.8	45.5	35	36.3	43.8	44.2
16	37.5	43.2	43.9	36	43.2	46.4	45.1
17	41.9	40.6	44.2	37	35.0	43.6	34.9
18	34.4	45.0	34.9	38	47.8	44.5	34.6
19	35.5	41.5	42.9	39	27.8	42.9	36.2
20	39.8	35.2	37.5	40	31.7	39.8	47.6

*The results in this table provide additional information in order to compare the breakdown voltages of long-term stored oils and well-processed oils.

Table II.2 AC breakdown voltages of transformer liquids in well-processed conditions

Sequence	Breakdown voltage (kV)			Sequence	Breakdown voltage (kV)		
	Gemini X	Midel 7131	FR3		Gemini X	Midel 7131	FR3
1	45.5	48.4	40.2	21	51.8	48.0	44.6
2	45.1	42.9	50.7	22	51.6	45.2	41.6
3	49.5	46.2	42.2	23	51.5	50.9	45.6
4	47.6	46.2	45.8	24	44.4	45.2	39.9
5	46.0	36.4	36.8	25	61.5	45.2	39.7
6	48.6	41.3	47.5	26	43.8	46.2	50.5
7	46.6	36.4	35.9	27	48.6	41.6	45.2
8	46.4	50.1	41.6	28	46.9	46.3	49.3
9	42.4	43.5	36.5	29	51.2	50.3	49.5
10	40.2	45.2	41.2	30	50.1	48.4	47.8
11	46.5	46.2	51.3	31	49.1	41.1	47.0

Appendix II. Test Results Used in Thesis

12	45.5	37.2	32.5	32	41.2	46.4	44.6
13	50.1	48.4	53.1	33	45.6	46.2	47.8
14	51.1	46.2	42.1	34	49.5	50.3	51.0
15	47.3	42.9	45.6	35	35.8	41.3	41.1
16	48.6	38.3	38.8	36	47.9	41.6	48.8
17	42.0	46.4	44.6	37	52.7	41.1	38.8
18	56.2	49.9	43.8	38	48.2	42.5	45.6
19	48.9	48.1	41.4	39	44.7	39.8	44.7
20	51.9	48.0	49.6	40	50.2	41.8	48.3

*The results in this table correspond to Figure 3.1, Figure 3.2 and Figure 3.3.

Table II.3 Parameters of AC breakdown strengths of mineral oil and esters

	New oil			Processed oil		
	Gemini X	Midel7131	FR3	Gemini X	Midel7131	FR3
Mean BDV (kV)	36.0	41.6	40.5	47.7	45.1	44.5
Lowest BDV (kV)	23.8	27.9	25.6	35.8	36.2	35.0
Highest BDV (kV)	48.9	48.0	49.9	58.2	53.3	53.1
Standard deviation (kV)	6.3	4.5	5.8	4.1	4.3	4.56
Coefficient (%)	17.5	10.5	14.3	8.6	9.7	10.3

*BDV=Breakdown voltage.

*The results in this table correspond to Figure 3.4.

Table II.4 500 breakdown voltage tests of transformer liquids to verify withstand voltage

Sequence	Gemini X (kV)	Sequence	Midel 7131(kV)	Sequence	FR3 (kV)
1	>34.6	1	>31.4	1	>30.2
...	>34.6	...	>31.4	...	>30.2
363	>34.6	19	>31.4	8	>30.2
364	15.3	20	27.3	9	22.3
365	16.0	21	28.1	10	24.6
366	>34.6	22	28.2	11	>30.2
367	>34.6	22	>31.4	12	>30.2
368	27.0	...	>31.4	13	>30.2
369	>34.6	500	>31.4	14	26.9
370	30.9			15	>30.2
371	>34.6			...	>30.2
372	>34.6			420	>30.2
373	>34.6			421	24.2
374	>34.6			422	>30.2
375	27.8			423	>30.2
376	>34.6			424	>30.2
377	>34.6			425	>30.2
378	>34.6			426	26.0
379	31.2			427	>30.2
380	>34.6			...	>30.2

Appendix II. Test Results Used in Thesis

381	>34.6				500	>30.2
382	25.1					
383	>34.6					
...	>34.6					
500	>34.6					

*The results in this table correspond to Figure 3.9, Figure 3.10 and Figure 3.11.

Table II.5 Parameters of cellulose particle effect on liquid breakdown voltages

Gemini X	Particle Content (>5 μ m)	312	700	3056	15220	2174200	641300		
	Mean BDV (kV)	47.2	41.7	33.7	27.9	22.4	22.1		
	Standard deviation (kV)	3.3	7.3	4.8	3.9	3.3	3.7		
	Highest BDV (kV)	54.3	55.5	40.8	35.3	32.0	30.0		
	lowest BDV (kV)	39.3	28.9	20.9	18.9	15.6	15.1		
Midel 7131	Particle Content (>5 μ m)	350	536	9177	18300	36600	226425	1132125	4528500
	Mean BDV (kV)	45.0	42.0	34.0	35.6	35.5	33.1	32.3	29.4
	Standard deviation (kV)	4.3	3.6	6.3	3.9	6.9	3.5	2.7	2.8
	Highest BDV (kV)	53.3	47.8	42.0	41.9	43.6	38.3	36.8	31.0
	lowest BDV (kV)	36.2	33.3	21.3	27.9	20.0	23.4	26.3	15.7
FR3	Particle Content (>5 μ m)	320	3170	18637	87960	1569700			
	Mean BDV (kV)	44.5	43.7	40.3	39.1	33.9			
	Standard deviation (kV)	4.6	4.2	3.3	5.7	4.4			
	Highest BDV (kV)	53.1	53.5	47.0	48.6	41.1			
	lowest BDV (kV)	35.0	34.2	33.7	25.2	23.7			

*The results in this table correspond to Figure 3.28.

Table II.6 Parameters of copper particle effect on liquid breakdown voltages

Gemini X	Particle Content (>5 μ m)	470	2543	3930	4503		
	Mean BDV (kV)	47.7	22.0	17.6	14.4		
	Standard deviation (kV)	4.1	3.3	2.6	2.3		
	Highest BDV (kV)	58.2	30.7	22.9	19.3		
	lowest BDV (kV)	35.8	14.1	12.1	9.8		
Midel 7131	Particle Content (>5 μ m)	350	2637	5987	12043	26110	48243
	Mean BDV (kV)	46.1	36.2	23.3	19.0	17.7	15.0
	Standard deviation (kV)	4.9	6.8	5.9	3.9	2.9	3.3
	Highest BDV (kV)	53.5	50.3	41.2	32.4	25.0	20.4
	lowest BDV (kV)	36.2	20.6	14.2	11.3	9.1	7.3
FR3	Particle Content (>5 μ m)	320	2510	5147	8660	14115	23963
	Mean BDV (kV)	44.5	38.0	31.8	26.6	23.1	21.0
	Standard deviation (kV)	4.6	5.0	4.5	2.9	2.4	1.9
	Highest BDV (kV)	53.1	48.1	42.1	34.2	28.3	26.4
	lowest BDV (kV)	35.0	23.7	18.7	18.3	17.7	16.9

*The results in this table correspond to Figure 3.29.

Appendix II. Test Results Used in Thesis

Table II.7 Threshold voltages of particle motion in transformer liquids

Distance to centre (mm)		1.5			1			0.5			0		
Threshold Voltage (kV)	Gemini X	5.8	5.9	5.8	6.1	5.9	6.2	9.2	8.8	9.1	10.9	10.6	10.7
	Midel 7131	4.7	4.5	4.7	6.8	6.9	6.8	8.8	8.9	8.9	11.2	11.1	10.6
	FR3	5.0	4.9	4.8	6.5	6.3	6.2	9.6	9.6	9.7	10.4	10.9	10.9

*The results in this table correspond to Figure 3.23.

Table II.8 Particle motion (distance from electrode (mm)) in transformer liquids at 20 kV

Frame	Gemini X	Frame	Gemini X	Frame	Midel7131	Frame	FR3
0	0.33	108	2.00	0	0.12	0	0.37
4	1.33	111	1.33	5	0.84	5	0.75
6	2.00	114	0.00	10	1.44	10	1.87
9	3.33	117	0.00	15	2.89	15	3.37
11	4.00	119	0.20	20	4.21	20	4.12
13	5.00	121	0.66	25	5.18	25	4.50
16	6.66	124	1.33	30	5.54	30	4.12
19	7.33	127	2.33	35	5.18	35	3.00
23	7.33	130	3.66	40	3.90	40	1.50
27	6.66	131	5.66	45	2.53	45	0.37
29	6.00	138	7.66	50	1.44	50	0.00
31	4.66	142	8.50	55	0.84	55	0.00
34	3.33	144	8.50	60	0.48	60	0.00
37	2.00	146	8.50	65	0.84	65	0.37
39	1.00	151	8.50	70	1.32	70	1.12
40	0.20	155	8.00	75	2.28	75	2.25
41	0.00	159	6.66	80	3.61	80	3.37
44	0.00	164	4.66	85	4.33	85	3.75
55	0.00	168	3.33	90	4.69	90	3.00
58	0.66	172	2.33	95	3.85	95	1.50
62	1.33	176	2.00	100	2.89	100	0.00
65	2.33	182	2.66	105	1.80	105	0.37
68	3.66	185	3.33	110	0.48	110	0.00
70	4.66	190	5.33	115	0.00	115	0.00
72	6.00			120	0.00	120	0.37
74	7.33			125	0.00	125	0.75
78	8.00			130	0.36	130	1.87
83	8.50			135	1.08	135	3.37
86	8.50			140	1.68	140	4.12
87	8.50			145	1.92	145	4.50
93	8.00			150	1.68	150	4.12
97	6.66			155	1.32	155	3.37
101	4.66			160	0.00	160	1.87
105	3.00			165	0.48		

*The results in this table correspond to Figure 3.25.

Appendix II. Test Results Used in Thesis

Table II.9 Swing voltages of particle motion in transformer liquids

Sequence		1	2	3	4	5	6	7	8	9	10
Swing Voltage (kV)	Gemini X	21.1	20.9	20.7	24.0	23.8	24.3	22.0	21.9	20.1	21.0
	Midel 7131	26.2	25.5	24.8	25.3	25.7	25.3	26.2	25.9	25.9	25.4
	FR3	25.0	25.3	24.7	24.3	24.5	24.7	25.4	25.2	24.6	25.3

*The results in this table correspond to Figure 3.26.

Table II.10 Breakdown voltages of particle motion in transformer liquids

Sequence		1	2	3	4	5	6	7	8	9	10
BDV (kV)	Gemini X	21.1	20.9	20.7	24.0	23.8	28.4	22.0	21.9	20.1	21.0
	Midel 7131	40.1	40.4	39.9	37.1	39.6	35.5	37.9	39.1	40.2	40.6
	FR3	35.4	35.9	34.4	34.2	36.1	35.3	34.7	33.9	30.2	36.6

*The results in this table correspond to Figure 2.27.

Table II.11 Parameters of water effect on breakdown voltages of transformer liquids

Gemini X	Absolute water content (ppm)	1.7	12.1	22.6	36.8	45.6	53.9			
	Relative water content (%)	3	22	41	67	83	98			
	Mean BDV (kV)	47	45	39	24	16	14			
	Standard deviation (kV)	3.0	3.2	4.4	3.5	3.6	3.7			
Midel 7131	Absolute water content (ppm)	78	156	286	338	650	806	988	1248	2080
	Relative water content (%)	3	6	11	13	25	31	38	48	80
	Mean BDV (kV)	45	42	43	39	38	38	25	24	8
	Standard deviation (kV)	3.7	4.4	5.2	6.4	5.8	7.5	5.7	5.0	2.8
FR3	Absolute water content (ppm)	33	66	132	220	264	330	484	638	781
	Relative water content (%)	3	6	12	20	24	30	44	58	71
	Mean BDV (kV)	44	38	40	42	38	30	14	11	10
	Standard deviation (kV)	5.3	9.1	10.7	10.8	10.6	8.4	3	2.1	1.4

*The results in this table correspond to Figure 3.28 and Figure 3.29.

Table II.12 Parameters of water effect for clean and relatively dirty Gemini X

Clean Gemini X	Relative water content (%)	3	22	26	41	43	67	83	98
	Mean BDV (kV)	47	45	44	39	38	24	16	14
	Standard deviation (kV)	3.0	3.2	5.8	4.4	5.1	3.5	3.6	3.7
Dirty Gemini X	Relative water content (%)	5	10	12	25	31	35	36	51
	Mean BDV (kV)	39	29	22	20	15	17	16	7
	Standard deviation (kV)	4.9	4.5	4.0	4.1	3.8	4.2	4.9	2.9

*The results in this table correspond to Figure 3.30.

Table II.13 Breakdown voltages of transformer liquids for various electrodes

Sphere electrode, ESA = 2.17 mm ²							
Sequence	Breakdown voltage (kV)			Sequence	Breakdown voltage (kV)		
	Gemini X	Midel7131	FR3		Gemini X	Midel7131	FR3
1	51.5	51.4	46.2	21	54.6	39.3	52.2
2	52.5	49.3	42.5	22	46.9	54.1	53.0
3	52.7	47.2	42.3	23	51.6	49.3	51.3

Appendix II. Test Results Used in Thesis

4	52.2	42.5	47.4	24	45.2	46.9	53.5
5	52.0	51.0	41.7	25	48.3	42.6	52.7
6	50.0	55.6	47.6	26	48.9	45.9	47.8
7	54.9	48.4	51.6	27	52.4	48.0	42.1
8	56.5	47.9	46.0	28	54.3	48.3	50.3
9	51.3	61.1	44.5	29	54.4	56.5	51.2
10	45.8	43.9	44.4	30	54.0	48.4	38.1
11	43.6	42.4	36.2	31	51.7	49.8	58.2
12	53.2	51.5	42.5	32	46.1	51.1	45.8
13	54.3	51.9	43.2	33	51.0	38.4	46.6
14	45.7	42.8	39.8	34	46.9	41.5	44.8
15	53.5	40.8	29.6	35	51.3	32.7	49.9
16	49.4	27.2	47.1	36	51.3	46.1	51.1
17	41.6	47.8	45.2	37	51.4	61.1	48.4
18	49.2	36.0	41.9	38	51.8	45.3	50.1
19	45.8	48.2	47.9	39	44.9	39.7	44.4
20	57.8	40.1	46.8	40	58.3	29.2	36.5
VDE electrode, ESA = 5.22 mm ² (in ascending sequence)							
Sequence	Breakdown voltage (kV)			Sequence	Breakdown voltage (kV)		
	Gemini X	Midel7131	FR3		Gemini X	Midel7131	FR3
1	35.8	33.0	32.5	21	48.9	45.3	44.7
2	40.2	37.2	35.9	22	49.1	45.8	45.2
3	41.2	38.3	36.5	23	49.2	46.2	45.6
4	42.0	38.8	36.8	24	49.5	46.2	45.6
5	42.4	39.4	38.8	25	49.5	46.2	45.6
6	43.8	39.8	38.8	26	50.1	46.3	45.7
7	44.4	41.1	39.7	27	50.2	46.4	45.8
8	44.7	41.3	39.9	28	51.1	47.6	47.0
9	44.7	41.7	40.2	29	51.2	48.1	47.5
10	45.1	41.8	41.1	30	51.5	48.4	47.8
11	45.5	42.3	41.2	31	51.6	49.0	48.3
12	45.5	42.6	41.4	32	51.8	48.0	48.8
13	45.6	42.8	41.6	33	51.9	49.2	49.3
14	46.0	43.0	41.6	34	52.6	49.5	49.5
15	46.4	43.1	42.1	35	52.7	49.9	49.6
16	46.5	43.5	42.2	36	52.8	50.2	50.5
17	46.6	44.5	43.8	37	54.8	50.4	50.7
18	46.9	45.2	44.6	38	54.9	50.7	51.0
19	47.3	45.2	44.6	39	56.2	50.9	51.3
20	47.6	45.2	44.6	40	61.5	53.3	53.1
Flat electrode, diameter = 20 mm, ESA = 283 mm ² (in ascending sequence)							
Sequence	Breakdown voltage (kV)			Sequence	Breakdown voltage (kV)		
	Gemini X	Midel7131	FR3		Gemini X	Midel7131	FR3
1	31.1	23.3	26.5	21	42.8	33.5	38.0

Appendix II. Test Results Used in Thesis

2	32.1	23.6	27.6	22	43.0	33.8	38.0
3	33.2	26.0	29.7	23	43.0	33.8	38.5
4	35.1	27.8	31.1	24	43.6	34.0	38.9
5	36.5	28.2	31.8	25	43.9	34.0	39.3
6	37.9	28.6	32.1	26	44.1	34.2	39.6
7	38.7	29.4	33.6	27	44.4	34.5	40.2
8	39.2	30.3	33.7	28	44.4	34.5	40.3
9	39.6	30.4	34.1	29	44.9	34.8	
10	39.8	30.5	34.2	30	44.9	35.0	
11	40.0	31.0	34.5	31	44.9	35.1	
12	40.6	31.8	35.9	32	45.5	35.3	
13	40.6	31.9	36.2	33	45.5	35.8	
14	40.6	32.3	36.4	34	45.5	36.4	
15	40.9	32.6	36.5	35	46.0	36.9	
16	41.1	32.7	36.5	36	46.0	38.5	
17	41.7	32.9	36.5	37	46.3	39.8	
18	41.9	33.0	36.9	38	46.6	39.9	
19	41.9	33.4	37.1	39	47.1	40.2	
20	42.5	33.5	37.2	40	47.7	41.6	

Flat electrode, diameter = 30 mm, ESA = 660 mm² (in ascending sequence)

Sequence	Breakdown voltage (kV)			Sequence	Breakdown voltage (kV)		
	Gemini X	Midel7131	FR3		Gemini X	Midel7131	FR3
1	30.3	24.2	24.5	21	39.1	36.2	34.5
2	34.2	25.8	24.6	22	39.3	37.4	34.9
3	35.5	25.8	25.5	23	39.5	37.4	34.9
4	36.3	30.2	29.9	24	39.5	37.7	35.1
5	36.4	30.4	30.1	25	39.6	37.8	35.2
6	36.5	31.1	30.3	26	39.7	37.8	35.3
7	36.6	31.6	30.4	27	39.7	38.1	35.8
8	36.6	32.0	31.6	28	39.8	38.3	35.9
9	37.2	32.9	32.1	29	39.9	39.0	36.2
10	37.3	33.0	32.1	30	40.0		36.6
11	37.6	33.1	32.4	31	40.3		36.7
12	38.0	33.8	32.4	32	40.3		36.8
13	38.2	34.2	32.5	33	40.4		36.9
14	38.3	34.6	32.8	34	41.0		37.4
15	38.4	34.7	33.0	35	41.1		37.5
16	38.4	35.5	33.1	36	41.3		37.6
17	38.5	35.6	33.3	37	41.8		37.9
18	38.7	35.7	33.5	38	42.3		38.0
19	38.8	35.8	33.6	39	43.2		38.0
20	39.0	35.9	34.2	40	43.3		39.2

Flat electrode, diameter = 40 mm, ESA = 1194 mm² (in ascending sequence)

Sequence	Breakdown voltage (kV)			Sequence	Breakdown voltage (kV)		
----------	------------------------	--	--	----------	------------------------	--	--

Appendix II. Test Results Used in Thesis

	Gemini X	Midel7131	FR3		Gemini X	Midel7131	FR3
1	28.6	23.6	27.4	21	36.8	33.3	
2	30.4	24.2	28.1	22	37.6	33.4	
3	31.4	25.2	30.4	23	37.6	33.7	
4	31.4	25.6	31.2	24	37.9	33.9	
5	32.0	25.8	31.8	25	38.1	34.0	
6	32.4	26.3	33.0	26	38.2	35.0	
7	32.5	26.3	33.2	27	38.6	35.7	
8	33.1	26.3	33.5	28	39.0	35.9	
9	33.3	26.4	34.1	29	39.2	36.4	
10	33.5	26.5	34.5	30	39.2	36.4	
11	33.6	26.9	34.8	31	39.3	36.5	
12	33.8	27.5	34.9	32	39.5	37.2	
13	33.9	27.5	35.0	33	39.5	37.9	
14	35.2	28.0	35.2	34	39.7	38.0	
15	35.7	29.3	35.7	35	40.2	39.0	
16	36.0	29.9	36.5	36	40.4		
17	36.3	31.4	36.6	37	40.5		
18	36.3	31.6	37.8	38	40.9		
19	36.7	32.0		39	41.5		
20	36.7	33.2		40	43.5		

Flat electrode, diameter = 50 mm, ESA = 1885 mm² (in ascending sequence)

Sequence	Breakdown voltage (kV)			Sequence	Breakdown voltage (kV)		
	Gemini X	Midel7131	FR3		Gemini X	Midel7131	FR3
1	26.7	15.8	20.9	21	35.2	25.9	
2	28.2	17.9	25.8	22	35.2	26.4	
3	29.2	18.7	26.9	23	35.2	26.4	
4	31.1	19.3	28.4	24	36.2	27.3	
5	31.5	19.6	28.6	25	36.2	28.3	
6	31.8	20.0	29.2	26	36.3	28.4	
7	32.2	20.1	29.3	27	36.3	28.7	
8	32.9	20.1	29.6	28	36.7	29.0	
9	33.2	20.2	30.2	29	36.7	29.2	
10	33.2	21.5	30.2	30	36.7	29.5	
11	33.7	22.9	30.3	31	36.8	29.9	
12	33.7	23.2	30.4	32	37.2	29.9	
13	33.7	23.8	30.5	33	37.3	29.9	
14	34.1	23.9	31.8	34	37.3	31.0	
15	34.4	24.2	35.0	35	37.4	31.4	
16	34.6	24.9	35.0	36	38.5	32.6	
17	34.6	25.2	35.0	37	38.9	33.1	
18	34.7	25.2		38	39.4	33.2	
19	34.7	25.6		39	39.4	33.2	
20	34.8	25.6		40	41.7	36.0	

Appendix II. Test Results Used in Thesis

Flat electrode, diameter = 50 mm, ESA = 1885 mm ² (in ascending sequence)							
Sequence	Breakdown voltage (kV)			Sequence	Breakdown voltage (kV)		
	Gemini X	Midel7131	FR3		Gemini X	Midel7131	FR3
1	33.4	16.2	20.8	11	32.5	25.4	28.1
2	31.0	16.4	21.1	12	32.4	25.8	28.1
3	29.0	20.1	21.3	13	34.3	25.8	28.2
4	26.7	23.4	21.8	14	33.9	26.2	28.3
5	32.2	23.5	22.0	15	29.6	26.9	28.4
6	32.3	23.7	23.5	16	32.8	26.9	28.5
7	27.2	23.9	24.8	17	27.5	27.2	28.7
8	32.5	24.2	26.6	18	32.9	27.3	28.8
9	28.1	24.5	26.7	19	33.0	27.5	28.9
10	26.3	24.6	27.5	20	21.2	28.9	29.2

*The results in this table correspond to Figure 3.33.

Table II.14 PD signals recorded in Gemini X at various ramping rates

Ramping rate = 2.0 kV/s									
Sequence	1	2							
Voltage (kV)	53.12	54.44							
PD amplitude (pC)	625	666							
Ramping rate = 1.0 kV/s									
Sequence	1	2	3	4	5	6	7	8	9
Voltage (kV)	38.68	39.5	42.2	49.08	49.54	51.02	51.96	54.96	55.86
PD amplitude (pC)	216	307	382	>666	>666	>666	>666	>666	>666
Ramping rate = 0.5 kV/s									
Sequence	1	2	3	4	5	6	7	8	9
Voltage (kV)	36.77	41.99	54.62	52.57	53.93	54.68	58.55	59.63	
PD amplitude (pC)	306	404	>666	>666	>666	578	>666	>666	
Ramping rate = 0.25 kV/s									
Sequence	1	2	3	4	5	6	7	8	9
Voltage (kV)	34.48	39.44	43.09	45.76	46.06	47.65	48.145	48.88	49.91
PD amplitude (pC)	186	207	516	>666	541	279	>666	>666	>666
Sequence	10	11	12	13	14	15	16	17	18
Voltage (kV)	49.29	49.37	49.45	49.53	49.61	50.15	51.02	51.05	51.75
PD amplitude (pC)	>666	560	>666	>666	>666	>666	>666	>666	>666
Sequence	19	20	21	22	23	24	25	26	27
Voltage (kV)	51.91	52.15	52.27	52.27	53.14	53.22	53.80	54.92	55.3
PD amplitude (pC)	>666	>666	556	552	>666	466	665	413	>666
Sequence	28	29	30	31	32	33	34	35	36
Voltage (kV)	55.42	55.47	55.82	55.88	56.68	57.13	57.21	57.33	58.38
PD amplitude (pC)	559	>666	>666	>666	>666	665	>666	>666	>666
Sequence	37	38	39	40	41	42	43		
Voltage (kV)	58.47	58.47	58.63	58.71	58.74	59.04	59.19		
PD amplitude (pC)	>666	>666	>666	530	>666	>666	>666		

Appendix II. Test Results Used in Thesis

*The results in this table correspond to Figure 4.3.

Table II.15 Maximum PD amplitudes with applied voltage in transformer liquids

Voltage (kV)	Maximum PD amplitude (pC)			Voltage (kV)	Maximum PD amplitude (pC)		
	Gemini X	Midel7131	FR3		Gemini X	Midel7131	FR3
22	0	78.26	0	29	313.28	319.04	157.99
23	80.32	133.44	0	30	353.89	361.09	211.94
24	141.93	141.93	60.97	31	-	-	233.95
25	174.01	166.81	68.42	32	-	-	231.33
26	219.44	190.17	113.94	33	-	-	271.26
27	260.51	218.05	141.47	34	-	-	322.69
28	292.56	241.84	168.36	35	-	-	343.24

*The results in this table correspond to Figure 4.5.

Table II.16 PDIV test results using IEC 61294 test procedure

Sequence	1	2	3	4	5	6	7	8	9	10	
PDIV (kV)	Gemini X	36.4	34.5	39.5	38.6	38.7	36.6	38.0	37.2	38.4	38.7
	Midel 7131	28.7	28.1	28.7	26.7	28.4	28.9	28.8	28.3	28.6	28.7
	FR3	36.1	33.5	34.7	34.0	35.8	34.6	35.3	34.5	33.6	33.7

*The results in this table correspond to Table 4.2.

Table II.17 PD repetition rates with applied voltage in transformer liquids around PDIV

Voltage (kV)	PD repetition rate (number/minute)			Voltage (kV)	PD repetition rate (number/minute)		
	Gemini X	Midel7131	FR3		Gemini X	Midel7131	FR3
16	0	0.5	0	24	8.5	30	25
17	0	1.5	0.15	25	-	59.5	45
18	0	2	0.5	26	14	-	65
19	0.3	3	1.5	27	-	73	168
20	0.75	3	3.5	28	32	96	482
21	-	9.5	4.5	29	52	146	810
22	4	23	6.5	30	61	186	
23	-	27.5	17				

*The results in this table correspond to Figure 4.6.

Table II.18 Maximum PD of transformer liquids at overstressed voltages

Voltage (kV)	Maximum PD amplitude (pC)			Voltage (kV)	Maximum PD amplitude (pC)		
	Gemini X	Midel7131	FR3		Gemini X	Midel7131	FR3
21	0	50	0	32	378.16	-	-
22	74.75	84.49	0	33	407.19	-	-
23	85.51	123.47	63	34	-	-	-
24	76.21	128.11	81	35	473.97	646.2	430
25	76.32	138.56	98	40	690	947	585
26	136.49	161.68	106	45	887.76	1027.1	656

Appendix II. Test Results Used in Thesis

27	-	255.61	169	50	1098.52	1275	884
28	223.54	310.39	171	55	1372.64	1840.88	1329
29	239.36	312.27	186	60	1765.41	2473	2032
30	266.38	415.18	261	65	2372.34	3891.4	2857
31	-	475.8	-	70	2759.54	6781	3721

*The results in this table correspond to Figure 4.7.

Table II.19 PD repetition rates of transformer liquids at overstressed voltages

Voltage (kV)	PD repetition rate (number/minute)			Voltage (kV)	PD repetition rate (number/minute)		
	Gemini X	Midel7131	FR3		Gemini X	Midel7131	FR3
21	0	3	0	32	52	-	-
22	37	6	0	33	61	-	-
23	12	12	168	34	-	-	-
24	5	23	482	35	35	614	2358
25	7	92	810	40	115	1178	5441
26	10	120	832	45	171	2132	8367
27	-	73	1448	50	305	2862	
28	10	96	1819	55	457	3463	
29	25	146	2201	60	568	4232	
30	44	186	1901	65	871	6400	
31	-	288	-	70	938	8058	

*The results in this table correspond to Figure 4.8.

Table II.20 PD equivalent currents of transformer liquids at overstressed voltage

Voltage (kV)	Equivalent current (μA)			Voltage (kV)	Equivalent current (μA)		
	Gemini X	Midel7131	FR3		Gemini X	Midel7131	FR3
21	0	4.94E-06	0	32	2.07E-04	-	-
22	1.02E-05	4.43E-06	0	33	2.58E-04	-	-
23	6.07E-06	1.11E-05	1.10E-04	34	-	-	-
24	4.55E-06	2.62E-05	2.34E-04	35	1.82E-04	0.00325	0.00613
25	6.50E-06	5.96E-05	3.61E-04	40	8.49E-04	0.00793	0.0178
26	1.17E-05	1.20E-04	4.72E-04	45	0.00162	0.01617	0.03029
27	-	1.85E-04	0.00119	50	0.00349	0.02586	0.0353
28	1.94E-05	2.65E-04	0.00171	55	0.0064	0.03302	0.04086
29	6.95E-05	4.28E-04	0.00233	60	0.00956	0.04326	0.05212
30	1.13E-04	6.23E-04	0.00277	65	0.01499	0.06873	0.06599
31	-	0.00112	-	70	0.02756	0.11383	0.11056

*The results in this table correspond to Figure 4.10.

Appendix II. Test Results Used in Thesis

Table II.21 PD equivalent powers of transformer liquids at overstressed voltage

Voltage (kV)	Equivalent power (W)			Voltage (kV)	Equivalent current (W)		
	Gemini X	Midel7131	FR3		Gemini X	Midel7131	FR3
21	0	1.36E-07	0	32	8.90E-06	-	-
22	2.05E-07	1.20E-07	0	33	1.13E-05	-	-
23	1.67E-07	3.46E-07	3.13E-06	34	-	-	-
24	1.33E-07	8.45E-07	7.43E-06	35	8.38E-06	1.53E-04	2.75E-04
25	2.18E-08	1.67E-06	1.42E-05	40	4.38E-05	4.22E-04	8.69E-04
26	4.17E-07	3.70E-06	1.60E-05	45	9.37E-05	9.53E-04	0.00159
27	-	6.73E-06	4.20E-05	50	2.21E-04	0.00167	0.00205
28	7.54E-07	1.00E-05	6.28E-05	55	4.39E-04	0.00225	0.00257
29	2.75E-06	1.66E-05	8.82E-06	60	7.06E-04	0.0031	0.00354
30	4.58E-06	2.51E-05	1.08E-04	65	0.00116	0.00524	0.00484
31	-	4.67E-05	-	70	0.00225	0.00916	0.00866

*The results in this table correspond to Figure 4.11.

Table II.22 Streamer repetition rates of streamers in Midel 7131 under various needle electrodes

Applied Voltage (kV)		16	17	18	19	20	21	22	23	24	25	29
Repetition rate (number/minute)	1 μm	0.5	1.5	2	3	3	9.5	23	27.5	30	29.5	-
	2 μm	0	0	0.5	1.5	3.5	4.5	6.5	8.5	5.5	11.5	33

*The results in this table correspond to Figure 5.8.

Table II.23 Streamer stopping lengths in Gemini X with instantaneous voltage at 80 kV

Positive streamers		Negative streamers		Positive streamers		Negative streamers	
Voltage (kV)	Stopping length (mm)						
107.4	50.0	-63.1	2.6	66.1	18.5	-95.5	0.7
110.3	50.0	-111.7	2.3	91.2	18.2	-112.2	0.7
111.8	50.0	-93.3	2.3	112.2	18.2	-31.0	0.7
107.4	39.1	-112.9	2.0	112.2	17.5	-50.9	0.7
107.7	37.4	-54.0	2.0	74.4	17.5	-20.7	0.7
113.1	36.4	-86.8	2.0	106.3	16.6	-57.1	0.7
112.2	35.4	-91.5	1.7	111.0	15.9	-86.8	0.7
111.1	34.4	-112.2	1.7	79.6	15.6	-85.2	0.4
100.5	32.1	-100.5	1.7	107.4	15.6	-93.6	0.3
111.6	30.8	-112.9	1.3	50.9	11.3	-51.4	0.3
112.6	28.5	-109.6	1.3	112.2	10.9	-63.6	0.3
112.6	27.5	-86.8	1.3	93.6	22.8	-113.1	0.3
95.5	26.8	-89.1	1.3	95.5	26.8	-103.8	0.3
103.6	26.8	-100.8	1.0	97.4	22.5	-80.0	0.3
84.9	26.5	-111.7	1.0	100.5	32.1	-97.4	0.3

Appendix II. Test Results Used in Thesis

109.6	25.8	-106.4	1.0	94.1	9.2	-113.1	0.3
93.3	25.8	-108.6	1.0	96.2	13.8	-103.8	0.3
113.1	25.2	-110.4	1.0	106.3	16.6	-82.5	0.3
109.4	25.2	-63.1	1.0	106.4	19.9	-102.4	0.3
110.5	24.8	-71.7	1.0	107.4	15.6	-84.9	0.3
111.7	23.8	-82.1	1.0	74.4	17.5	-97.4	0.3
111.7	23.5	-77.4	0.7	79.6	15.6	-100.8	0.3
93.6	22.8	-112.6	0.7	89.4	21.5	-113.1	0.3
103.8	22.8	-87.2	0.7	91.2	18.2	-102.4	0.3
74.4	22.8	-95.5	0.7			-41.1	0.3
109.7	22.8	-111.7	0.7			-74.4	0.3
97.4	22.5	-112.6	0.7			-112.3	0.2
89.4	21.5	-111.1	0.7			-112.6	0.2
106.4	19.9	-111.7	0.7			-105.0	0.2
111.7	19.2	-105.2	0.7			-104.0	0.1
60.2	18.9	-105.2	0.7			-68.9	0.1

*The results in this table correspond to Figure 5.15.

Table II.24 Propagation of positive streamers in transformer liquids

Gemini X		Midel 7131		FR3	
Propagation duration (μs)	Stopping length (mm)	Propagation duration (μs)	Stopping length (mm)	Propagation duration (μs)	Stopping length (mm)
3.0	2.2	2.0	1.5	2.7	2.1
4.6	7.8	1.7	3.3	7.0	9.0
4.6	2.2	7.3	11.2	6.7	8.8
4.3	4.3	6.8	7.9	5.2	5.5
5.0	6.8	4.8	7.8	6.6	10.2
4.6	3.8	4.7	6.6	6.4	8.3
5.1	5.1	9.1	15.2	8.3	9.2
4.6	5.6	8.5	14.3	8.8	11.3
5.9	8.8	5.8	7.1	8.1	13.2
9.4	13.7	7.5	12.2		
7.8	9.3				
8.6	17.1				
10.9	13.0				
9.5	11.5				
6.3	9.5				
10.1	15.5				

*The results in this table correspond to Figure 5.18.

Appendix II. Test Results Used in Thesis

Table II.25 Propagation of negative streamers in transformer liquids

Gemini X		Midel 7131		FR3	
Propagation duration (μs)	Stopping length (mm)	Propagation duration (μs)	Stopping length (mm)	Propagation duration (μs)	Stopping length (mm)
6.5	1.2	8.0	3.8	1.8	0.7
90.7	16.0	2.3	1.3	1.6	0.6
123.4	19.7	1.6	0.5	1.4	0.5
130.0	21.8	1.5	0.9	1.7	0.9
		4.6	2.4	0.8	0.4
		3.7	1.7	2.0	1.0
		5.6	1.6	3.0	1.2
		2.9	0.3	2.9	1.2
		2.8	0.4	2.8	1.4
		4.1	0.8	2.2	0.6
		2.8	1.1	32.4	17.8
		3.7	1.3	39.7	17.0
		1.9	0.6	50.0	22.2
		3.7	1.1	29.6	11.9
		1.0	0.4	49.1	20.4
		2.5	0.8	57.3	23.3
		0.6	0.2	34.0	12.6
		2.8	1.0	60.4	23.7
		1.0	0.5	39.7	20.0
		5.0	3.0	47.1	24.4
		0.8	0.3	46.9	22.2
		1.5	0.4	28.5	13.7

*The results in this table correspond to Figure 5.19.

Table II.26 Breakdown voltages of transformer liquids with gap distance

Sequence	Breakdown voltages for Gemini X (kV)					
	2 mm	10 mm	20 mm	50 mm	75 mm	85 mm
1	12.9	37.5	45.6	88.2	132.0	141.0
2	9.9	30.6	52.7	91.3	132.3	147.5
3	14.5	37.5	52.9	90.3	136.8	134.4
4	15.6	30.6	45.6	91.3	115.0	141.0
5	16.1	30.6	46.6	87.1	125.8	141.0
6	19.9	37.5	46.6	91.3	125.8	134.4
7	16.7	30.6	45.6	85.8	125.8	145.5
8	18.8	37.5	38.7	92.7	132.3	141.0
9	16.9	38.4	45.6	87.9	138.9	141.0
10	17.2	30.6	44.6	78.5	138.9	141.0
Average	15.9	33.4	46.5	88.4	130.4	140.8
Standard deviation	2.9	3.8	4.0	4.1	7.4	4.9

Appendix II. Test Results Used in Thesis

Sequence	Breakdown voltages for Midel 7131 (kV)					
	2 mm	10 mm	20 mm	50 mm	75 mm	100 mm
1	11.7	22.5	36.6	65.3	101.9	129.9
2	11.9	25.0	36.6	71.9	115.1	125.8
3	15.2	25.5	37.3	71.9	115.1	132.3
4	18.3	25.5	36.6	71.9	108.5	134.4
5	18.1	25.5	36.6	65.3	108.5	121.3
6	11.5	25.0	35.2	73.9	101.9	127.8
7	16.5	25.0	35.2	78.1	93.3	129.9
8	18.4	25.0	36.3	65.3	106.4	129.9
9	18.5	27.7	33.6	65.3	99.9	127.1
10	17.5	24.4	36.0	69.5	104.0	127.8
Average	15.6	25.1	36.0	69.8	104.5	128.4
Standard deviation	3.1	1.3	1.1	4.5	7.1	3.5
Sequence	Breakdown voltages for FR3 (kV)					
	2 mm	10 mm	20 mm	50 mm	75 mm	100 mm
1	21.2	30.6	33.3	69.5	107.1	127.8
2	16.7	30.6	36.3	73.6	113.7	129.9
3	16.5	24.6	38.0	85.7	109.2	121.3
4	16.5	27.3	38.4	87.8	115.7	127.8
5	17.1	24.1	37.0	87.8	113.7	129.9
6	17.5	24.1	38.0	89.8	109.2	140.1
7	17.6	24.6	38.0	74.6	115.7	140.1
8	17.6	24.6	36.3	85.3	109.2	134.4
9	16.5	24.6	36.3	81.2	109.2	134.4
10	18.0	24.6	37.3	72.6	115.1	145.1
Average	17.1	25.5	37.3	82.0	114.0	133.7
Standard deviation	1.4	2.6	1.5	7.5	5.5	6.8

*The results in this table correspond to Figure 5.32.

Table II.27 Breakdown voltages with various needle electrodes in Midel 7131

Sequence	Breakdown voltages (kV) using needle with 1 μm tip curvature					
	2 mm	10 mm	20 mm	50 mm	75 mm	100 mm
1	21.2	30.6	33.3	69.5	107.1	127.8
2	16.7	30.6	36.3	73.6	113.7	129.9
3	16.5	24.6	38.0	85.7	109.2	121.3
4	16.5	27.3	38.4	87.8	115.7	127.8
5	17.1	24.1	37.0	87.8	113.7	129.9
6	17.5	24.1	38.0	89.8	109.2	140.1
7	17.6	24.6	38.0	74.6	115.7	140.1
8	17.6	24.6	36.3	85.3	109.2	134.4
9	16.5	24.6	36.3	81.2	109.2	134.4
10	18.0	24.6	37.3	72.6	115.1	145.1
Average	17.1	25.5	37.3	82.0	114.0	133.7

Appendix II. Test Results Used in Thesis

Standard deviation	1.4	2.6	1.5	7.5	5.5	6.8
Sequence	Breakdown voltages (kV) using needle with 50 μm tip curvature					
	2 mm	10 mm	20 mm	50 mm	75 mm	100 mm
1	18.2	29.2	37.6	72.6	93.3	123.6
2	24.2	21.7	36.2	64.9	107.1	125.8
3	22.8	25.9	32.8	64.9	95.4	112.7
4	21.4	21.4	36.3	64.9	102.3	125.8
5	22.8	24.1	36.3	64.9	95.4	125.8
6	22.2	23.6	36.3	72.6	98.7	112.7
7	20.6	21.7	32.8	61.8	91.4	130.2
8	19.8	23.4	37.6	72.6	102.3	125.8
9	21.9	23.3	36.2	64.9	95.4	125.8
10	19.7	24.4	36.3	72.6	107.1	123.6
Average	21.4	23.9	35.8	66.5	98.7	122.7
Standard deviation	1.8	2.3	1.8	3.4	5.8	5.7
Sequence	Breakdown voltages (kV) using needle with 700 μm tip curvature					
	2 mm	20 mm	30 mm	40 mm	50 mm	100 mm
1		59.1	78.43	90.2	79.12	129
2		59.1	80.16	73.63	80.16	121.2
3		59.1	76.36	82.38	88.1	117.05
4		59.1	73.94	80.19	79.48	117.05
5		60.1	73.59	73.63	82.59	123.27
6		66.3	59.08	80.19	80.16	125.69
7		66.3	73.59	80.19	73.59	117.05
8		59.1	72.9	71.9	81.2	118.07
9		66.3	70.5	72.59	88.2	118.09
10		59.1	71.86	90.2	81.2	125.69
Average		61.7	73.0	78.3	81.4	121.2
Standard deviation		3.5	5.7	5.9	4.3	4.4

*The results in this table correspond to Figure 5.34.

Table II.28 Probabilities of breakdowns induced by negative streamers in Midel 7131

Sequence	Breakdowns induced by which polarity streamer using needle with 1 μm tip curvature					
	2 mm	10 mm	20 mm	50 mm	75 mm	100 mm
1	P	P	P	P	P	P
2	P	P	P	P	P	P
3	N	P	P	P	P	N
4	N	P	P	P	P	P
5	P	P	P	P	P	P
6	P	P	P	P	P	P
7	N	P	P	P	P	P
8	P	P	P	P	P	P
9	P	P	P	P	P	P

Appendix II. Test Results Used in Thesis

10	p	P	P	P	P	P
Probability (%)	30	0	0	0	0	10
Sequence	Breakdowns induced by which polarity streamer using needle with 50 μm tip curvature					
	2 mm	10 mm	20 mm	50 mm	75 mm	100 mm
1	P	P	P	P	P	P
2	N	P	P	P	P	P
3	N	P	P	P	P	P
4	P	P	P	P	P	P
5	N	B	P	P	P	N
6	N	B	P	P	P	P
7	N	P	P	P	N	P
8	N	P	P	P	P	P
9	N	P	P	P	P	P
10	P	P	P	P	P	P
Probability (%)	70	20	0	0	10	10
Sequence	Breakdowns induced by which polarity streamer using needle with 700 μm tip curvature					
	2 mm	20 mm	30 mm	40 mm	50 mm	100 mm
1	N	N	N	N	P	P
2	N	N	N	P	P	P
3	N	N	N	P	N	P
4	N	P	N	P	P	P
5	N	N	P	P	P	P
6	N	N	P	P	P	P
7	N	N	P	P	P	P
8	N	N	N	P	P	P
9	N	N	N	P	P	N
10	N	N	N	P	P	P
Probability (%)	100	90	70	20	10	10

*P/N indicates breakdowns induced by positive streamers/negative streamers.

*For a restroke breakdown, the breakdown is induced by the first streamer.

*The results in this table correspond to Figure 5.35.

Table II.29 Breakdown voltages of Midel 7131 with ground electrodes

Sequence	Breakdown voltages (kV) using plane electrode with 1256 mm^2					
	2 mm	10 mm	20 mm	50 mm	75 mm	100 mm
1	15.8		36.3	57.4	92.3	109.2
2	18.5		35.2	57.7	87.9	115.1
3	18.5		30.4	58.7	88.1	115.1
4	17.8		30.9	58.7	94.0	108.5
5	18.1		31.4	52.2	88.1	121.3
6	19.3		29.8	62.5	96.4	117.1
7	18.1		32.0	62.5	96.4	115.1

Appendix II. Test Results Used in Thesis

8	18.3		32.0	63.2	91.9	115.1
9	18.3		32.0	56.7	94.0	115.1
10	18.2		34.1	64.3	93.9	121.2
Average	18.1		32.4	59.7	92.1	114.6
Standard deviation	0.9		2.1	3.7	3.4	3.8
Sequence	Breakdown voltages (kV) using plane electrode with 7853 mm ²					
	2 mm	10 mm	20 mm	50 mm	75 mm	100 mm
1	11.1	18.2	30.5	57.4	79.1	104.0
2	11.1	19.7	31.4	57.4	79.1	102.6
3	13.5	21.4	27.7	58.4	79.1	109.2
4	11.1	21.8	30.4	58.4	77.7	102.6
5	16.6	16.7	29.3	58.4	77.7	100.5
6	14.5	21.4	28.2	58.4	79.1	100.5
7	14.0	21.1	27.7	58.4	79.1	100.5
8	16.7	16.9	29.3	57.4	85.3	100.5
9	16.8	21.9	31.4	58.4	77.7	100.5
10	15.9	21.6	28.2	58.4	84.3	100.5
Average	14.1	20.1	29.4	58.1	79.8	102.2
Standard deviation	2.4	2.1	1.5	0.5	2.7	2.8

*The results in this table correspond to Figure 5.36.

Table II.30 Comparison of breakdown strengths of Gemini X using IEC 60156 and ASTM D1816

Breakdown sequence	1	2	3	4	5	6	7	8	9	10
IEC 60156 (kV)	28.6	22.1	22.9	22.1	21.3	15.9	-	-	-	-
ASTM D1816 (kV)	22.7	17.4	26.9	18.7	19.4	17.4	17.7	23.2	23	23.3

*The results in this table correspond to Figure I.2.

Table II.31 Particle contents of stored FR3 oil after each filtration cycle

Particle diameter (µm)	Stored oil	1 st cycle	2 nd cycle	3 rd cycle	4 th cycle	5 th cycle
1	250807	12302	853	1103.3	565.5	700
2	15117	1823	550	700	409	500
5	6976.7	1102	523	426.66	540	420
15	130	112	90	40	65	45
25	80	65	50	10	5	5
50	9	7	6.666	0	0	0
100	1	0	0	0	0	0
200	0	0	0	0	0	0

*The results in this table correspond to Figure I.7.

Table II.32 Preparation of electrodes and conditioning effect for Midel 7131 oil

Sequence	BDV (kV)						
----------	----------	----------	----------	----------	----------	----------	----------

Appendix II. Test Results Used in Thesis

1	32.7	21	39.8	41	43.3	59	29.1
2	24.6	22	43.1	42	41.9	60	44.9
3	32.5	23	48.9	43	49.1	61	27.6
4	21.5	24	40.6	44	39.5	62	31.3
5	21.1	25	47.1	45	38.5	63	41.3
6	29.5	26	45.2	46	39.5	64	44
7	35.3	27	37.7	47	38.9	65	45.2
8	45.5	28	48.2	48	38.7	66	45.5
9	41.1	29	42.2	49	45.5	67	38.9
10	35.8	30	40.5	50	40.1	68	45.6
11	39.1	31	44.9	Change to new oil		69	42.9
12	27.7	32	41.1	sample		70	43.3
13	40.1	33	31.3	51	27.8	71	41.9
14	39.9	34	43.2	52	29.3	72	43.2
15	26	35	44	53	32	73	45.6
16	42.4	36	46	54	32		
17	40.4	37	45.5	55	28		
18	45.2	38	44.2	56	30.2		
19	28.2	39	45.6	57	25.5		
20	35	40	38.4	58	22.9		

*The results in this table correspond to Figure I.9.

Appendix III. List of Publications

- [1] X. Wang and Z.D. Wang, "Particle Effect on Breakdown Voltage of Mineral and Ester Based Transformer Oils," in *2008 Conference on Electrical Insulation and Dielectric Phenomena*, Quebec, Canada, 2008, pp. 598-602.
- [2] X. Wang and Z.D. Wang, "Discussion on the Effectiveness of IEC1294:1993 ' Insulating Liquids – Determination of the Partial Discharge Inception Voltage (PDIV) – Test Procedure'," in *2009 International Electrical Insulation Conference*, Birmingham, UK, 2009, No. 1-5.
- [3] Z.D. Wang, L. Qiang, X. Wang, and X. Yi, "Pre-Breakdown Study on Ester Transformer Liquids under Lightning Impulse and AC voltage," in *CIGRE 2010 Proceeding*, Paris, France, 2010.
- [4] X. Wang, Z.D. Wang, and J. Noakhes, "Motion of Conductive Particles and the Effect on AC breakdown Strengths of Esters," in *2011 International Conference on Dielectric Liquids*, Trondheim, Norway, 2011, No. 11-2.
- [5] X. Wang, Z.D. Wang, C. Perrier, and S. Northcote, "Electrode Area Effect on Dielectric Breakdown Strengths of Mineral Oil and Esters," in *2011 International Symposium on High Voltage Engineering*, Hannover, Germany, 2011, No. E-047.
- [6] Z.D. Wang, Q. Liu, X. Wang, P. Jarman, and G. Wilson, "Discussion on possible additions to IEC 60897 and IEC 61294 for insulating liquid tests," *IET Electric Power Applications*, vol. 5, pp. 486-493, June, 2011.
- [7] P. Jarman, G. Wilson, P. Dyer, F. Perrot, D. Walker, M. Lashbrook, J. Noakhes, Q. Liu, X. Wang, X. Yi, and Z.D. Wang, "Electrical Performance of Ester Insulating Liquids for Power Transformers," in *2012 CIGRE SC A2 & D1 Joint Colloquium*, Kyoto, Japan, 2012. (Accepted)



References

- [1] W. H. Bartley, "Analysis of Transformer Failures," in *2003 International Association of Engineering Insurers*, Stockholm, Sweden, 2003.
- [2] D. Martin, I. Khan, J. Dai, and Z. D. Wang, "An Overview of the Suitability of Vegetable Oil Dielectrics for Use in Large Power Transformers," in *2006 European Conferences for the Maintenance and Management of High Voltage Electrical Equipment (2006 Euro TechCon)*, Chester, United Kingdom, 2006.
- [3] P. Hopkinson, L. Dix, C. P. McShane, H. R. Moore, S. Moore, J. Murphy, T. Prevost, and S. D. Smith, "Progress Report on Natural Esters for Distribution and Power Transformers," in *2006 IEEE Transmission and Distribution Conference and Exhibition*, 2006, pp. 15-17.
- [4] D. P. Stockton, J. R. Bland, T. McClanahan, J. Wilson, D. L. Harris, and P. McShane, "Natural Ester Transformer Fluids: Safety, Reliability, Environmental Performance," in *2007 IEEE Petroleum and Chemical Industry Technical Conference*, 2007, pp. 1-7.
- [5] C. Perrier and A. Beroual, "Experimental Investigations on Insulating Liquids for Power Transformers: Mineral, Ester, and Silicone Oils," *IEEE Electrical Insulation Magazine*, vol. 25, pp. 6-13, 2009.
- [6] www.midel.com, "The First Midel 7131 Insulated 238 kV Power Transformer," 2004.
- [7] www.cooperpower.com, "Medium and Large Power Transformer Users List Retrofill & New Installations," December, 2008.
- [8] M. Amaah, S. M. Islam, S. Chami, and G. Ienco, "Analyses of Physical Characteristics of Vegetable Oils as an Alternative Source to Mineral Oil-based Dielectric Fluid," in *2005 IEEE International Conference on Dielectric Liquids*, 2005, pp. 397-400.
- [9] D. F. Binns and K. T. Yoon, "Comparison between Insulating Properties of Transformer Oil and a Low-flammability Ester Midel 7131," *IEE Physical Science, Measurement and Instrumentation*, vol. 129, pp. 182-185, 1982.
- [10] Z. D. Wang, A. Darwin, and R. Martin, "New Insulation Fluids: Use of Environmentally Friendly Fluids in Power Transformers," in *2007 CIGRE Colloquium*, Bruges, Belgium, 2007, pp. 04-07.
- [11] X. Wang and Z. D. Wang, "Particle Effect on Breakdown Voltage of Mineral and Ester Based Transformer Oils," in *2008 Conference on Electrical Insulation and Dielectric Phenomena*, Quebec, Canada, 2008, pp. 598-602.
- [12] Nynas, *Transformer Oil Hand Book*. Sweden, 2001.
- [13] Nynas, *Product Data Sheet - Nytro Gemini X*, 2008.
- [14] D. Martin, "Evaluation of the Dielectric Capability of Ester based Oils for Power Transformers," in *Department of Electrical Engineering and Electronics*, University of Manchester, 2007, p. 225.
- [15] www.midel.com, "Midel 7131 Transformer Fluid - Technical Data," January, 2007.
- [16] www.cooperpower.com, "Envirotemp FR3 Fluid - Testing Guide," July, 2004.

References

- [17] N. Felici, "High-Field Conduction in Dielectric Liquids," *IEEE Transactions on Electrical Insulation*, vol. EI-20, pp. 233-238, 1985.
- [18] M. G. Danikas, "Study of Some Factors Affecting the Breakdown Strength of Transformer Oil," in *1988 International Conference on Dielectric Materials, Measurements and Applications*, 1988, pp. 9-12.
- [19] A. A. Zaky and R. Hawley, *Conduction and Breakdown in Mineral Oil*. London, UK: Peter Peregrinus Ltd., 1973.
- [20] Z. Krasucki, "Breakdown of Liquid Dielectrics," *Proceedings of the Royal Society of London, Series A, Mathematical and Physical Sciences*, vol. 294, pp. 393-404, 1966.
- [21] N. Hayakawa, H. Sakakibara, H. Goshima, M. Hikita, and H. Okubo, "Breakdown Mechanism of Liquid Nitrogen Viewed from Area and Volume Effects," *IEEE Transactions on Dielectrics and Electrical Insulation*, vol. 4, pp. 127-134, 1997.
- [22] A. Beroual and R. Tobazeon, "Prebreakdown Phenomena in Liquid Dielectrics," *IEEE Transactions on Electrical Insulation*, vol. EI-21, pp. 613-627, 1986.
- [23] O. Lesaint and R. Tobazeon, "Study of the Generation by Sharp Electrodes of a Gaseous Phase in Dielectric Liquids Subjected to High AC or Step Voltages," *IEEE Transactions on Electrical Insulation*, vol. EI-20, pp. 269-273, 1985.
- [24] C. Hosticka, "Dependence of Uniform/ Nonuniform Field Transformer Oil Breakdown on Oil Composition," *IEEE Transactions on Electrical Insulation*, vol. EI-14, pp. 43-50, 1979.
- [25] T. V. Top, G. Massala, and O. Lesaint, "Streamer Propagation in Mineral Oil in Semi-uniform Geometry," *IEEE Transactions on Dielectrics and Electrical Insulation*, vol. 9, pp. 76-83, 2002.
- [26] G. Massala and O. Lesaint, "Positive Streamer Propagation in Large Oil Gaps: Electrical Properties of Streamers," *IEEE Transactions on Dielectrics and Electrical Insulation*, vol. 5, pp. 371-381, 1998.
- [27] R. Hancox and H. Tropper, "The Breakdown of Transformer Oil under Impulse Voltages," *IEE Proceedings Part A: Power Engineering*, vol. 105, pp. 250-262, 1958.
- [28] P. K. Watson and J. B. Higham, "Electric Breakdown of Transformer Oil," *IEE Proceedings Part II: Insulating Materials*, vol. 100, pp. 168-174, 1953.
- [29] M. G. Danikas, "Breakdown of Transformer Oil," *IEEE Electrical Insulation Magazine*, vol. 6, pp. 27-34, 1990.
- [30] S. Palmer and W. A. Sharpley, "Electric Strength of Transformer Insulation," *Proceedings of the IEE Part A: Power Engineering* vol. 116, pp. 2029-2037, 1969.
- [31] F. M. Clark, "Water Solution in High-Voltage Dielectric Liquids," *Transactions of the American Institute of Electrical Engineers*, vol. 59, pp. 433-441, 1940.
- [32] A. S. Asem and A. F. Howe, "Drying of Power Transformer Insulation," *Proceedings of the IEE Part C: Generation, Transmission and Distribution*, vol. 129, pp. 228-232, 1982.
- [33] G. D. Golovan, "Water Solubility in Transformer Oils with Various Hydrocarbon Compositions," *Chemistry and Technology of Fuels and Oils* vol. 20, pp. 387-391, August 1984.
- [34] "Method for Determination of Water in Liquid Dielectrics by Automatic Coulometric Karl Fischer Titration," in *IEC 60814*, 1985.

References

- [35] D. Chandler, "Two Faces of Water," *Nature*, vol. 417, p. 491, 2002.
- [36] O. Koreh, K. Torkos, M. Bashir Mahara, J. Boressay, and V. Izvekov, "Study of Water Clusters in Insulating Oils by Fourier Transform Infrared Spectroscopy," *IEEE Transactions on Dielectrics and Electrical Insulation*, vol. 5, pp. 896-902, 1998.
- [37] S. Itahashi, Y. Hayashi, K. Ohta, and M. Sone, "The Effect of the State of Bound Water in Aged Transformer Oil on Conductivity," in *1999 IEEE International Conference on Dielectric Liquids*, 1999, pp. 286-289.
- [38] S. Itahashi, H. Mitsui, T. Sato, and M. Sone, "State of Water in Hydrocarbon Liquids and Its Effect on Conductivity," *IEEE Transactions on Dielectrics and Electrical Insulation*, vol. 2, pp. 1117-1122, 1995.
- [39] K. Farooq, "The Effect of Particulate and Water Contamination on the Dielectric Strength of Insulating Oils," in *1996 IEEE International Symposium on Electrical Insulation* Montreal, Quebec, Canada, 1996, pp. 728 - 732.
- [40] J. K. Nelson, B. Salvage, and W. A. Sharpley, "Electric Strength of Transformer Oil for Large Electrode Areas," *Proceedings of the IEE*, vol. 118, pp. 388-393, 1971.
- [41] M. E. Zein El-Dine and H. Tropper, "The Electric Strength of Transformer Oil," *Proceedings of the IEE - Part C: Monographs*, vol. 103, pp. 35-45, 1956.
- [42] I. Fofana, H. Borsi, and E. Gockenbach, "Moisture Uptake of Mineral Oil at Different Air Relative Humidities and Temperatures," in *2000 Conference on Electrical Insulation and Dielectric Phenomena 2000*, pp. 276-279 vol.1.
- [43] D. Martin and Z. D. Wang, "A Comparative Study of the Impact of Moisture on the Dielectric Capability of Esters for Large Power Transformers," in *2006 IEEE Conference on Electrical Insulation and Dielectric Phenomena*, 2006, pp. 409-412.
- [44] M. Krins, M. Reuter, H. Borsi, and E. Gockenbach, "Breakdown and Flashover Phenomena Related to the Presence of High Absolute Water Contents in Clean and Carbonized Transformer Oil," in *2002 Conference on Electrical Insulation and Dielectric Phenomena*, 2002, pp. 252-255.
- [45] H. Borsi, "Dielectric Behavior of Silicone and Ester Fluids for Use in Distribution Transformers," *IEEE Transactions on Electrical Insulation*, vol. 26, pp. 755-762, 1991.
- [46] K. Brinkman and M. Beyer, "Uber die Hochvakuum-Trocknung und Entgasung von Isolierolen fur Hochspannungskabeln," *ETZ-A*, vol. 81, 1960.
- [47] K. Miners, "Particles and Moisture Effect on Dielectric Strength of Transformer Oil Using VDE Electrodes," *IEEE Transactions on Power Apparatus and System*, vol. PAS-101, pp. 751-756, 1982.
- [48] W. G. Chadband, "The Electrical Breakdown of Insulating Oil," *Journal of Power Engineering*, vol. 6, pp. 61 - 67, Mar 1992.
- [49] Y. Du, A. V. Mamishev, B. C. Lesieutre, M. Zahn, and S. H. Kang, "Moisture Solubility for Differently Conditioned Transformer Oils," *IEEE Transactions on Dielectrics and Electrical Insulation*, vol. 8, pp. 805-811, 2001.
- [50] C. G. Garton and Z. Krasucki, "Bubbles in Insulating Liquids: Stability in an Electric Field," *Proceedings of the Royal Society of London, Series A: Mathematical and Physical Sciences*, vol. 280, pp. 211-226, 1964.

References

- [51] G. Berg, L. Lundgaard, and F. K. Hansen, "Elongation of Water Drops in Oil during Transient Electric Fields," in *2005 IEEE International Conference on Dielectric Liquids*, 2005, pp. 189-192.
- [52] G. Taylor, "Disintegration of Water Drops in an Electric Field," *Proceedings of the Royal Society of London, Series A: Mathematical and Physical Sciences*, vol. 280, pp. 383-397, 1964.
- [53] CIGRE, "Effect of Particles on Transformer Dielectric Strength," in *Working Group 17 of Study Committee 12*, 2000.
- [54] L. Dascalescu, A. Samuila, and R. Tobazeon, "Cylindrical Conductive Particles in the Proximity of an Electrode Affected by a High-intensity Electric Field," *Journal of Electrostatics*, vol. 37, pp. 173-196, 1996.
- [55] S. M. Makkawy, "Movement of Charged Conducting Particles under AC Voltages in Insulating Liquids," in *1996 IEEE International Symposium on Electrical Insulation*, 1996, pp. 585-588 vol.2.
- [56] R. Tobazeon, "Behaviour of Spherical and Cylindrical Particles in an Insulating Liquid Subjected to a DC Uniform Field," in *1993 IEEE International Conference on Conduction and Breakdown in Dielectric Liquids*, 1993, pp. 415-420.
- [57] F. Carraz, P. Rain, and R. Tobazeon, "Particle-initiated Breakdown in a Quasi-uniform Field in Transformer Oil," *IEEE Transactions on Dielectrics and Electrical Insulation*, vol. 2, pp. 1052-1063, 1995.
- [58] K. Asano, K. Anno, and Y. Higashiyama, "The Behavior of Charged Conducting Particles in Electric Fields," *IEEE Transactions on Industry Applications*, vol. 33, pp. 679-686, 1997.
- [59] S. Birlasekaran, "The Movement of a Conducting Particle in Transformer Oil in AC Fields," *IEEE Transactions on Electrical Insulation*, vol. 28, pp. 9-17, 1993.
- [60] C. Choi, K. Yatsuzuka, and K. Asano, "Motion of a Conductive Particle in Viscous Fluid Simulating Liquified Plastic Waste," in *1999 IEEE Conference on Industry Applications*, 1999, pp. 1831-1836 vol.3.
- [61] P. Rain and R. Tobazeon, "Behaviour of Free Conducting Particles and Their Role on Breakdown in Oils under AC and DC Voltages," in *1992 International Conference on Dielectric Materials, Measurements and Applications*, 1992, pp. 96-99.
- [62] S. Birlasekaran and M. Darveniza, "Microdischarges from Particles in Transformer Oil," *IEEE Transactions on Dielectrics and Electrical Insulation*, vol. EI - 11, pp. 162-163, 1976.
- [63] T. Zinoulis, I. Argirakis, D. W. Auckland, and W. G. Chadband, "The Role of Particles in Discharge Initiation in Liquids," in *1993 IEEE International Conference on Dielectric Liquids*, 1993, pp. 421-425.
- [64] H. Kurita, O. Usui, T. Hasegawa, and H. Fujii, "Effect of Particles on Partial Discharge Inception in Oil Immersed Insulating System," in *1999 IEEE International Conference on Dielectric Liquids*, 1999, pp. 126-131.
- [65] N. G. Trinh, C. Vincent, and J. Regis, "Statistical Dielectric Degradation of Large-Volume Oil-Insulation," *IEEE Transactions on Power Apparatus and Systems* vol. PAS-101, pp. 3712-3721, 1982.
- [66] IEC, "IEC 60970: Insulating Liquids - Methods for Counting and Sizing Particles," 2007.

References

- [67] H. Miyahara, "Influence of Micro Particles in Fluid on the Impulse and AC breakdown Strengths of Low-viscosity Silicone Liquid Immersed Insulating Systems," Hitachi City, Japan: Japan AE Power Systems Corporation, 2008, p. 6.
- [68] K. N. Mathes and J. M. Atkins, "Influence of Particles on Partial Discharges and Breakdown in Oil," in *1978 IEEE International Symposium on Electrical Insulation*, 1978.
- [69] H. Naoshi, O. A. Aloys, and A. Kiyomitsu, "The Effect of Contaminant in Breakdown Time Lag of Uniform Electric Field Using Impulse Breakdown in Mineral Oil," in *1999 IEEE International Conference on Dielectric Liquids*, 1999, pp. 207-210.
- [70] J. A. Kok, *Electrical Breakdown of Insulating Liquids*. New York: Interscience Publishers, Inc., 1961.
- [71] A. Lobeira and J. Sabau, "Counting and Sizing Particles in Insulating Mineral Oils," Miami: Beckman Coulter, 1999, p. 6.
- [72] W. B. Wiegand, C. R. Boggs, and D. W. Kitchin, "Effect of Carbon Black on Insulating Oils," *Journal of Industrial and Engineering Chemistry*, vol. 23, pp. 273-276, 1931.
- [73] M. Krins, H. Borsi, and E. Gockenbach, "Influence of Carbon Particles on the Breakdown and Partial Discharge Inception Voltage of Aged Mineral Based Transformer Oil," in *1996 International Conference on Dielectric Materials, Measurements and Applications*, 1996, pp. 251-254.
- [74] M. Krins, H. Borsi, and E. Gockenbach, "Impact of Carbon Particles on the Electrical Strength of Different Solid/Liquid Interfaces in a Non-uniform Field," in *1998 IEEE International Symposium on Electrical Insulation*, 1998, pp. 623-626 vol.2.
- [75] M. Krins, H. Borsi, and E. Gockenbach, "Impact of Carbon Particles on the Impulse Flashover Behavior of Different Solid/Liquid Interfaces in a Non-uniform Field," in *1998 International Symposium on Electrical Insulating Materials*, 1998, pp. 363-368.
- [76] M. Khalifa, *High-Voltage Engineering- Theory and Practice*. New York: Marcel Dekker, 1990.
- [77] G. Chen and M. H. Zuber, "Pre-breakdown Characteristics of Contaminated Power Transformer Oil," in *2007 Conference on Electrical Insulation and Dielectric Phenomena*, 2007, pp. 659-662.
- [78] A. P. Sullivan and P. K. Kilpatrick, "The Effects of Inorganic Solid Particles on Water and Crude Oil Emulsion Stability," *Journal of Industrial and Engineering Chemistry Research*, vol. 41, pp. 3389-3404, 2002.
- [79] A. Ozawa, S. Mikami, K. Nitta, M. Shinmura, S. Washizu, and Y. Wada, "Electrical Conduction and Polarization in Cellulose in Relation to its Water Content," in *1989 International Conference on Conduction and Breakdown in Solid Dielectrics*, 1989, pp. 15-19.
- [80] H. Kurita, T. Hasegawa, and K. Kimura, "Dielectric Breakdown Characteristics of Clean Oil," in *1992 IEEE International Symposium on Electrical Insulation* Baltimore, MD, USA, 1992, pp. 433-436.
- [81] T. V. Oommen and S. R. Lindgren, "Bubble Evolution from Transformer Overload," in *2001 IEEE Conference on Transmission and Distribution and*

References

- Exposition*, 2001, pp. 137-142 vol.1.
- [82] F. M. Clark, "The Role of Dissolved Gases in Determining the Behavior of Mineral Insulating Oils," *Journal of the Franklin Institute*, vol. 215, pp. 39-67, 1933.
- [83] F. M. Clark, "Dielectric Strength of Mineral Oils," *Transactions of the American Institute of Electrical Engineers*, vol. 54, pp. 50-55, 1935.
- [84] H. Tropper, "The Effect of Dissolved Gases on the Electrical Conduction and Breakdown of Insulating Oil," *Journal of Electrochemical Society*, vol. 108, pp. 144-150, 1961.
- [85] A. M. Sletten, "Electric Strength and High-Field Conduction Current in n-Hexane," *Nature*, vol. 183, pp. 311-312, 1959.
- [86] A. M. Sletten and T. J. Lewis, "The Influence of Dissolved Gases on the Dielectric Strength of N-hexane," *British Journal of Applied Physics*, vol. 14, pp. 883-888, 1963.
- [87] A. Nosseir, R. Hawley, and N. Clothier, "Effect of a Dissolved Electronegative Gas (Sulphur Hexafluoride) on the Breakdown Strength of Liquid Dielectrics," *Nature*, vol. 206, pp. 494-494, 1965.
- [88] A. Nosseir and R. Hawley, "Effect of Dissolved SF₆ on High Field Conductivity in Mineral Oils " *British Journal of Applied Physics*, vol. 16, pp. 1633-1642, 1965.
- [89] A. H. Mufti and A. O. Arafa, "Conduction Current-stress Characteristics of Mineral Oil under the Effect of Electronegative Dissolved Gases," in *1996 International Conference on Conduction and Breakdown in Dielectric Liquids*, 1996, pp. 234-237.
- [90] K. C. Kao, "Deformation of Gas Bubbles and Liquid Drops in an Electrically Stressed Insulating Liquid," *Nature*, vol. 208, pp. 279-280, 1965.
- [91] M. Cevallos, M. Butcher, J. Dickens, A. Neuber, and H. Krompholz, "Bubble Dynamics and Channel Formation for Cathode Initiated Discharges in Transformer Oil," in *2005 IEEE Conference on Pulsed Power*, 2005, pp. 1235-1238.
- [92] T. Aka-Ngnui and A. Beroual, "Bubble Dynamics and Transition into Streamers in Liquid Dielectrics under a High Divergent Electric Field," *Journal of Physics D: Applied Physics*, vol. 34, pp. 1408-1412, 2001.
- [93] J. A. Scott, "Effect of Oil Pressure on Insulation Strength," *Transactions on the American Institute of Electrical Engineers*, vol. 53, pp. 308-309, 1934.
- [94] W. G. Hoover and W. A. Hixson, "Dielectric Strength of Oil with Variations of Pressure and Temperature," *Transactions on the American Institute of Electrical Engineers*, vol. 68, pp. 1047-1050, 1949.
- [95] Y. Toriyama, T. Sato, and H. Mitsui, "Dielectric Breakdown of Insulating Liquids," *British Journal of Applied Physics*, vol. 15, pp. 203-205, 1964.
- [96] S. M. Korobejnikov and E. V. Yanshin, "Bubble Model: Time Dependent Pressure Effect in Liquids," in *1990 International Conference on Conduction and Breakdown in Dielectric Liquids*, 1990, pp. 360-364.
- [97] K. C. Kao and J. P. C. McMath, "Time-Dependent Pressure Effect in Liquid Dielectrics," *IEEE Transactions on Electrical Insulation*, vol. EI-5, pp. 64-68, 1970.
- [98] I. Y. Megahed and A. A. Zaky, "Influence of Temperature and Pressure on Conduction Currents in Transformer Oil," *IEEE Transactions on Electrical*

References

- Insulation*, vol. EI-4, pp. 99-103, 1969.
- [99] Y. Kawaguchi, H. Murata, and M. Ikeda, "Breakdown of Transformer Oil," *IEEE Transactions on Power Apparatus and Systems*, vol. PAS-91, pp. 9-23, 1972.
- [100] A. A. Zaky and A. Nosseir, "Electrical Breakdown of Mineral Oil under Uniform Field," *Journal of Physics D: Applied Physics*, vol. 10, pp. 1761-1767, 1977.
- [101] I. Y. Megahed and A. A. Zaky, "Effect of Electrode Material, Oxygen and Organic Additive on the Breakdown Strength of Mineral Oil under Non-uniform Fields," *Journal of Electrostatics*, vol. 12, pp. 345-351, 1982.
- [102] H. S. Endicott and K. H. Weber, "Electrode Area Effect for the Impulse Breakdown of Transformer Oil," *Power Apparatus and Systems, Part III. Transactions of the American Institute of Electrical Engineers*, vol. 76, pp. 393-397, 1957.
- [103] K. H. Weber and H. S. Endicott, "Area Effect and Its Extremal Basis for the Electric Breakdown of Transformer Oil," *Power Apparatus and Systems, Part III. Transactions of the American Institute of Electrical Engineers*, vol. 75, pp. 371-381, 1956.
- [104] K. H. Weber and H. S. Endicott, "Extremal Area Effect for Large Area Electrodes for the Electric Breakdown of Transformer Oil," *Power Apparatus and Systems, Part III. Transactions of the American Institute of Electrical Engineers*, vol. 76, pp. 1091-1096, 1957.
- [105] S. J. Laihonen, U. Gafvert, T. Schutte, and U. W. Gedde, "Influence of Electrode Area on Dielectric Breakdown Strength of Thin Poly(ethylene terephthalate) Films," in *2004 Conference on Electrical Insulation and Dielectric Phenomena*, 2004, pp. 563-567.
- [106] W. R. Wilson, "A Fundamental Factor Controlling the Unit Dielectric Strength of Oil," *Power Apparatus and Systems, Part III. Transactions of the American Institute of Electrical Engineers*, vol. 72, pp. 68-74, 1953.
- [107] E. Simo, "Large Scale Dielectric Test of Transformer Oil with Uniform Field Electrodes," *IEEE Transactions on Electrical Insulation*, vol. EI-5, pp. 121-126, 1970.
- [108] J. C. Devins, S. J. Rzad, and A. J. Schwab, "Prebreakdown Phenomena in Sphere - Sphere Electrode Configurations in Dielectric Liquids," *Applied Physics Letters*, vol. 31, pp. 313-314, 1977.
- [109] P. E. Frayssines, O. Lesaint, N. Bonifaci, A. Denat, and F. Devaux, "Prebreakdown and Breakdown Phenomena under Uniform Field in Liquid Nitrogen and Comparison with Mineral Oil," *IEEE Transactions on Dielectrics and Electrical Insulation*, vol. 10, pp. 970-976, 2003.
- [110] E. F. Kelley and R. E. Hebner, "Prebreakdown Phenomena Between Sphere - Sphere Electrodes in Transformer Oil," *Applied Physics Letters*, vol. 38, 1981.
- [111] H. Yamashita, K. Yamazawa, and Y. S. Wang, "The Effect of Tip Curvature on the Prebreakdown Streamer Structure in Cyclohexane," *IEEE Transactions on Dielectrics and Electrical Insulation*, vol. 5, pp. 396-401, 1998.
- [112] F. M. J. McCluskey, A. Denat, and O. Lesaint, "Breakdown and Prebreakdown Phenomena in Liquids under Positive Impulse Voltages," *IEEE Transactions on Dielectrics and Electrical Insulation*, vol. 1, pp. 377-382, 1994.
- [113] R. Hanaoka, Y. Iwasa, S. Takata, Y. Nakagami, and K. Takamoto, "Impulse

References

- Creepage Discharges in Rapeseed Ester Oil," in *2004 Conference on Electrical Insulation and Dielectric Phenomena*, 2004, pp. 663-666.
- [114] O. Lesaint, A. Saker, P. Gournay, R. Tobazeon, J. Aubin, and M. Mailhot, "Streamer Propagation and Breakdown under AC Voltage in Very Large Oil Gaps," *IEEE Transactions on Dielectrics and Electrical Insulation*, vol. 5, pp. 351-359, 1998.
- [115] Q. Liu and Z. D. Wang, "Streamer Characteristic and Breakdown in Synthetic and Natural Ester Transformer Liquids under Standard Lightning Impulse Voltage," *IEEE Transactions on Dielectrics and Electrical Insulation*, vol. 18, pp. 285-294, 2010.
- [116] A. Beroual, M. Zahn, A. Badent, K. Kist, A. J. Schwabe, H. Yamashita, K. Yamazawa, M. Danikas, W. D. Chadband, and Y. Torshin, "Propagation and Structure of Streamers in Liquid Dielectrics," *IEEE Electrical Insulation Magazine*, vol. 14, pp. 6-17, 1998.
- [117] O. Lesaint, "On the Relationship between Streamer Branching and Propagation in Liquids: Influence of Pyrene in Cyclohexane," *Journal of Applied physics D*, vol. 33, p. 1360, 2000.
- [118] O. Lesaint, "Prebreakdown Phenomena in Liquids and Their Relations with Breakdown Properties in High Voltage Applications," in *CIGRE Colloquium Bruges 2007*. vol. PS1 Bruges, Belgium, 2007, p. 01.
- [119] T. V. Top and A. Lesaint, "Streamer Initiation in Mineral Oil. Part II: Influence of a Metallic Protrusion on a Flat Electrode," *IEEE Transactions on Dielectrics and Electrical Insulation*, vol. 9, pp. 92-96, 2002.
- [120] O. Lesaint, P. Gournay, A. Saker, R. Tobazeon, J. Aubin, and M. Mailhot, "Streamer Propagation and Breakdown under AC in Mineral Oil for Gaps up to 80 cm," in *1996 International Conference on Conduction and Breakdown in Dielectric Liquids*, 1996, pp. 251-254.
- [121] A. Nosseir and I. Y. Megahed, "Pre-breakdown Conduction Current Pulses in Insulating Oils under Non-uniform Field Conditions " *Journal of Physics D: Applied Physics*, vol. 3, pp. 1205-1211, 1970.
- [122] W. G. Chadband, "From Bubbles to Breakdown, or Vice-versa," in *1993 IEEE International Conference on Conduction and Breakdown in Dielectric Liquids*, 1993, pp. 184-193.
- [123] O. Lesaint and R. Tobazeon, "Streamer Generation and Propagation in Transformer Oil under AC Divergent Field Conditions," *IEEE Transactions on Electrical Insulation*, vol. 23, pp. 941-954, 1988.
- [124] O. Lesaint and G. Massala, "Positive Streamer Propagation in Large Oil Gaps: Experimental Characterization of Propagation Modes," *IEEE Transactions on Dielectrics and Electrical Insulation*, vol. 5, pp. 360-370, 1998.
- [125] O. Lesaint, P. Gournay, and R. Tobazeon, "Investigations on Transient Currents Associated with Streamer Propagation in Dielectric Liquids," *IEEE Transactions on Electrical Insulation*, vol. 26, pp. 699-707, 1991.
- [126] L. E. Lundgaard, D. Linhjell, and G. Berg, "Streamer/leaders from a Metallic Particle between Parallel Plane Electrodes in Transformer Oil," *IEEE Transactions on Dielectrics and Electrical Insulation*, vol. 8, pp. 1054-1063, 2001.
- [127] C. T. Duy, O. Lesaint, A. Denat, and N. Bonifaci, "Streamer Propagation and

References

- Breakdown in Natural Ester at High Voltage," *IEEE Transactions on Dielectrics and Electrical Insulation*, vol. 16, pp. 1582-1594, 2009.
- [128] Y. Kamata and Y. Kako, "Flashover Characteristics of Extremely Long Gaps in Transformer Oil under Non-Uniform Field Conditions," *IEEE Transactions on Electrical Insulation*, vol. EI-15, pp. 18-26, 1980.
- [129] IEC, "IEC 60599: Mineral oil Impregnated Electrical Equipment in Service- Guide to the Interpretation of Dissolved and Free Gases Analysis," 1999.
- [130] J. Fleszynski, B. Lutynski, and J. I. Skowronski, "Effect of Impurities on the Breakdown of Insulating Oil in Long Gaps," *Journal of Electrostatics*, vol. 7, pp. 47-55, 1979.
- [131] F. M. J. McCluskey, O. Lesaint, and A. Denat, "Breakdown Processes over Large Distances in Insulating Liquids of Distinct Chemical Compositions," in *1994 IEEE International Symposium on Electrical Insulation*, 1994, pp. 426-429.
- [132] J. C. Devins, S. J. Rzad, and R. J. Schwabe, "Breakdown and Prebreakdown Phenomena in Liquids," *Journal of Applied Physics*, vol. 52, pp. 4531-4545, 1981.
- [133] Y. Nakao, H. Itoh, S. Hoshino, Y. Sakai, and H. Tagashira, "Effects of Additives on Prebreakdown Phenomena in N-hexane," *IEEE Transactions on Dielectrics and Electrical Insulation*, vol. 1, pp. 383-389, 1994.
- [134] S. SIngebrigtsen, "The Influence of Chemical Composition on Streamer Initiation and Propagation in Dielectric Liquids," in *Department of Chemistry*. vol. PhD Trondheim: Norwegian University of Science and Technology, 2008.
- [135] P. Rain, C. Boisdon, O. Lesaint, and R. Tobazeon, "Behavior of Streamers under Divergent AC Fields in Transformer Oils at Large Gaps," *IEEE Transactions on Electrical Insulation*, vol. 26, pp. 715-725, 1991.
- [136] L. E. Lundgaard, "Discharges in AC-stressed Oil Gaps," in *1993 IEEE International Conference on Conduction and Breakdown in Dielectric Liquids*, 1993, pp. 337-341.
- [137] A. Cavallini, G. C. Montanari, and F. Ciani, "Analysis of Partial Discharge Phenomena in Paper-oil Insulation Systems as a Basis for Risk Assessment Evaluation," in *2005 IEEE International Conference on Dielectric Liquids*, 2005, pp. 241-244.
- [138] C. Vincent, N. G. Trinh, R. Olivier, and J. Aubin, "Behavior of an Oil-paper Interface in Presence of Carbon Particle Contamination," in *1994 IEEE International Symposium on Electrical Insulation*, 1994, pp. 534-537.
- [139] T. Van Top and O. Lesaint, "Effect of Electrode Geometry and Cellulose Particles on Streamer Initiation in Oil under Divergent AC Fields," in *1997 International Conference on Properties and Applications of Dielectric Materials*, 1997, pp. 178-181 vol.1.
- [140] Y. Torshin, "The Universal Discharge Mechanism in Mineral Oil and Possible Estimation of its Breakdown Voltage," in *2002 International Conference on Dielectric Liquids*, 2002, pp. 107-110.
- [141] O. Lesaint and T. V. Top, "Streamer Initiation in Mineral Oil. Part I: Electrode Surface Effect under Impulse Voltage," *IEEE Transactions on Dielectrics and Electrical Insulation*, vol. 9, pp. 84-91, 2002.
- [142] O. Lesaint, "'Streamers' in liquids: Relation with Practical High Voltage Insulation and Testing of Liquids," in *2008 IEEE International Conference on Dielectric*

References

- Liquids*, 2008, pp. 1-6.
- [143] D. Martin and Z. Wang, "Statistical Analysis of the AC Breakdown Voltages of Ester Based Transformer Oils," *IEEE Transactions on Dielectrics and Electrical Insulation*, vol. 15, pp. 1044-1050, 2008.
- [144] IEC, "IEC 60296: Fluids for Electrotechnical Applications - Unused Mineral Insulating Oils for Transformers and Switchgear," 2003.
- [145] IEEE, "IEEE C57.147: Guide for Acceptance and Maintenance of Natural Ester Fluids in Transformers," 2008.
- [146] IEC, "IEC 61099: Insulating Liquids- Specifications for Unused Synthetic Organic Esters for Electrical Purposes," 2010.
- [147] H. Hirose, "Maximum Likelihood Parameter Estimation in the Extended Weibull Distribution and its Applications to Breakdown Voltage Estimation," *IEEE Transactions on Dielectrics and Electrical Insulation*, vol. 9, pp. 524-536, 2002.
- [148] F. A. M. Rizk and C. Vincent, "Testing for Low Breakdown Probability with Special Reference to Liquid Insulation," *IEEE Transactions on Power Apparatus and Systems*, vol. 96, pp. 1892-1900, 1977.
- [149] H. Z. Ding, Z. D. Wang, and P. Jarman, "Dielectric Strength of Aged Transformer Oils: Experimental Studies and Statistical Analysis of Breakdown voltage," in *2005 International Symposium on High Voltage Engineering*, China, 2005.
- [150] R. Gnanadesikan, *Statistical Data Analysis*: American Mathematical Society, 1983.
- [151] C. Huber-Caron, N. Balakrishnan, M. S. Nikulin, and M. Mesbah, *Goodness-of-Fit Tests and Model Validity*. Washington D.C. USA: Hamilton Printing Company, 2002.
- [152] D. Martin and Z. Wang, "Statistical Analysis of the AC Breakdown Voltages of Ester Based Transformer Oils," *Dielectrics and Electrical Insulation, IEEE Transactions on*, vol. 15, pp. 1044-1050, 2008.
- [153] J. K. Nelson and C. Shaw, "The Impulse Design of Transformer Oil-Cellulose Structures," *IEEE Transactions on Dielectrics and Electrical Insulation*, vol. 13, pp. 477-483, 2006.
- [154] W. Lick and M. Muhr, "Strength Investigations on Long Oil Gaps," in *IEEE International Conference on Dielectric Liquids*, Austria, 2002, pp. 228-230.
- [155] M. J. Heathcote, *J&P Transformer Book*: Reed Educational and Professional Publishing Ltd, 1998.
- [156] M. G. Danikas, "Technical Report of Particles in Transformer Oil," *IEEE Electrical Insulation Magazine*, vol. 7, pp. 39-40, March 1991.
- [157] IEC, "IEC 60422: Mineral Insulating Oils in Electrical Equipment- Supervision and Maintenance Guidance," 2005.
- [158] IEC, "IEC 1203: Synthetic Organic Esters for Electrical Purposes - Guide for Maintenance of Transformer Esters in Equipment," 1992.
- [159] M. Pompili and C. Mazzetti, "Effect of Reduced Viscosity on the Electrical Characteristics of Transformer and Switchgear Oils," in *2002 IEEE International Symposium on Electrical Insulation*, 2002, pp. 363-366.
- [160] J. K. Nelson and M. J. Lee, "Electrokinetic Phenomena in Dielectric Liquids," in *1986 IEEE International Symposium on Electrical Insulation*, Washington, 1986, pp. 90-94.

References

- [161] L. Dascalescu, M. Mihailescu, and R. Tobazeon, "Modeling of Conductive Particle Behavior in Insulating Fluids Affected by DC Electric Fields," *IEEE Transactions on Industry Applications*, vol. 34, pp. 66-74, 1998.
- [162] S. Jayaram, "Effects of Thermal and Viscous Drag Forces on AC Breakdown Characteristics of Transformer Oil," in *1993 Conference on Electrical Insulation and Dielectric Phenomena*, 1993, pp. 396-401.
- [163] ASTM, "ASTM D5023: Standard Practice for Maintaining Constant Relative Humidity by Means of Aqueous Glycerin Solutions," 2003.
- [164] P.Schuster, G.Zundel, and C.Sandorfy, *The Hydrogen Bond*. Amsterdam: North-Holland Publishing Company, 1976.
- [165] M. Beyer and H. Borsi, "Comparison of the Electric and Dielectric Behaviour of Different Insulating Fluids," in *1990 International Conference on Conduction and Breakdown in Dielectric Liquids*, 1990, pp. 524-528.
- [166] N. Hayakawa, H. Sakakibara, H. Goshima, M. Hikita, and H. Okubo, "Mutual Contribution of Area and Volume Effects on Breakdown Strength in Liquid Nitrogen," in *1996 International Conference on Conduction and Breakdown in Dielectric Liquids*, 1996, pp. 333-336.
- [167] W.Hauschild and W.Mosch, *Statistical Techniques for High-Voltage Engineering*: Peter Peregrinus Ltd., London, 1992.
- [168] H. Goshima, N. Hayakawa, M. Hikita, H. Okubo, and K. Uchida, "Weibull Statistical Analysis of Area and Volume Effects on the Breakdown Strength in Liquid Nitrogen," *IEEE Transactions on Dielectrics and Electrical Insulation*, vol. 2, pp. 385-393, 1995.
- [169] M. Kaufhold, H. Aninger, M. Berth, J. Speck, and M. Eberhardt, "Electrical Stress and Failure Mechanism of the Winding Insulation in PWM-inverter-fed Low-voltage Induction Motors," *IEEE Transactions on Industrial Electronics*, vol. 47, pp. 396-402, 2000.
- [170] E. A. Cherney and J. Cross, "Electric-Field Distortions at Solid-Liquid Dielectric Interfaces," *IEEE Transactions on Electrical Insulation*, vol. EI-9, pp. 37-42, 1974.
- [171] A. Cavallini, M. Conti, A. Contin, and G. C. Montanari, "Advanced PD Inference in On-field Measurements. II. Identification of Defects in Solid Insulation Systems," *IEEE Transactions on Dielectrics and Electrical Insulation*, vol. 10, pp. 528-538, 2003.
- [172] H. C. Hall and R. M. Russek, "Discharge Inception and Extinction in Dielectric Voids," *Proceedings of the IEE, Part II: Power Engineering*, vol. 101, pp. 47-55, 1954.
- [173] J. Dai and Z. D. Wang, "A Comparison of the Impregnation of Cellulose Insulation by Ester and Mineral oil," *IEEE Transactions on Dielectrics and Electrical Insulation*, vol. 15, pp. 374-381, 2008.
- [174] D. A. Nattrass, "Partial Discharge Measurement and Interpretation," *IEEE Electrical Insulation Magazine*, vol. 4, pp. 10-23, 1988.
- [175] E. O. Forster, "Partial Discharges and Streamers in Liquid Dielectrics - The Significance of the Inception Voltage," *IEEE Transactions on Electrical Insulation*, vol. 28, pp. 941 - 946, December 1993.
- [176] H. Yamashita, "Partial Discharge Measurements in Dielectric Liquids under

References

- Impulse Voltage," *IEEE Transactions on Electrical Insulation*, vol. 28, pp. 947-955, 1993.
- [177] IEC, "IEC 61294: Determination of the Partial Discharge Inception Voltage (PDIV) Test Procedure of Insulating Liquids," 1993.
- [178] C. Mazzetti, M. Pompili, and R. Schifani, "A Comparative Evaluation of Partial Discharge Inception Voltage of Power Transformer Liquids," in *1988 IEEE International Symposium on Electrical Insulation* Boston, MA, 1988, pp. 31 - 34.
- [179] M. Pompili, C. Mazzetti, M. Libotte, and E. O. Forster, "The Effect of the Definition Used in Measuring Partial Discharge Inception Voltages," *IEEE Transactions on Electrical Insulation*, vol. 28, pp. 1002-1006, 1993.
- [180] IEC, "IEC 60270: High-voltage test techniques - Partial discharge measurements," 2000.
- [181] C. Mazzetti, M. Pompili, H. Yamashita, and E. O. Forster, "A Comparison of Streamer and Partial Discharge Inception Voltages in Liquid Dielectrics," in *1992 International Conference on Dielectric Materials, Measurements and Applications*, 1992, pp. 93-95.
- [182] M. Pompili, C. Mazzetti, and R. Bartnikas, "PD Pulse Burst Characteristics of Transformer Oils," *IEEE Transactions on Power Delivery*, vol. 21, pp. 689-698, 2006.
- [183] C. Mazzetti, M. Pompili, and E. O. Forster, "A Study of Partial Discharge Measurements in Dielectric Liquids," *IEEE Transactions on Electrical Insulation*, vol. 27, pp. 445-450, 1992.
- [184] D. Linhjell, L. Lundgaard, and G. Berg, "Streamer Propagation under Impulse Voltage in Long Point-plane Oil Gaps," *IEEE Transactions on Dielectrics and Electrical Insulation*, vol. 1, pp. 447-458, 1994.
- [185] D. J. Swaffield, P. L. Lewin, G. Chen, and S. G. Swingler, "Partial Discharge Characterization of Streamers in Liquid Nitrogen under Applied AC Voltages," *IEEE Transactions on Dielectrics and Electrical Insulation*, vol. 15, pp. 635-646, 2008.
- [186] I. Fafana, V. Wasserberg, H. Borsi, and E. Gockenbach, "Retrofilling Conditions of High Voltage Transformers," *IEEE Electrical Insulation Magazine*, vol. 17, pp. 17-30, 2001.
- [187] B. Halpern and R. Gomer, "Field Emission in Liquids," *Journal of Chemical Physics*, vol. 51, pp. 1031-1047, 1969.
- [188] B. Halpern and R. Gomer, "Field Ionization in Liquids," *Journal of Chemical Physics*, vol. 51, pp. 1049-1056, 1969.
- [189] P. Rain and O. Lesaint, "Prebreakdown Phenomena in Mineral Oil under Step and AC Voltage in Large-gap Divergent Fields," *IEEE Transactions on Dielectrics and Electrical Insulation*, vol. 1, pp. 692-701, 1994.
- [190] S. Ingebrigtsen, H. S. Smalo, P. O. Astrand, and L. E. Lundgaard, "Effects of Electron-attaching and Electron-releasing Additives on Streamers in Liquid Cyclohexane," *IEEE Transactions on Dielectrics and Electrical Insulation*, vol. 16, pp. 1524-1535, 2009.
- [191] Y. Inuishi, "Effect of Space Charge and Structure on Breakdown of Liquid and Solid," *IEEE Transactions on Electrical Insulation*, vol. EI-17, pp. 488-492, 1982.
- [192] L. Lundgaard, D. Linhjell, G. Berg, and S. Sigmond, "Propagation of Positive and

References

- Negative Streamers in Oil with and without Pressboard Interfaces," *IEEE Transactions on Dielectrics and Electrical Insulation*, vol. 5, pp. 388-395, 1998.
- [193] M. Duval and A. DePabla, "Interpretation of Gas-in-oil Analysis Using New IEC Publication 60599 and IEC TC 10 Databases," *IEEE Electrical Insulation Magazine*, vol. 17, pp. 31-41, 2001.
- [194] M. Duval, "A Review of Faults Detectable by Gas-in-oil Analysis in Transformers," *IEEE Electrical Insulation Magazine*, vol. 18, pp. 8-17, 2002.
- [195] M. Duval and J. Dukarm, "Improving the Reliability of Transformer Gas-in-oil Diagnosis," *IEEE Electrical Insulation Magazine*, vol. 21, pp. 21-27, 2005.
- [196] M. Duval, "The Duval Triangle for Load Tap Changers, Non-mineral oils and Low Temperature Faults in Transformers," *IEEE Electrical Insulation Magazine*, vol. 24, pp. 22-29, 2008.
- [197] I. Khan, Z. D. Wang, and I. Cotton, "Dissolved Gas Analysis of Alternative Fluids for Power Transformers," *IEEE Electrical Insulation Magazine*, vol. 23, pp. 5 - 14, September 2007.
- [198] M. Duval, "Dissolved Gas Analysis and the Duval Triangle," in *AVO New Zealand*, New Zealand, 2006.
- [199] I. Khan, Z. D. Wang, J. Dai, I. Cotton, and S. Northcote, "Fault Gas Generation in Ester based Transformer Fluids and Dissolved Gas Analysis (DGA)," in *2008 International Conference on Condition Monitoring and Diagnosis*, 2008, pp. 909-913.
- [200] T. H. Dang, A. Denat, and O. Lesaint, "Degradation of Organic Molecules by Streamer and Spark Discharges in Water: A Measurement of the Energetic Efficiency," in *2008 IEEE International Conference on Dielectric Liquids*, 2008, pp. 1-4.
- [201] I. Fofana, J. Sabau, D. Bussieres, and E. B. Robertson, "The Mechanism of Gassing in Power Transformers," in *2008 IEEE International Conference on Dielectric Liquids*, 2008, pp. 1-4.
- [202] I. H. Atanasova and R. Frotscher, "Carbon Oxides in the Interpretation of Dissolved Gas Analysis in Transformers and Tap Changers," *IEEE Electrical Insulation Magazine*, vol. 26, pp. 22-26.
- [203] IEEE, "IEEE C57.104: Guide for the Interpretation of Gases Generated in Oil-Immersed Transformers -Description," 1991.
- [204] N. A. Muhamad, B. T. Phung, T. R. Blackburn, and K. X. Lai, "Comparative Study and Analysis of DGA Methods for Transformer Mineral Oil," in *2007 IEEE Lausanne Power Tech*, 2007, pp. 45-50.
- [205] www.rswww.co.uk, *RS Arcrylic Based Sealing Compound*.
- [206] M. Duval, "Calculation of DGA Limit Values and Sampling Intervals in Transformers in Service," *IEEE Electrical Insulation Magazine*, vol. 24, pp. 7-13, 2008.
- [207] J. Dai, I. Khan, Z. D. Wang, and I. Cotton, "Comparison of HYDRAN and Laboratory DGA Results for Electric Faults in Ester Transformer Fluids," in *2007 International Conferences on Electrical Insulation and Dielectric Phenomena*, 2007, pp. 731-734.
- [208] N. A. Muhamad, B. T. Phung, and T. R. Blackburn, "Dissolved Gas Analysis (DGA) of Partial Discharge Fault in Bio-degradable Transformer Insulation Oil,"

References

- in *2007 Australian Universities Power Engineering Conference*, 2007, pp. 1-6.
- [209] www.cooperpower.com, "Envirotemp FR3 Fluid - Dissolved Gas Guide," 2006.
- [210] L. G. Wad, *Organic Chemistry*: Pearson Prentice Hall, 2006.
- [211] V. Sokolov, A. Bassetto, J. Mark, and T. V. Oommen, "Transformer Fluid: A Powerful Tool for the Life Management of an Ageing Transformer Population," in *2001 European Conferences for the Maintenance and Management of High Voltage Electrical Equipment (2001 Euro TechCon)* Chester, United Kindom, 2001.
- [212] www.cooperpower.com, "Environmental Technology Verification Report - Cooper Power Systems Envirotemp FR3 Vegetable Oil-Based Insulating Dielectric Fluid," 2002.
- [213] B. M. David and H. S. Thomas, *Flavor Chemistry of Lipid Foods*. Champaign, Illinois, USA: American Oil Chemists' Society, 1989.
- [214] B. M. David and H. S. Thomas, *Flavor Chemistry of Fats and Oils*. Champaign, Illinois, USA: American Oil Chemists' Society, 1985.
- [215] J. Pai, S. Lomanno, and W. Nawar, "Effect of Heat Treatments on the Volatile Composition of Coconut Oil," *Journal of the American Oil Chemists' Society*, vol. 56, pp. 494-497, 1979.
- [216] N. Artman and D. Smith, "Systematic Isolation and Identification of Minor Components in Heated and Unheated Fat," *Journal of the American Oil Chemists' Society*, vol. 49, pp. 318-326, 1972.
- [217] M. Brodnitz, W. Nawar, and I. Fagerson, "Autoxidation of Saturated Fatty Acids. II. The Determination of the Site of Hydroperoxide Groups in Autoxidizing Methyl Palmitate," *Lipids*, vol. 3, pp. 65-71, 1968.
- [218] CIGRE, "Recent Developments in DGA Interpretation," in *Joint Task Force D1.01/A2.11*, 2006.
- [219] X. Chen and W. Chen, "Research of Relationship between Partial Discharge and Dissolved Gases Concentration in Oil," in *2005 International Symposium on High Voltage Engineering* Beijing, China, 2005.
- [220] C. Vincent, C. Benoit, and R. Olivier, "Comparative Evaluation of Parameters of the Dielectric Breakdown Test on Transformer Oil," in *1996 International Conference on Conduction and Breakdown in Dielectric Liquids*, Roma, Italy, 1996, pp. 337-341.
- [221] www.baur.at, "Data Sheet- BAUR Oil Tester DPA75," 2010.
- [222] IEC, "IEC 60156: Insulating liquids - Determination of the breakdown voltage at power frequency - Test method," 1995.
- [223] ASTM, "ASTM D1816: Standard Test Method for dielectric breakdown voltage of insulating oils of petroleum origin using VDE electrodes," 2004.
- [224] BS, "BS 8471: Guide to Particle Sizing Methods," 2007.
- [225] V. Lakhiani, "Transformer Life Management Condition Assessment and Dissolved Gas Analysis," Crompton Greaves Ltd., 2006.
- [226] I. Fofana, H. Borsi, and E. Gockenbach, "Fundamental Investigations on Some Transformer Liquids under Various Outdoor Conditions," *IEEE Transactions on Dielectrics and Electrical Insulation*, vol. 8, pp. 1040-1047, 2001.